University of Naples Federico II
Department of Structures for Engineering and Architecture
Ph.D. Program in Structural, Geotechnical Engineering and Seismic Risk,
XXXIII Cycle

Gaetano Cantisani

Seismic Collapse Assessment of Older Non-Residential Single-Storey Steel Buildings

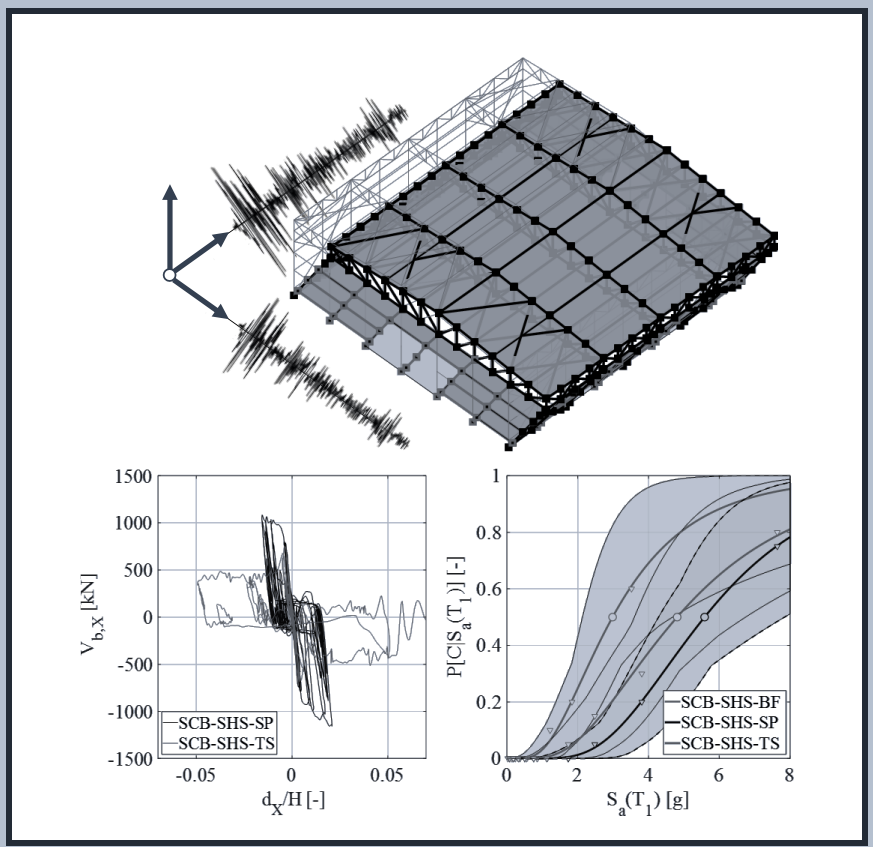

2021

University of Naples Federico II

Department of Structures for Engineering and Architecture

Ph.D. Program in Structural, Geotechnical Engineering and Seismic Risk

Coordinator: *Prof. Eng. Luciano Rosati*

XXXIII Cycle

Gaetano Cantisani

Ph.D. Thesis

Seismic Collapse Assessment of Older Non-Residential Single-Storey Steel Buildings

Tutor: *Prof. Eng. Gaetano Della Corte*

Co-Tutor: *Prof. Eng. Raffaele Landolfo*

April 2021

ACKNOWLEDGMENTS

Here I am, officially leaving my role as a *student* for life. I never imagined I could make it this far, really! In this long journey, many people contributed in several ways to bring me up to be the person I am today, helping me more than one might think. I really thank all of them for having been part of this. However, there are people I cannot help but mention in this manuscript, at the end of my *PhD*. A *necessary, yet not sufficient* way to deeply express my gratitude to them.

First, I would like to thank my tutor, Prof. Gaetano Della Corte, for guiding me like a father during the last four years of my life. His academic tutoring gave me the possibility to highly improve my skills as an engineer, as well as my scientific knowledge. His kindness and honesty are very rare. I will owe him for the rest of my life.

I am grateful to Prof. José Miguel Castro and Prof. Alessandro Zona, as reviewers of my thesis. Their suggestions and comments were very helpful to improve the present work.

Moreover, a special thank is addressed to my *roommates* in Via Claudio, my colleagues who have shared with me the experience of the *PhD* journey, supporting and enduring me the whole time. Among them, I would like to thank Milena, the special gift of these last three years. I really thank her to believe in me more than I do.

Also, a big thank to my parents for always being there (even if I suspect they did not really understand what I was doing!).

“Why do we fall, sir?
So that we can learn to pick ourselves up.”
(Batman Begins, 2005)

TABLE OF CONTENTS

LIST OF FIGURES

LIST OF TABLES

Chapter I

INTRODUCTION

I.1 Background and motivation

Non-residential older steel buildings represent a significant fraction of the Italian building stock. Such buildings were usually made as single-story buildings (SSBs), with various structural layouts as a function of geometrical dimensions and architectural constraints. The primary application of such buildings is for industrial purpose (Arcelor Mittal, 2012), but single-story solutions are appropriate for many other uses (e.g., commercial uses). Thus, the economic value of these buildings can significantly vary due to the building destination of use, but in any case, building owners can be considerably interested to protect their own investments relying on realistic evaluation of losses in case of seismic events (Silva *et al.*, 2020a). Additionally, risks of fatalities and/or injuries play an important role in making decisions for strategies aimed to reduce the impact of rare events, such as severe earthquakes.

Figure I.1 shows examples of non-residential older steel building in Italy. Reticular trusses were mainly used as the structural system to carry gravity loads (Belleri *et al.*, 2017). Usually, concentric bracing was used to resist horizontal loads, such as wind or seismic loads, as well as to guarantee out-of-plane stability

of the columns and trusses. Also, such buildings were often equipped with overhead cranes used to move crane weights inside the building.

Figure I.1 Examples of non-residential older steel buildings in Italy.

Depending on the building use, different types of envelope panels have been used, varying the thermal insulation characteristics of the building. Figure I.2 shows examples of envelope panels for existing single-storey steel structures in Italy.

Particularly, the figure shows examples of typical opening layout used for such type of structures.

Figure I.2 Examples of envelope panels and opening arrangements.

Figure I.3 shows examples of connections in non-residential older steel buildings e.g., column base connections, truss-to-column connections, and roof brace connections. Usually, IPE or HE shapes were used for the main columns of the building. The main trusses were mostly made by using built-up (back-to-back) angle or UPN shapes. Both welded and bolted connections were normally used for any of the connections. Exposed column base connections with base plate stiffeners and anchor bolts were also usually adopted.

Figure I.3 Examples of main connections from non-residential older steel buildings.

As shown by recent earthquakes in Italy, existing industrial buildings can exhibit extensive damage and/or non-negligible collapse risk (Belleri *et al.* 2015, Magliulo *et al.* 2014) triggered by poor connection details. The available literature mainly refers to precast industrial buildings since a few cases of damaged single-story steel buildings were documented during the past Italian earthquakes. However, a French report of the Chile Earthquake in 2010 (Martin *et al,* 2010)

shows several damaged and collapsed non-residential steel buildings. The report focuses on severe damages occurred to cladding systems. Buckling of braces was also highlighted. Collapse was mainly triggered by failure of column base connections and main beam-to-column connections. Prediction and prevention of structural collapse has been the major objective of earthquake engineering since its inception. Indeed, collapse is the main source of injuries and loss of lives, and one of the biggest challenges in the context of earthquake engineering simulations. More specifically, from a structural seismic engineering perspective, collapse is a term referring to the loss of ability of a structural system to resist gravity loads in the presence of seismic effects (Ibarra and Krawinkler, 2005). Despite such definition gives a clear physical perspective of the problem, the assessment of the capacity of a structure to resist an earthquake without collapse remains a rather difficult technical task (Villaverde, 2007). This is due to the complexity of the various aspects involved in the evaluation process. Adequate prediction of seismic hazard, ground motion selection, identification of all the possible modes of collapse, and an accurate modelling of cyclic component deteriorations, non-linear dynamic analyses based on reliable numerical algorithms are aspects deserving careful attention and in-depth study. Especially, from the point of view of the structural modelling, it is currently recognized that the models should be able to predict the dynamic response of deteriorating systems (Della Corte *et al.*, 2002, Adam and Ibarra, 2014). Unfortunately, such deteriorating models are only available for a limited number of structural components, and often include empirical factors needing calibration for specific applications. Besides, input ground motions, as well as key structural properties, can produce large dispersion in the numerically predicted structural response. Therefore, the collapse potential of a structural system should be quantified by means of a probabilistic-based methodology (Zareian and Krawinkler, 2007, Iervolino, 2017). The main output of such probabilistic analysis is a collapse fragility curve, which expresses the

probability of collapse as a function of the selected ground motion intensity measure. Eventually, it is worth noting that numerical studies show that collapse could also significantly contribute to the expected annual losses (Cantisani and Della Corte, 2019, 2020, Silva *et al.*, 2020b).

The difficulties in predicting the earthquake-induced collapse of buildings significantly increase when existing buildings are considered. Existing building structures have been designed according to the limited knowledge of the time in which they were built. Typically, the absence of capacity design rules and ductility requirements, result in failures of structural components, e.g. connections, which might exhibit limited ductility, thus leading to premature global collapse. The modelling difficulties become exacerbated in this case, due to the lack of adequate knowledge in terms of the cyclic inelastic response.

Within this context, this thesis presents a study on the collapse fragility assessment of existing single-storey steel buildings. The study is part of a wider ongoing research project called RINTC-E (Iervolino *et al.* 2019). The general goal of the project is to evaluate the structural reliability, expressed in terms of annual failure rate, of several building types designed according to past design codes. In fact, such structures constitute a vast majority of the Italian building stock.

I.2 Scope and objectives

The present work aims to evaluate the seismic performance of older non-residential single-story steel buildings by focusing on collapse risk evaluation. The work considered archetype buildings designed in Italy during the decade 1980s-1990s, by simulating the design process with application of codes and standards of practice relevant to that time.

The objectives of the work are: (i) to identify the seismic collapse mechanisms for typical older industrial steel buildings and define relevant engineering demand parameters (EDP) to use in seismic performance assessment; (ii) to develop guidelines for modelling structural and non-structural components; (iii) to build collapse fragility curves for selected archetype SSBs starting from results of non-linear dynamic analyses on 3D Finite Element (FE) models with bi-directional ground motion input.

I.3 Thesis outline

Following the main objectives discussed in the previous Section, the presented dissertation is organized as follows.

In Chapter II, key structural characteristics arising from the use of older design codes and standards of practice are highlighted and discussed. Several building archetypes were designed with various design assumptions for the main building components and connections, as well as for the building envelope.

Chapter III provides description of the modelling issues for the building damageable components. First, the state-of-the-art about available mechanical models is presented. Then, an extensive description of the implemented modelling strategies is discussed. Modelling of both structural and non-structural components is addressed. Especially, the Chapter presents a proposal for an improvement over available models simulating the structural response of envelope panels.

In Chapter IV, the seismic collapse mechanisms for the selected building archetypes are investigated by means of non-linear static (pushover) analysis of 3D finite element models. The pushover results are also used to identify the collapse capacity by means of selected EDPs.

Chapter V extends the contents of Chapter IV considering time-history analysis with bi-directional ground motion inputs. A comparison with predictions obtained by means of the pushover analysis is also provided.

Chapter VI is dedicated to build collapse fragility curves. Results from the analysis of the different building archetypes are compared and discussed. Fragility curve parameters are reported, as well as uncertainties in the relevant parameter estimation.

Eventually, Chapter VII outlines the main conclusions.

References

Adam C., Ibarra L.F. 2014. Seismic Collapse Assessment. *Encyclopedia of Earthquake Engineering, Springer. DOI 10.1007/978-3-642-36197-5_248-1.*

Arcelor Mittal. 2012. Steel Buildings in Europe, Technical article. Freely available on: https://constructalia.arcelormittal.com/en/news_center/articles/design_guides_steel_buildings_in_europe.

Belleri A., Torquati M., Riva P., Nascimbene R. 2015. Vulnerability assessment and retrofit solutions of precast industrial structures. *Earthquakes and Structures 8(3): 801 – 820.*

Belleri A., Torquati M., Marini A., Riva P. 2017. Simplified building models as advanced seismic screening tools for steel industrial buildings. *Journal of Constructional Steel Research 138: 51 -64.*

Cantisani G., Della Corte G. 2019. Simplified Displacement-Based Economic Loss Assessment of Single-Storey Steel Buildings. *SECED Conference on Earthquake risk and Engineering towards a resilient world,* 9-10 September, Greenwich, England.

Cantisani G., Della Corte G., Sullivan T.J., Roldan R. 2020. Displacement-Based Simplified Seismic Loss Assessment of Steel Buildings. *Journal of Earthquake Engineering 24sup1: 146 – 178.*

Della Corte G., De Matteis G., Landolfo R., Mazzolani F.M. 2002. Seismic analysis of MR steel frames based on refined hysteretic models of connections. *Journal of Constructional Steel Research 58: 1331 – 1345.*

Ibarra L.F., Krawinkler H. 2005. Global collapse of frame structures under seismic excitations. *Report No. PEER 2005/06,* Pacific Earthquake Engineering Research Center, University of California at Berkley, Berkley, California.

Iervolino I. 2017. Assessing uncertainty in estimation of seismic response for PBEE. Earthquake Engineering and Structural Dynamics 46: 1711 – 1723.

Iervolino I., Spillatura A., Bazzurro P. 2019. RINTC-E Project: towards the assessment of the seismic risk of existing buildings in Italy. *Proceedings of the 7th ECCOMAS Thematic Conference on Computational Methods in Structural Dynamics and Earthquake Engineering,* Crete, Greece.

Magliulo G., Ercolino M., Petrone C., Coppola O., Manfredi G. 2014. The Emilia Earthquake: Seismic Performance of Precast Reinforced Concrete Buildings. *Earthquake Spectra 30(2): 891 – 912.*

Martin C., Beyer K., Colbeau-Justin L., Devaux M., Quistin P., Vezin J.M., Wenk T. 2010. Le Seisme du Chili M_w=8.8: Rapport de la Mission AFPS/SGEB du 9 au 16 avril 2010. *Association Francaise du Genie Parasismique,* Paris.

Silva A., Castro J.M., Monteiro R. 2020a. A rational approach to the conversion of FEMA P-58 seismic repair costs to Europe. *Earthquake Spectra 00(0): 1 –12.*

Silva A., Castro J.M., Monteiro R. 2020b. Brace-to-frame connection modelling effects on seismic loss assessment of steel concentrically-braced frames. *Journal of Constructional Steel Research 172: 1 –14.*

Silva A., Macedo L., Monteiro R., Castro J.M. 2020c. Earthquake-induced loss assessment of steel buildings designed to Eurocode 8. *Engineering Structures 208: 1 –15.*

Villaverde R. 2007. Methods to Assess Seismic Collapse Capacity of Building Structures: State of the Art. *Journal of Structural Engineering 133(1): 57 – 66.*

Zareian F., Krawinkler H. 2007. Assessment of probability of collapse and design for collapse safety. *Earthquake Engineering and Structural Dynamics 26: 1901 – 1914.*

Chapter II

SINGLE-STOREY OLDER STEEL BUILDINGS: Design of archetype buildings

II.1 Overview of the design codes and practice in the 1980s-1990s

Nowadays, seismic design of structures in Italy is carried out using a state-of-art of technics and strategies developed to counteract earthquakes by dissipating input seismic energy thanks to controlled building damages. The seismic action is modelled by using pseudo-acceleration spectra which accounts for the probabilistic genesis of the action itself, built considering the probabilistic seismic hazard approach and by varying the return period as a function of the design limit state of interest. To obtain satisfactory energy dissipation, rules concerning details for ductility requirements and capacity design must be adhered. Such rules are included in the actual European codes (CEN, 2003) and the national Italian code (*CS.LL.PP.*, 2018). On the contrary, past structural codes provisions did not include any rules in terms of capacity design or details for ductility requirements.

Therefore, design of structures by neglecting such aspects can lead to uncontrolled collapse mechanisms with an uncertain amount of structure overstrength and global ductility. This clearly led to structural deficiencies which needs to be quantified in order to have an idea of risk in overpassing a certain limit state.

To better understand the evolution of such design code prescriptions, a summary of its main changes during the past years is described. The first Italian seismic code was a consequence of the 1908 Messina earthquake. After this event, the concept of the equivalent lateral force was introduced into the structural code, but only for such municipalities which experienced severe earthquakes (i.e., municipalities heavily damaged by an earthquake). This was introduced with the *Regio Decreto n.18 aprile 1909 n.193* and, until 1974 no changes were made, except for adding those municipalities which experienced earthquakes in that period. For example, in 1927, the *Regio Decreto n.431* defined two seismic zone categories for the calculation of the equivalent horizontal forces. Subsequently, the *Legge n.64 02 02 1974* stated that the seismic classification should have been made based on proved scientific and technical arguments. Therefore, the law introduced several changes: (i) a new seismic zone classification system; (ii) consideration of site amplification effects; (iii) introduction of modal analysis (instead of equivalent static analysis), coupled with a design spectrum, as a tool for seismic design of buildings. Though only implicitly, this was the first seismic code considering the concepts of yielding structures and ductility. After the Friuli Venezia Giulia (1976) and Irpinia (1980) earthquakes, the national territory was classified in three seismic categories by means of several Ministerial Decrees (between 1981 and 1984), considering 45% of the national territory affected by earthquakes. For the first time, the seismic classification was based on a probabilistic analysis (Meletti *et al., 2014*). In 2002, the Puglia and Molise earthquake led to a new seismic classification, considering four different seismic zones, and including the entire national territory. The four zones were identified

by considering ranges of the expected value of the bedrock acceleration experienced at the site of interest. For completeness, Figure II.1 shows maps concerning the variation of the seismic classification of the Italian territory through the years.

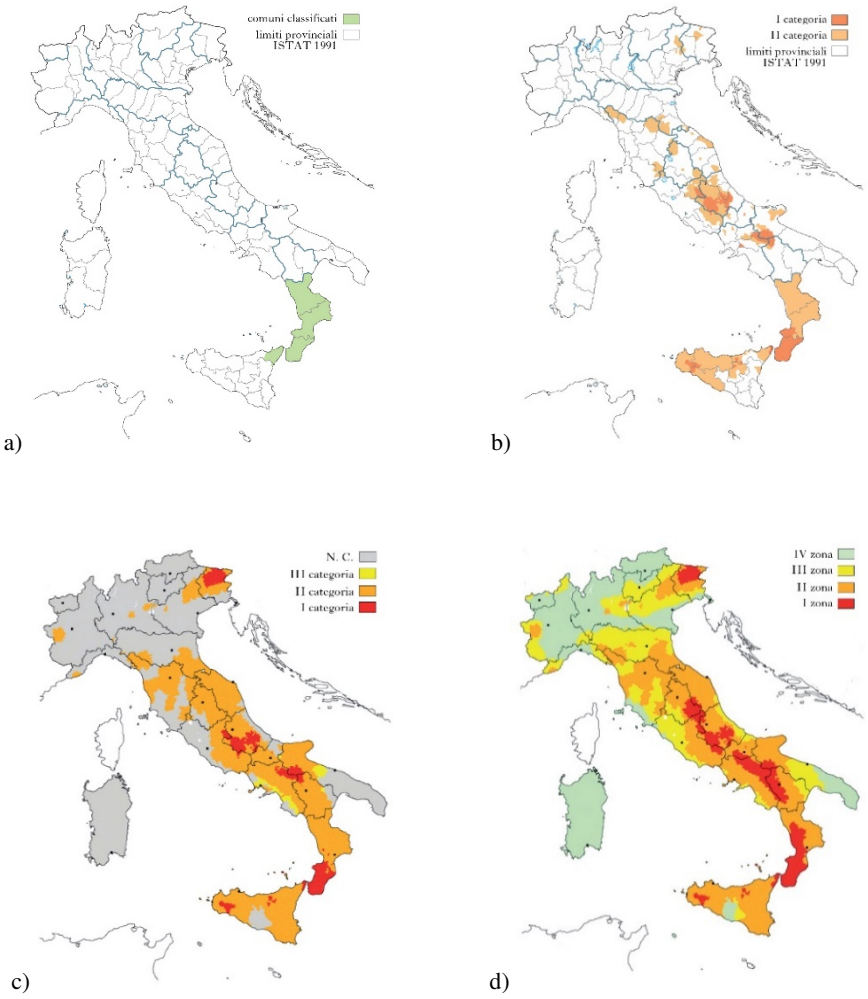

Figure II.1 Evolution of seismic zone classification: (a) 1909; (b) 1974; (c) 1984; (d) 2003 (http://www.treccani.it/enciclopedia/memoria-e-mappa-sismica_%28L%27Italia-e-le-sue-Regioni%29/)

The evolution of seismic action models and classifications led also to improvements of technical design prescriptions, especially for reinforced concrete structures. For instance, with the *Decreto Ministeriale 24 01 1986*, a new requirement about a mandatory connection between isolated foundation elements of a given building was explicitly added to the code. Another example is provided by consideration of requirements about the gap between adjacent buildings. Shear reinforcement at column ends and limitation of percentage of reinforcement into the elements were prescribed after the *Decreto Ministeriale 16 01 1996*. It is only with the *OPCM 3274 (2003)* that the seismic structural code experienced new major modifications. Most importantly, capacity design rules and ductility requirements were introduced explicitly. Such prescriptions were then completed with the Ministerial Decree of 2008 (CS.LL.PP., 2008). and, subsequently, the actual code prescriptions (CS.LL.PP., 2018). Regarding steel structures, indication concerning the importance of an appropriate design of connections, especially for dissipative zones, were made only after the *OPCM 3274*. This clearly led to potentially poor seismic behaviour of steel structures designed prior to the new millennium. Minor design differences could be seen among codes of the past century.

The presented work focuses on the assessment of structural response for buildings designed in the decade 1980s-1990s. Two main design codes were used designing steel buildings during those years. Specifically, the design for vertical loads was carried out according to the rules given in the *Decreto Ministeriale 12 02 1982* (CS.LL.PP., 1982a) (DM82). More general information on design load combinations, and particularly the design values of wind load, were instead specified in the *Circolare 24 05 1982* (CS.LL.PP., 1982b). Regarding the design of structural steel members and connections, designers used the *CNR* guidelines (C.N.R., 1988). The CNR guidelines could be regarded as the state-of-the-art approach for designing steel structures in Italy in those years. The guidelines were

based on the allowable stress method. No information was provided regarding the special case of seismic actions, which were treated as any other design load in terms of structural verifications. On the contrary, the *Decreto Ministeriale 24 01 86* (CS.LL.PP., 1986) provided the rules only for calculation of the equivalent static seismic forces (both horizontal and vertical components). Such seismic forces were calculated according to Equation (2.1) and Equation (2.2), respectively for the horizontal and vertical components:

$$F_h = C \cdot R \cdot I \cdot W \tag{2.1}$$

$$F_v = m \cdot C \cdot I \cdot W \tag{2.2}$$

In both the equations, W is the seismic weight of the building, which was the sum of the permanent structural and non-structural loads, plus a fraction of the variable loads as a function of the building type. The coefficient R appearing in Equation (2.1) considered the dynamic effects. However, it was generally fixed equal to 1. Instead, the coefficient I considered the need of more protection (which was intended to be equivalent to more strength) to structures destined to manage emergency after an earthquake. Thus, for such "important" structures, I was larger than 1, otherwise, it was set equal to 1. Finally, in calculating the vertical action, the coefficient m was generally set equal to 2. The most important factor in the definition of the building seismic actions was the C coefficient, which quantified the building site seismicity. C generally varied with the site, according to the Italian seismic risk classification of the territory previously discussed. Therefore, the equivalent seismic static base shear force was a fraction of the seismic weight of the building. Despite the presence of such seismic actions into the codes, design of seismic resistant buildings could be regarded as design for a generic force

acting on the structure. In most cases, especially in light buildings (it is the case of non-residential steel buildings), such force was not the one governing the design output. This result was not only a consequence of the relatively small intensity of the design seismic action, but also a consequence of neglecting any capacity-design and ductility requirements. Therefore, relatively brittle failure modes could be well expected in case of older steel buildings.

II.2 Archetype buildings adopted as case studies

This section summarizes the simulated design of the archetype buildings. As discussed in the previous chapter, these are the buildings considered in assessing the seismic reliability within the activities of the RINTC-E research project. Older single-story steel buildings were considered made by reticular truss beams in the transverse (portal frame) direction, whilst vertical concentric braces were considered in the longitudinal direction. The main geometric characteristic and structural schemes adopted for the considered archetypes are depicted in Figure I.1. Since past numerical studies (Scozzese *et al.*, 2018a, 2018b) demonstrated that structural behavior of code-conforming non-residential steel building slightly changed by varying the main building geometry, the study focuses on the assessment of the structural response of older SSBs by changing design assumptions and structural schemes used for design purpose. This is the reason why, at least in this part of the project, a unique geometrical configuration was considered in defining the archetype case studies. The generic archetype comprises five main portal frames with truss beams in the transverse (X-) direction. In the longitudinal (Y-) direction, concentric braces provide stiffness and resistance against vertical and horizontal loads. To stabilize the upper truss chords, roof braces were used. Also in this case, a concentric brace configuration was used. A reticular truss beam was also designed in the longitudinal direction, to stabilize upper and bottom chord of end member of the main truss system. Also,

concentric braces were used to fix out-of-plane displacements at the bottom truss member intersections in which secondary column elements were placed. Indeed, secondary column elements were designed as simply supported beam loaded with horizontal wind loads due to pressure in cladding elements. Therefore, it was necessary to stiff out-of-plane truss direction to provide an adequate top support to secondary columns.

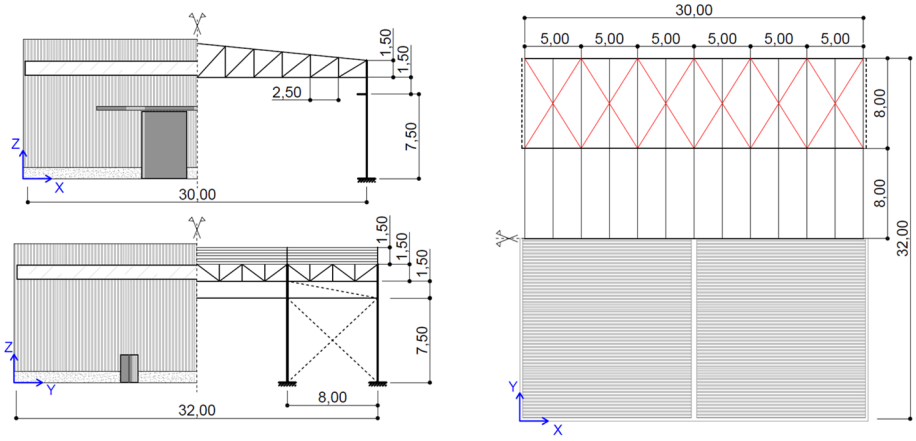

Figure II.2 General views of the archetype buildings.

As indicated in Figure I.1, truss beams had a span length of 30 *m*, while each portal frame was shifted by the previous of 8 *m.* Within this selected geometry, several structural schemes were considered. Figure II.3 shows these main structural assumptions. In the transverse direction, two alternatives were selected: (i) a continuous column for the whole height of the building with a pinned column base and a truss beam providing moment action. (ii) A nominally fixed column base and a nominally pinned truss-to-column connection. The first case study will be indicated by the acronym PCB (pinned column base). The second case will be referred to as a "semi-continuous column base" (SCB) because analysis revealed a semirigid and partial strength connection. In the longitudinal direction, two

shape of member cross sections and two types of connections were selected for the vertical brace elements: (i) hollow square cross sections and welded gusset plate connections (SHS); (ii) closely spaced built-up angle sections with bolted gusset plate connections (2L). For all the considered structural schemes and connection details, an old "Fe 430" was used as structural steel, both for member and connections. For bolts, design was carried out by varying in some cases the bolt class. Such information will be then addressed when necessary in the subsequent part of the dissertation.

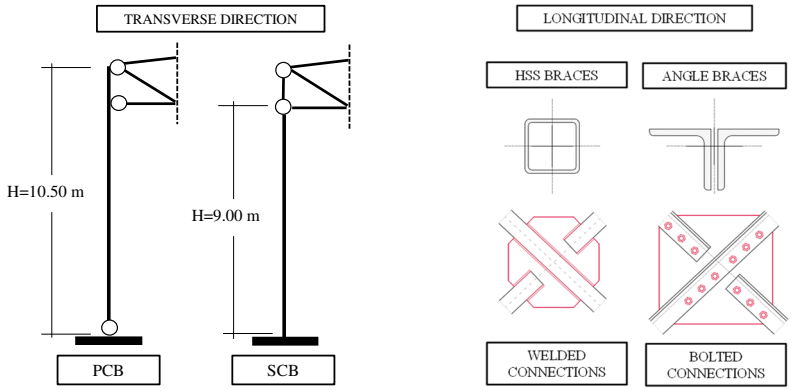

Figure II.3 Structural schemes for the archetype buildings.

Two main envelope types were considered. Figure II.4(a) shows a structural detail concerning the envelope made by means of sandwich panels (SP). As shown in the figure, the single panel was connected to the generic structural member by means of bolted connections. Figure II.4(b) shows a detail of the envelope made by means of trapezoidal sheeting (TS), connected to the generic structural member by means of screw connections. These two envelope typologies were then used alternatively to generate two different cladding systems. Instead, only the solution made by means of trapezoidal sheeting was used as roofing, eventually completed on-site with thermal insulation and weather shield. This choice was done to extend

the study by implicitly considering variation of the building destination of use and its economic value. In fact, the envelope made by sandwich panels reflects a refined building envelope, perhaps with offices inside in which economic and social activities can be carried out. On the other hand, an envelope made by a single layer of trapezoidal sheeting reflects a poor building envelope, in which there are no requirements concerning thermal insulation or aesthetic refinement of the building. In this case, the building can be considered as warehouse or similar.

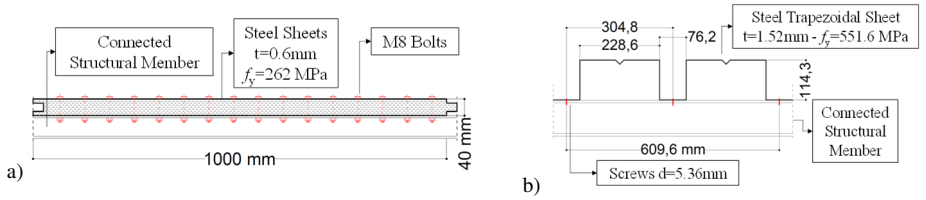

Figure II.4 Cladding panels considered: (a) Sandwich panel; (b) Trapezoidal sheeting.

To consider variability of the failure risk with the site earthquake characteristics, the case study buildings were designed in three different locations. The selected three sites reflect variation of the seismic hazard from low (Milano, Italy), through medium (Napoli, Italy), to high (L'Aquila, Italy). The assessment of the structural response was started for the buildings located at L'Aquila i.e., at the site of highest seismic intensity. This made it possible to identify the structural response characteristics and the corresponding modelling issues. Although this thesis work is mainly concerned with modelling and analysis of the response of the buildings located at L'Aquila, information regarding design aspects are included here for comparison.

Considering assumptions made in defining structural schemes, envelope details and the building sites, Figure II.5 shows the assessment framework discussed in

the following chapters of the dissertation (the acronym BF correspond to the assessment of the bare frame structure, i.e., without considerations concerning the envelope). Therefore, twelve different numerical models will be generated and analyzed both with static and dynamic non-linear procedures.

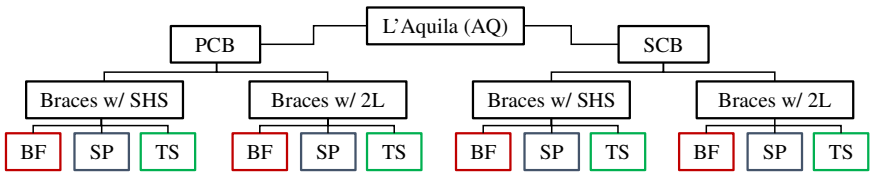

Figure II.5 Summary of the case studies investigated in next Chapters.

II.2.1 Design loads and load combinations

Permanent non-structural loads considered were the cladding weight (0.12 kN/m^2), the runway beam weight (1.55 *kN/m*) and the overhead crane weight (150 *kN*). In variable loads, the crane working load was considered (100 *kN*). Additional variable loads were described subsequently.Table II-1 provides characteristic values for the snows loads for the three building sites considered in the research project, as well as other imposed loads. As one can see, the larger value of snow load was registered in L'Aquila.

Table II-1 Design values of snow loads for the archetype buildings.

SITE [-]	**ZONE [-]**	**a_s [m]**	**q_s [kN/m^2]**
L'Aquila (AQ)	I	716	1.52
Napoli (NA)	II	17	0.60
Milano (MI)	I	120	0.90

Table II-2 shows characteristic value for wind actions in terms of pressure by varying the building site. Additionally, such pressure was turn into an equivalent horizontal and vertical force acting on the structure, normalized to the building weight, as a quantitative information to compare wind and seismic actions acting on the structure. This gave a preliminary idea on the amount of overstrength which will be expected to the structure.

Table II-2 Design values of wind loads for the archetype buildings.

SITE [-]	ZONE [-]	a_s [m]	q_w [kN/m2]	$F_{w,h}/W$ [-]	$F_{w,v}/W$ [-]
L'Aquila (AQ)	II	716	0.61	0.21	0.30
Napoli (NA)	III	17	0.76	0.26	0.37
Milano (MI)	I	120	0.46	0.16	0.22

Finally, Table II-3 shows calculation concerning the seismic force (both for horizontal and vertical component). The coefficient *C,* described in the previous section, was calculated by means of the coefficient *S*, which was defined as a function of the seismic zone. Relationship between *C* and *S* is described by Equation (2.3).

$$C = \frac{S-2}{100} \tag{2.3}$$

Table II-3 Design values of seismic loads for the archetype buildings.

SITE [-]	S [-]	C [-]	R [-]	I [-]	$F_{s,h}/W$ [-]	$F_{s,v}/W$ [-]
L'Aquila (AQ)	9	0.07	1	1	0.07	0.14
Napoli (NA)	6	0.04	1	1	0.04	0.08
Milano (MI)	NC	0.00	1	1	0.00	0.00

Comparing seismic and wind global forces acting on the structure, one can see the larger amount of wind forces despite of the seismic ones. This clearly gives a large amount of overstrength in assessing response for lateral loads. As a conclusion, gravity and wind actions for the case studies produced structural effects always larger than seismic effects.

As reported in the *CNR* guidelines, two different load combination were used: (i) a gravity load combination, which maximized the effects of vertical loads acting on the structure, without considering any type of horizontal action; (ii) a lateral load combination, which maximized the effect of horizontal loads acting on the structure, by alternatively considering the wind loads and the seismic loads and by neglecting the contribution given by the snow loads.

II.3 Main aspects in the archetype building design

Archetype buildings were designed according to the indication provided by the design codes and guidelines discussed in Section II.1. For this reason, design was carried out by applying the allowable stress method and using an allowable stress σ_a = 190 *MPa.* As already discussed, neither capacity design rules nor ductility detailing was required by the code. The following section details criticisms arising from carrying out simulated design for such building typology. Two subsections were considered, separating issues arising from both the transverse and longitudinal building direction, produced by different structural schemes assumed during the design hypothesis.

II.3.1 The transverse truss

Evaluation of internal forces in the main truss system was done by considering simplified 2D structural schemes and assuming pinned connections for all truss members. Since the internal force demand due to snow loads was always larger

compared to wind (or seismic) loads, the design of the main trusses was always governed by the gravity loads. These load effect "hierarchy" had radically different consequences on the two considered structural schemes (i.e., PCB and SCB). In fact, in the PCB structural scheme, the main truss system was designed as an equivalent beam with fixed ends. Equivalent bending moments at the truss ends were used to design chord members and relevant connections (i.e., the truss-to-column connections) at the two ends of each truss. In this case, the resistance of connections was not large enough to allow yielding of the connected members or formation of plastic hinges into the columns when horizontal loads are applied. On the contrary, in the SCB structural scheme, the main truss system was designed as a simply supported equivalent beam. This led to larger equivalent bending moment at the middle of the truss if compared with that expected in the PCB case. Therefore, larger member cross sections and more robust connections were expected in the central part of the truss for the PCB case compared with the SCB case.

In the PCB case, horizontal actions drastically change distribution of axial forces into the main truss. In the SCB case, the structural scheme for the design of the truss is not affected by the horizontal actions. In fact, horizontal loads do not produce drastic variations of axial forces in the main truss members. In fact, the resistance to the lateral forces is provided by the two columns acting as two cantilevers. Obviously, the two cantilevers did account for the global overturning moment produced by horizontal loads reacting with bending moments at the column base, opposite to what happened in the PCB case.

Figure II.6 shows a detailed sketch of the designed truss-to-column connections for the PCB and SCB cases. Differences resulting from the preceding discussion about the internal force demand according to the different design schemes are apparent from the figure. Both the top and the bottom chord member cross section

are shown, as well as general connection arrangement. One other paramount detail concerns the column cross section profile, which was used for the whole height of the main truss system in the case of PCB (Figure II.6(a)). Then, truss-to-column connections were used to connect truss members to the main column. On the contrary, in the SCB case (Figure II.6(b), truss-to-column connection developed at the beginning of the main truss height. Consequently, the column cross section was interrupted at the height of 9.00 *m*. Results of such interruption did generate a new vertical truss member at the end of the truss, with respect to the PCB case, as shown in the figure.

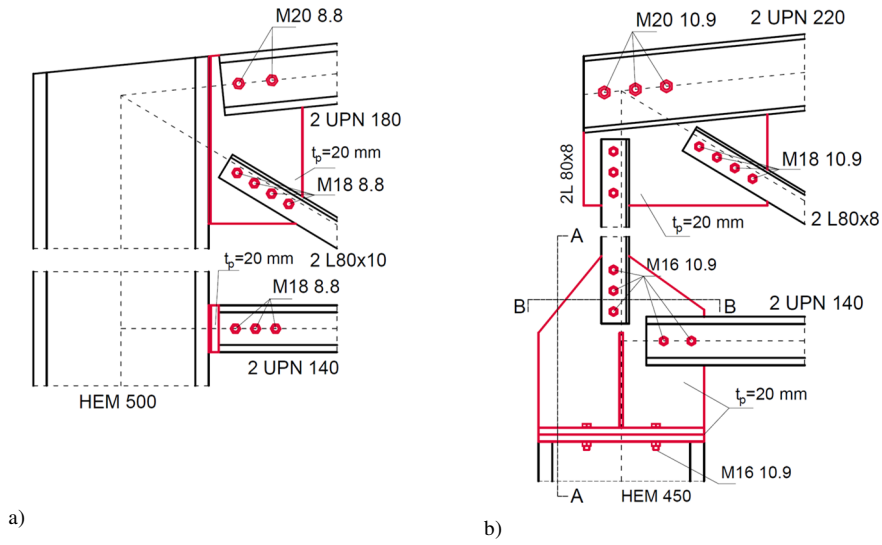

Figure II.6 Truss-to-column connections: (a) PCB case; (b) SCB case.

II.3.2 Columns and column base connections

Columns were designed considering both resistance checks and deformability checks. In fact, as suggested in the *CNR* guidelines, a limit to the horizontal displacements needed to be considered, to reduce damage of non-structural elements. Such limitation was fixed as displacement limitation of 1/500 of the building height, which was 10.50 *m* for the assumed geometry. Instead, resistance checks were made to have an appropriate resistance against the lateral-torsional buckling behavior. As a result of the simulated design carried out by varying the building site, deformability requirements proved to be more severe than the buckling check, thus column cross sections were chosen to satisfy such deformability target.

Although the two structural schemes should have the same (or rather comparable) initial lateral stiffness, the PCB structural scheme showed smaller lateral stiffness than the SCB case. This led to slightly different column cross section, as suggested in Figure II.6. Motivation behind such difference was due to the different structural models used to design the transverse building direction. In fact, the PCB case was largely influenced by the presence of the main truss system, which can be regarded as a semi-rigid moment-rotation response at the top of the column. On the other hand, the SCB case was not influenced by such deformability, as also noted when truss-to-column connection results were discussed. In this case, design of the building was carried out by keeping the assumption of a fixed connection at the column end, whatever it will be the connection detail. In fact, classification of joint, as reported in the recent version of the Eurocode (CEN, 2009), was totally neglected during the design phase of older steel buildings. Connections were designed just considering resistance checks, assuming simplified action distributions in bolts and/or welds. Thus, both theoretically and

practically, the SCB case can be regarded as the stiffer solution if compared with the PCB case during the design phase.

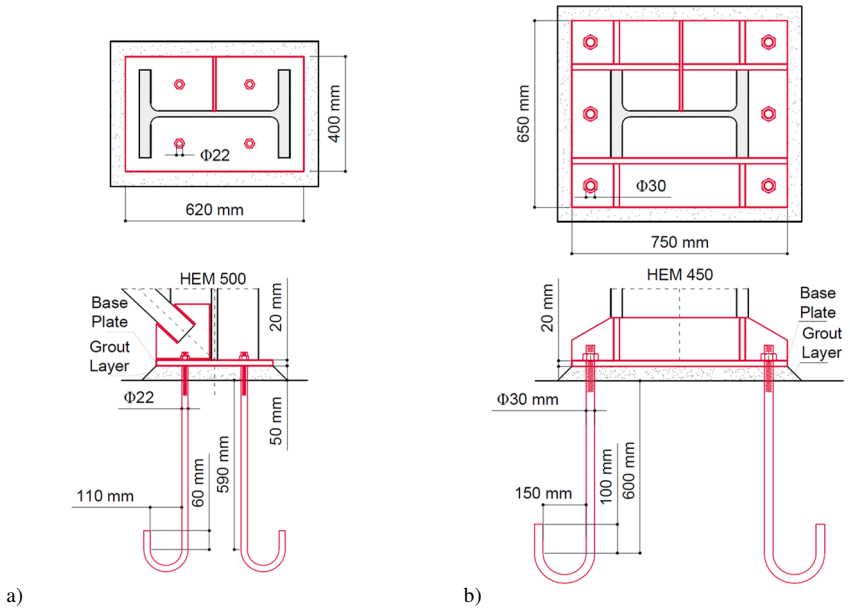

Figure II.7 Column base connections: (a) PCB case; (b) SCB case.

Column base connections were also significantly influenced by the differences in the two structural schemes. In the PCB case, the column base connection was designed as a pinned connection. Design was governed by the braced frame direction, in which vertical and horizontal actions were transferred by the brace in tension. Design for such actions required a smaller number of anchors in comparison with the SCB case. A connection with four anchors were adopted, in view of the need to provide some stability during the erection phase. Anchors were designed by using the same *Fe430* structural steel used for members. Although no tension force was predicted to occur under the design loads, the anchor length was conservatively selected equal to the minimum suggested by the code for tension bars. On the other hand, the SCB column base connection was designed as a fixed

connection. Design was governed by the portal frame direction, in which bending moment and shear forces were transferred by the column. Therefore, bending moments arising from the horizontal loads were considered to design anchors. A larger number of anchors was needed for this structural scheme. Additionally, vertical stiffeners were added according to the engineering practice of the 1980s-1990s.

Figure II.7 shows a detail of the designed column base connections, respectively for the PCB and the SCB case. One can immediately compare differences in size of both base plates and anchors between the PCB and the SCB case. It is worthy to note that similar anchor details were adopted for the two structural schemes.

II.3.3 The longitudinal bracing system

The braced frames in the longitudinal direction of the buildings were designed assuming a pinned structural scheme. This made it possible to carry out relatively simple hand calculations. Also for this direction, wind loads were dominant in defining the maximum axial forces necessary to design both brace cross sections and their connections. However, another code limitation should be considered in designing compressed members. In fact, the *CNR* guidelines (CNR, 1988) specified that the geometrical slenderness λ (i.e., the ratio between the member buckling length and the cross-section radius of inertia) for compressed members should not exceed the value of 200. Obviously, the slenderness limitation can be satisfied by different cross section shapes with different cross section areas. For instance, Figure II.8 shows a comparison between some selected cross-section shapes satisfying the slenderness limitation for a given length of the brace (equal to 5.50 *m* for the X- and 8.14 *m* for the single diagonal bracing in the considered case study buildings). As one can see, hollow squared cross sections (SHS) offer a more rational solution. A large increase of area can be observed when comparing

the SHS solution with the closely spaced built-up angle section (2L) solution. UPN shapes are the worst case in terms of structural efficiency.

Despite SHSs ensure a more rational design solution, issues could be originated in this case because of the welded connections to be made on site. As an alternative to the SHS shapes with welded connections, the case of back-to-back L shapes (2L) braces with bolted connections was also considered worthy of investigation.

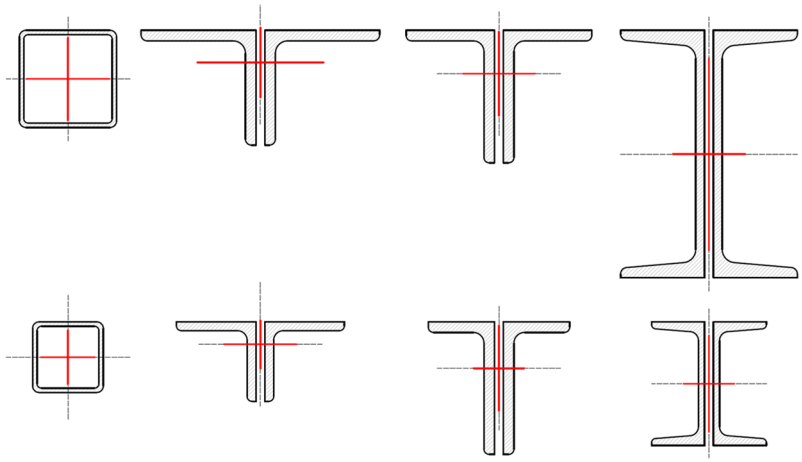

Figure II.8 Brace cross section shapes fulfilling the global slenderness limitation.

Therefore, the design of the brace cross sections was governed by the slenderness limitation. In fact, the tensile resistance of the brace cross section (the minimum between the gross and net cross section resistances) was always larger than the axial force demand once a given shape was selected to satisfy the slenderness limitation. Since capacity design was not a code requirement, both the welded and bolted connections were designed by considering the axial forces arising from the lateral load design combination (i.e., design for wind loads). Fillet welds were designed by considering a minimum value of the effective throat thickness, as suggested in the *CNR* guidelines. In designing the bolted connections, a minimum

number of three bolts was considered. Shear forces arising from any eccentricities were considered in the design of the connections. Although the design principles were the same in the two cases of welded and bolted connections (i.e. for the case of SHS and 2L braces), a significant difference in the design output was obtained in terms of connection resistance relative to the member resistance. In case of SHS braces and welded connections, the combination of having a smaller cross section area and a minimum value of the effective throat thickness implied overstrength of the SHS welded connections allowing yielding and strain hardening of the brace prior to connection failure. On the other hand, the bolted connection resistance resulted insufficient to allow yielding of the brace.

Figure II.9 shows some examples of both the welded (Figure II.9(a)) and bolted brace-to-column connections (Figure II.9(b)).

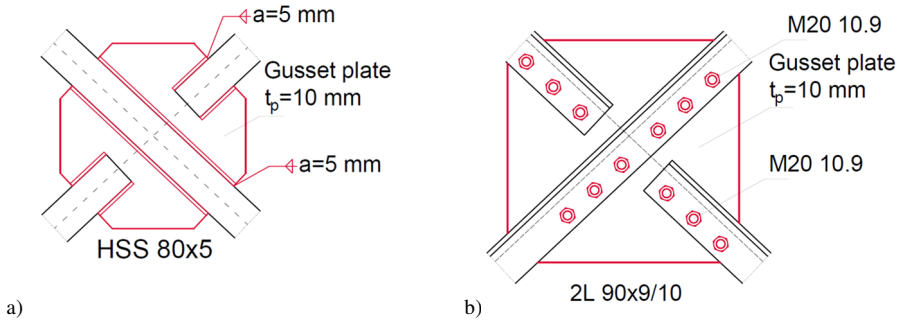

Figure II.9 Brace-to-column connections: (a) welded SHS braces; (b) bolted 2L braces.

References

CEN. 2003. Eurocode 8: Design of structures for earthquake resistance – Part 1: General rules, seismic actions and rules for buildings. *Brussels, Belgium: European Committee for Standardization*.

CEN. 2009. Eurocode 3: Design of steel structures – Part 1-8: Design of joints. *Brussels, Belgium: European Committee for Standardization*.

CNR. 1988. Costruzioni di acciaio: Istruzioni per il calcolo, l'esecuzione, il collaudo e la manutenzione (1988). CNR-UNI 10011. *Rome, Italy: UNI - Ente Nazionale Italiano di Unificazione*.

CS.LL.PP. 1982a. Criteri generali per la verifica di sicurezza delle costruzioni e norme tecniche per i carichi ed i sovraccarichi (DM 12 febbraio). *Rome, Italy: Gazzetta Ufficiale della Repubblica Italiana 56*.

CS.LL.PP. 1982b. Istruzioni relative ai carichi, ai sovraccarichi ed ai criteri generali per la verifica di sicurezza delle costruzioni (C 24 maggio). *Rome, Italy: Gazzetta Ufficiale della Repubblica Italiana 140.*

CS.LL.PP. 1986. Norme tecniche per le costruzioni in zone sismiche (DM 24 gennaio). *Rome, Italy: Gazzetta Ufficiale della Repubblica Italiana 108*.

CS.LL.PP. 2008. Norme tecniche per le costruzioni. *Rome, Italy: Gazzetta Ufficiale della Repubblica Italiana 29*.

CS.LL.PP. 2018. Aggiornamento delle norme tecniche per le costruzioni. *Rome, Italy: Gazzetta Ufficiale della Repubblica Italiana 42*.

Meletti C., Stucchi M., Calvi G.M. 2014. La classificazione sismica in Italia, oggi. *Progettazione Sismica 5(3):13 – 23.*

Scozzese, F., Terracciano G., Zona A., Della Corte G., Dall'Asta A., Landolfo R. 2018a. Modelling and seismic response analysis of Italian code-conforming single-storey steel buildings. *Journal of Earthquake Engineering 22 (sup2): 2104 – 2133.*

Scozzese, F., Terracciano G., Zona A., Della Corte G., Dall'Asta A., Landolfo R. 2018b. Analysis of seismic non-structural damage in single-storey industrial steel buildings. *Soil Dynamics Earthquake Engineering 114: 505 – 519.*

Chapter III

STRUCTURAL MODELS FOR COLLAPSE ASSESSMENT

III.1 Literature overview

It is nowadays well known that collapse prevention is one of the main objectives of a performance-based design. An appropriate knowledge of the structural response against the strong earthquakes, meaning those potentially triggering collapse, is needed to avoid catastrophic failures. However, as (unfortunately) proved by past events, structural collapse due to earthquake actions can occur due to several reasons (mainly, uncertainties of seismic actions, insufficient lateral resistance and low-ductile failure modes in case of older buildings). In fact, buildings have partially or totally collapsed during several past earthquakes (e.g., Chile in 1985, Mexico City in 1985, Northridge in 1994, Kobe in 1995, Christchurch in 2011, Emilia Romagna in 2012, Nepal in 2015 among many others). Many of the observed collapses have occurred in older buildings, which were designed with inadequate design standards. Therefore, assessing the structural response for collapse risk evaluation of such "non-conforming" buildings is important and can allow safeguarding human lives besides to reducing economic losses if appropriate actions are taken. Indeed, the 2015 National

Earthquake Hazards Reduction Program (NEHRP) Recommended Seismic Provisions for New Buildings and Other Structures (Building Seismic Safety Council 2015 p.4) asserts that "Most earthquake injuries and deaths are caused by structural collapse". However, dealing with structural collapse modelling is not a trivial task. Researchers have pointed out that several factors are involved in the definition of the collapse limit state. According to Villaverde (2007), the following factors should be mentioned: (i) characteristics of the ground motion, such as intensity, frequency content and duration; (ii) structural dynamic properties; (iii) post-elastic and post-buckling behavior of the structural components, especially their strength and stiffness degradation in case of repeated inelastic deformation demand; (iv) P-Delta effects; (v) interaction between structural and non-structural components; (vi) soil-structure interaction. Complex numerical models built with the objective to capture global collapse are not frequently used, due to the complexity of the topic and analysis. The complexity is reflected in the fact that a variety of approaches has been pursued such as non-linear static or dynamic analysis, equivalent single degree of freedom (SDOF) or more realistic multi-degree of freedom (MDOF) structural models. Tests on full-scale buildings and small-scale models have been carried out to obtain an experimental validation of analytical methodologies (e.g., Vian and Bruneau, 2001, 2003, Kanvinde, 2003, Lignos *et al.*, 2008), also improving the understanding of the conditions leading structures to collapse during earthquakes. This section tries to summarize the consolidated knowledge and most recent advances in the field of the seismic collapse assessment, considering both the aspect of the implemented methodologies aimed at evaluating building collapse and the most implemented component modelling strategies. The focus will be on collapse assessment of steel structures.

III.1.1 Overview of component modelling for collapse assessment

As stated in Zareian *et al.* (2010), collapse of a building during and shortly after an earthquake is the consequence of the loss of the building structural system integrity due to failure in one, or several, components. Two collapse modes were depicted as the most common in observing collapse cases of buildings from past earthquakes. Such collapse modes are called *sidesway* collapse and *vertical* collapse. Distinction between them was related to the components which experienced damages during the earthquake. The same classification was reported in a recent paper by Wu *et al.* (2018) in studying the seismic behavior of steel moment resisting frames. However, such classification is mainly related to collapse assessment starting from ductile structural systems, in which large displacements are expected in approaching such a limit state (i.e., large influence of P-Delta effects). Therefore, the assumptions of adequate capacity-based design rules should be made to confine yielding into predetermined zones. However, damage to brittle components might propagate rapidly to global collapse. Also, the cited collapse mode classification can be difficult to apply when damaging components triggering collapse are simultaneously belonging to both the gravity and lateral load resisting system. According to Della Corte *et al.* (2002), the assessment of collapse needs the capability to predict deterioration in strength and stiffness of structural components, realistically representing the building damage and the sequence of events which lead to the loss of strength and stiffness of the whole building. The effects of strength and stiffness deteriorations on the seismic response of structures are discussed in several papers and analytical models have been developed (Della Corte *et al.*, 2002, Ibarra *et al.* 2002, Ibarra *et al.* 2005, Ibarra and Krawinkler 2005, Zareian 2006, Haselton and Deierlein 2006, Zareian and Krawinkler 2007). Unfortunately, most of the available models for strength and stiffness deteriorations are still largely empirical, and information on parameter uncertainties could be missing. Also, detailed procedures and

compliance criteria properly assessing the structural response of existing steel structures are deemed necessary (Araùjo and Castro, 2016). Existing analytical models for predicting the structural response of ductile components can also be employed for properly modelling the response of existing steel building, when the relevant observed/predicted phenomena can be satisfactory simulated by them. Therefore, the subsequent parts of the section present existing modelling strategies focusing on different steel structural components, by considering the components or structural assemblages which are usually encounters in single-story non-residential buildings.

III.1.1.1 Modelling of ductile structural components

Most of the available technical literature is focused on the modeling of ductile components, i.e., components fulfilling specific design rules for ductility. Such ductile components show relatively stable hysteretic loops, or at least a smooth degradation process.

Focusing on the behavior of beams and columns, Lignos (2008) developed a database providing a collection of experimental test results, as well as calibration of modelling parameters considering strength and stiffness deterioration. Moreover, Lignos proposed a modification to an existing deterioration model based on the experimental observations. More recently, the same author and other researchers (Lignos *et al.*, 2019, Suzuki and Lignos, 2021) worked on the characterization of the hysteretic response of wide flange and hollow square steel columns under cyclic loading.

The seismic performance of single brace members was comprehensively discussed by Tremblay (2002). The author examined the response of single diagonal bracing members based on 76 cyclic loading tests. Equations were proposed to assess the minimum brace compressive strength and statistical

evaluations were carried out to account for uncertainties of the main parameters affecting the brace response. Especially, the ductility exhibited by the bracing members up to fracture was found to be strongly dependent on both the global and the local brace slenderness. The effect of the brace arrangement in the seismic response of braced structures, such as the concentric configuration with X-braces, was extensively described in the paper by Palmer *et al.* (2012). By means of experimental results, the paper highlighted the effect of the center splice detail on the brace behavior, also demonstrating the role of the tension brace as out-of-plane support for the compression brace. Also, the paper by Dicleli and Calik (2008) proposed an analytical model dealing with the brace axial force-deformation response. The paper by Uriz *et al.* (2008) extensively described modelling strategies to satisfactory simulate brace behavior, considering brace buckling, asymmetric cyclic behavior and yielding in tension. The modelling strategy, which is the most used in the technical literature, consider force-based beam-column elements with discretized brace cross section. Imperfections in the brace geometry gave the possibility to well predict brace buckling of the specimen, as well as the complex non-linear M-N interaction which develops into the brace itself. The fracture life of the brace under cyclic loading condition was studied by several authors. This is the most severe cause of the strength and stiffness degradations. In fact, in the case of seismic actions, low-cycle fatigue might trigger brace fracture. Some predictive equations were proposed accounting for such phenomenon, as well as the possibility to trace propagation of fracture. Several authors proposed different models based on local strain-related parameters (Lignos and Karamanci 2013, Hsiao *et al.*, 2013, Kumar and Sahoo, 2018, Sen *et al.* 2019). More recently, Hsiao *et al.* (2013) and Sen *et al.*, (2019) discussed the possibility to upgrade the numerical model by tracing the brace response beyond fracture.

Most of the experimental tests and analytical models for connections mainly consider the behavior up to limited damage. Since connections are nowadays designed to ensure yielding of dissipative members according to capacity design rules, past research mainly focused on quantification of connection elastic stiffness and resistance. Information concerning the cyclic response to large and repeated deformation demands are limited or absent. On the contrary, cases for which connections participate explicitly to the inelastic response of the structure are well documented in the literature. This is the case of braced frame structures, in which the inelastic connection response directly affects the cyclic response of the whole bracing system. Hsiao *et al.* (2012) discussed the gusset plate connection behavior of welded SHS braces. The paper focused on the out-of-plane connection behavior due to brace buckling. An extensive modelling strategy was described. Several numerical models were also discussed and compared with experimental tests.

III.1.1.2 Modelling of low-ductility structural components

The lack of knowledge for older structural components, which frequently do not satisfy modern requirements for ductility, is apparent from the technical literature. Especially, the inelastic behavior of connections with poor seismic details is not adequately studied. However, connections might play a fundamental role in defining the global resistance and ductility. The section tries to collect the information available to model low-ductile structural components.

Recently, some issues concerning non-conforming steel structural components (i.e., those not designed with implementation of capacity design rules or ductility requirements) have been addressed. Sen *et al.* (2016, 2017) discuss the performance of *non-ductile* concentric braces by reviewing existing structures with different brace-to-frame connection details. Information concerning typical

structural deficiencies can be found, as well as information on drift capacity due to premature brace fracture. Also, common failure mechanisms in the brace connections were discussed. Particularly, the papers emphasized that 20 different deficiencies could be identified and classified in the analyzed case studies. As suggested by such results, failure in brace connections lead to abrupt loss in the lateral frame resistance, with a large amount of loss of the energy dissipation capacity and a large increase in global P-Delta effects. Sizemore *et al.* (2017) presented a parametric study for low-ductility concentrically braced frames. Numerical models were developed to replicate full-scale experiments on two-story buildings. The modeling framework was calibrated by using the experimental data. Results clearly highlighted the detrimental effect of connection failures. Sen *et al.* (2019) provided some guidelines for modelling *nonductile* concentric braced frames. The paper focused on typical structural details of US bracing systems. However, the described modelling strategies are not yet sufficient to cover all the other possible deficiencies which can be found in existing steel structures. In fact, many other component damages have been documented in buildings which experienced earthquakes (Tremblay *et al.*, 1996). A critical analysis of the available technical literature has shown that the current knowledge on the seismic behavior of steel members and connections must be used in a more versatile perspective. Existing analytical models, available experimental tests and engineering judgment should be used for properly assessing the structural response of existing steel structures for seismic collapse risk evaluation.

In the following, Section III.2 is focused on the structural components that were identified for the older single-story non-residential archetype buildings examined in this study. Using the available literature information, simplified ways to model the response of such components are proposed. These modelling issues might help future researchers in selecting the relevant topics to be treated (both

experimentally and analytically) to fulfill the knowledge gap for the seismic response assessment of similar existing steel structures.

III.1.1.3 Non-structural components

Realistic numerical models of (both existing and new) structures should consider explicitly the non-structural elements. Usually, such elements are not part of the main structural system. Notwithstanding, the "non-structural" components might provide not negligible global stiffness and resistance contributions with respect to the global structural response. Modelling of steel-made non-structural components for seismic actions are not sufficiently treated in the literature. Existing studies are mainly related to assess the resistance and elastic stiffness of individual panels or assemblages of panels and secondary steelwork (Davies J.M., 2006, ECCS, 1995, AISI, 2013). Trapezoidal sheeting, sandwich panels and other common types are covered within these studies to estimate the in-plane shear strength and elastic stiffness of the sub-assemblage (i.e., sheets plus secondary steelwork and connections). In some cases, such elements are explicitly designed to provide enough lateral strength and stiffness avoiding the use of braces (i.e., *stressed skin design* (Davies J.M., 2006)). With more specific reference to the seismic response, Tremblay *et al.* (2004) evaluated the possibility to use the envelope roofing system as ductile dissipative element, while De Matteis G. (2005) addressed the effects of such envelope panels on the seismic performance. A recent experimental campaign on the behavior of steel decks (O'Brien *et al.*, 2017) pointed out some pivot aspects of the problem, particularly related to the variability of the energy dissipation of the system, as well as the effect of the connection type and geometrical layout. Shrestha *et al.* (2009) suggested the use of equivalent truss elements to simulate the in-plane structural response of a metal deck plus connections. However, detailed information on system discretization and quantification of ductility up to failure of such components are missing.

Therefore, further studies are needed concerning the identification of a robust methodology for assessing collapse by including non-structural elements, as well as modelling strategies suitable to that scope.

Trying to fulfil such knowledge gap in modelling the envelope panel response, especially accounting for strength and stiffness degradation in case of cyclic loading, a proposal of an improvement over existing models was developed specifically for trapezoidal sheeting (Cantisani and Della Corte, 2019). The choice reflected the availability of a significant number of experimental results concerning the in-plane response of the sheeting panel response. On the contrary, very few experimental studies can be found in the literature concerning the sandwich panel response. The proposed model is based on the models presented by ECCS (1995) and AISI (2013) for predicting the stiffness and resistance. In addition, information is provided to represent the post-peak branch of the response, based on experimental results provided by O'Brien *et al.* (2017). Figure III.1(a) shows the parameters relevant to the geometrical characterization of the sheeting, as well as the number/location of connections. The assembled sheeting is reported in Figure III.1(b), which also indicates the position of additional steelworks and a sketch of the mechanical model for the experimental test assemblage. A statistical analysis was carried out by comparing the theoretical values of resistance and elastic stiffness with the experimental results from the database. Figure III.2 shows a sketch of generic test results in terms of in-plane shear force (S) versus shear deformation (γ) relationship. Figure III.2(a) highlights some characteristic response points, which were identified during the experimental tests. The elastic stiffness (G') and peak shear resistance (S_{max}) were quantities measured during the generic test. Thus, the yielding resistance (defined as 40% of S_{max}) and the yielding shear deformation ($\gamma_y = 0.4S_{max}/G$') were calculated. In addition, the shear deformation associated with 20% loss in shear resistance ($\gamma_{80\%}$) was measured. In the study, to obtain information for representing

the post-peak branch of the in-plane shear response, three additional parameters were considered (Figure III.2(b)): (1) the shear deformation corresponding to the peak shear resistance ($\gamma(S_{max})$ or $\gamma_{100\%}$); (2) the shear deformation at the last available point from the test results (γ_{max}); (3) the shear resistance corresponding to the last available point from the test results (S_{res}).

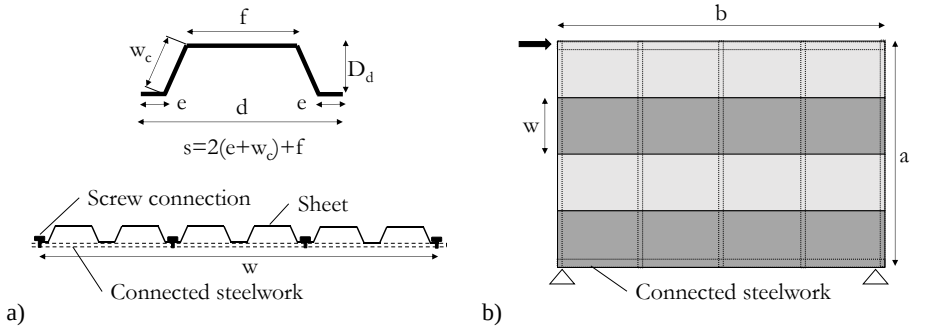

Figure III.1 Trapezoidal sheeting geometry:
(a) cross section geometry and connection location, (b) experimental test assemblage (reproduced from O'Brien et al. [2017]).

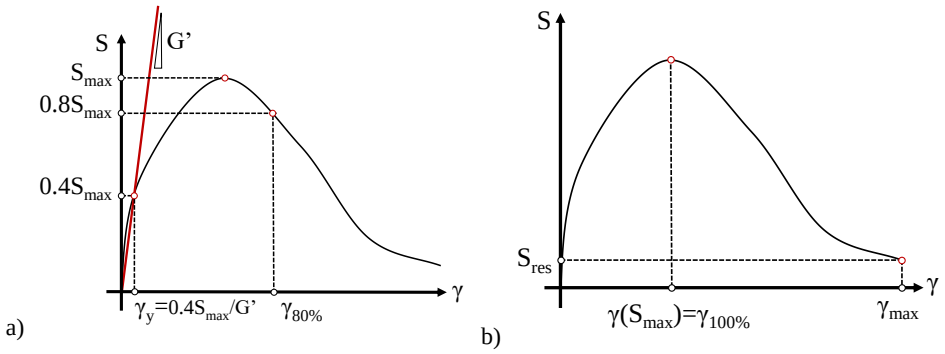

Figure III.2 Mechanical parameters from experimental tests:
(a) parameters explicitly provided by O'Brien et al. (2017) and (b) additional parameters evaluated as part of this study from the test results in O'Brien et al. (2017).

An empirical trilinear model has been proposed as shown in Figure III.3. Specifically, the AISI model was adopted for calculating the peak resistance, while the ECCS model was selected for the elastic stiffness. Those choices were made because the theoretical vs. experimental result comparisons indicated more accurate predictions obtained using the ECCS model for the elastic stiffness and the AISI model for the maximum resistance (Cantisani and Della Corte, 2019).

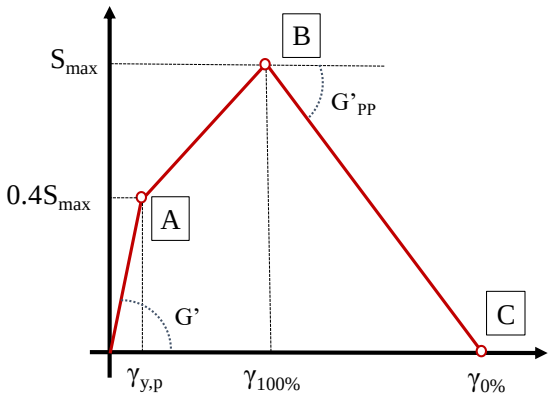

Figure III.3 Proposed trilinear model in estimating trapezoidal sheeting response.

The theoretical maximum resistance and stiffness were then corrected by empirical coefficients, as shown by Equation (3.1) and Equation (3.2). In addition, Equation (3.3) and Equation (3.4) were proposed to calculate the shear deformation at the peak resistance point, and the post-peak negative stiffness (G'_{PP}). Particularly, G'_{PP} was defined as the following ratio: $(S_{max} - S_{res})/(\gamma_{max} - \gamma_{100\%})$. The set of semi-empirical equations allows the calculation of parameters for a tri-linear simplified model. The new equations matched the experimental stiffness and resistance of the sample on average, while keeping the same dispersion provided by the original AISI and ECCS models. In addition, the equations allow calculating the deformation at the peak force resistance and the

slope of an assumed post-peak descending linear branch in the force-deformation response, with a dispersion comparable to that observed for the elastic stiffness. Details of such statistical analysis, as well as details concerning the validation of the model against experimental tests, can be found in Cantisani and Della Corte (2019).

$$S_{\max} = 1.20 \cdot S_{\max,AISI} \tag{3.1}$$

$$G' = 1.23 \cdot G'_{ECCS} \tag{3.2}$$

$$\gamma_{100\%} = 4.36 \cdot \frac{0.40 \cdot S_{\max}}{G'} \tag{3.3}$$

$$G'_{PP} = G'_{ECCS} \left[5.78 \cdot \left(12.97 \cdot \left(\frac{0.40 \cdot S_{\max}}{G'} \right)^{-0.8} \right)^{-1.40} \right] \tag{3.4}$$

The proposed model is a simplification of the complex mechanical behaviour characterizing the in-plane shear response of the whole structural system (i.e., sheeting, secondary steelwork and relevant connections). However, it allows to simulate the in-plane structural behaviour of trapezoidal sheeting with screw connections starting from parameters related to the specimen geometry and basic mechanic properties of the relevant components (such as mechanical parameters of the steel sheeting and the fasteners). Notwithstanding, additional tests should be carried out to prove the reliability of the analytical model by varying the type of connections (switching to welded connections or other fastener types) and connections layout, as well as the sheeting geometry.

III.1.2 Overview of methods to identify global collapse

As previously discussed, models which include strength and stiffness degradation of critical components are needed to assess collapse of structures. However, another fundamental aspect of the collapse assessment process is to identify the conditions triggering global collapse of a structural system. This section of the dissertation summarizes major findings available in the technical literature, highlighting differences among methods.

One of the most common definition of structural collapse refers to the loss of ability of a structural system to resist gravity loads in the presence of seismic effects (Ibarra and Krawinkler, 2005). Such definition of global collapse was also used by Krawinkler and Zareian (2007), which identified such collapse mode as the analytical condition for which large displacements lead to large P-Delta effects, large enough to counterbalance the first order base (or story) shear resistance. Several methodologies accounting for collapse evaluation coherently with such definition can be found in the literature. For example, Mehanny and Deierlein (2000) proposed a methodology based on the evaluation of a plastic zone damage index. Such index was used to calculate reduced members strength and stiffness, accounting for damage accumulation due to repetition of inelastic deformations. Within a new structural model, which was built starting from the calculated reduced strength and stiffness of the members, a gravity load analysis was carried out to quantify stability of the structure. The structure was considered stable if the gravity load multiplier was larger than 1. Similarly, Della Corte (2001) introduced a damage index to quantify the structure ability to sustain gravity loads after an earthquake. In the work of Della Corte (2001), the post-earthquake damaged structure was used to perform a non-linear static analysis by increasing the gravity loads and measuring the residual gravity-load carrying capacity. The paramount role of strength degradation in modelling the component

response was also emphasized by the same author. In the FEMA guidelines (FEMA, 2000a, 2000c), structural collapse is evaluated by using both non-linear static and non-linear dynamic analyses. Particularly, when non-linear dynamic analyses are used to assess structural response, the collapse condition is considered triggered with the occurrence of dynamic instability. This corresponds to a physical phenomenon in which a small increase in the ground motion intensity generates a large increase in relevant values representing the structural response (e.g., a relevant structure displacement), theoretically an infinitely large value. According to the same guidelines, in the case of non-linear static analysis, global collapse can be assumed to occur whenever the base shear lateral displacement curve attains a negative slope and reaches afterward a point in which the base shear force resistance is zero. In fact, this structural condition implies no lateral resistance and the inability of the structure to resist gravity loads. This is in line with the concepts presented by Della Corte (2001) and Mehanny and Deierlein (2000). Using non-linear dynamic simulations, Vamvatsikos and Cornell (2002) discussed identification of the collapse limit state by using incremental dynamic analyses (IDA). In this case, given the generic IDA curve (i.e., a relationship between an engineering demand parameter, EDP, and the earthquake intensity measure, IM), collapse is defined as the value of the IM for which the IDA curve becomes flat. The idea is that the flattening of the curve is an indicator of dynamic instability. Thus, collapse definition corresponds to that proposed in the FEMA guidelines. However, authors argued on the difficulties of the mathematical identification of such condition for the generic IDA curve. Additionally, both DM-based and IM-based approaches were discussed. A DM-based approach considers identification of the structural collapse by limiting values of the structural response (DM means Damage Measure), also identifying regions where the numerical model may not be trustworthy. On the contrary, an IM-based approach considers identification of a specific IM value for which collapse is triggered. For

example, the FEMA guidelines used the 20% tangent slope approach, which can be regarded as an IM-based approach. Therefore, collapse is identified corresponding to the last point on the IDA curve with a tangent slope equal to 20% of the elastic slope. A similar approach was that discussed by Karamanci and Lignos (2014) in assessing collapse response of concentrically braced frame structures. In that paper, collapse was identified during time history analysis when the first order story shear resistance of the structure was overcame by the second order P-Delta effects, leading to the occurrence of dynamic instability, a concept that is again in line with the ones presented by Mehanny and Deierlein (2000) and Della Corte (2001). A similar approach was used also in other papers (Eads *et al.*, 2012, Wu *et al.*, 2018, Hamidia *et al.*, 2013). More recently, the RINTC project (Iervolino *et al.* 2018) considered the identification of the global collapse with the use of pushover analysis. Global collapse was assumed to occur at a drift value which corresponded to a 50% drop of the global base shear force resistance with respect to its maximum value. To evaluate such a condition, 3D non-linear finite element models were built and analyzed. The limit drift was then used to assess the occurrence of collapse during non-linear dynamic analyses. Clearly, the proposed RINTC criterion is a compromise between different needs. In fact, severe convergence issues could arise in tracing the response when strong strength degradation occurs (Hall, 2018). Besides, the criterion also considered the larger level of uncertainties which characterize the component modelling for large post-peak deformations. Since available hysteresis models are still large empirical and model uncertainties are nowadays not completely quantified, the proposed criterion better represents a balance between the accuracy of the collapse assessment and the simplifications needed to avoid numerical issues and uncertain results.

Ground motions variability and uncertainties can produce significantly different structural responses, especially when the structure is near to collapse (Kanvinde,

2003). For that reason, probabilistic approaches have been introduced in the process of collapse prediction to consider such aspects. Research results (Ibarra and Krawinkler, 2005, Zareian and Krawinkler, 2007, Zareian *et al.*, 2010) have highlighted the importance of a probabilistic framework to assess collapse of structures that integrate possible sources of variability. Consequently, the attention was shifted towards different aspects of the problem, such as identification of suitable performance measures to assess structural collapse. In assessing such critical structural response, a metric to quantify collapse risk was needed. To this purpose, Zareian and Krawinkler (2007) and Zareian et al. (2010) proposed two performance measure for assessment of the collapse potential of a building. This is in line with the probabilistic approach used to quantify the three levels of uncertainties which characterize the collapse performance (i.e., ground motion intensity, seismic demand and seismic capacity). Such performance measures are a *tolerable probability of collapse* at a discrete hazard level, and a *tolerable mean annual frequency (MAF) of collapse*. The cited papers present methods for quantifying such performance measures.

Nowadays, indication concerning the limit values for the probabilistic performance measures are missing. Only the SAC/FEMA guidelines (FEMA, 2000b) recommend that the probability of seismic collapse should be less than 2% in 50 years. Quantification of the collapse probability of structures is still not available and, it is also still a challenge because of the multiple reasons highlighted in this literature overview. In this context, the RINTC-e research project is addressed to fulfill this knowledge gap.

III.2 Modelling issues for non-residential single-storey older steel buildings

In developing non-linear models for assessing the seismic response of non-residential single-story older steel buildings, several modelling issues should be faced. The focus of the discussion here is on the archetype buildings described in Chapter II. The section is subdivided into sub-sections related to each structural component characterizing the structural response of the bare frame system. An additional sub-section is specifically related to the modelling of the building envelope components (both the panels and the secondary structural steel work, with all relevant connections).

A sketch of each considered numerical model is depicted hereafter. For each model, highlights concerning the major modelling aspects are indicated, helping the readers in identifying the main structural weaknesses and modelling issues. The considered component responses are treated more specifically in the remaining part of the chapter. The main assumptions for each structural component are summarized, as well as examples of the implemented structural response for both monotonic and cyclic loading conditions.

III.2.1.1 PCB case studies

Figure III.4(a) shows a sketch of the implemented numerical model for case studies with pinned column base connections in the transverse direction (i.e., PCB cases) and SHS braces in the longitudinal direction. Such model was analysed by considering both the bare frame (BF) structure and by adding the envelope, respectively made by sandwich panels (SP) or trapezoidal sheeting (TS). The model for the transverse (X-) direction considered the explicit modelling of shear failure of bolted truss-to-column connections. An explicit modelling of brace

buckling and yielding, as well as fracture was considered for the vertical braces in the longitudinal direction, as well as for the roof braces. Equivalent geometrical imperfections were modelled to obtain out-of-plane buckling of braces. Additionally, column base connections were explicitly modelled to behave non-linearly, accounting for the interaction between shear and axial forces, both in the elastic and inelastic range of response. Figure III.4(b) shows the numerical model for the PCB case studies with longitudinal 2L braces. It is worth remembering here (Chapter II) that the 2L braces have bolted end connections, while the SHS braces have welded end connections. For the 2L braces, the bearing failure of the brace connections was explicitly modelled because failures of connections were anticipated to occur prior to yielding of the braces. Equivalent geometrical imperfections were used also in this case to represent brace buckling but considering in-plane buckling in this case because of the geometrical characteristics of the braces.

III.2.1.2 SCB case studies

Figure III.5(a) and (b) show the numerical model for the buildings with semi-continuous column base connections in the transverse direction (SCB case studies), using SHS or 2L braces, respectively. The main difference with respect to the PCB case was the modelling of the column base connections for the response in the transverse (X-) direction. In these cases, the column base connections were modelled explicitly in terms of their moment-rotation response up to anchor fracture. Additionally, the moment-rotation non-linear responses of truss-to-column connections were modelled explicitly in both transverse and longitudinal directions (i.e., both in-plane and out-of-plane). In the longitudinal (Y-) direction, yielding and hardening of SHS braces developed prior to anchor yielding in the column base connections. In the case of 2L braces, bearing of the

bolted connections developed prior to anchor yielding in the column base connections.

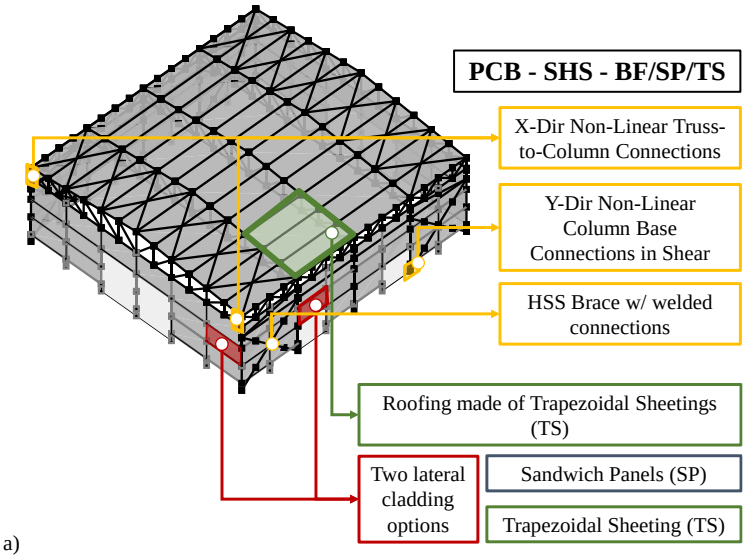

a)

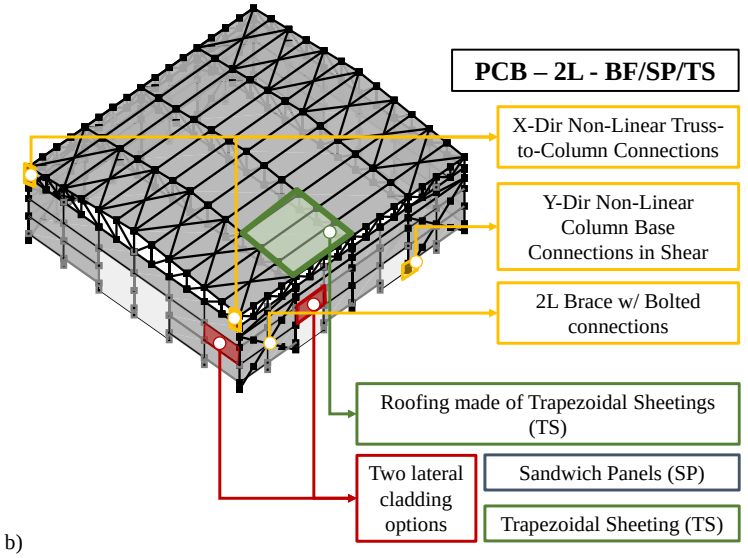

b)

Figure III.4 PCB case study models: (a) SHS braces; (b) 2L braces.

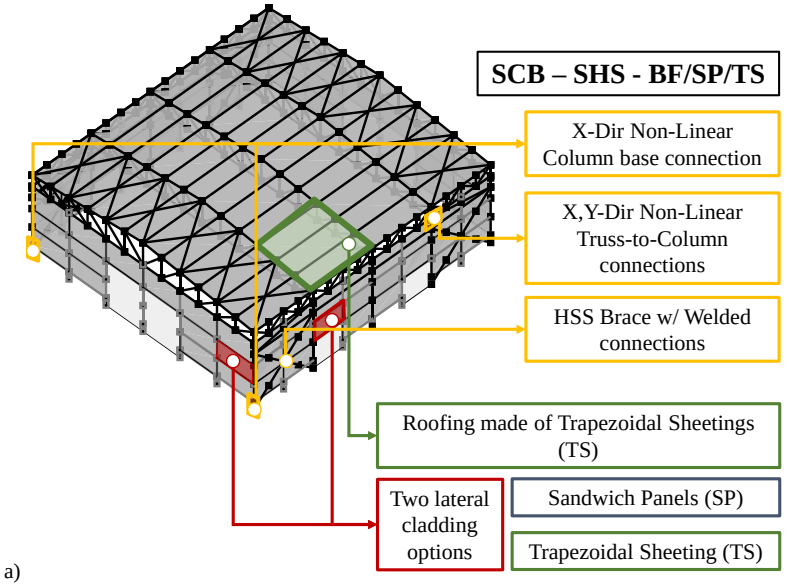

a)

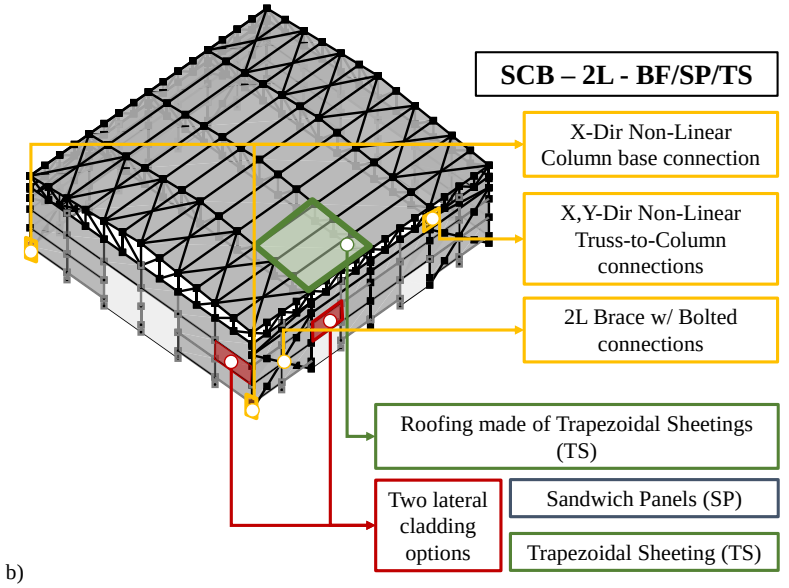

b)

Figure III.5 SCB case study models: (a) SHS braces; (b) 2L braces.

These results allowed to neglect the column base connection behavior in the longitudinal (Y-) direction of the SCB case studies. Therefore, the model mainly focused on brace and brace connection behavior. Distinctions were made in modelling brace imperfections between the SHS and 2L case studies. In the case of SHS braces, out-of-plane imperfections were modelled. On the contrary, in-plane imperfections were modelled in the case of 2L braces. Several additional modelling aspects needed to be considered for such case studies, as specifically treated in the following sections. Roof braces were modelled with an imperfect geometry and by considering the non-linear behavior. The model was analysed considering both the bare frame (BF) structure and by adding the envelope, made either of sandwich panels (SP) or trapezoidal sheeting (TS).

III.2.2 General modelling aspects

The non-linear numerical models were built-in and analysed by means of the open-source software *OpenSees* (McKenna *et al.*, 2010). However, for the linear buckling analysis, which was specifically carried out to identify the buckling modes of the vertical bracing system, the commercial software *SAP2000* (CSI, 2011) was used, because *OpenSees* does not include an option for the linear buckling analysis.

The Giuffré-Menegotto-Pinto (*Steel02*) *uniaxialMaterial* model was used to simulate the steel stress-strain relationship. Nominal values were used for the Young modulus E_s = 210 GPa and the Poisson ratio ν = 0.3 (CEN, 2005). The yield strength was estimated starting from the nominal value of the older *Fe 430* structural steel f_y = 275 MPa (CNR, 1988). Then, an overstrength factor γ_{Rd} = 1.15 was applied to consider the random variability (CS.LL.PP, 2018) , thus obtaining an expected yield strength equal to f_{ye} = 316.25 MPa. The mean ultimate strength

f_u = 479 MPa and mean ultimate strain ε_u = 34% were assumed according to recent statistical evaluations (Badalassi *et al.*, 2017). The post-elastic kinematic hardening ratio was used in modelling the non-linear stress-strain relationship of brace members. The value $E_p = 0.01E_s$ was selected according to Hsiao *et al.* (2012).

Geometric non-linearities were considered by means of the P-Delta formulation as the default option. However, several elements in the model required using the co-rotational formulation, as described in the following sections.

The mass matrix of the bare structure was formed by lumped masses derived from the real spatial distribution of the structural elements. Additionally, masses of the the overhead crane were considered. The overhead crane was assumed located at the support bracket of the second main frame. Therefore, it was assumed that the crane cannot operate with larger plan eccentricities and the planar asymmetric location of the crane masses was considered. The maximum crane load was assumed to act during the generic earthquake event. The cladding and roofing panel masses were assigned to nodes according to an influence area criterion.

Structural damping was modelled using a classical Rayleigh damping model, i.e. with a damping matrix proportional to the mass matrix and the elastic stiffness matrix. The damping ratio was set equal to 5% for two selected vibration modes which corresponded to global frame displacements in the two main building directions (i.e., transverse and longitudinal). The 5% value was based on information provided in FEMA-355F (2000b). In OpenSees, damping is automatically considered for all the beam-column elements of the numerical model (both linear and non-linear). For springs and truss elements, damping is deactivated by default and it needs to be manually activated. Attention was given to keep damping not activated for those elements with unrealistically large elastic

stiffness (i.e., for springs simulating rigid connections or plastic hinges). This is an important step to avoid structural overdamping due to unrealistically large values in the elastic stiffness matrix (Finley, 2008).

III.2.3 Column modelling

The building columns were modelled as elastic beam-column elements. In fact, pushover analyses indicated neither yielding nor buckling of columns. However, since bi-directional ground motion input was used to assess structural response by using non-linear dynamic procedures, plastic and buckling resistance verifications were also carried out when post processing the time-history results. A specific section of the dissertation in Chapter V will discuss this specific aspect of the model. Since columns in the PCB case studies were subjected to strong local interaction with some cladding panel elements, a co-rotational formulation was needed to represent some cladding detachments. To help the reader understanding this specific aspect, the corresponding model is described in Chapter IV along with the observed nonlinear static response.

III.2.4 Brace modelling

All the brace members in all the archetype buildings were modelled using the same basic options. Force-based beam-column elements with fiber discretized cross sections were always adopted. The co-rotational formulation was used to represent geometric non-linearities, since the model had to follow the post-buckling response of the generic brace for large displacement demand. Differences between SHS and 2L braces had to be considered because of the different failure modes. In the case of SHS braces, the model represented explicitly the initiation and propagation of brace fracture, according to the modelling strategy proposed by Hsiao *et al.* (2013). The Hsiao's model was implemented as a new *uniaxialMaterial* into the *OpenSees* software. According

to the Hsiao's model, a limit value of the maximum strain range (MSR_C) can trigger fracture of the brace. The limit value depends on both global and local brace slenderness, as well as steel mechanical properties. Once the MSR_C limit is reached, the tension stress in the corresponding fiber of the cross section drops to zero. The brace member was discretized with 16 sub-elements and 5 integration points were used per each element. Besides, geometrical imperfections were represented by means of out-of-plane displacements with sinusoidal shape and maximum amplitude e_0. The value for e_0 was calibrated to obtain buckling in the numerical model corresponding to the buckling axial force resistance calculated according to Eurocode (EC3) formulations (CEN, 2005). Elastic buckling loads were calculated by using simplified 2D numerical models of the longitudinal building direction, considering elastic interaction developed between tensile and compressive brace of the X-configuration and the effect of the elastic stiffness of brace connections. To this end, linear buckling analyses were performed with SAP2000. The main results of the linear buckling analysis are graphically summarized in Figure III.6(a) and (b), for PCB-SHS and SCB-SHS models respectively.

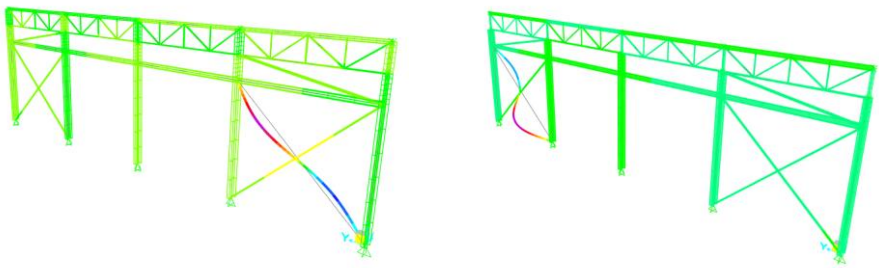

a) b)

Figure III.6 Examples of buckling modes:(a) PCB-SHS Y-2D model; (b) SCB-SHS Y-2D model.

The figures show one example of buckling mode associated to the continuous brace in the X-configuration. In both cases, analyses show a predominance of the

S-shape buckling mode for the continuous brace, with negligible values of the out-of-plane displacement at the central node. Therefore, the implemented non-linear models neglected the central node displacement in defining and calibrating the imperfection shapes.

A sketch of the implemented numerical model is described in Figure III.7(a), while Figure III.7 (b) and (c) show examples of the cyclic stress-strain relationship and global response of a generic brace, respectively.

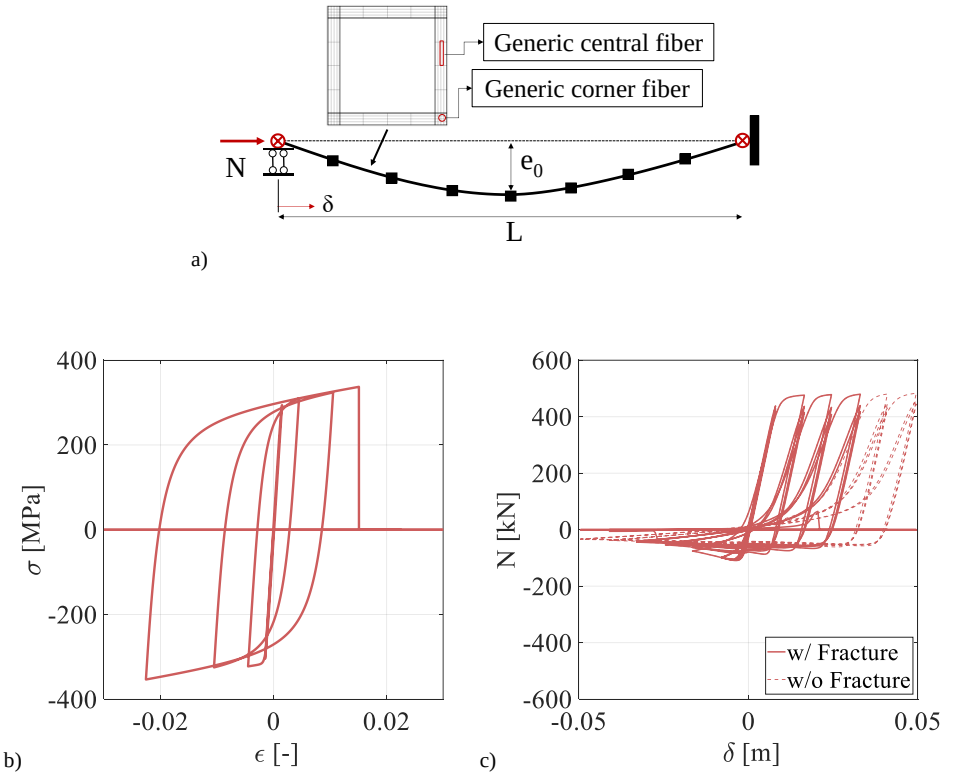

Figure III.7 SHS brace modelling and response: (a) brace model ;(b) stress-strain relationship; (c) cyclic response simulation.

The out-of-plane rotational stiffness and resistance of the gusset plates at the brace ends were implemented by means of zero length elements, following the model formerly proposed by Hsiao *et al.* (2012) for brace members in new buildings and later extended by Sen *et al.* (2019) to the case of brace end connections representative of existing buildings. Information provided by Sen *et al.* (2019) was also used to predict the tensile resistance of gusset plates. Instead, the modified Thornton method, as proposed by Yam & Cheng (2002), was used to evaluate the gusset plate compression resistance. Force-based checks were carried out to check the resistance of welds, which was not a dominant failure mode in the considered cases. In the case of 2L braces with bolted connections, the larger cross section area determined a change in the hierarchy of failure modes, with connection failure taking place prior to brace yielding in tension. Therefore, connection failure was explicitly considered in the numerical model. Analysis indicated that connection failure was in the form of bolt bearing failure. Unfortunately, the technical literature provides scarce information with reference to simplified and explicit modelling of such connection response. In fact, the connection geometry, the number of bolts and shear planes per bolt, the clearance between the bolt shanks and the holes, as well as the eccentricity of the applied loads can all have effect on the deformation capacity. Moze and Beg (2019) provided information concerning the ductility of single bolt-to-plate connections in case of monotonic loading conditions. Due to lack of more specific information on the seismic response, the work by Moze and Beg was used to build a non-linear force-displacement relationship for the considered bolted gusset plate brace connections. The strength and stiffness were estimated by means of the component method (CEN, 2009). The implemented modelling strategy resembles the one adopted by Martin *et al.* (2017) and Couchaux *et al.* (2017). According to such preceding studies, the implemented model should lead to conservative results, since force redistribution after first bearing failure is not explicitly

considered. The simplified modelling approach could be justified due to the limited information available in the technical literature and in consideration of the following additional factors, which were not included in the study by Moze and Beg: (i) the actual clearance between each bolt and the corresponding hole is uncertain due to both fabrication and erection imperfections; (ii) the eccentricity between the cross section centroid and the bolt row axis; (iii) the number of shear planes to transfer shear forces; (iv) the influence of the bolt assembly geometry and possible interactions multiple failure modes (such as failure at the net cross section area, the Whitmore resistance of the gusset plate).

Figure III.8(a) shows the implemented numerical model for a generic brace-to-gusset plate connection, while Figure III.8(b) shows an example of monotonic and cyclic responses of a connection.

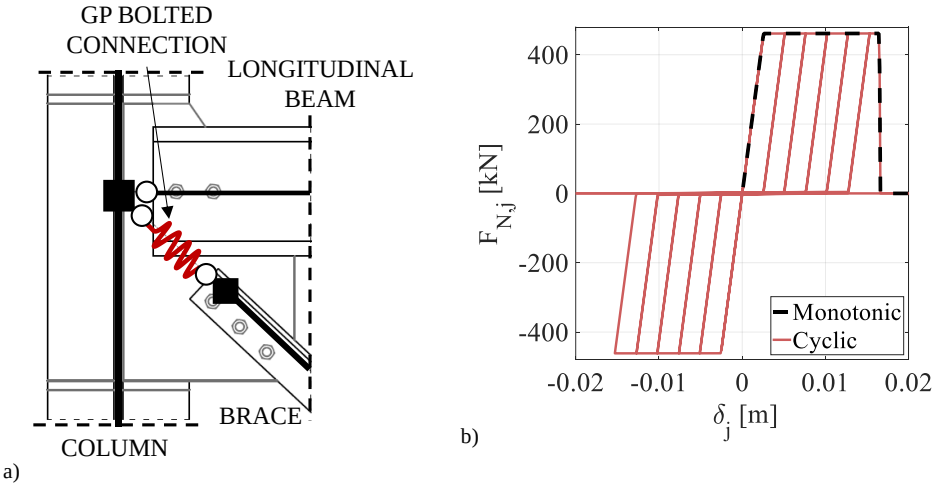

Figure III.8 Bolted gusset plate connection modelling (a) and response example (b)

An additional significant difference with respect to the SHS brace model was in the implementation of the equivalent geometrical imperfections to represent

buckling. In fact, the 2L brace exhibit in-plane buckling. In any case, a sinusoidal shape was considered, with the maximum imperfection amplitude e_0 calibrated according to the buckling axial force resistance predicted by means of the EC3 formulations. As for the SHS braces, also for the 2L braces the elastic buckling loads were calculated according to the numerical results obtained by performing linear buckling analysis of simplified 2D models. Figure III.9 highlights the main results of such buckling analyses. Particularly, a continuous S-shape was predicted as the buckling mode of the continuous brace in X-configuration (Figure III.9(a)). On the contrary, discontinuous braces did not interact each other in the relevant buckling modes (Figure III.9(b)).

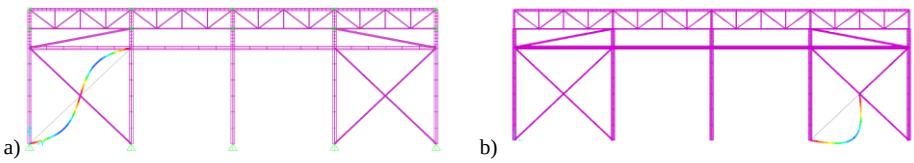

Figure III.9 Examples of buckling modes:(a) PCB-2L Y-2D model; (b) SCB-2L Y-2D model.

Roof braces were also modelled by discretizing the generic brace and using force-based beam-column elements with fiber discretized cross sections. Since neither yielding nor fracture in tension was expected for such braces, four elements were used to discretize a brace, thus reducing the computational time but allowing to obtain reasonable predictions of brace buckling and inelastic post-buckling behaviour (D'Aniello *et al.*, 2013). Obviously, to represent buckling and post buckling responses, an imperfect geometry was considered, as well as the use of the co-rotational formulation for representing the geometrical non-linearity. A sinusoidal imperfect geometrical shape was then used, with the same calibration of the initial camber as already explained for the main vertical bracing members.

III.2.5 Column base connection modelling

In modelling column base connections, two different behaviours were considered depending on the structural characteristics (i.e., PCB or SCB). Therefore, the section is subdivided into two parts, one per each type of behaviour.

III.2.5.1 Modelling of column base connections for the PCB case studies

In the PCB cases, the moment capacity of the column base connections was neglected for the assessment of the response in the transverse direction. In fact, according to EC3, the designed connections could be approximated to pinned connections. To support such modelling choice, simplified 2D pushover analyses were carried out considering explicitly the column base connection behaviour in terms of moment-rotation connection response. Such results were then compared with those obtained with the simplified 2D model with pinned restraints at the column ends. The analysis has shown that both stiffness and resistance of the column base connections did not affect the observed collapse mechanism. Besides, the collapse drift capacity, calculated according to the criteria described in section III.3, did not change by changing the model of the column base connections. On the contrary, for the response to lateral forces in the longitudinal direction, the axial and shear force resistance of the connections were explicitly represented, also considering the force interaction. The model was based on the study presented by Gresnigt *et al.* (2008). One important aspect of the model is that it represents the mechanical and geometrically non-linear response of the portion of anchors projecting outside the concrete foundation. The idea was to represent the anchors by means of force-based beam column elements with fiber discretized cross sections. However, for the search of simplifications in the overall (complex) structural model and considering the relatively small moment capacity

of the column base connections, only one equivalent beam column element was used, with an equivalent circular cross section. To consider the geometrical non-linearity, the co-rotational formulation was adopted in consideration of the large local deformations that anchors could be subjected to. Additionally, the model comprises the mechanical behaviour of the portion of the anchors embedded into the concrete foundation. The information provided by Fabbrocino *et al.* (2004) was adopted to model a non-linear zero-length element with tension-only force capacity, also considering the anchor hooks mechanical behaviour. A parallel (linear) spring with compression-only stiffness was then used for modelling the column base connection response in compression. Figure III.10(a) shows a sketch of the implemented model, while Figure III.10(b) shows an example of both monotonic and cyclic responses in terms of connection shear force ($F_{V,j}$) vs. connection horizontal displacement (δ_j).

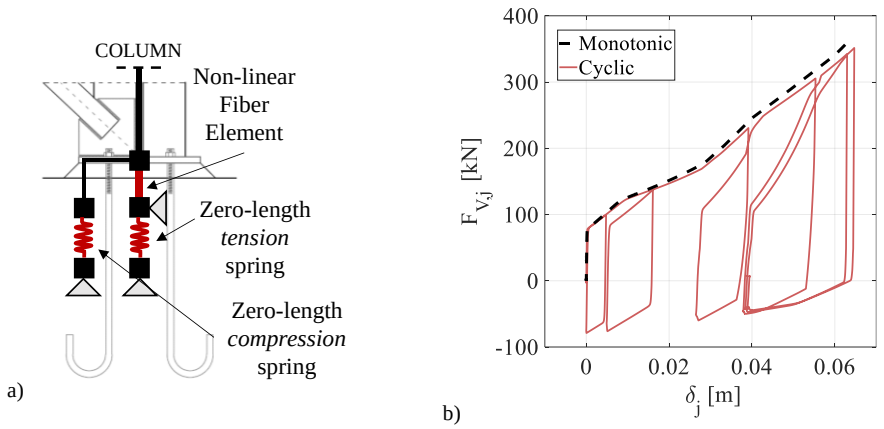

Figure III.10 Column base connection modelling: (a) PCB connection model and (b) example of numerical simulations.

III.2.5.2 Modelling of column base connections in the SCB case studies

In the SCB cases, the column base connection moment (M_j) vs. rotation (θ_j) response in the transverse direction was explicitly modelled by means of a zero-length rotational spring. The model, which is depicted in Figure III.11(a), is a rather simplified representation of the non-linear response of the column base joint rotational response. The simplification was due to the limited knowledge available in the literature regarding older column base connections, with vertical stiffeners and multiple anchors. In fact, such connection type is not covered by the current version of EC3, while the base plate stiffeners are expected to highly affect the connection response (Della Corte and Landolfo, 2017, Della Corte *et al*., 2018). Additionally, the EC3 model considers a constant value of the axial force eccentricity during the loading history (i.e., the ratio between the applied bending moment and axial force is kept constant in the analysis of the moment-rotation response). However, this is not true during an earthquake, when axial forces are almost constant while bending moments largely vary. Additionally, the cyclic response of this type of connection is relatively complex, because of the presence of several connection components which interact each other (Torres *et al.,* 2016, Della Corte and Landolfo, 2017, Della Corte *et al.,* 2017, 2018). Considering a simplified model approach, Figure III.11(b) shows an example of both cyclic and monotonic connection response. As one can see, the cyclic response is dominated by pinched hysteresis loops, due to the tension yielding of anchors. The model included consideration of base plate stiffeners by exploiting background concepts behind EC3. In fact, the plastic resistance and rotational stiffness were evaluated according to the method proposed by Della Corte *et al.* (2018). A constant value of the axial force acting on the connection was considered (i.e., non-proportional loading path, as considered in the technical literature), using the value developed by the application of the gravity loads. The ultimate connection rotation was obtained from the experimental results provided by Della Corte & Landolfo

(2017), considering the closest column base specimen with to the one presented in this case study, in terms of both connection geometry and anchor details. The ultimate connection rotation was reached with anchor fracture after significant bending of the base plate and anchor axial deformations.

As shown in Chapter IV, the rotation capacity of the column base connection played a fundamental role in assessing the global collapse capacity of the examined structures. Indeed, the plastic mechanism of the building in the portal frame direction was characterized by the formation of plastic hinges at the column bases. Unfortunately, there is no much experimental information about the rotation capacity of column base connections having the geometrical and material properties as those of the archetype buildings considered here. Gomez *et al.* (2010) and Grauvilardell *et al.* (2005) provided information concerning the seismic performance of column base connections by considering experimental test results.

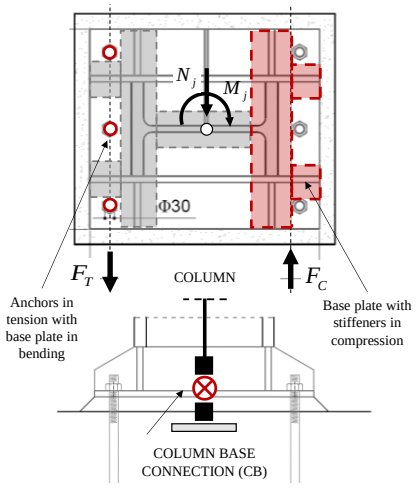

a)

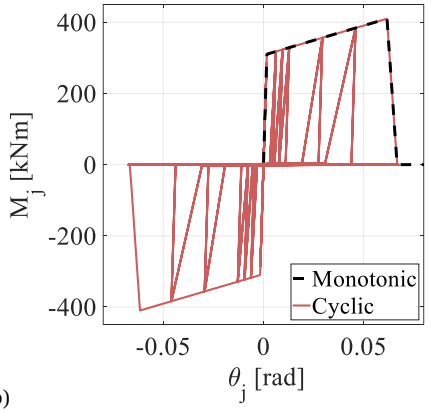

b)

Figure III.11 Column base connection modelling: (a) SCB connection model; and (b) example of numerical simulations.

Grauvilardell *et al.* (2005) summarized a synopsis of column base experimental and analytical studies. Anchor rod yielding and failure were indicated as a typical failure mode. However, information concerning the ultimate rotation capacity was not provided. On the contrary, Gomez *et al.* (2010) focused on seven specimens by varying the column cross section, the base plate thickness, the weld details and the mechanical properties of the relevant components. The experimental results described by Gomez *et al.* (2010) show that anchor rods fractured for cycles of amplitude not smaller than 7%. However, the geometrical and material characteristics (especially the anchor rod steel) of the connections considered in that report are rather different from those corresponding to the case studies examined here. Della Corte and Landolfo (2017) report a connection rotation capacity equal to approximately 6% for the specimen having a failure mechanism that is close the one predicted for the designed connections. were instead used to assign a value for the column base connection rotation capacity. Therefore, the rotation capacity was assumed equal to approximately 0.06 rad.

With reference to the response in the longitudinal direction, the connection resistance was large enough to allow for brace yielding and strain hardening up to fracture. Therefore, the model considered a perfect restraint condition to displacements in the longitudinal direction at the column bases. However, force-based checks were subsequently carried out when processing the time-history results to verify that the assumption remained valid under more complex loading conditions.

From the overview of the available research results, it was clear that modelling of column base connections in terms of ultimate response due to seismic actions has not reached complete maturity yet. There is a need to better simulate the connection strain hardening response, the post-peak descending branch, any cyclic strength and stiffness degradations, as well as the possible force interactions.

Those aspects were out of the scope of this dissertation, which is addressed to quantify the risk of collapse using state-of-the art models available in the technical literature, rather than to develop new models. However, some contributions could be identified in the direction of enhancing the modelling ability as shown by Figure III.10 and Figure III.11. The importance of appropriate models of column base connections for assessing the structural response of both new and existing buildings will be confirmed by the numerical results presented in the following chapters, and it also find confirmation in recent papers form other authors (Falborski *et al.*, 2020).

III.2.6 Truss-to-column connection modelling

For all the archetype building structures (i.e., both the PCB and SCB case studies), the non-linear force-deformation response of truss-to-column connections needed to be explicitly modelled. In fact, as it will appear more clearly in Chapters IV and V, the seismic response is strongly affected by the truss system. Different modelling strategies were adopted for the PCB and SCB case studies in consideration of the different geometrical characteristics. These models are described in detail in the following, separately for the PCB cases and the SCB case studies.

III.2.6.1 Modelling of truss-to-column connections for the PCB case studies

In the PCB cases, the response to both gravity and lateral loads in the transverse direction (i.e., the portal frame direction) is governed by the distribution of the axial forces in the main truss system. Therefore, all truss member connections were modelled, considering explicitly their elastic stiffness and plastic resistance. The model parameters were calculated by exploiting the background of the component method implemented in EC3 for connections. A similar approach was previously adopted by other researchers (Pietrapertosa *et al., 2004*, Henriques *et*

al., 2014). Simple preliminary static analysis revealed that the resistance of truss-to-column connections was particularly important. In fact, failure of such connections was expected to occur prior to any column or column base connection yielding.

The main truss system was modelled with truss elements for the top chord, diagonal and vertical members. Instead, elastic beam-column elements were used for the bottom chord members, because out-of-plane displacements were not restrained by braces at some nodes. Figure III.12 shows a sketch of the implemented numerical model. Red circles highlight the position of longitudinal braces needed to restrain out-of-plane displacements due to the presence of secondary columns belonging to the envelope system.

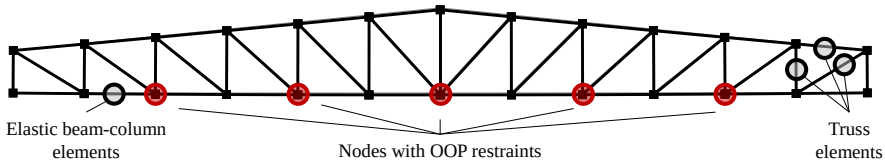

Figure III.12 Main truss model with indication of finite elements used.

Axial springs were introduced to represent explicitly deformations of bolts in shear and plates in bearing, considering both the elastic and the plastic range of the response. Especially, both the bottom and top chord truss-to-column connections were modelled explicitly by considering the shear failure of bolts, which was found to be the failure mode. To model the ductility of the bolts failing in shear, results provided by Henriques *et al.* (2014) were considered, as well as their suggestions concerning the strain hardening response. The post-peak descending branch in the force-deformation response was considered as a vertical drop in the shear force resistance (i.e., the model neglected any force redistributions after rupture of one bolt). Figure III.13(a) shows a sketch of the

implemented model in the case of PCB structures. An example of the implemented numerical model in terms of cyclic and monotonic responses is depicted in Figure III.13(b), which refers to the truss-to-column connection of the bottom chord. The effects of bolt-to-hole clearances were not included in the model. The numerical simulations in Figure III.13(b) clearly show the relatively low ductility developed by the truss-to-column connections. The very small local ductility of truss-to-column connections will reflect into a quasi-brittle global failure of the PCB portal frames (Chapter IV). The truss-to-column connections at the top chord locations were very similar those described for the bottom chord, but with smaller connection resistance.

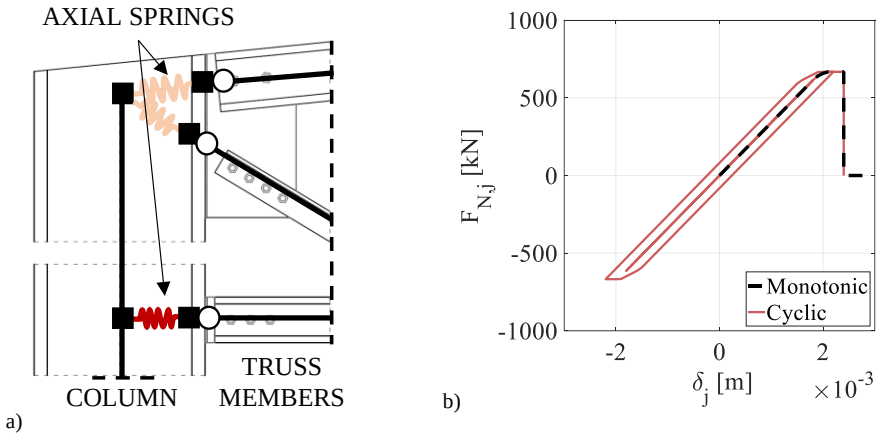

Figure III.13 Truss-to-column connection modelling: (a) PCB case mechanical model with (b) example of numerical results.

III.2.6.2 Modelling of truss-to-column connections in the SCB case studies

In the SCB cases, the modelling strategies for truss-to-column connections were extensively studied to consider the possibility of failure propagating to connections in the main member trusses. As one can see in Figure III.14(a), the

column was interrupted at the height of 9.00 *m*, while a rigid element was used to simulate column-to-truss eccentricity. The possibility to transfer any significant bending moment from the column to the truss members was investigated by considering the in-plane (IP) connection rotational stiffness and resistance (TCC_{IP}), along with rotational stiffness at all other nodes of the main truss system. The connection rotational stiffness was estimated by applying the component method.

Two alternative models of the main truss system were considered: the first model assumed pinned connections for all members; the second model considered the connection rotational stiffness (and resistance) by means of additional (rotational) springs (Figure III.14(b)). Analysis of the structure response when the rotational stiffness of connections was included showed that there was no significant propagation of bending moments from the main column to truss members. Therefore, to reduce the number of degrees of freedom, truss members were modelled as pinned and all the inelasticity was concentrated into the truss-to-column connection, by means of the non-linear spring labelled as TCC_{IP} in Figure III.14(a). Figure III.14(b) shows an example of both monotonic and cyclic simulations concerning the in-plane (IP) and out-of-plane (OOP) behaviour of the truss-to-column connection in terms of relationship between the applied moment (M_j) and the connection rotation (θ_j). The cyclic behaviour followed a peak-oriented reloading rule in line with the observed cyclic behaviour of typical beam-to-column bolted connections (Tsai and Popov, 1990, Shi *et al.*, 2007). The connection strain hardening was neglected as a simplification to this model. Indeed, results from preliminary pushover analysis did not show any significant bending moment demand to this connection. The out-of-plane connection (TCC_{OOP}) behaviour characterized the longitudinal building response. Figure III.16(a) shows the position of the zero-length non-linear spring used to model the longitudinal behaviour of the truss-to-column connection. An example of the non-

linear response of such component is depicted in Figure III.14(b), comparing the moment-rotation response between the IP and the OOP connection behaviour. The TCC_{OOP} is characterized by smaller strength and stiffness, since the connection lever arm reduced for the OOP behaviour with respect to the IP behaviour.

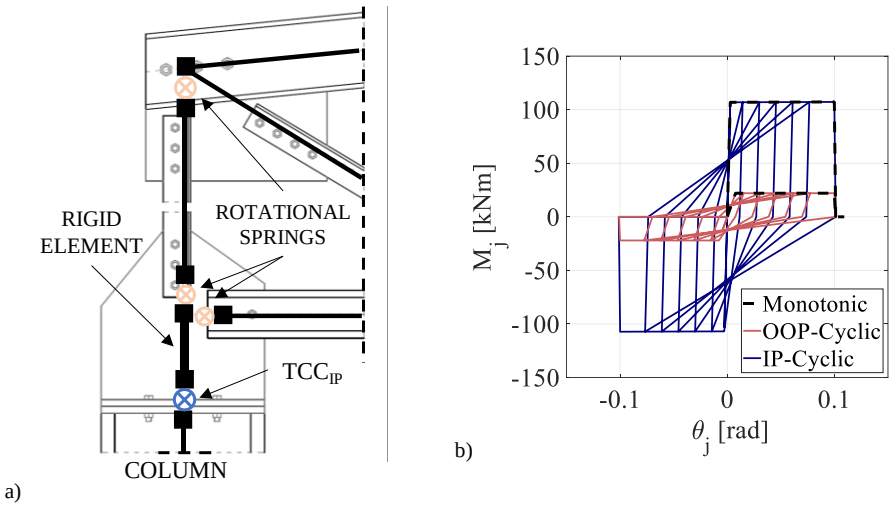

Figure III.14 Truss-to-column connection modelling: (a) SCB mechanical model with (b) example of numerical results.

III.2.7 Additional aspects concerning the SCB connection modelling

Additional modelling aspects had to be considered specifically for the SCB models. These additional aspects are characteristics of only the SCB models because of two main differences with the PCB models. The first difference concerns the interruption of the main column at the height of 9.00 *m*, where both transverse and longitudinal trusses are connected. The second difference is related to the effect of the column base connection yielding. In fact, in the PCB models, yielding of column base connections took place in the longitudinal direction.

Such differences introduced variation of the force path developed into the structure with respect to the PCB models. Particularly, increase of axial forces in the longitudinal truss system and horizontal chord members can cause additional connections yielding. Therefore, non-linear models for such connection were needed to assess the consequences of such failures for the whole building structural response. Figure III.15 shows a sketch of the longitudinal direction with indication of the considered additional non-linear connections considered in the SCB numerical models.

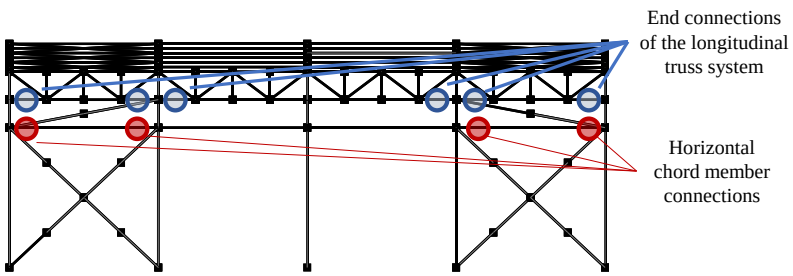

Figure III.15 Additional modelling issues in longitudinal direction of SCB models.

Figure III.16(a) shows the model for the gusset plate connections of the longitudinal trusses. A zero-length element was used to simulate the gusset plate (labelled as GP_{AX}), including the Whitmore section yielding and fracture, according to suggestions by Sen *et al.* (2019). To simulate the cyclic behaviour, the *Steel02* material model was used. An example of both monotonic and cyclic simulations is depicted in Figure III.16(b) in terms of axial force ($F_{N,j}$) vs. axial displacement relationship (δ_j). As shown in the figure, a symmetric response to tensile and compressive forces was assumed, because no buckling of the gusset plate was predicted to occur.

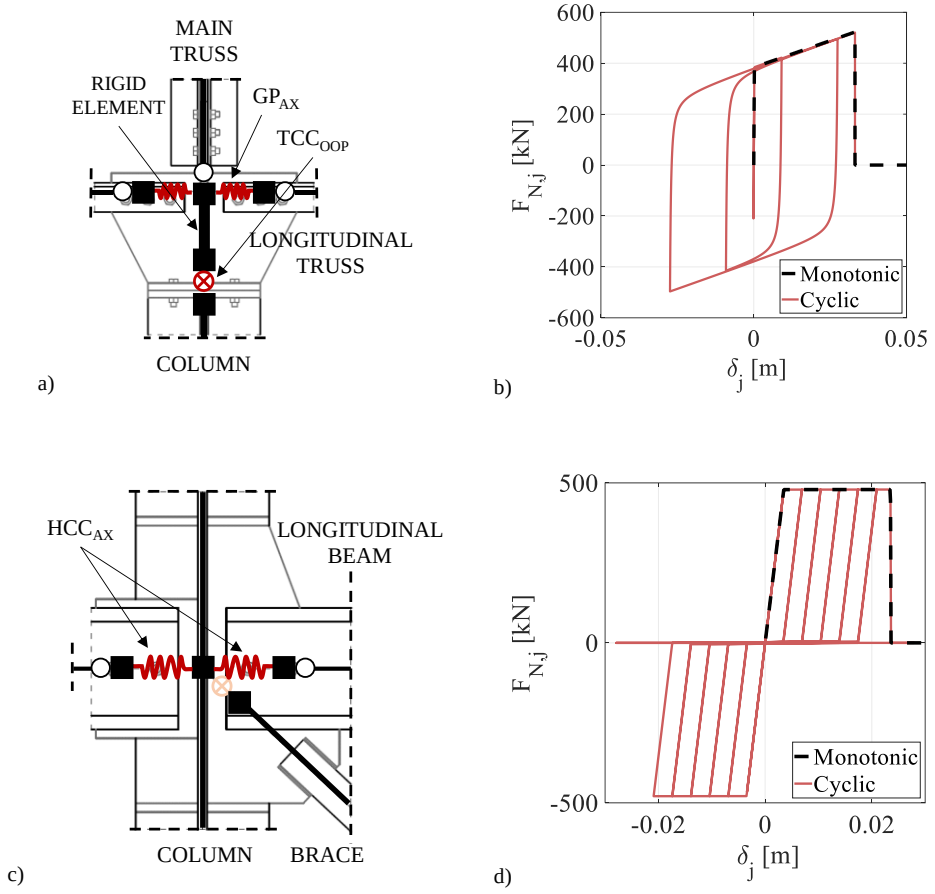

Figure III.16 (a) Gusset plate model and (b) examples of monotonic and cyclic responses. (c) Bracing chord member connection model and (d) examples of monotonic and cyclic responses.

Figure III.16(c) shows the model for the bracing chord member connections, which was also in this case implemented as an axial spring simulating the non-linear response of the weakest connection component (labelled as *HCC*$_{AX}$ in the figure), which in the specific case was plate bearing (Figure III.16(d)). Following the same approach proposed in Section III.2.4, the EC3 component method and information concerning the connection ductility provided by Moze and Beg (2019) were used to obtain a simplified monotonic response curve for the

connection. Strain hardening was neglected, and no force redistribution was considered based on the same considerations that were previously discussed for the bolted connections of the vertical brace with 2L cross sections (section III.2.4). Besides, results from the structural analysis illustrated in Chapters IV and V will demonstrate that such connection models did not significantly affect the global building performance.

III.2.8 Envelope panels and secondary steelwork modelling

For steel buildings, the building envelope is usually made of panel elements connected to secondary steelwork. The secondary steelwork is in turn connected to the main structural elements. Two examples of such building envelopes were described in Chapter II, with reference to the case study buildings. Specifically, it was assumed that both cladding and roofing panels were connected to secondary structural elements by means of several connections, which are typically designed to sustain the wind loads. Intrinsic in-plane stiffness and resistance are obvious, and they might affect the overall building response to horizontal (wind or seismic) loads (Mazzolani *et al.*, 1996, De Matteis and Landolfo, 2000, CNR, 2009). With specific reference to single-story steel buildings, recent studies (Scozzese *et al.*, 2018a, 2018b) have addressed the role of cladding panels for new buildings, i.e. buildings designed according to modern design criteria. The studies show that the effect of the cladding on the global structure response is usually significant if high-level performance is investigated (e.g., damage limitation), while the effect on collapse did not appear always important. However, in case of existing buildings where premature and relatively brittle failure modes might occur, the role of the building envelope might be more important in terms of global collapse. Besides, in Scozzese *et al.* (2018b) high-quality cladding panels (i.e., sandwich panels with bolted connections) were considered, while for existing buildings simpler and lower quality cladding panels (e.g., single trapezoidal sheeting with screwed

connections) might be found. Therefore, developing a proper mechanical model of the building envelope panels, with consideration of the secondary steelwork and relevant connections, was one of the objectives of this research study.

III.2.8.1 Modelling of the secondary steelwork

Figure III.17(a) and Figure III.17(b) show a sketch of the secondary steel structure in both the longitudinal and transverse building directions.

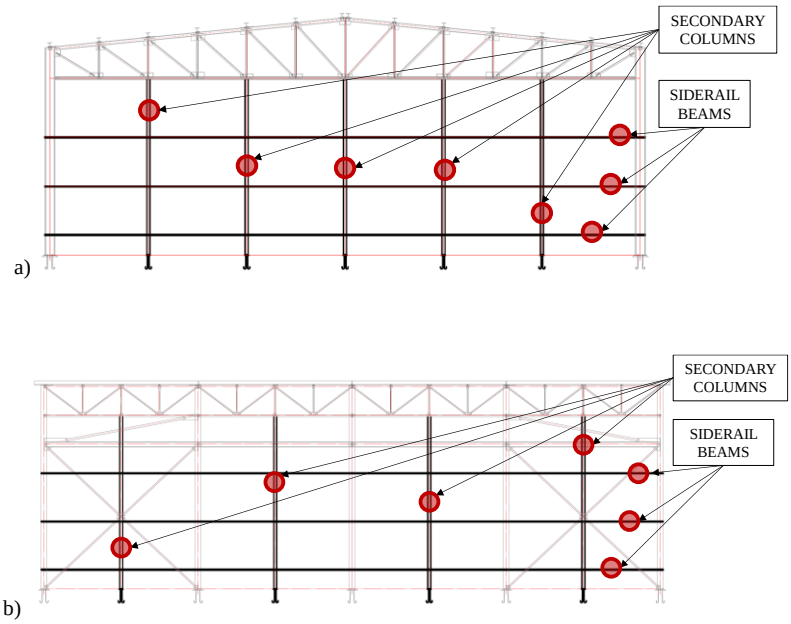

Figure III.17 Secondary steel structure: (a) transverse direction; (b) longitudinal direction.

To correctly reproduce a realistic load path between the primary and secondary structures, secondary steel elements were modelled explicitly. The proposed mechanical model tried to reproduce the local interactions between the envelope elements and the main structure. A sketch of the proposed numerical model is shown in Figure III.18 for both transverse and longitudinal directions. All the

secondary columns were explicitly modelled, as well as all the siderail beams, meshing the external surfaces of the building in both transverse and longitudinal directions. The siderail beams were modelled as elastic truss elements, while the columns were modelled as elastic beam-column elements and considering the P-Delta effects. The moment-rotation response of the connections at the base of the secondary columns was not included in the model, assuming they could be approximated to perfect hinges.

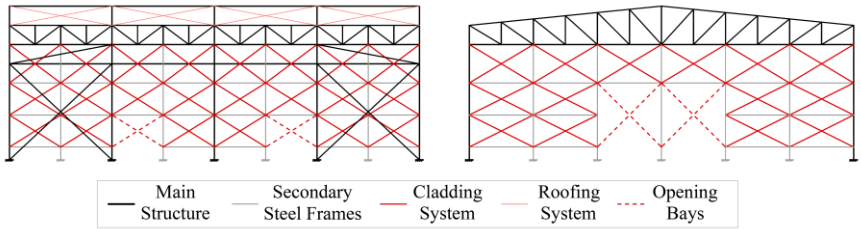

Figure III.18 Sketch of the implemented model for the building envelope.

III.2.8.2 Modelling of secondary siderail-to-column connections

The secondary steelworks were connected to the main structure by means of bolts designed considering out-of-plane actions produced by wind loads. Such connections were explicitly included into the numerical models, since preliminary analyses showed that they could fail during a sufficiently strong earthquake causing local detachments of the panels.

Thus, the proposed mechanical model was built by adding zero-length elements for connecting two nodes with the same coordinates. To simplify the numerical model, eccentricity between the envelope layer and the main frame plane was neglected. This is expected to produce some overestimation of the building lateral

stiffness, and deserves further, more detailed, investigations. Figure III.19(a) and Figure III.19(b) show sketches of the implemented model considering a generic column and a corner column, respectively. Cladding elements, which will be discussed subsequently, were connected to the secondary nodes at the ends of the secondary elements and steelwork. Such secondary nodes were mechanical connected with the main column nodes by means of the previously mentioned zero-length elements, represented with a non-linear spring (SC-CON). The force-deformation response of the SC-CON springs followed the same rules proposed for the PCB truss-to-column connections. Indeed, analysis of the connection failure modes did predict shear failure of the bolts taking place prior to bearing failure or net cross section failure.

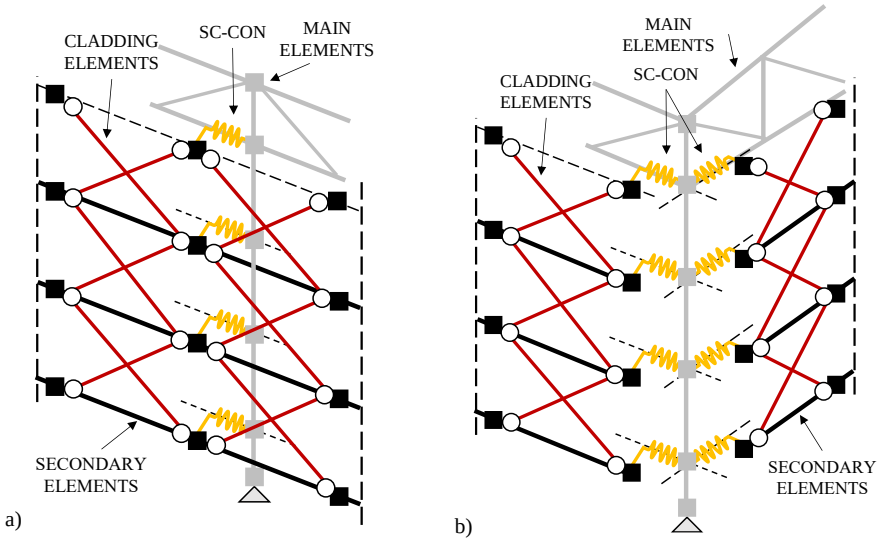

Figure III.19 Sketches of the building envelope model considering secondary connections: (a) generic column; (b) corner column.

III.2.8.3 Cladding and roofing panels non-linear response

The in-plane force-displacement response of cladding and roofing panels was calibrated starting from experimental results available in the technical literature. The calibration procedure is summarized in Figure III.20(a) and (b), respectively using experimental results of sandwich panels (SP) extracted from the paper by De Matteis & Landolfo (1999) and the relevant monotonic test of trapezoidal sheeting (TS) extracted from the report by O'Brien *et al.* (2017). Geometry of these two specimens were already described in Chapter II. In both cases, experimental tests included structural response of panels and cladding-to-frame connections. In fact, according to the experimental results, failure of the SP specimen occurred by bolt bearing against the sheeting. Similarly, failure of the TS specimen occurred by bearing and tilting of screw connections.

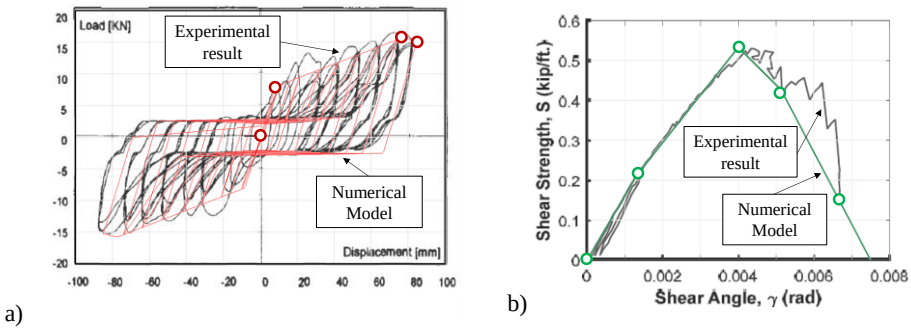

Figure III.20 (a) Experimental results (De Matteis & Landolfo, 1999) vs. numerical model for sandwich panels; (b) Experimental results (O'Brien et al., 2017) vs. numerical model for trapezoidal sheeting.

For the case of SP calibration, the considered numerical model neglected the structural response exhibited by the specimen at each first cycle of the generic displacement step, since the response in the first cycle appeared much different from those exhibited in the following cycles, which were more similar each other.

The analytical model was assumed to behave symmetrically. For the TS calibration, the selected specimen was tested only considering monotonic loading conditions. A quadrilinear analytical model was used to fit the observed experimental response. The first two branches were used to model the elastic response and the specimen strain hardening. For simulating the descending branch of the response curve, a linear relationship was chosen to fit the relative minimum values of the resistance from the observed structural response, thus conservatively approximating the complex (and uncertain) experimental response which was observed after reaching the maximum resistance value. The adopted numerical model is shown in Figure III.21(a), in which an example of panel assembly is illustrated. Two equivalent truss elements which are connected to the secondary nodes are used to represent the overall force-deformation response of the panels including the effects of the connections. Figure III.21(b) shows the in-plane force-displacement response for the cladding system made by sandwich panels (SP). This response is for a single panel but comprises the panel-to-frame connections that were part of the tested specimen (De Matteis & Landolfo, 1999). Starting from the single panel response, panels belonging to the same sub-area perimeter were assumed to behave as elements working in parallel. Figure III.21(c) shows the in-plane force-displacement response for the adopted trapezoidal sheeting (TS), used for both cladding and roofing systems. In this last case, the relationship comprises also the side-by-side connections between adjacent sheets, as they were included in the tested specimen and characterized failure of the specimen (O'Brien *et al*, 2017) by means of a mix of bearing and tilting failure.

The nature of screw connections, which characterized the structural response of TSs, led to a rather brittle failure mode in comparison with the response of the SPs, in which bolted connections were strong enough to allow bearing failure without tilting.

Openings in the building envelope were considered by applying a 50% reduction to both the initial stiffness and resistance (ECCS, 1995) for the relevant elements in the global structural models (in Figure III.17(c), bays with openings are highlighted using dashed lines for the equivalent braces).

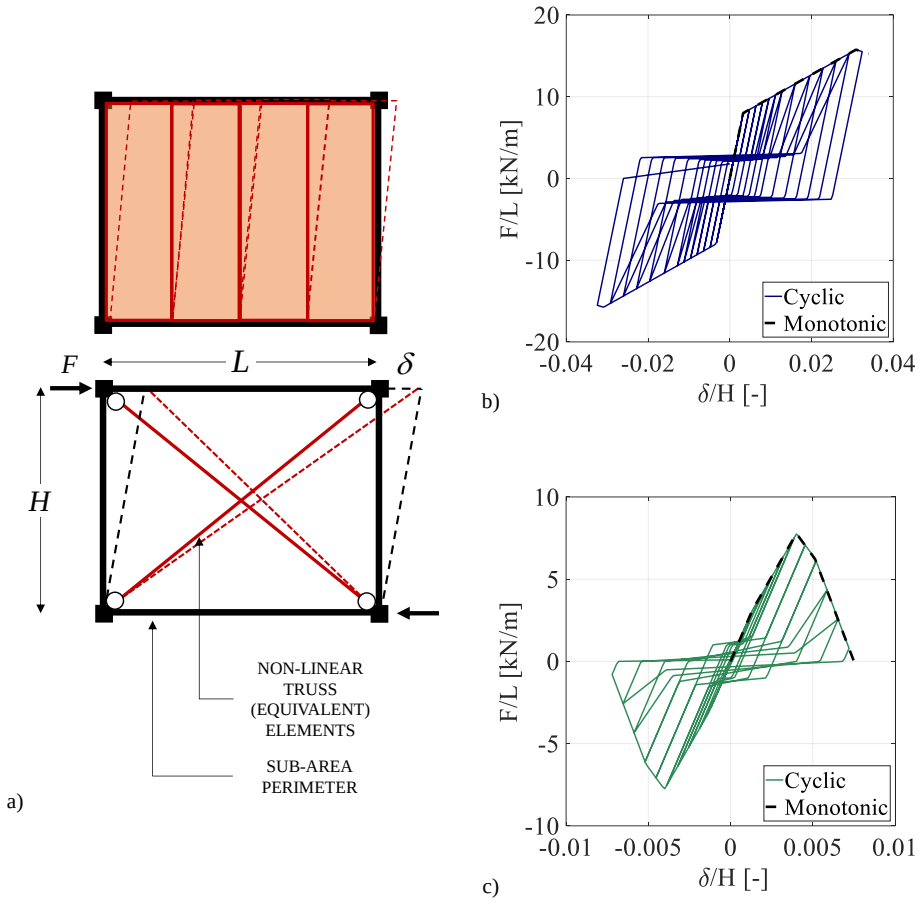

Figure III.21 (a) Mechanical model for a basic unit of the cladding and roofing systems; Cladding models: (b) sandwich panel response; (b) trapezoidal sheeting response.

III.3 Seismic collapse criteria

This section summarizes the criteria used to assess collapse for the investigated single-story steel buildings subjected to ground motions. The procedure adopted to identify collapse was agreed within the RINTC research project. Such procedure was then adopted also for this study to make results comparable to those obtained by other research groups working on different building types. According to the RINTC procedure collapse means that an appropriate engineering demand parameter (*EDP*) exceeds a limit value, or capacity (EDP_C). The EDP should be selected to be representative of the global structural response, e.g. the inter-story drift is used for multi-story buildings. For the single-storey buildings examined in this study, the ratio between the displacement at the column tip for both the building directions and the building height (H = 10.50 m) was considered representative of the global response. The collapse threshold was then defined as the EDP corresponding to a 50% strength degradation in terms of the base shear force resistance obtained through a pushover analysis. Since 3D numerical models were built and analysed, the EDP_C value was evaluated and checked for the two main building directions. It was assumed that the collapse capacity could be separately evaluated by means of an independent pushover analysis in each of the two main building directions. A graphical explanation of the collapse criteria is shown qualitatively in Figure III.22, in which two different pushover curves represent the non-linear response for two main building directions, i.e. the X- and Y- directions. The 50% reduction was assumed to represent a reasonable limit, because of the limitations and uncertainties of currently available mechanical models for the structural components. Therefore, bounding the numerical response of the building in a range for which all the main sources of non-linearities are considered (Figure III.23) should not compromise the trustworthiness of the model.

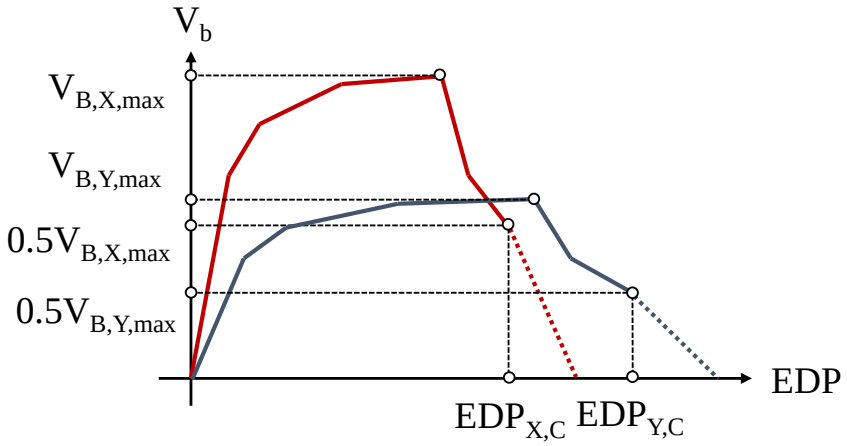

Figure III.22 Global collapse criteria RINTC-compliant.

The assessment of dynamic instability due to seismic actions on 3D numerical models has not been investigated in the technical literature so far. Interactions between the structural elements in the two main building directions could be foreseen to be one important issue to consider. Besides, additional modelling issues should be faced e.g., (i) the non-linear behavior of the secondary column elements and their column base connections; (ii) the possibility to develop stabilizing tensile forces in the longitudinal braces for large drifts in the transverse direction; (iii) a proper representation of the column base connection biaxial response, i.e. for bending moments acting both in the longitudinal and transverse planes; (iv) explicit modelling of the strength and stiffness degradation when anchor bolts in column base connections are subjected to a combination of axial and shear forces; (v) a proper representation of the maximum inelastic strain until the occurrence of fracture in anchors bolts subjected to a combination of axial and shear forces. For all these aspects, specific research studies should be addressed to improve the current knowledge and to extensively characterize appropriate modelling strategies to develop confidence in numerical results up to the dynamic

instability condition. Therefore, the choice of using the selected EDPs to assess the collapse limit state was considered a reasonable compromise between accuracy of the analysis and reliability of the available hysteresis models for members and connections.

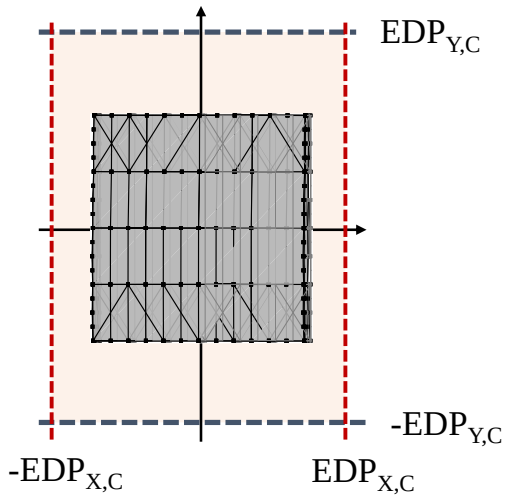

Figure III.23 Collapse domain considering the RINTC criteria.

The collapse criteria depicted in Figure III.22 implicitly assume that the force resistance would continue to reduce if the drift increases. However, there could be cases in which a gain in resistance is obtained following a strong degradation in strength. A practical example of this type of behavior is given by braced frames, where after brace or connection failure and consequent abrupt loss in the system strength, the frame still possesses some residual stiffness and resistance because of some moment-capacity at beam-column joints (Sizemore *et al.*, 2017, Hines *et al.*, 2009, Sen et al., 2019, Bèland *et al.*, 2020). In such cases, the analyst should identify the progressive sequence of damages leading to the abrupt loss of the building lateral resistance, keeping trace of the subsequent response by means of

a rigorous time-history response analysis. For the archetype single-story buildings considered in this study, this was an issue of limited importance, because of the small or very small force redistribution capacity.

However, one important issue to identify an EDP_C strictly following the RINTC criteria appears for the braced frame direction. In case of braces the available criteria to identify the triggering and propagation of brace fracture is dependent on the loading history. Therefore, the EDP_C value could change significantly from static to time history analysis. For the same reason, the limit does also depend on the ground motion considered. Similarly, the interaction of axial and shear forces acting on column base anchors leads to a path-dependent failure mode also for this component. Therefore, additional failure criteria were considered in addition to those set in Figure I.13. To take into account implications of brace fracture, the maximum strain range was considered according to the modelling criteria described in Section III.2.4. As described in the following Chapter V, the response history analysis for each ground motion considered a limit to the MSR parameter to trigger and propagate fracture through the brace (Hsiao *et al.*, 2013). However, to represent a possible range of values for the MSR_C parameter during the pushover analysis, two alternative limits were considered: (i) MSR_1 = half of the capacity according to Hsiao *et al.* (2013), to consider the case of an ideal symmetric dynamic response in terms of *MSR*; (ii) MSR_2 = the capacity according to Hsiao *et al.* (2013), to consider the case of a monotonic loading response up to brace fracture. In such a way, it was possible to identify with the pushover analysis the occurrence of a 50% loss in the base shear force resistance and the corresponding drift. This will allow to compare the *static* collapse criteria (i.e., obtained using the two MSR_C values previously discussed) within the actual "dynamic" identification of brace fracture. Similarly, to consider the possibility of triggering base anchor fracture due to axial and shear forces, the peak strain demand on the equivalent beam-column elements (described in Section III.2.5) was evaluated

and limited to the material deformation capacity evaluated according to Section III.2.2. Additionally, the maximum forces developed into the anchors were checked. Comparison was carried out with the anchor axial force resistance obtained developing the ultimate strength, f_u (Section III.2.2).

References

AISI. 2013. North American Standard for the Design of Profiled Steel Diaphragm Panels. *American Iron and Steel Institute, AISI S310-13*.

Araújo M., Castro J.M. 2016. A Critical Review of European and American Provisions for the Seismic Assessment of Existing Steel Moment-Resisting Frame Buildings. *Journal of Earthquake Engineering 22(8): 1336 – 1364*.

Badalassi, M., Braconi, A., Cajot, L.-G., Caprili S., et al. 2017. Influence of variability of material mechanical properties on seismic performance of steel and steel-concrete composite structures. *Bulletin of Earthquake Engineering 15: 1559-1607*.

Beland T., Tremblay R., Fahnestock L.A., Hines E.M. 2020. Contribution of the gravity beam-column connections to the seismic reserve capacity of steel buildings. *The 17th World Conference on Earthquake Engineering 17 WCEE.* Sendai, Japan, September 13th to 18th.

CEN. 2003. Eurocode 8: Design of structures for earthquake resistance – Part 1: General rules, seismic actions and rules for buildings. *European Committee for Standardization, Brussels, Belgium.*

CEN. 2005. EN 1993-1-1: Design of steel structure – part 1-1: General rules and rules for buildings. *European Committee for Standardization, Brussels, Belgium*.

CEN. 2009. Eurocode 3: Design of steel structures– Part 1-8: Design of joints. *European Committee for Standardization, Brussels, Belgium.*

CNR. 1988. Costruzioni di acciaio: Istruzioni per il calcolo, l'esecuzione, il collaudo e la manutenzione (1988). CNR-UNI 10011. *Rome, Italy: UNI - Ente Nazionale Italiano di Unificazione*.

CNR. 2009. Istruzioni per la valutazione delle azioni e degli effetti del vento sulle costruzioni (1988). CNR-DT 207/2008. *Rome, Italy: UNI - Ente Nazionale Italiano di Unificazione*.

CSI. 2011. SAP2000 Linear and Nonlinear Static and Dynamic Analysis and Design of Three-Dimensional Structures. *CSI Computer & Structures,* Berkeley, California.

CS.LL.PP. 2018. Aggiornamento delle norme tecniche per le costruzioni. *Rome, Italy: Gazzetta Ufficiale della Repubblica Italiana 42*.

Couchaux M., Martin P.O., Rodier A. 2017. Static and cyclic behaviour of bolted gusset plate connections: numerical and analytical modelling. *Proceedings of EUROSTEEL 2017, Copenhagen, Denmark*.

D'Aniello M., La Manna Ambrosino G., Portioli F., Landolfo R. 2013. Modelling aspects of the seismic response of steel concentric braced frames. *Steel and Composite Structures 15(5): 539 – 566.*

Davies J.M. 2006. Developments in stressed skin design. *Thin-Walled Structures 44: 1250 – 1260.*

De Matteis G., Landolfo R. 2000. Modelling of lightweight sandwich shear diaphragms for dynamic analyses. *Journal of Constructional Steel Research 53: 33 – 61.*

De Matteis G. 2005. Effect of lightweight cladding panels on the seismic performance of moment resisting steel frames. *Engineering Structures 27: 1662 – 1676.*

De Matteis G., Landolfo R. 1999. Structural behaviour of sandwich panel shear walls: An experimental analysis. *Material and Structures 32: 331-341.*

Della Corte G. 2001. Seismic Stability of Elasto-Plastic Frames. *Ph. D Thesis. University of Naples, Federico II.*

Della Corte G., Cantisani G., Landolfo R. 2017. Seismic response of built-up steel columns with semi-continuous base-plate connections. *Proceedings of EUROSTEEL 2017,* Copenhagen, Denmark.

Della Corte G., Cantisani G., Landolfo R. 2018. Battened Steel Columns with Semi-Continuous Base Plate Connections: Experimental Results vs. Theoretical Predictions. *Key Engineering Materials 763: 243 – 250.*

Della Corte G., De Matteis G., Landolfo R., Mazzolani F.M. 2002. Seismic analysis of MR steel frames based on refined hysteretic models of connections. *Journal of Constructional Steel Research 58: 1331 – 1345.*

Della Corte G., Landolfo R. 2017. Lateral loading tests of built-up battened columns with semi-continuous base-plate connections. *Journal of Constructional Steel Research 138*: *783-798.*

Dicleli M., Calik E. 2008. Physical Theory Hysteretic Model for Steel Braces. *Journal of Structural Engineering 134(7): 1215 – 1228.*

Eads L., Miranda E., Krawinkler H., Lignos D.G. 2013. An efficient method for estimating the collapse risk of structures in seismic regions. *Earthquake Engineering and Structural Dynamics 42(1): 25 – 41.*

ECCS. 1995. European recommendations for the application of metal sheeting acting as a diaphragm – Stressed skin design. *European Convention for Constructional Steelwork, PUB88*. https://store.steelconstruct.com/site.

Falborski T., Torres-Rodas P. Zareian F., Kanvinde A. 2020. Effect of Base-Connection Strength and Ductility on the Seismic Performance of Steel Moment-Resisting Frames. *Journal of Structural Engineering 146(5) 1 – 15.*

FEMA. 2000a. Recommended seismic design criteria for new steel moment-frame buildings. *Report No. FEMA A-350. SAC Joint Venture. Federal Emergency Management Agency, Washington DC.*

FEMA. 2000b. State of Art report on performance prediction and evaluation of steel moment-frame buildings. *Report No. FEMA 355F. Federal Emergency Management Agency, Washington DC.*

FEMA. 2000c. Prestandard and commentary for the seismic rehabilitation of buildings. *Report No. FEMA 356. Federal Emergency Management Agency, Washington DC.*

Finley A. 2008. Unintended Consequences of Modeling Damping in Structures. *Journal of Structural Engineering 134(4):581 – 592.*

Grauvilardell J.E., Lee D., Hajjar J.F., Dexter R.J. 2005. Synthesis of design, testing and analysis research on steel column base plate connections in high seismic zones. *Structural Engineering Report No. ST-04-02, Department of Civil Engineering, University of Minnesota*.

Gresnigt N., Romeijn A., Wald F., Steenhuis M. 2008. Column bases in shear and normal force. *Heron 53 (2/3):145–166*.

Gomez I., Kanvinde A., Deierlein G. 2010. Exposed column base connections subjected to axial compression and flexure. *Final Report Presented to the American Institute of Steel Construction (AISC).*

Hines E.M., Appel M.E., Cheever P.J. 2009. Collapse Performance of Low-Ductility Chevron Braced Steel Frames in Moderate Seismic Regions. *Engineering Journal 46(3): 149 – 180.*

Hall J.F. 2018. On the descending branch of the pushover curve for multistory buildings. *Earthquake Engineering and Structural Dynamics 47: 772 – 783.*

Haselton C.B., Deierlein G.G. 2006. Assessing seismic collapse safety of modern reinforced concrete moment frame buildings. *John A. Blume Earthquake Engineering Center Report No TR 156, Department of Civil Engineering, Stanford university.*

Henriques J., Jaspart J.P., Da Silva L.S. 2014. Ductility requirements for the design of bolted lap shear connections in bearing. *Advanced Steel Constructions* 10(1): *33-52*.

Hsiao P.C., Lehman D.E., Roeder C.W. 2012. Improved analytical model for special concentrically braced frames. *Journal of Constructional Steel Research 73: 80 – 94.*

Hsiao P.C., Lehman D.E., Roeder C.W. 2013. A model to simulate special concentrically braced frames beyond brace fracture. *Earthquake Engineering and Structural Dynamics 42: 183 – 200.*

Ibarra L., Medina R., Krawinkler H. 2005. Hysteretic models that incorporate strength and stiffness deterioration. *Earthquake Engineering and Structural Dynamics 34: 1489 - 1511.*

Ibarra L.F., Krawinkler H. 2005. Global collapse of frame structures under seismic excitations. *Report No. PEER 2005/06*, Pacific Earthquake Engineering Research Center, University of California at Berkley, Berkley, California.

Iervolino I., Spillatura A., Bazzurro P. 2018. Seismic Reliability of Code-Conforming Italian Buildings. *Journal of Earthquake Engineering 22:sup2 5 – 27.*

Kanvinde A.M. 2003. Methods to evaluate the dynamic stability of structures – Shake table tests and nonlinear dynamic analyses (EERI paper competition winner). *Proceedings of EERI meeting.* Portland, February.

Karamanci E., Lignos D.G. 2014. Computational Approach for Collapse Assessment of Concentrically Braced Frame. *Journal of Structural Engineering 140(8): 1 – 15.*

Krawinkler H., Zareian F. 2007. Prediction of collapse – How realistic and practical is it, and what can we learn from it? *Tall Building Journal 16(5): 633 – 653.*

Kumar P.C.A., Sahoo D.R. 2018. Fracture ductility of hollow circular and square steel braces under cyclic loading. *Thin-Walled Structures 130: 347 – 361.*

Lignos D.G. 2008. Sidesway collapse of deteriorating structural systems under seismic excitations. *PhD Dissertation*, Department of Civil and Environmental Engineering, Stanford University, California.

Lignos D.G., Karamanci E. 2013. Predictive Equations for Modelling Cyclic Buckling and Fracture of Steel Braces. *10th International Conference on Urban Earthquake Engineering*, Tokyo, Japan.

Lignos D.G., Hartloper A.R., Elkady A., Deirlein G.G., Hamburger R. 2019. Proposed Updates the the ASCE 41 Nonlinear Modeling Parameters for Wide-Flange Steel Columns in Support of Performance-Based Seismic Engineering. *Journal of Structural Engineering 145(9): 1 – 13.*

Martin P.O., Rodier A., Couchaux M., Kanyilmaz A., Degèe H. 2017. Assessment of the ductile behavior of CBF structures considering energy dissipation in bolted joints. *Proceedings of EUROSTEEL 2017, Copenhagen, Denmark.*

Mazzolani F.M., Landolfo R., De Matteis G. 1998. Analysis of the contributing effect of building panels on steel structure resistance to seismic and aeolian phenomena. *Technical final report, European Community Commission, Executive Committee F6 'Steel Structures', Agreement no. 7210-SA/421*. Brusselles.

McKenna, F., Scott, M. H., Fenves, G. L. 2010. Nonlinear Finite-Element Analysis Software Architecture Using Object Composition. *Journal of Computing in Civil Engineering 24(1), 95-107.*

Mehanny S.S., Deierlein G.G. 2000. Modeling of assessment of seismic performance of composite frames with reinforced concrete columns and steel beams. *Report No. 135, The John A. Blume Earthquake Engineering Center.* Department of Civil and Environmental Engineering, Stanford University.

Može P., Beg D. 2014. A complete study of bearing stress in single bolt connections. *Journal of Constructional Steel Research 95: 126 – 140.*

O'Brien, P., Eatherton M.R., Easterling W.S. 2017. Characterizing the load-deformation behavior of steel deck diaphragms using past test data. *Cold-Formed Steel Research Consortium Report Series, CFSRC R-2017-02*.

Palmer K.D., Roeder C.W., Lehman D.E., Okazaki T., Shield C.K. Powell J. 2012. Concentric X-Braced Frames with HSS Bracing. *International Journal of Steel Structures 12(3): 443 – 459.*

Pietrapertosa C., Piraprez E., Jaspart J.P. 2004. Ductility requirements in shear bolted connections. *Connection in Steel Structures V, Amsterdam, Belgium, June 3-4.*

Scozzese F., Terracciano G., Zona A., Della Corte G., Dall'Asta A., Landolfo R., 2018a. Modelling and seismic response analysis of Italian code-conforming single-storey steel buildings. *Journal of Earthquake Engineering 22(sup2): 2104 – 33.*

Scozzese F., Terracciano G., Zona A., Della Corte G., Dall'Asta A., Landolfo R., 2018b. Analysis of seismic non-structural damage in single-storey industrial steel buildings. *Soil Dynamics and Earthquake Engineering 114: 505 – 19.*

Shi G., Shi Y., Wang Y. 2007. Behaviour of end-plate moment connections under earthquake loading. *Engineering Structures 29: 703 – 716.*

Sizemore J.G., Fahnestock L.A., Hines E.M., Bradley C.R. 2017. Parametric Study of Low-Ductility Concentrically Braced Frames under Cyclic Static Loading. *Journal of Structural Engineering 143(6): 1 – 12.*

Sen A.D., Sloat D., Ballard R., Johnson M.M., Roeder C.W., Lehman D.E., Berman J.W. 2016. Experimental Evaluation of the Seismic Vulnerability of Braces and Connections in Older Concentrically Braced Frames. *Journal of Structural Engineering 142(9):1 – 15.*

Sen A.D., Swatosh M.A., Ballard R., Sloat D., Johnson M.M., Roeder C.W., Lehman D.E., Berman J.W. 2017. Development and Evaluation of Seismic Retrofit Alternatives of Older Concentrically Braced Frames. *Journal of Structural Engineering 143(5):1 – 17.*

Sen A.D., Roeder C.W., Lehman D.E., Berman J.W. 2019. Nonlinear modelling of concentrically braced frames. *Journal of Constructional Steel Research 157: 103 – 120.*

Shrestha K., Franquet J., Rogers C.A. 2009. OpenSees modeling of the inelastic response of steel roof deck diaphragms. *Behaviour of Steel Structures in Seismic Areas – STESSA 2009.*

Suzuki Y., Lignos D.G. 2021. Experimental Evaluation of Steel Columns under Seismic Hazard-Consistent Collapse Loading Protocols. *Journal of Structural Engineering 147(4): 1 – 18*

Takeuchi T., Matsui R. 2015. Cumulative Deformation Capacity of Steel Braces under Various Cyclic Loading Histories. *Journal of Structural Engineering 141(7): 1 – 11.*

Torres P.R., Zareian F., Kanvinde A. 2016. Hysteretic Model for Exposed Column-Base Connections. *Journal of Structural Engineering 142(12): 1 – 13.*

Tremblay R., Martin E., Yang W. 2004. Analysis, Testing and Design of Steel Roof Deck Diaphragms for Ductile Earthquake Resistance. *Journal of Earthquake Engineering 8(5): 775 – 816.*

Tremblay R. 2002. Inelastic seismic response of steel bracing members. *Journal of Constructional Steel Research 58: 665 – 701.*

Tsai K.C., Popov EP. 1990. Cyclic behavior of end-plate moment connections. *Journal of Structural Engineering 116(11):2917 – 2930.*

Uriz P., Filippou F.C., Mahin S.A. 2008. Model for Cyclic Inelastic Buckling of Steel Braces. *Journal of Structural Engineering 134(4): 619 – 628.*

Vamvatsikos D., Cornell C.A. 2002. Incremental Dynamic Analysis. *Earthquake Engineering and Structural Dynamics 31, 491 – 514.*

Vian D. and Bruneau M. 2001. Experimental investigation of P-Delta effects to collapse during earthquakes. *Technical report MCEER-01-0001*, University at Buffalo - Department of Civil, Structural and Environmental Engineering.

Vian D. Bruneau M. 2003. Tests to structural collapse of single degree of freedom frames subjected to earthquake excitations. *Journal of Structural Engineeering 129(12): 1676 – 1685.*

Villaverde R. 2007. Methods to Assess Seismic Collapse Capacity of Building Structures: State of the Art. *Journal of Structural Engineering 133(1): 57 – 66.*

Wu T.Y., El-Tawil S., McCormick J. 2018. Seismic Collapse Response of Steel Moment Frames with Deep Columns. *Journal of Structural Engineering 144(9): 1 – 12.*

Yam M.C.H., Cheng J.J.R. 2002. Behavior and design of gusset plate connections in compression. *Journal of Constructional Steel Research 58: 1143 – 1159.*

Zareian F. 2006. Simplified performance-based earthquake engineering. *Ph.D Dissertation*. Department of Civil and Environmental Engineering, Stanford University, Stanford California.

Zareian F., Krawinkler H. 2007. Assessment of probability of collapse and design for collapse safety. *Earthquake Engineering and Structural Dynamics 36(13): 1901 – 1914.*

Zareian F., Krawinkler H., Ibarra L., Lignos D. 2010. Basic Concepts and Performance Measures in Prediction of Collapse of Buildings under Earthquake Ground Motions. *The Structural design of Tall and Special Buildings 19: 167 – 181.*

Chapter IV

NON-LINEAR STATIC ANALYSIS

IV.1 Introduction

Seismic analysis of both new and existing buildings requires analysis methods adequately accounting for all sources of non-linearity as a function of the structural characteristics and/or the input actions (i.e., ground motions). The analysis should be able to identify all potential damages to both structural and non-structural elements. The assessment is generally carried out simplifying the process with the introduction of discrete limit states (e.g., collapse). Two main analysis methods are currently used: (i) non-linear static analysis and (ii) non-linear time history analysis. The choice between the two procedures strictly depends on the objectives of the study. In the non-linear static analysis procedure, usually known as pushover analysis, the most typical implementation assumes that the deformed shape of the structural system remains constant during the time history, regardless of the level of deformation demand. The deformed shape is obviously the first mode of vibration and equivalent seismic forces are calculated according to well-established principles of structural dynamics (Chopra, 2007). The assumption works well when higher mode effects can be neglected, both in the elastic and inelastic deformation ranges. Such static method of analysis is usually adopted when assessing the structural response of regular buildings.

Nevertheless, some extensions have been proposed for structures with irregular behavior (Peres *et al.*, 2018). If the underlying assumptions are valid, then the static analysis is easier to carry out and allows to identify the main potential weaknesses and collapse mechanisms. For instance, Hall (2018) stated that calculating a pushover curve is an essential step in design or assessment of a major structure. However, limitations of the static analysis should be always considered. Several criticisms were highlighted, for example, in the work by Krawinkler and Seneviratna (1998). Time history analysis is the reference method to consider for seismic response assessment in the context of performance-based earthquake engineering, i.e. to obtain a probabilistic description of the seismic performance. For that scope, a sufficiently large number of realistic ground-motions should be used (Baltzopoulos *et al.*, 2018, Giannopoulos and Vamvatsikos, 2018). Besides, time-history analysis requires the representation of the hysteresis response of the structure components, including the potentially important effects of strength and stiffness deteriorations (Della Corte *et al.*, 2002, Ibarra *et al.* 2005). Unfortunately, such hysteresis models are not always available, and the models often require significant judgement for their applications. Therefore, both the larger analysis difficulties and more expensive post-processing of the numerical results make the method more complex and time consuming. Usually, a limit value of an engineering demand parameter (EDP) is used as the capacity for a selected performance limit state. The EDP should adequately represent the response of the structure at the global level. Evaluation of the capacity in terms of the global EDP can be carried out by using, for example, a pushover analysis. Therefore, a combination of the two methods of analysis, static and dynamic, could be considered. Indeed, in complex non-linear numerical models, a preliminary pushover assessment can help structural engineers in understanding complex structural behavior, as well as in giving quantification in terms of both global and local engineering demand parameters. The study presented in this dissertation

adopted such a combined approach, with the static analysis performed first and the time-history response analysis second. The first main objective of the static analysis was to identify the main damageable components requiring non-linear modelling for the subsequent time-history analysis. This chapter is addressed to describe the results from the static non-linear analysis of the archetype buildings presented in Chapter II. Special attention was given to identify the failure modes and the global displacement capacity for the subsequent assessment of the collapse risk by means of the time-history analyses. The chapter also compares the response observed for the various building archetype emphasizing the effects of the relevant design assumptions and the role of the building envelope.

IV.2 Preliminary modal analysis

Evaluation of the vibration modes of a structural model is the first step to be carried out even if a static analysis method is chosen. In fact, the modes of vibration are needed to evaluate the patterns of the statically "equivalent" seismic loads. Additionally, values of the dominant structural vibration periods will be subsequently used for choosing an appropriate set of ground motions to consider the record-to-record variability in structural response (Chapter V). This section summarizes results of modal analysis carried out on the numerical models described in Chapter III. Because of the large number of degrees of freedom, each model is characterized by several vibration modes. However, this section describes only the modes that were important to represent the "global" response. Many local modes which have effects on the details of the local force and deformation demand but do not change the overall system response are not described here.

IV.2.1 Translational modes of vibration in the transverse direction

Figure IV.1 summarizes the modal analysis results for the bare frame model with pinned column base connections in the transverse direction and vertical SHS braces in the longitudinal direction (PCB-SHS-BF). Results are shown in terms of displacement shape in 3D, plan and transverse views. A mainly translational vibration mode in the transverse direction was predicted by the analysis to be the first vibration mode, with a vibration period equal to 1.03 *s*. The plan view shows a non-uniform distribution of displacements among the five portal frames. Indeed, this was a consequence of the asymmetric behavior generated by the overhead crane masses, which were modelled by applying them at the second portal frame (starting from the bottom in the figure) (Chapter III).

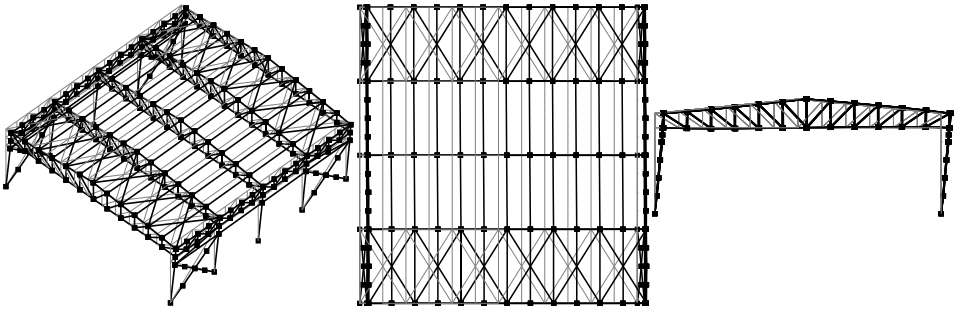

Figure IV.1 Transverse vibration mode in 3D, plan and transverse views for the PCB-SHS-BF case.

Similarly, Figure IV.2 shows the transverse vibration mode for the bare frame model with semi-continuous column base connections in the transverse direction and vertical SHS braces in the longitudinal direction (SCB-SHS-BF). Also in this case the selected vibration mode was the first one, with a vibration period of 0.78 *s*. The plan view shows a rather uniform transverse displacement shape, with a maximum value in the second portal frame. This result is in line with the previous

case. Differences between the two transverse periods of vibration, respectively for the PCB and the SCB case, are a consequence of the effect of the main truss axial stiffness and the rotational stiffness of the column base connections to the portal frame lateral stiffness. In the PCB case, the main truss axial stiffness significantly contributed to defining the boundary conditions at the top of the column. On the contrary, in the SCB case, the portal frame lateral stiffness was dominated by the rotational stiffness of the column base connections. Implications of the design assumptions yield to PCB cases more flexible than the SCB cases.

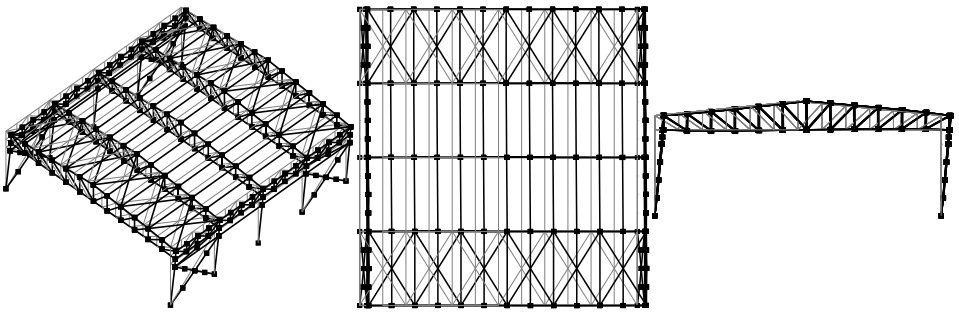

Figure IV.2 Transverse vibration mode in 3D, plan and transverse views for the SCB-SHS-BF case.

Numerical models including the building envelope panels were built starting from the structural response of both sandwich panels with bolted connections (SPs) and trapezoidal sheeting with screw connections (TSs), as extensively discussed in the previous chapter. However, modal results obtained by varying the envelope panel type were predicted to be practically coincident, with minor differences in vibration periods due to minor differences in the panel (in-plane) stiffness. For this reason, in this section both the model with SPs and TSs will be considered (both labelled as *ENV* models). The modal response of the PCB-SHS-ENV model shows the transverse main vibration mode highlighted in Figure IV.3, with 3D, plan and transverse views. Also in this case, the vibration mode for the transverse

direction was found to be the first one, with a vibration period approximately equal to 0.55 *s* in both cases. Furthermore, the vibration mode obtained by explicitly modelling the envelope panel response shows practically the same roof displacement distribution as obtained within the BF model. However, benefits on the increase of the building lateral stiffness provided by the presence of the envelope become apparent comparing values of the vibration periods, which are approximately halved passing from the bare frame model to the *ENV* models.

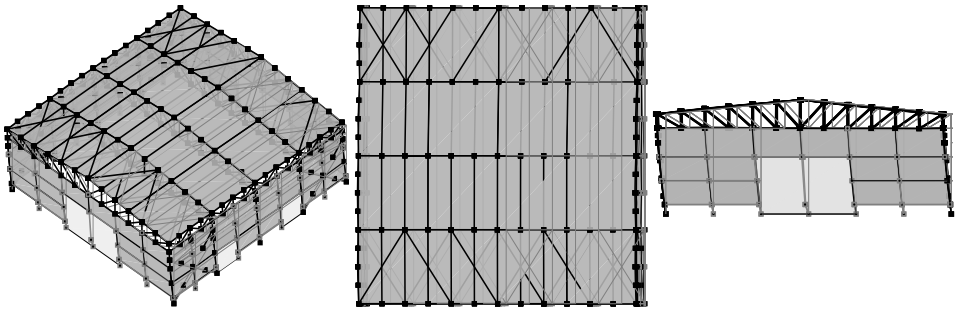

Figure IV.3 Transverse vibration mode in 3D, plan and transverse views for the PCB-SHS-ENV case.

The same consideration can be made looking at the results of the SCB-SHS-ENV models, in which the first vibration mode was found to be the translational one with a vibration period equal to 0.45 *s* (both for the SPs and for the TSs envelope types). Results are summarized in Figure IV.4. The distribution of modal displacements is approximately uniform also in this case, with slightly larger values obtained at the second portal frame because of the additional overhead crane masses. The same structural models were also analyzed by changing cross section and connection details of the longitudinal braces. However, modal results did not show any significant variation when the transverse direction was analyzed. Numerical differences in values of the vibration periods were found and are summarized in Table IV-1 for completeness. Such small variation in the values

were related only to variations in the structural masses due to changes in the longitudinal brace cross sections. More precisely, the 2L braces had a larger cross section than the SHS braces, thus generating a slight increase of the vibration periods.

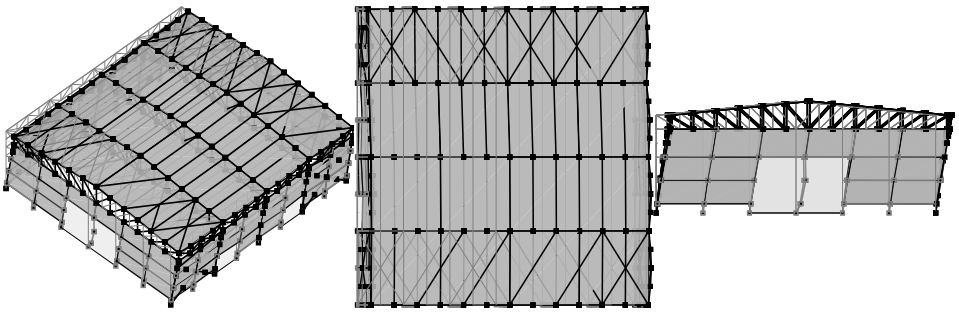

Figure IV.4 Transverse vibration mode in 3D, plan and transverse views for the SCB-SHS-ENV.

Table IV-1 Transverse vibration mode characteristics.

MODEL [-]	ENV TYPE [-]	M [t]	M_X* [% M]	T_X [s]
PCB-SHS	BF	140.57	99.07 %	1.03
	SP	166.03	91.23 %	0.55
	TS	166.03	91.15 %	0.56
SCB-SHS	BF	136.58	98.49 %	0.78
	SP	160.78	89.47 %	0.45
	TS	160.78	89.35 %	0.45
PCB-2L	BF	142.14	99.07 %	1.03
	SP	168.16	91.00 %	0.55
	TS	168.16	90.92 %	0.56
SCB-2L	BF	138.15	98.48 %	0.79
	SP	162.35	89.57 %	0.45
	TS	162.35	89.44 %	0.46

In the table, information concerning the modal participating masses in the transverse direction (M_X^*) as a percentage of the total building masses are reported. Values are always larger (or slightly smaller) than 90%, thus identifying practically the predominance of the translational vibration mode in the dynamic response of the building.

IV.2.2 Longitudinal translational modes of vibration

Figure IV.5 shows the main longitudinal vibration mode, with 3D, plan and longitudinal elevation views. Such mode of vibration was found to be the fifth in the modal analysis results, with a vibration period equal to 0.26 *s*. Large differences in periods of vibration were observed with respect to the transverse direction. Obviously, such differences were a direct consequence of the presence of the vertical braces leading to much stiffer response. Asymmetry of masses did not generate any appreciable asymmetric response in terms of displacements.

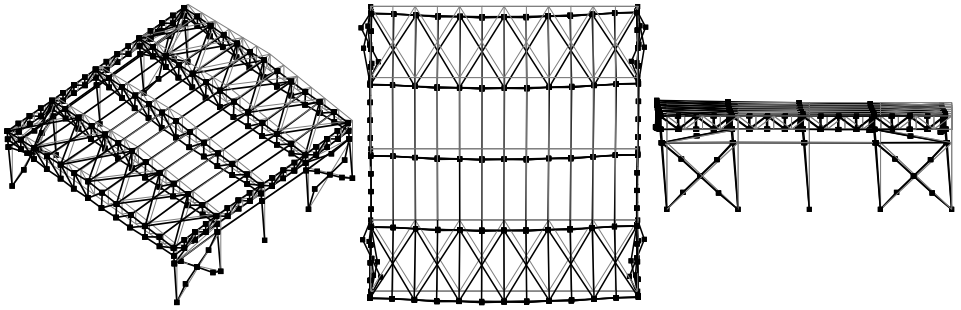

Figure IV.5 Longitudinal vibration mode in 3D, plan and transverse views for the PCB-SHS-BF case.

Figure IV.6 shows the longitudinal vibration mode in the case of SCB-SHS-BF model. In this case, such vibration mode was found to be the third one, with a vibration period equal to 0.25 *s*, practically equal to the longitudinal vibration

mode of the PCB-SHS-BF model. Differences are related to variations of column cross sections (from HE 500 M to HE 450 M).

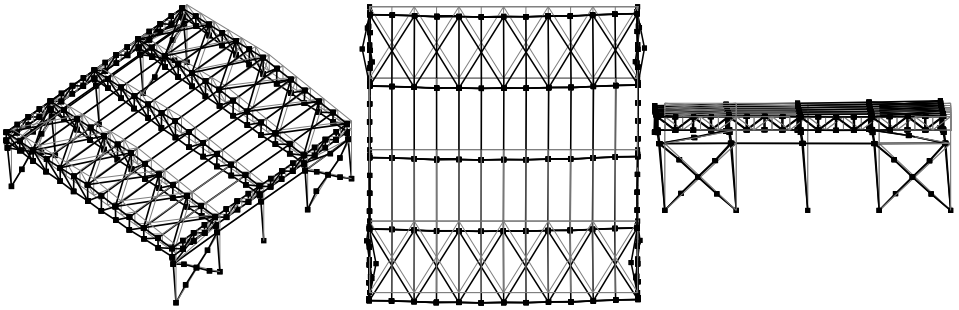

Figure IV.6 Longitudinal vibration mode in 3D, plan and transverse views for the SCB-SHS-BF case.

Figure IV.7 shows the same longitudinal vibration mode from the PCB-SHS-ENV model, which was found to be the fourth mode provided by the analysis. The structural behavior did not change compared with the bare frame model, thus showing a clear translational mode of vibration.

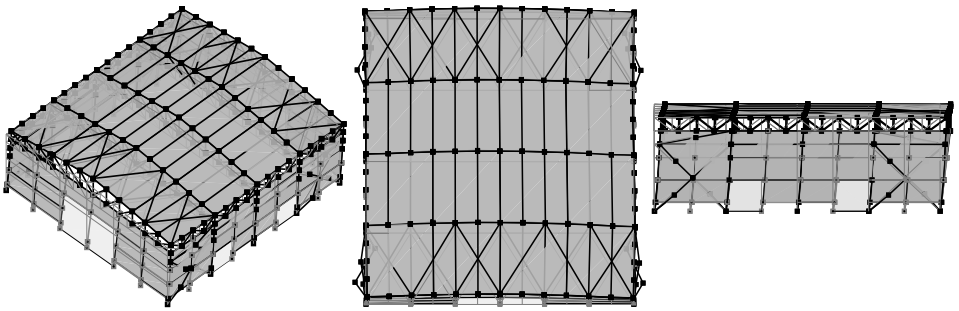

Figure IV.7 Longitudinal vibration mode in 3D, plan and longitudinal views for the PCB-SHS-ENV case.

The corresponding vibration period slightly reduced from 0.26 *s* to 0.23 *s*. This result clearly confirms that the effect of the building envelope in the braced frame

direction is almost negligible in terms of the initial lateral stiffness, because of the already large lateral stiffness provided by the bracing system. Eventually, the modal analysis did not suggest significant asymmetric response also in this case.

The same comments can be done looking at the SCB-SHS-ENV model, which is depicted in Figure IV.8. In this case, the main translational vibration mode in the longitudinal direction was found to be the third mode, with a vibration period of 0.22 *s*. Again, the small decrease of the vibration period with the respect to the bare frame model confirms the negligible role of the building envelope for the longitudinal direction response.

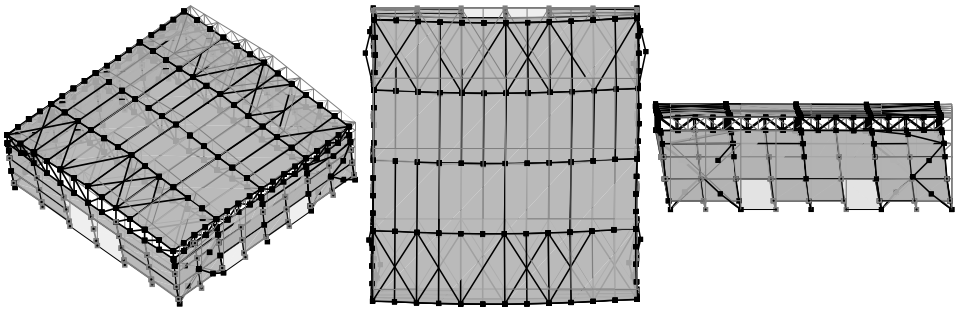

Figure IV.8 Longitudinal vibration mode in 3D, plan and longitudinal views for the SCB-SHS-ENV case.

Changing the vertical brace cross sections did not change the longitudinal modal response. Figure IV.9 shows the vibration modes in a 3D view, both for the BF and the ENV models. Vibration periods were equal to 0.26 *s* and 0.23 *s*, for the PCB-BF and PCB-ENV models, respectively. Similarly, the vibration periods were equal to 0.25 *s* to 0.22 *s*, for the SCB-BF and SCB-ENV models, respectively.

Table IV-2 summarizes results for the longitudinal direction in terms of vibration periods and modal participant masses for the longitudinal building direction

(M_Y^*). As one can see, differences obtained by varying the structural layouts and brace cross sections were small, thus indicating negligible effects of the structural scheme for the transverse direction and the vertical brace cross sections for the longitudinal direction. For all the models, the selected vibration mode excited more than the 85% of the total building mass in the longitudinal direction.

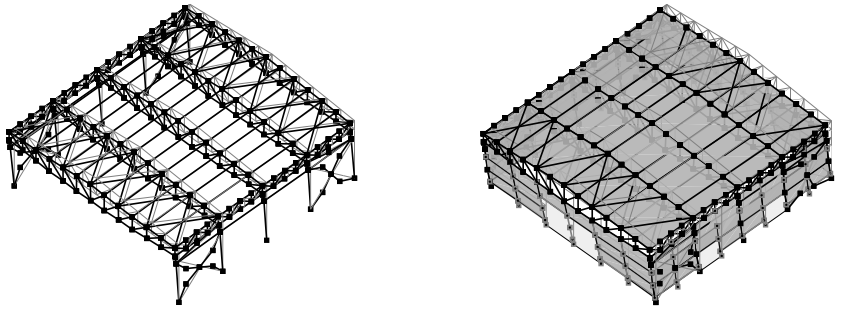

Figure IV.9 Longitudinal vibration modes in 3D view for the SCB-2L without and with envelope.

Table IV-2 Longitudinal vibration mode characteristics.

MODEL [-]	ENV TYPE [-]	M [t]	M_Y^* [% M]	T_Y [s]
PCB-SHS	BF	140.57	92.40 %	0.26
	SP	166.03	87.59 %	0.23
	TS	166.03	87.35 %	0.23
SCB-SHS	BF	136.58	92.99 %	0.25
	SP	160.78	89.23 %	0.22
	TS	160.78	88.82 %	0.22
PCB-2L	BF	142.14	92.00 %	0.26
	SP	168.16	87.38 %	0.23
	TS	168.16	87.14 %	0.23
SCB-2L	BF	138.15	92.65 %	0.25
	SP	162.35	89.12 %	0.22
	TS	162.35	88.72 %	0.22

IV.2.3 Torsional vibration modes

Torsional modes were also predicted by the modal analysis in all the examined cases. Such modes were always characterized by corresponding periods of vibration intermediate between the two translational modes in the longitudinal and transverse directions. Such irregularity in the building modal response is a consequence of the absence of a rigid diaphragm at the roof level coupled with the effect of the eccentricity of masses. Particularly, eccentric masses (i.e., masses of the overhead crane and the crane working load) were a significant fraction of the total building mass. Therefore, they significantly influenced torsional behavior of the building.

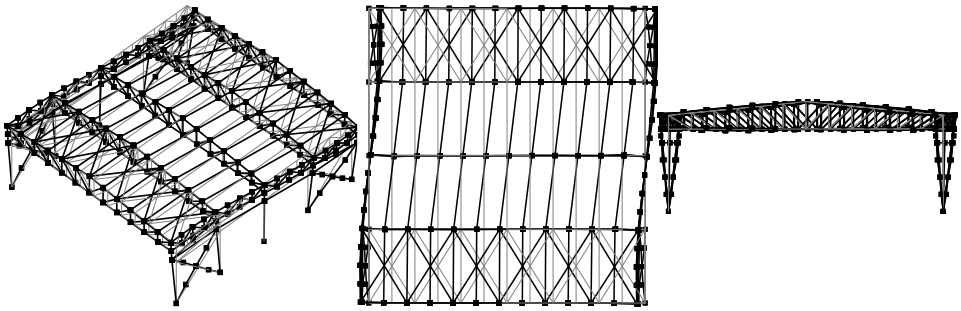

Figure IV.10 Example of torsional modes of vibration in the PCB-SHS-BF case.

Example of the torsional vibration modes are highlighted by Figure IV.10 and Figure IV.11, which show torsional vibration modes with both 3D, plan and transverse views in the case of numerical models without and with the envelope panels included. A quantification of the relative importance of such phenomenon during the dynamic response will be carried out in the relevant chapter of this dissertation.

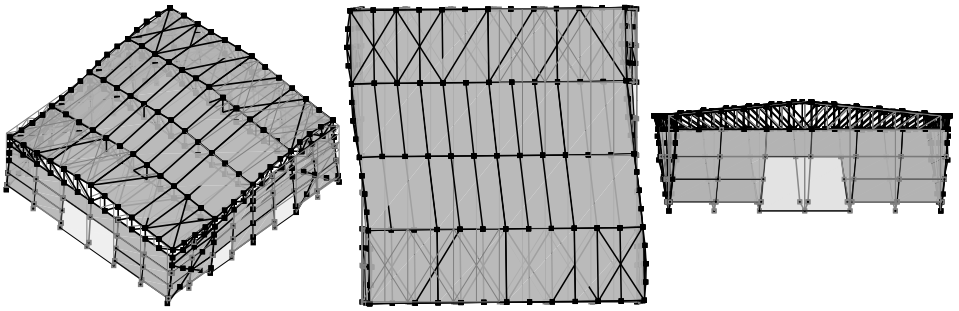

Figure IV.11 Example of torsional modes of vibration in the PCB-SHS-ENV case.

IV.2.4 Vibration modes involving mainly vertical displacements

Vertical vibration modes are obviously expected in structural models which includes masses with vertical degrees of freedom. The importance of such vibration modes in the structural response needed to be quantified. Also, the possibility to have coupling of both horizontal and vertical vibration modes should be checked looking at the modal analysis results. In the examined cases, because of the span length (30 *m*), modes concerning vertical vibrations of the building trusses were found to have vibration periods in between those corresponding to the main translational modes. However, differences in the structural schemes led to differences in the "vertical" mode vibration periods. Particularly, the PCB models show several vertical vibration modes (for both the BF and ENV models) with vibration periods in between those of the transverse and longitudinal translational modes. Examples are summarized in Figure IV.12 for the PCB case, with and without the building envelope. The plotted vibration modes refer to a vibration period of 0.31 *s* and 0.24 *s*, for the BF and ENV models, respectively.

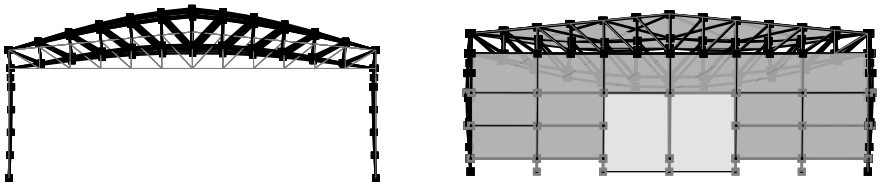

Figure IV.12 Example of vertical vibration modes in the PCB cases.

For the SCB cases the "vertical" modes of vibration were characterized by smaller vibration periods compared with the longitudinal translational modes (i.e., vibration periods smaller than 0.22 *s*). The increase in the "vertical" vibration period for the PCB cases was a consequence of the different modelling approaches developed for the main truss axial stiffness. Indeed, effect of connection axial stiffness was directly considered in the PCB cases, whilst it was neglected in the SCB cases, since the truss axial stiffness did not play any important role in terms of the main translational modes.

The role of the vertical ground motion components in assessing the overall structural response of such buildings was out of the scope of this study. This is an aspect deserving investigation in future research studies.

IV.3 Pushover analysis results

In this section, results obtained by the non-linear static analysis are described and discussed. The section is subdivided into two sub-sections, each one describing the response in one of the two main building directions. In every case, modal pushover analysis was preliminarily carried out, to obtain a force pattern proportional to the relevant translational mode shape.

IV.3.1 Transverse direction

Figure IV.13 summarizes results of non-linear static analyses in the transverse (i.e., X-) direction, plotting the relationship between the base shear force in the transverse direction ($V_{b,X}$) and the displacement of the top column in the same direction (d_X/H, H = 10.50 *m*). For the sake of simplicity, only the PCB-SHS and SCB-SHS pushover curves were plotted since no variation in the transverse direction response was observed when the 2L brace configuration was used as vertical bracing elements and connections. A rather different structural response was observed comparing the PCB to SCB case studies, independent of the envelope type. A detailed description of the evolution of the non-linear response is described subsequently, respectively considering the PCB and the SCB case studies.

IV.3.1.1 PCB case study

Figure IV.13(a) shows results for the PCB case by varying the envelope model (in the plots, the acronym BF stands for bare frame). Also, the discussed (RINTC-compliant) collapse condition is highlighted with an empty circle. Consequently, the last part of the pushover curve was represented by a dashed line. In fact, the structural response beyond the considered collapse threshold was not of interest for the purposes of the subsequent non-linear dynamic analyses. Focusing on the BF curve, one can observe an example of elastic-brittle structural response. All the drops in lateral strength were a consequence of a main truss-to-column connection failure due to shear bolt failure. Indeed, low ductility of the bolts in shear led to an abrupt loss of the building lateral strength. However, the structural response following the 50% loss of base shear force resistance was found to be stable (i.e., an increase in displacement provided an increase in lateral strength). The drift capacity was estimated to be 2% of the building height (H = 10.50 *m*).

Nevertheless, a zero value of the base shear force resistance was reached at approximately 3% of lateral drift, because of redistribution of axial forces among the portal frames. After reaching such drift, every portal frame formed a mechanism with zero lateral resistance.

The building envelope significantly increased both the lateral stiffness and resistance. The ratio between the maximum base shear force resistance for the SP model and the BF model was equal to 1.86, while it was equal to 1.21 when the TS model was considered with respect to the BF model. A relatively small increase of the collapse drifts was also obtained with a value of 2% for the BF model becoming 2.51% for the SP model and 2.2% for the TS model. The observed response was largely a consequence of the non-conforming connection local response. Looking at the details in the evolution of the SP model response, one can identify the first non-linear event as yielding of the cladding-to-frame connections, which corresponded to bearing of the bolted connections described in Chapter III. Then, local siderail-to-column connection failures occurred prior to reaching the maximum base shear force (very small drops in the pushover curve prior to reaching the maximum lateral resistance identify such failures). The descending branch of the curve was triggered due to truss-to-column connection failure, as obtained for the BF model. Then, both truss-to-column and siderail-to-column connection failures occurred, thus leading to subsequent vertical drops in the pushover curve while reaching a very small base shear force resistance. However, the resistance tended to increase after such failures and up to a lateral drift equal to 3%. This was due to residual shear forces in secondary column elements which were modelled as elastic elements. Inelasticity of such elements needed to be explicitly considered to identify the condition of zero lateral shear force resistance. Similarly, for the TS model the envelope structural response totally developed prior to reaching a lateral drift equal to 1%. This was due to the poorer structural behavior of the screws when compared to the bolted connections

used for the SPs. Indeed, in the TS case, a bearing-tilting mechanism with small ductility characterized the screw connection response. After losing the envelope resistance contribution, the structural displacements increased linearly with a reduced stiffness until the truss-to-column connection resistance was also reached. However, the lateral stiffness of the TS model in the phase where the contribution of the TS is lost does not coincide with the lateral stiffness of the BF model, because of the presence of both the roofing panels and the secondary columns increasing the stiffness. Like the SP case, in the TS case the loss in resistance following the peak value was due to truss-to-column connection failures.

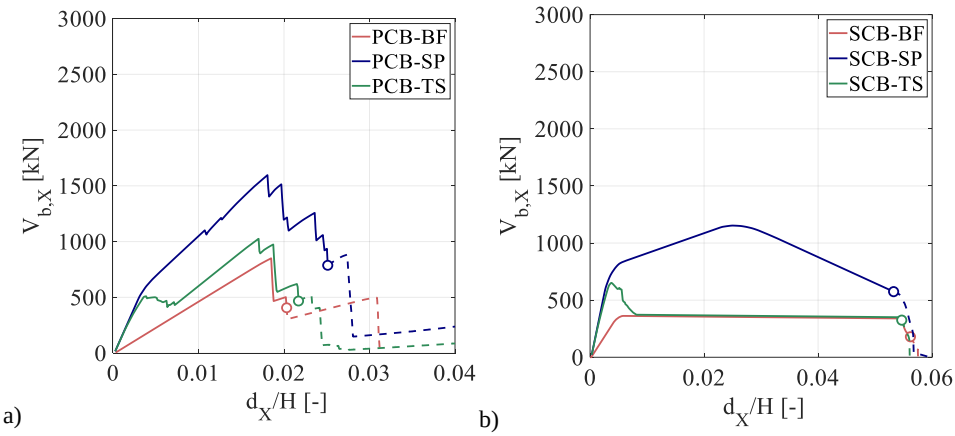

Figure IV.13 Pushover curves in the transverse direction: (a) PCB cases; (b) SCB cases.

IV.3.1.2 SCB case studies

Figure IV.13(b) shows results concerning the SCB case studies. Also, the (RINTC-compliant) collapse condition is highlighted with an empty circle. Consequently, the last part of the pushover curve was represented by a dashed line since it was not considered during the assessment by means of non-linear dynamic

analyses. The structural response of the BF model was dominated by the column base connection yielding, due to combined axial forces and bending moments. Because of the ductile yielding of anchors, a 50% drop in lateral shear force resistance was reached for a lateral drift equal to 5.6%. All the plastic branch of the pushover was due to column base connection yielding and strain-hardening. However, strain-hardening was partially overwhelmed by the global P-Delta effect. The same collapse mechanism was observed looking at the SP and TS models. Differences can be noted when comparing the elastic branch of the pushover curves and the post peak behaviours. The increase of the lateral stiffness, already noticed and described with the modal analysis, was confirmed by the pushover analysis. The ratio between the maximum lateral base shear force resistance of the BF and SP models resulted equal to 3.20, while it is equal to 1.80 when the TS model is considered. Collapse lateral drifts did not change significantly, since the collapse mechanism did not change (i.e., no siderail-to-column connection failures were involved approaching the descending branch of the pushover). Starting from a drift of 5.6% for the BF case study, values were obtained equal to 5.3% for the SP model and 5.5% for the TS model), due to changes in the maximum base shear force resistance. Both the SP and TS pushover curves clearly showed the development of damage in cladding elements, as described starting from the single panel structural component (See Chapter III for further details). In these cases, no failures in the siderail-to-column connections were observed.

IV.3.1.3 Pushover deformed shapes

To better highlight the described structural response, Figure IV.14 shows the building deformed shape for the PCB-SHS-SP model, with transverse elevation and plan views. Similar deformed shapes were obtained for the TS model. From the left to the right, the figure shows: (i) a deformed shape considering a drift

corresponding to the maximum base shear force resistance in the transverse direction, (ii) a drift which identified the structural response beyond the first truss-to-column connection (TCC) and siderail-to-column connection failures and (iii) a drift for which the lowest value of the base shear force resistance was observed. Drift values are indicated in the figure. The plot shows the progressive cladding detachment, as well as the change of the column deformed shape following the relevant TCCs failures. Additionally, relative lateral drifts between adjacent portal frames are shown in the figure, thus highlighting the slightly asymmetric behavior produced by the overhead crane and crane loads.

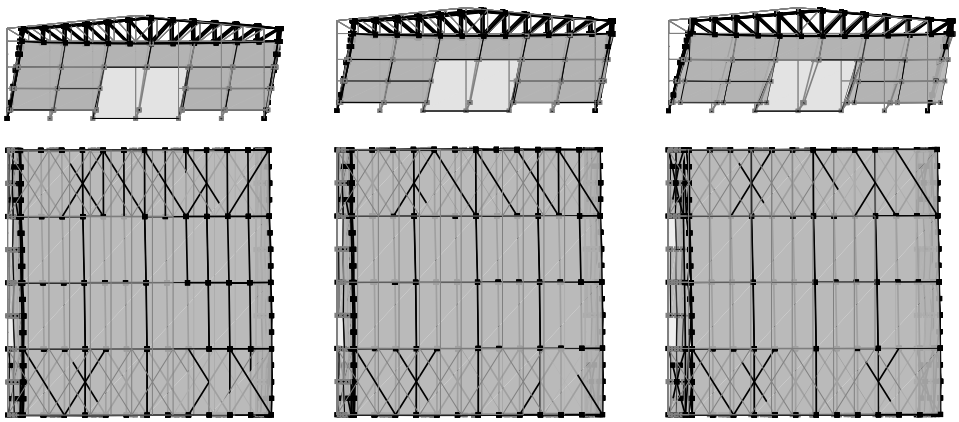

Figure IV.14 Deformed shapes of the PCB-SHS-SP structure at selected steps of the pushover analysis.

In the same way, Figure IV.15 shows a plot of the 3D deformed shape for the SCB-SHS-SP case study. From the left to the right, the figure shows: (i) a deformed shape considering a drift corresponding to yielding of the bolted cladding-to-frame connections, (ii) a drift corresponding to the maximum base shear force resistance in the transverse direction, (ii) the drift corresponding to the considered collapse limit state of the whole building.

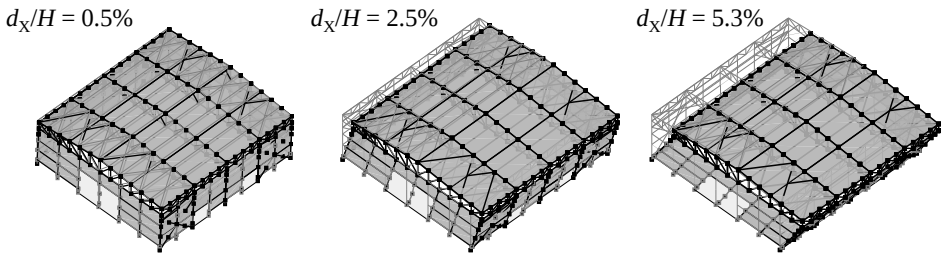

Figure IV.15 Deformed shapes of the SCB-SHS-SP structure at selected steps of the pushover analysis.

Roof drifts were more similar among the five portal frames in this case compared with the PCB model. As previously discussed, no failure of siderail-to-column connections were observed.

IV.3.1.4 Component response

Figure IV.16(a) illustrates the relationship between the forces in the top chord truss-to-column connections (F_{TCC}) and the drift used to build the pushover curve for the PCB case (d_X/H). Both the left (continuous lines) and the right (dashed lines) connection forces are shown for the five portal frames. As one can see, all the TCCs reached their plastic resistance and eventually the ultimate displacement capacity, thus reaching a zero value of the connection force in the plot. This observation holds true for all the numerical models (i.e., varying the cladding type). However, slightly differences in drift values triggering the connections failure were observed passing from the BF model to both the SP and TS models. Particularly, lateral drifts triggering connections failure reduced with the presence of the cladding panels. Connection failures started from the right side and, almost simultaneously, propagated to the left side.

Figure IV.16(b) shows the relationships between the in-plane bending moments in the column base connections (M_{CBC}) and the drifts used to build the pushover

curve for the SCB case (d_X/H). Both the left (continuous lines) and the right (dashed lines) connections are shown for the five portal frames. Differences in connection resistances were related to the value of the axial forces acting at the column base connection due to gravity loads. Every column base connection yielded for lateral drift value approximatively equal to 0.5%. Eventually, they reached the rotation capacity, thus generating a drop up to zero resistance. The rotation capacity was reached almost simultaneously in every portal frame. Also, the plot shows practically the same moment-drift response by varying the considered numerical model (i.e., by varying the cladding panel).

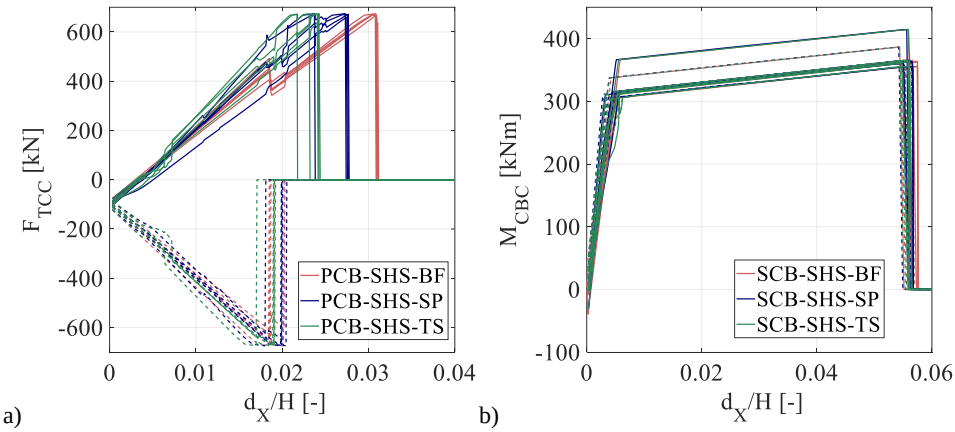

Figure IV.16 (a) PCB truss-to-column connection response; (b) SCB column-base connection response.

IV.3.1.5 Summary of the results

The study of the response in the transverse direction allows to make some comments about the performance of portal frames designed according to different structural schemes. The PCB model appears to have larger base shear force resistance due to gravity load design implications. On the contrary, the SCB case appears to have very relatively smaller resistance, because the design of the

columns was governed by lateral loads. However, the ductility of the SCB cases was approximately twice that of the PCB cases. The effects of the envelope panels were significant in every case, in terms of both lateral stiffness and resistance. Failures of siderail-to-column connections were observed in the PCB case and they highly affected the global collapse of the building. However, minor differences were observed in the value of the displacement capacity, which is therefore dominated by the main structure response characteristics.

IV.3.2 Longitudinal direction: SHS braces

This section summarizes results of longitudinal pushover analysis for the SHS brace configuration (i.e., braces made by using square hollow sections and welded connections between the gusset plate and the brace). The analysis results are summarized in the form of a relationship between the base shear force resistance in the longitudinal direction ($V_{b,Y}$) and the displacement of the column tip in the same direction (d_Y/H, H = 10.50 m). In the case of SHS, two pushover curves are considered, differing for the adopted limit to the maximum strain range triggering fracture of braces. The two limits will be labelled as MSR_1 and MSR_2 according to the discussion presented in Chapter III, Section III.3. Results are separately described for the PCB and the SCB case studies, respectively.

IV.3.2.1 PCB case studies

Figure IV.17(a) shows the structural response for the PCB-SHS case. The BF model showed non-linear response starting from very small values of the building lateral drifts. This early nonlinearity is due to two main structural components: (i) vertical braces, which buckle for a lateral drift approximately equal to 0.1%; (ii) column base connections, which yield due to the combined vertical and horizontal forces transmitted by the corresponding braces in tension. The braces yield in tension at a much larger drift (approximately equal to 1%) as a consequence of

the additional system deformability due to this early anchor yielding. Following the brace yielding in tension, strain hardening could develop up to brace fracture. It is worth noting that slope of the pushover curve in this phase of yielded and strain-hardened braces was also due to a moment-frame action produced by the columns and the longitudinal truss system globally acting as a beam. The pushover response curve shows that the limit value of the parameter *MSR* plays a very important role: (i) using the MSR_1 limit, the braces started to fracture for a drift equal to 1.8% (the first brace to fracture was one of the compressed braces, because of the concomitant bending moment at the middle of the brace). Subsequently, brace fracture was triggered in the tension braces, leading to an almost instantaneous propagation of fracture through the cross sections and consequent separation of the fractured brace into two separate parts. The 50% loss of the base shear force resistance occurred at a drift equal to 2.7%. Following that event, the pushover curve tended to increase with the lateral drift, exhibiting a lateral stiffness due to the secondary moment frame action previously mentioned. Since the time-history response analysis described in the following Chapter V did not show longitudinal drift demands larger than those investigated with the pushover analysis up to brace fracture, the post-fracture response was not modelled with a detailed representation of subsequent potential failures of the columns and longitudinal trusses. With the MSR_2 capacity value, brace fracture occurred at a drift equal to 3.7%, while the 50% loss of base shear force resistance was reached for a lateral drift equal to 4.7%. Delay in brace fracture led to increase of strain demand in anchors. In fact, the model predicted triggering of anchors fracture prior to brace fracture (3.2%). As previously mentioned, such failure mode was not explicitly modelled. Therefore, the pushover curve did not show any drop in lateral resistance due to this non-linear event.

The SP model showed a negligible increase in the building elastic lateral stiffness in comparison with the BF model confirming a conclusion already commented

with reference to modal analysis results. On the contrary, the maximum base shear force resistance increased up to 1.25 (MSR_1) and 1.11 (MSR_2) with respect to the BF model. The first non-linear event was the buckling of the vertical braces. Subsequently, yielding of the anchors occurred, thus generating a large increase of shear forces in the siderail-to-column connections close to the column base connections for which anchor yielding occurred. Eventually, failures of those connections were predicted to occur for a drift approximately equal to 0.5%. Thus, detachment of the cladding was predicted by the numerical model also in this building direction. The small drops in the pushover curve correspond to siderail-to-column connection failures. Despite a negligible global effect introduced by such failure mode, the local behavior was strongly affected by them. Indeed, anchor fracture occurs for a drift equal to 1.4% (the event highlighted with an empty triangle in the pushover curve), thus introducing a significant difference with respect to the BF model analysis results. The pushover curves were continued for larger drift values to identify the occurrence of brace fracture. for a subsequent comparison with results from dynamic analyses. Considering the MSR_1, vertical brace fracture was predicted for a drift equal to 2.1%, which was also the lateral drift for which the 50% loss of base shear force resistance was reached. Similar to the BF model, the pushover curve shows a positive stiffness following brace fracture due to secondary moment frame actions and, in this case also the additional contribution from the building envelope. Considering the MSR_2 limit, brace fracture occurred at a drift equal to 3.8%, while the drift corresponding to the 50% loss of the base shear force resistance was 4.2%. After brace fracture, the base shear force resistance increased due to the moment frame actions, coherently with the results of the bare frame model. However, the subsequent non-linear dynamic analysis described in Chapter V, will indicate that the behavior of the structure for such large drifts is not a concern, because collapse occurs predominantly in the transverse building direction.

The TS model exhibited a response very close to that of the SP model. Comparing the TS model with the BF model, a negligible increase of the building elastic lateral stiffness is observed, while the peak shear force resistance either increases of a factor equal to 1.04 MSR_1 case or decreases of a factor 0.93 MSR_2 case. Buckling of braces was the first non-linear event. Then, siderail-to-column connection failures were predicted to occur, followed by cladding detachment and yielding of anchors. The maximum strain in the anchors was reached for a lateral drift equal to 1.7%. Investigation of the structural response by neglecting anchor failures shows that brace fracture would occur for lateral drifts equal to 1.8% and 2.3%, for the MSR_1 and the MSR_2 limits, respectively. There were severe numerical convergence difficulties following the first brace fracture in tension.

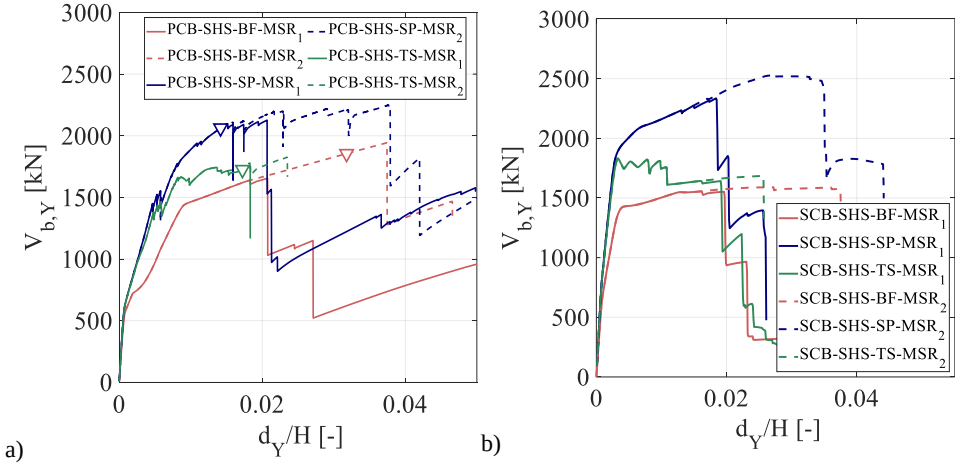

Figure IV.17 Pushover curves in the longitudinal direction: (a) PCB-SHS cases; (b) SCB-SHS cases.

Consequently, such pushover curves do not show the secondary moment frame effect. The results were considered acceptable, without further efforts in solving the convergence issues, because of the following multiple reasons: (i) the TS envelope response completely developed up to complete connection failures for a

drift smaller than 1%; (ii) the brace fracture corresponds to a loss of more than 50% of total base shear force resistance.

IV.3.2.2 SCB case studies

Figure IV.17(b) shows the response obtained for the SCB-SHS model. The pushover curve without considering envelope (i.e., for the BF model) linearly increases up to brace buckling. Subsequently, the lateral stiffness reduced to approximately one half of the initial stiffness. The following non-linear event was yielding of the braces in tension. After brace yielding, the pushover curve shows a relatively very small increase of the base shear force resistance, because no moment frame action can take place in the SCB case. In fact, the main columns were interrupted at the height of the longitudinal trusses which are supported on top of the columns. However, the model predicted a relatively small increase of axial forces in the chord members of the bracing system. Consequently, yielding of the gusset plate connections at the longitudinal truss ends took place. Also, connections bearing of the horizontal chord members was observed. In both cases, the model indicates that the corresponding deformation capacity was not exceeded. Subsequently, brace fracture started the pushover curve descending branch. Considering the MSR_1 limit, brace fracture was triggered for a drift value equal to 1.6% (brace in compression) or equal to 2% (brace in tension), while a 50% loss of the base shear force resistance occurred at a drift equal to 2.3%. Collapse drift capacity was achieved after fracture of two brace in tension. The negligible base shear force resistance due to secondary moment-frame actions were progressively eliminated by the truss-to-column connection failures. Indeed, the plastic resistance of the truss-to-column connections was reached, and large rotations were predicted at the column top after yielding of such components. Therefore, the pushover curve practically drops to zero immediately following the brace fractures. Using the MSR_2 limit, brace fracture was triggered at a drift equal

3.8%. Also in this case, several convergence problems were encountered due to fracture of braces in tension. For the same reasons already discussed with reference to the PCB case, the descending branch of the pushover was not needed in consideration of the predominance of collapse in the transverse direction during the time-history analysis. Therefore, the obtained results were considered satisfactorily for the purposes of this study.

In the SP model, the bare frame and the envelope system reacted to the horizontal loads practically as parallel resisting systems. The increase of the lateral stiffness with respect to the BF model was negligible, while the maximum shear force resistance increased with respect to the BF model of a factor equal to 1.50 (MSR_1) or 1.60 (MSR_2). Yielding of the cladding panels was predicted after brace buckling. Longitudinal drifts were similar to those corresponding to brace yielding (0.4%). Brace fracture with the MSR_1 limit occurred at 1.5% of lateral drift in the braces subjected to compression, and at 1.8% in the braces subjected to tension. A 50% loss of the shear force resistance occurred at a drift equal to 2.6%. The descending branch of the pushover curve was practically a vertical line. In fact, redistribution of horizontal forces was not possible after brace fracture (because no secondary moment frame action can be developed). A similar behavior was obtained with the MSR_2 limit. In this case, brace fracture started at a lateral drift equal to 3.2%, while collapse was reached with a drift equal to 4.4%.

Similar to the SP model, the TS model showed a negligible increase of elastic lateral stiffness with respect to the BF model. However, the screw connections started to fail at a drift equal to 0.5%. The contribution of the TSs was totally lost at a drift equal to 1%, approximately. The structural response following such non-linear events was very close to the response of the bare frame. Compared to the BF model, minor differences were observed in the value of the base shear force resistance, due to the shear forces in the secondary columns (not included in the

BF model). Also in this case, fracture of braces in tension dominated the descending branch of the pushover curve. Brace fracture (MSR_1) was triggered at a drift equal to 2% (approximately) for the braces in tension. The 50% drop in the base shear force resistance was reached at a drift equal to 2.3%. When the MSR_2 limit was used, the descending branch of the pushover curve started at a drift equal to 2.6%.

IV.3.2.3 Pushover deformed shapes

Examples of the displaced configurations for the examined case study structures are provided with Figure IV.18. Figure IV.18(a) shows the deformed shape of the BF model, with both elevation and plan views, while varying the considered drift (numerical drift values are shown in the figure). Three steps were considered: (i) a step corresponding to the yielding of the anchors in the column base connections; (ii) a step corresponding to the achievement of the maximum base shear force resistance, (iii) a step after brace fracture in tension. The longitudinal elevation views allow visualization of the anchor displacements for both the elastic and inelastic branch of the structural response. The absence of anchor yielding at the column bases with braces in compression can be noted. In the plan views, the progression of the out-of-plane (OoP) buckling for braces in compression is clearly visible. Differences in the inelastic displacement shapes between the two braced bays can be observed. The differences were a consequence of the structural details for brace connections. Indeed, the X-brace configuration was designed with one continuous brace in one direction and two spliced braces welded to a central gusset plate. The continuous brace in compression has a sinusoidal out-of-plane (OoP) displacement shape with two opposite maximum displacements at middle point along their axis. On the contrary, only one spliced brace in compression exhibits significant out-of-plane displacements, with a maximum at the middle point along their axis. When

fracture of brace in tension occurs, compressed braces in the same bay lose their out-of-plane restraint. Consequently, significant OoP displacements at the central node of the braced bay are observed. These numerical results agree with the experimental results presented by Palmer *et al.* (2012). Clearly, after brace fracture the torsional response of the roof increased.

Figure IV.18(b) shows the deformed shape of the SP model, with both longitudinal and plan views, considering various significant steps in the pushover analysis. The response resembles the one observed for the TS model. Three steps were considered: (i) a step prior to the first drop in resistance due to siderail-to-frame connection failure; (ii) a step corresponding to the column base connection failure due to excessive strain in anchors, (iii) a step after brace fracture in tension. In the elevation views, it is possible to visualize cladding detachment and the consequent unusual main column deformed shape after cladding-to-frame connection failures and column base connection yielding. In the plan views, progression of out-of-plane (OOP) buckling for the braces in compression replicates what is observed for the BF model. Eventually, when fracture occurred for braces in tension, OoP displacements for both the compressed and tensile braces were observed.

Figure IV.19(a) shows the deformed shape of the SCB-BF model, with both longitudinal and plan views, at different steps in the pushover response. Three analysis steps were considered: (i) a step corresponding to yielding of braces in tension; (ii) a step corresponding to the achievement of the maximum base shear force resistance, (iii) a step immediately following brace fracture in tension (MSR_1). The figure confirms the OoP displacement behavior of the braces as previously described. Additionally, the last plot on the right shows triggering of truss-to-column connection failures.

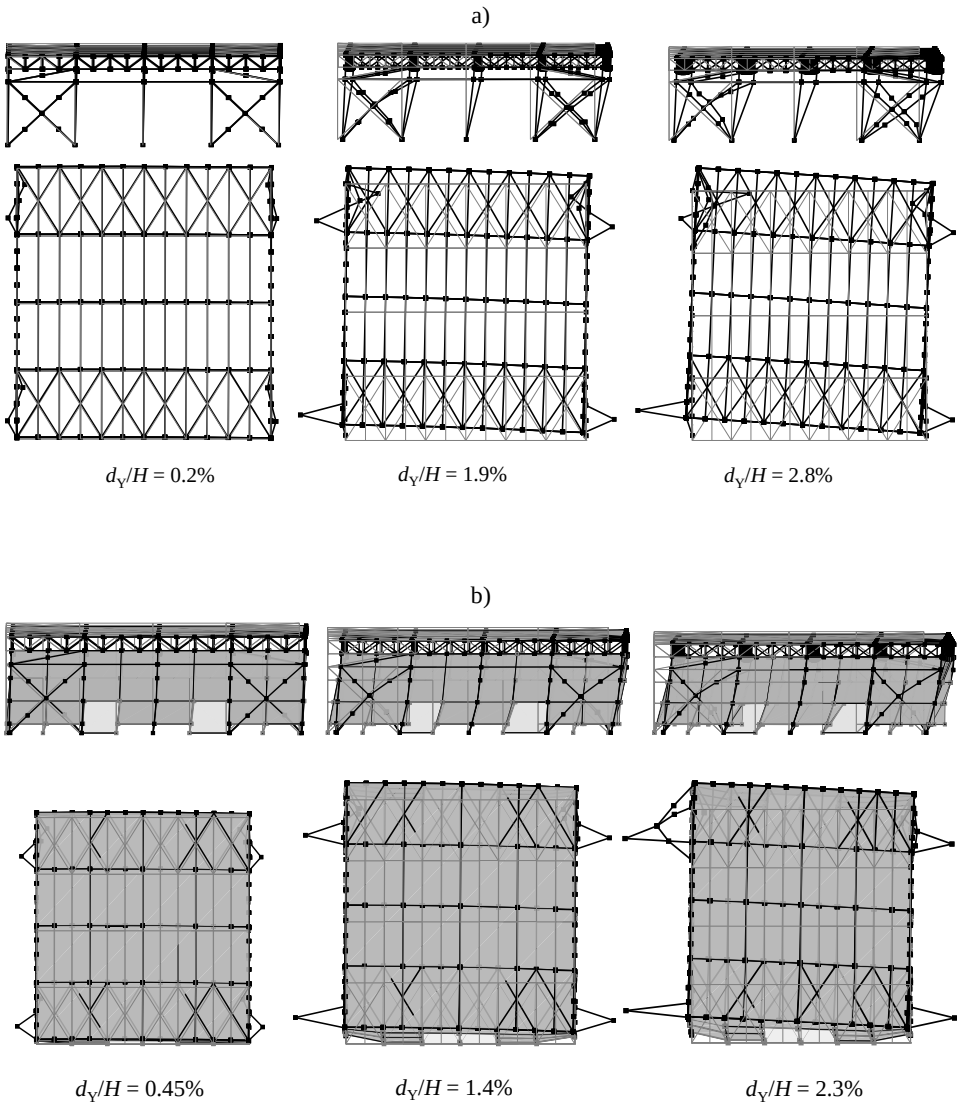

Figure IV.18 Displacement shapes of the PCB-SHS structures at selected steps of the pushover analysis: (a) BF model; (b) SP model.

Similarly, Figure IV.19(b) shows the deformed shape of the SCB-TS model, with both longitudinal and plan views, by using three analysis steps: (i) a step corresponding to the achievement of the maximum base shear force resistance,

which is coincident with the yielding of braces in tension, (ii) a step after the complete loss of the base shear force resistance contribution from the TS cladding elements, (iii) a step after brace fractures in tension (MSR_1).

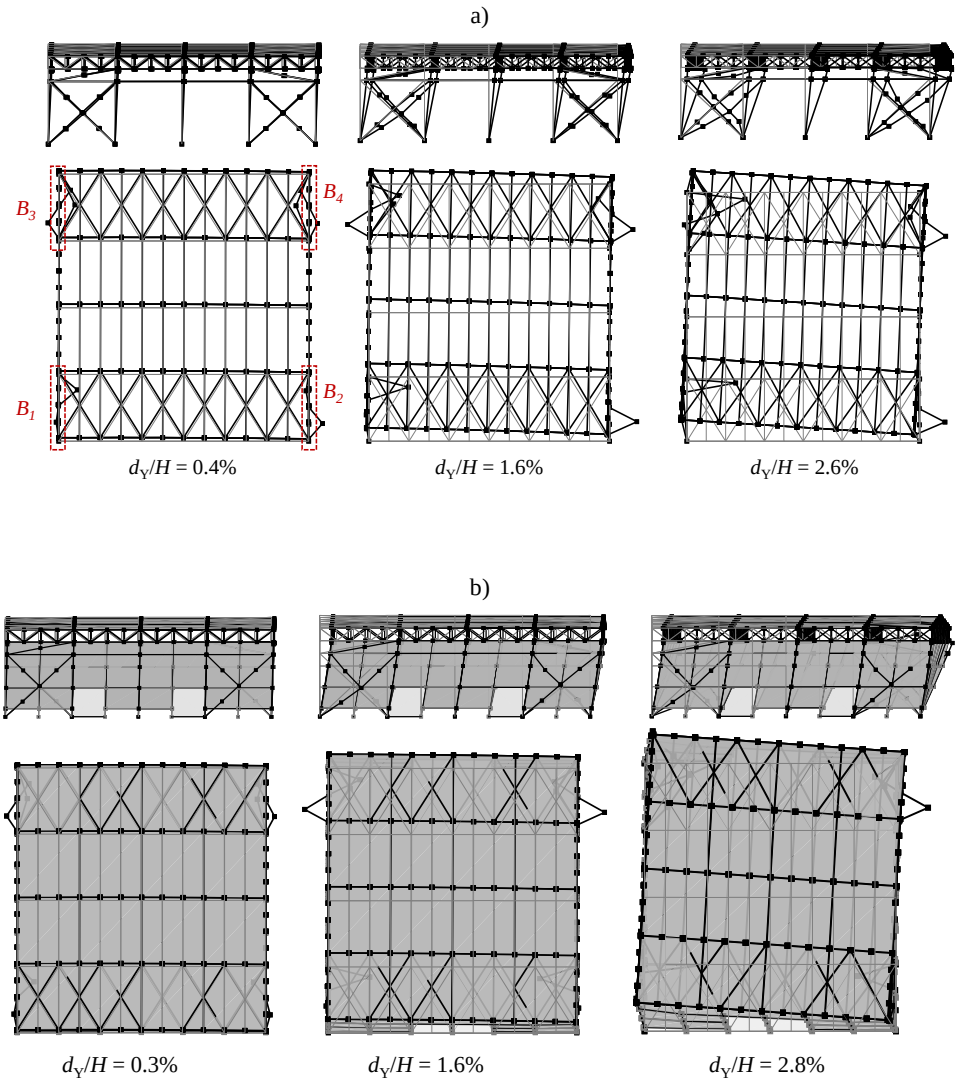

Figure IV.19 Displacement shapes of the SCB-SHS structures at selected steps of the pushover analysis: (a) BF model; (b) SP model.

The deformed shapes are very similar to those described for the SCB-BF model. No cladding detachment was predicted by the numerical model for these case studies (i.e., for both the TS and SP models). Indeed, the building envelope did not change the collapse mechanisms.

IV.3.2.4 Component response

Since anchor fractures dominated the structural response of the PCB case studies in the longitudinal direction, Figure IV.20(a) shows the relationship between the equivalent anchor strain (ε_A) and the pushover drift (d_Y/H), both for left-side anchors (continuous line) and right-side anchors (dashed lines). The ultimate strain anchor capacity (Chapter III) is depicted as a black dashed line in the plot.

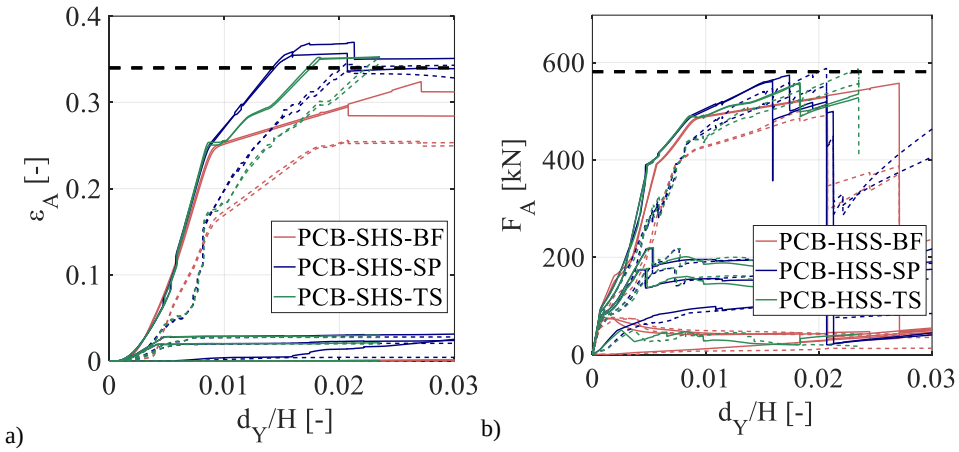

Figure IV.20 (a) Strains and (b) resultant forces in anchors for the PCB column base connections.

Differences between the relationship obtained from the BF model and those obtained from the SP/TS models were related to the presence of the envelope panels. The slope of the relationship in Figure IV.20(a) highly increased with

respect to the BF model after yielding of brace in tension (1%). Figure IV.20(b) shows values of the resultant forces acting on the base anchors (F_A), while the anchor force resistance is depicted as a black dashed line in the plot. Forces in the anchors did not exceed their resistance when anchor strain was smaller than the considered limit.

To better describe the evolution of the non-linear response of braces, in Figure IV.21 the brace axial force (N_{BR}) vs. the brace axial deformation (δ_{BR}) relationship is plotted for the SCB-BF model, considering both the MSR_1 and the MSR_2 fracture criteria. The figure is subdivided into 4 sub-plots, each one referring to one of the four braced bays (Figure IV.19 shows names of the bays).

Continuous braces are plotted with dashed lines, while spliced braces are plotted with dotted lines. Eventually, single braces at the second level are plotted with continuous lines. One can observe the highly asymmetric component response, due to the large value of the brace slenderness. For the MSR_1 capacity value, brace fracture was predicted to occur first on compressed brace of the B_1 bay. Eventually, only the left-side bays (Figure I.23(a) and (b)) experienced fracture of tensile braces, thus degrading the longitudinal base shear force resistance up to the 50% of the maximum value. This was a consequence of the asymmetric masses due to the overhead crane and the crane loads. On the contrary, using the MSR_2 capacity value, the first brace to fracture was the tensile brace of the B_1 bay. In any case, brace fracture occurred only at the first “story” of the braced bay. No brace fracture or weld failures were observed for the “second-story” braces in any of the four braced bays.

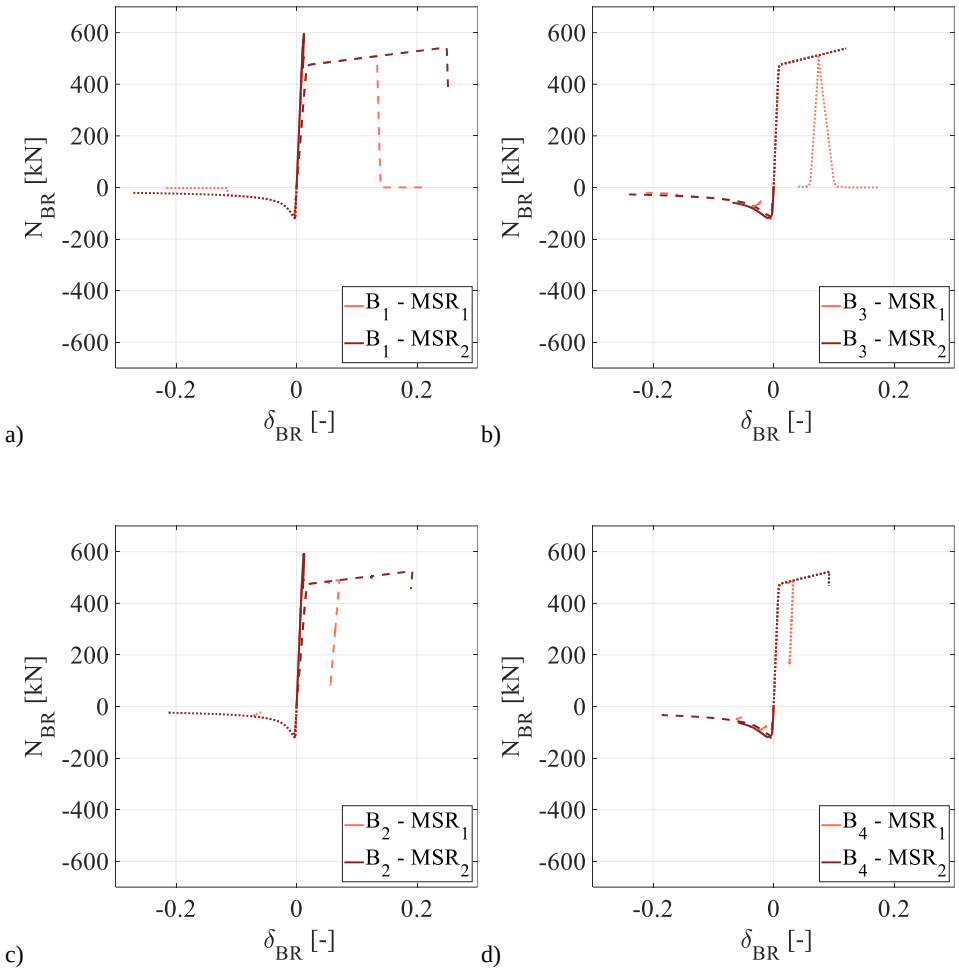

Figure IV.21 Brace axial forces in the SCB-BF model:
(a) Left-bottom bay (B_1); (b) Left-top bay (B_3); (c) Right-bottom bay (B_2); (d) Right-top bay (B_4).

IV.3.2.5 Summary of the results

In all the examined case studies, the global collapse condition was reached immediately following the tension brace fracture. As shown by the pushover

curves, secondary moment-frame actions can have different impacts, depending on the structural layouts. Minor importance was given to the secondary moment-frame action in this study, because global collapse of the 3D buildings examined in this dissertation is largely dominated by the response in the transverse (portal frame) direction. This aspect will be thoroughly discussed in the following Chapter V dealing with time-history response analysis and, eventually, in Chapter VI discussing the collapse fragility curves.

A second interesting observation suggested by the static analysis results is relevant to the brace fracture criteria. From the pushover results, drifts corresponding to the attainment of the MSR_1 and MSR_2 limits were calculated per each case. Then, the results suggest that such drifts depend on the cladding type.

IV.3.3 Longitudinal direction: 2L braces

The structural response to lateral loads in the longitudinal direction is discussed in this section with reference to braces made of built-up section with two L shapes back-to-back and bolted connections. The pushover results are shown in Figure IV.22, for both the PCB and SCB case studies. For the type of braces investigated here, connection failure occurs prior than brace fracture. Henceforth, there is no need to consider the two alternative brace fracture criteria as done for the SHS braces. Consequently, only one pushover curve will be provided per each case study.

IV.3.3.1 PCB case studies

The pushover curves of the PCB-2L models are depicted in Figure IV.22(a). The BF response is characterized by yielding of anchors at the column base connections simultaneously with in-plane buckling of the braces. As shown in the figure, connections of braces in tension yielded at a lateral drift equal to 0.8%.

The deformation capacity of every connection was exhausted almost simultaneously at a drift equal to approximately 1.2%. Following connection failure, secondary moment frame actions took place, thus preserving the system stability to horizontal loads up to column buckling. The global collapse condition (i.e., 50% loss of base shear force resistance) was predicted to occur at a drift equal to 1.3%. This event is highlighted with an empty circle in the figure. The structural response considering the contribution of either the TSs or the SPs is also shown in Figure IV.22(a). In both models (i.e., SP and TS), anchor fracture did not take place, contrary to what happened in the case studies equipped with SHS braces and welded connections. Consequently, collapse was reached due to brace connection failure, in the form of bearing of the bolts and consequent gusset plate fracture. In more detail, the SP model shows an increase of maximum shear force resistance with respect to the bare frame model of approximately 30%. As already shown by the modal analysis results, the increase of lateral stiffness with respect to the BF model was practically negligible. The structural response was governed by the local interaction between the bare frame and the envelope due to progressive siderail-to-column connection failures. Such failures correspond to the vertical drops visible in the pushover curve. The first occurrence of brace connection failure was observed at a lateral drift equal to 1.2%, while the 50% loss of the base shear force resistance occurred at a drift equal to 1.4%. Convergence issues did not allow to trace the last part of the pushover curve. For the TS case, the increase of the lateral shear force resistance was by a factor equal to 1.16 with respect to the bare frame model. A negligible increase of the lateral stiffness was predicted by the numerical model. Also, detachment of the cladding panels from the (main and secondary) columns was observed, and they correspond to the vertical drops in the pushover curve. Eventually, brace connection failure started to happen at a lateral drift equal to 1.2%, and global collapse was reached at a drift equal to 1.4%. In this case, the analysis was able to show the secondary

moment-frame action. As previously discussed, the secondary moment-frame action was not important for the buildings examined in this study, because global collapse of the 3D building was largely dominated by failures occurring in the portal frames.

IV.3.3.2 SCB case studies

The structural responses obtained with the SCB-2L models are shown in Figure IV.22(b). The results are very similar to those described in the SCB-SHS case studies. The BF model shows an increase of the base shear force until brace buckling and tensile brace connection yielding occurred (at a drift equal to 0.3%). The brace connection resistance was large enough to develop brace buckling, but insufficient to develop brace yielding in tension

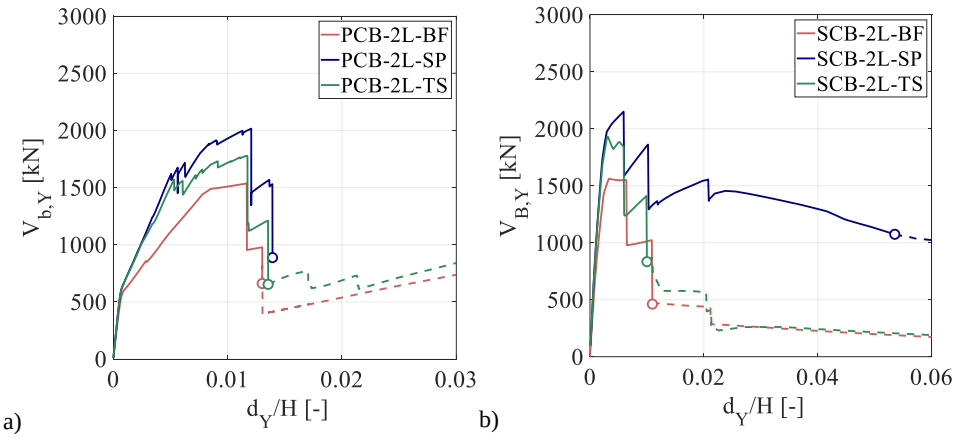

Figure IV.22 Pushover curves in the longitudinal direction: (a) PCB-2L cases; (b) SCB-2L cases.

The first brace connection failure was reached with a lateral drift equal to 0.6%, while the global collapse capacity was reached at a lateral drift equal to 1.1%. After this event, the structural response became strongly irregular, with a strong amplification of torsional roof displacements. For this reason, the lateral

resistance did not drop to zero but smoothly decreased with increasing the control joint displacement. Figure IV.22(b) shows the response with envelope panels. In both the SP and TS models, a minor increase of the lateral stiffness was observed with respect to the bare frame, confirming the results from modal analysis. An increase of the maximum shear force resistance with respect to the BF model was obtained, with factors equal to 1.34 and 1.24, for the SP and TS models, respectively. As observed for the SCB-SHS case studies, including the envelope system originated different post-peak structural responses, because differences in cladding-to-frame connections led to different peak connection resistance and post-peak stiffness and strength degradation. In the SP case, the brace connection failure was compensated by the sandwich panel force contribution, thus obtaining a less severe strength degradation following the peak. In fact, SPs acted as equivalent braces after the occurrence of the brace connection failures. For this reason, the global collapse condition occurred with a lateral drift equal to 5.3%. In the TS case, the structural response practically coincides with the BF response. Indeed, the TS contribution is practically lost when brace connection failures occurred (0.6%), and global collapse occurred with a lateral drift equal to 1%.

IV.3.3.3 Deformed shapes

Figure IV.23(a) shows the structure displacement shapes from analysis of the PCB-2L case study at the following analysis steps: (i) a step corresponding to the yielding of the anchors in column base connections, (ii) a step corresponding to the bearing of bolts in the brace connections, (iii) a step corresponding to brace connection failures and global collapse. In-plane (IP) brace buckling occurred in the case of 2L brace cross sections. However, the buckled shapes of braces are qualitatively similar to those already observed for the SHS braces. Displacements of nodes at the column bases due to yielding of the anchors are also clearly visible. Figure IV.23(b) shows similar results for the SP case study, using the same

analysis steps considered for the BF and TS case studies, because of the similarities in response. In the figure, cladding detachments are also clearly visible, as well as IP buckling of braces and inelasticity triggered in column base connections.

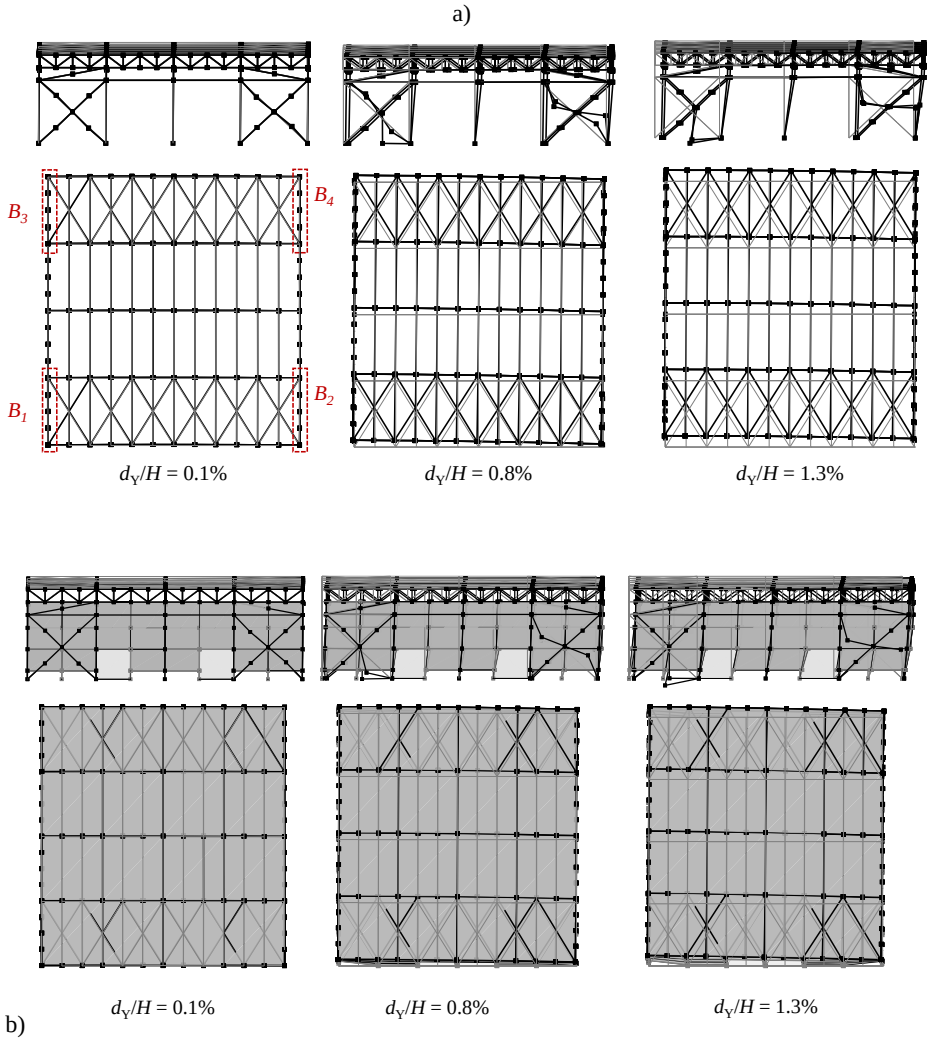

Figure IV.23 Displacement shapes for the PCB-2L structures at selected steps of the pushover analysis: (a) BF model; (b) SP model.

Figure IV.24 plots the elevation views of the deformed shapes for the SCB-2L-TS numerical model, as an example. Differences with respect to the PCB-2L-SP were mainly due to the absence of column base connection inelastic displacements. Indeed, column base connections were strong enough to allow brace connection yielding and failure. Also, IP buckling inelastic displacements are shown in the plots. Eventually, failure of truss-to-column connections are depicted in the last plot on the right. Similarly, Figure IV.25 shows deformed shapes in plan view during pushover analysis for the SCB-2L case studies. In all the cases, the same pushover drifts were considered. The considered drifts correspond to the following analysis steps: (i) the drift corresponding to brace yielding in tension, (ii) the drift for which the global collapse limit state was triggered, for both the BF and TS models, (iii) the drift corresponding to 50% loss of the building lateral strength for the SP model (i.e. global collapse). Similar deformed shapes were observed among the three considered case studies. Indeed, in the SCB cases the envelope panels and the secondary steel structure acted practically as parallel lateral resisting systems. No cladding detachment was predicted for such case studies, as already confirmed by the SCB-SHS structural analysis.

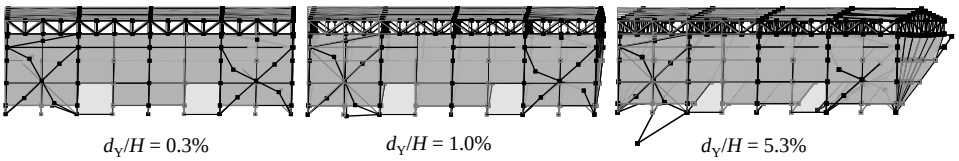

Figure IV.24 Longitudinal displacement shapes of the SCB-2L-SP structure at selected steps of the pushover analysis.

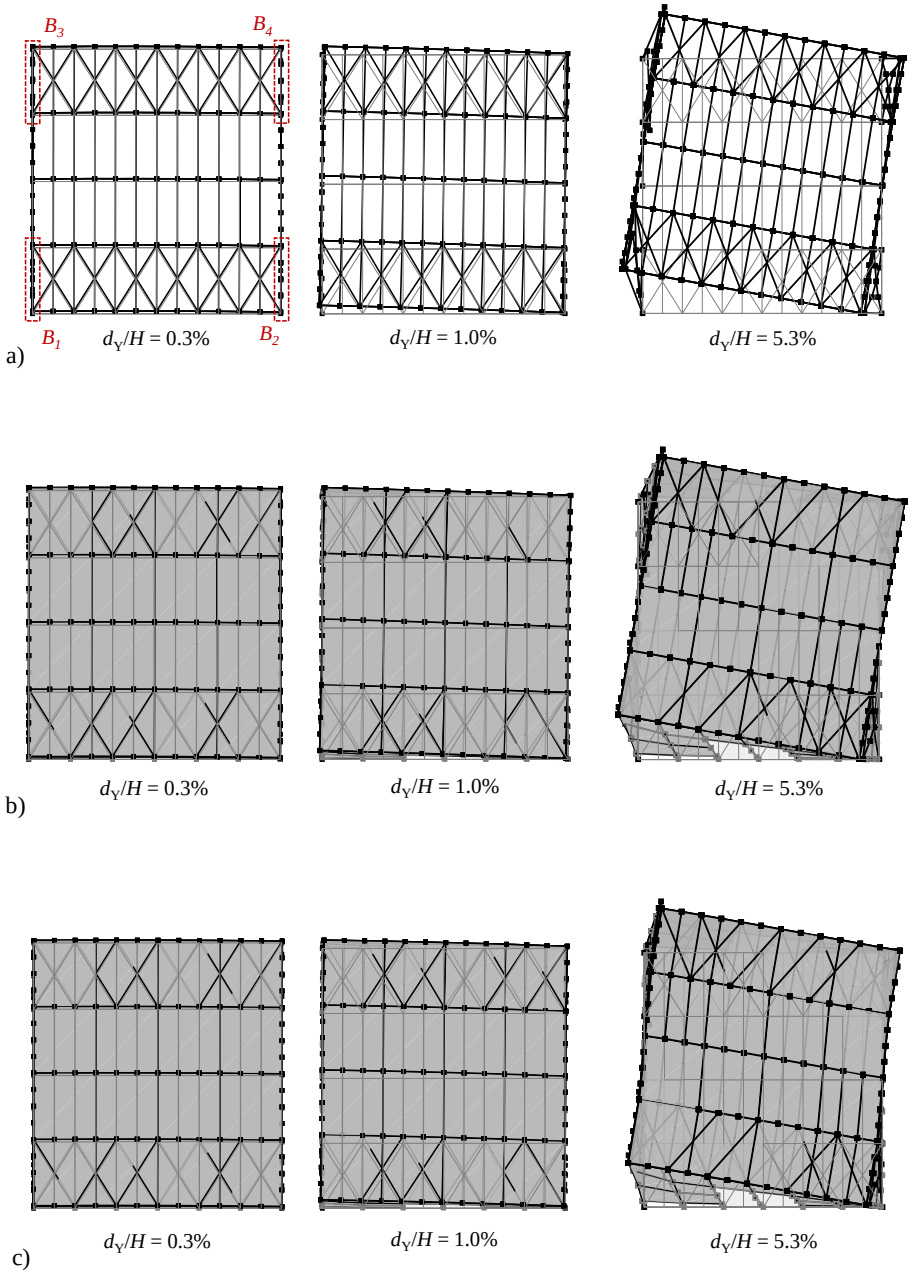

Figure IV.25 Plan views of the displacement shapes of the SCB-2L structures at selected steps of the pushover analysis: (a) BF model; (b) SP model; (c) TS model.

IV.3.3.4 Component response

Figure IV.26(a) shows the relationship between the equivalent anchor strain (ε_A) and the pushover drift (d_Y/H), for both the left-side anchors (continuous line) and right-side anchors (dashed lines). The relationship resembles that obtained for the PCB-HSS case studies. However, as suggested by the pushover analysis results, brace connection failures anticipated anchor fractures, as confirmed by the plot (the strain anchor capacity, ε_u, is depicted as black dashed line in the plot).

Figure I.22(b) shows values of the resultant forces acting on the base anchors (F_A), while the anchor fracture resistance is depicted as a black dashed line in the plot. The forces in the anchors never exceeded the corresponding resistance. The abrupt reduction of the anchor forces was due to brace connection failures, as suggested by the corresponding drift values.

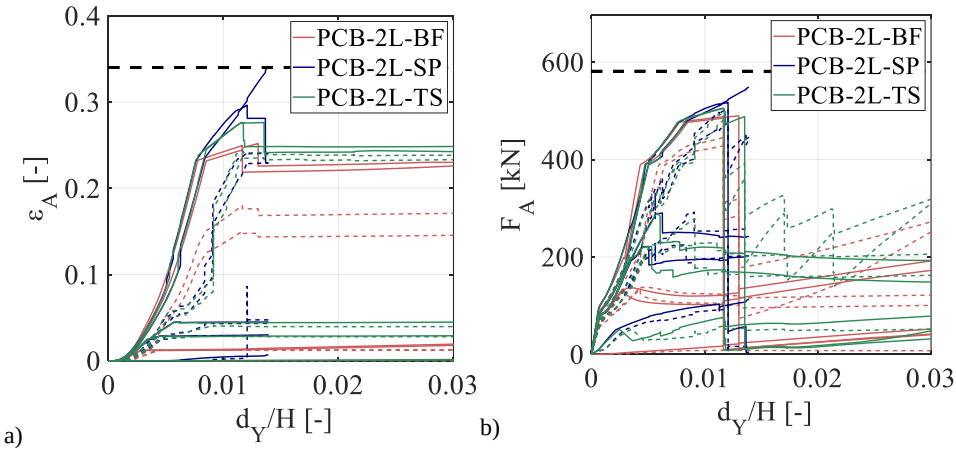

Figure IV.26 (a) Strains and (b) resultant forces in anchors for the PCB-2L column base connections.

Since brace connections were fundamental components for assessing global collapse for the examined case studies with 2L brace cross sections and the

relevant connection details, a post process of the brace connection component response was carried out and summarized hereafter. The post process was done similarly to what was presented for brace components in Figure IV.21, and it is summarized in Figure IV.27.

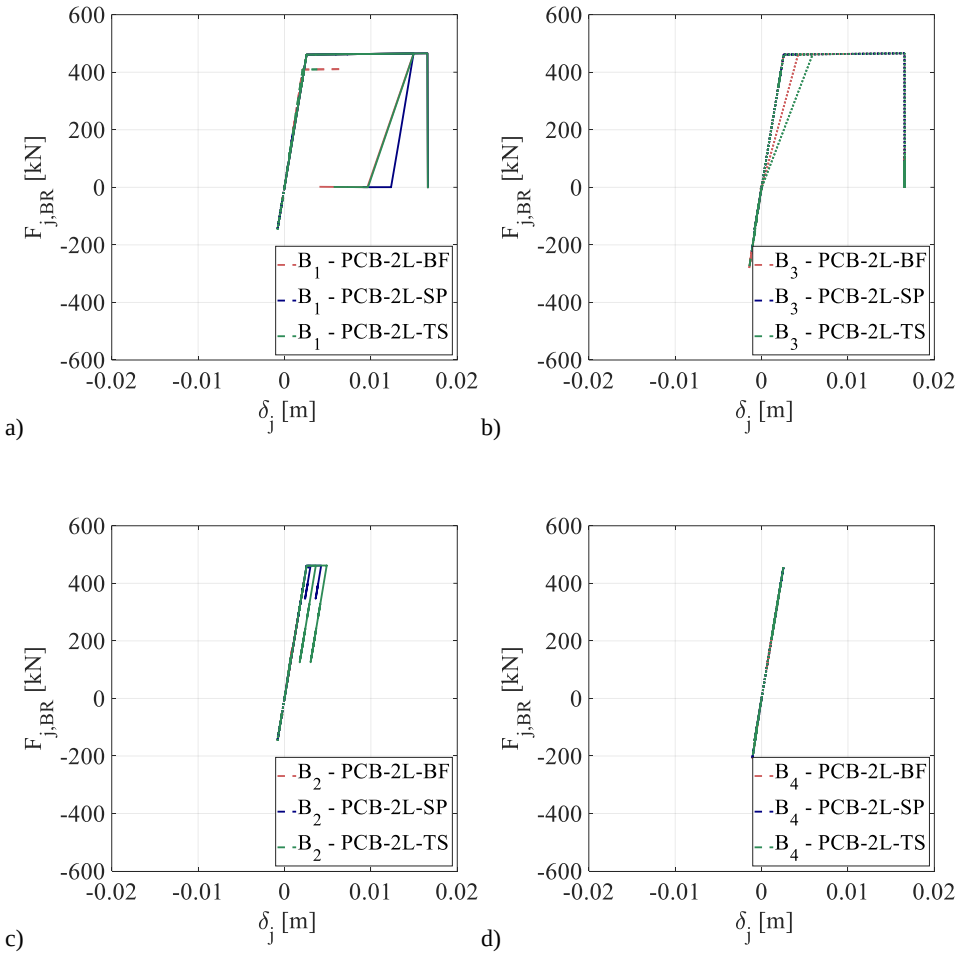

Figure IV.27 Brace connection forces in the PCB-2L models:
(a) Left-bottom bay (B1); (b) Left-top bay (B3); (c) Right-bottom bay (B2); (d) Right-top bay (B4).

The figure shows the brace connection force (F_{BR}) vs. the connection displacement (δ_j) relationship arising from all the three PCB-2L models. The figure is subdivided into 4 plots, thus splitting brace response within the four braced bays (Figure IV.23Figure IV.25(a) shows information concerning bays location). Connections of continuous braces are plotted with continuous lines, while connections of spliced braces are plotted with dotted lines. Eventually, connections on single braces at the second level are plotted with dashed lines. Brace connection failures were triggered only for bays B_1 and B_3, corresponding to the bays in the left-side of the building. Additionally, in bay B_1 the plastic resistance of the brace connections at the second level were reached, but only for the TS and BF models. Therefore, such plastic resistance was achieved after the first brace connection failures at the first level. As one can see, the bay B_2 is slightly interested by development of connection plastic deformations, while connections located in the bay B_4 remained in the elastic range.

Figure IV.28 shows the brace connection force (F_{BR}) vs. the connection displacement (δ_j) relationship concerning the analysis of the three SCB-2L models. The figure is subdivided into 4 plots, considering the response of the four braced bays (see Figure IV.25Figure IV.25(a) for information about the braced bays location and numbering). The results resemble those observed in the PCB cases, with brace connection yielding and failure in both braced bays B_1 and B_3. On the contrary, the braced bays B_2 and B_4 show relatively smaller connection plastic deformations (B_2) or practically elastic behaviour (B_4) up to the maximum considered drifts.

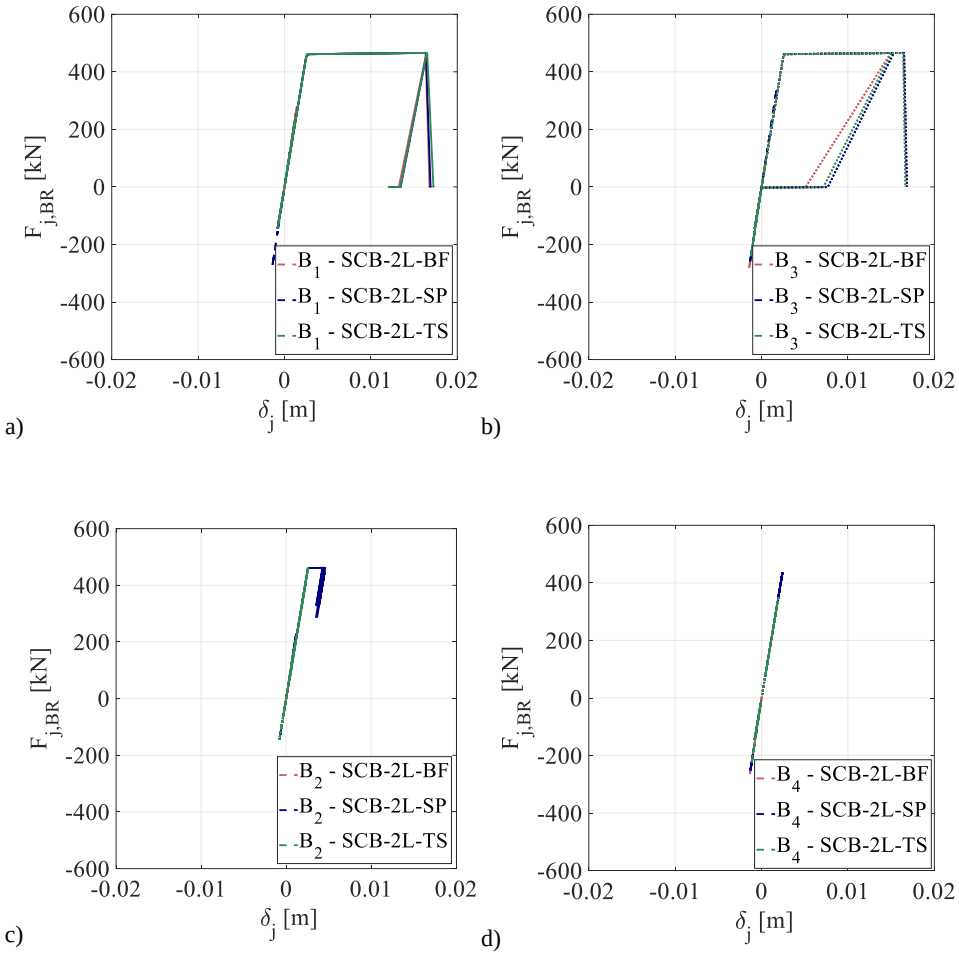

Figure IV.28 Brace connection forces in the SCB-2L models:
(a) Left-bottom bay (B1); (b) Left-top bay (B3); (c) Right-bottom bay (B2); (d) Right-top bay (B4).

IV.3.3.5 Summary of the results

In all the examined case studies, the global collapse condition was reached immediately following the tension brace connection failure. For the PCB cases,

numerical models did not predict anchor fractures prior to failures of brace connections. As suggested by the observation of the brace connections response, inelastic behavior mainly developed on the left braced side. Depending on the structural arrangement in the transverse direction (i.e., PCB or SCB), inelastic deformations may or may not develop in the vertical brace connections at the second level.

Structural response by considering cladding panels may be significantly affected by the cladding type in the case of SCB models. In fact, the better performance of SPs allowed to have larger collapse drift capacity with respect to TSs. On the contrary, PCB models had shown similar collapse drift capacities for both the cladding types.

IV.3.4 Main pushover analysis results

The present chapter focused on the main structural analysis results obtained via the non-linear static procedure for the archetype buildings.

The numerical results show that the envelope panels may have or may not have an important effect on the structural response, depending on the type of cladding and the characteristics of the bare structural frame. Concerning the type of cladding, the buildings with bolted sandwich panels exhibited better structural performance, compared to the buildings with single trapezoidal sheeting and screwed connections. In fact, better cladding-to-frame connection details of sandwich panels exhibited larger ductility values if compared with the screw connection details of trapezoidal sheeting. Effect of different local cladding behavior led to differences in both maximum base shear force resistance and descending branch of the pushover curves. Concerning the characteristics of the bare structural frames, it was observed a strong interaction between the cladding

panels and the PCB bare frame structure. On the contrary, cladding panels behave as parallel system with the bare frame structure in the case of SCB models.

In case of pinned column base connections (PCB), the building response was strongly influenced by the cladding siderail-to-column connection failures, which triggered cladding panel detachments. Compared to the SCB models, the PCB models had larger base shear force resistance in the transverse portal frame direction. However, the SCB models showed significantly larger collapse drift capacity. With reference to the behavior of the longitudinal braced frames, in case of SHS braces, failure of the column base anchors occurred prior to brace fracture in the case of PCB connections, whilst the opposite was observed for the SCB connections. Therefore. the collapse drift capacity of the PCB cases resulted smaller than that observed for the SCB models. In cases where built-up angle sections (2L) and bolted connections were adopted, results show the worst structural response due to early (and almost brittle) end brace connection failure.

Collapse mechanisms were clearly identified for the transverse (X) building direction, corresponding to sidesway global collapse triggered by connection failures in every examined case. Truss-to-column connection failure caused the exceedance of the collapse limit state for PCB case studies, while column base connections failures dominated collapse of the SCB cases. In the longitudinal (Y) building direction, fracture of braces (SHS) or brace connections (2L), as well as column base connection failures, triggered drop in lateral base shear force resistance larger than 50% of the maximum value. In every case, the collapse limit state was triggered. However, non-negligible effects of secondary moment-frame actions can produce additional lateral strength and stiffness to postpone global collapse to larger drift values. Such effects were not fully represented by the models, leading to some conservative estimations of the drift to collapse. However, the following Chapter V will show that during the time-history analysis

with bidirectional ground motions most of the collapses occur due to the fragility of the transverse portal frames. Therefore, this limitation of the braced frame model was accepted as a reasonable compromise between accuracy and simplicity, in view of the results from the time-history analysis.

References

Baltzopoulos G., Baraschino R., Iervolino I. 2018. On the number of records for structural risk estimation in PBEE. *Earthquake Engineering and Structural Dynamics 2018: 1 – 18.*

Chopra A.K. 2007. Dynamics of structures: Theory and applications to earthquake engineering. Upper Saddle River, N.J: Pearson/Prentice Hall.

Della Corte G., De Matteis G., Landolfo R., Mazzolani F.M. 2002. Seismic analysis of MR steel frames based on refined hysteretic models of connections. *Journal of Constructional Steel Research 58: 1331 – 1345.*

Giannopoulos D., Vamvatsikos D. 2018. Ground Motion Records: To rotate or not? *Earthquake Engineering and Structural Dynamics 47(12): 2410 – 2425.*

Hall J.F. 2018. On the descending branch of the pushover curve for multistory buildings. *Earthquake Engineering and Structural Dynamics 47: 772 – 783.*

Hsiao P.C., Lehman D.E., Roeder C.W. 2013. A model to simulate special concentrically braced frames beyond brace fracture. *Earthquake Engineering and Structural Dynamics 42: 183 – 200.*

Ibarra L., Medina R., Krawinkler H. 2005. Hysteretic models that incorporate strength and stiffness deterioration. *Earthquake Engineering and Structural Dynamics 34: 1489 - 1511.*

Krawinkler H., Seneviratna G.D.P.K. 1998. Pros and cons of a pushover analysis of seismic performance evaluation. *Engineering Structures 20: 452-464.*

AISI. 2013. North American Standard for the Design of Profiled Steel Diaphragm Panels. *American Iron and Steel Institute, AISI S310-13.*

Palmer K.D., Roeder C.W., Lehman D., Shield C. K. Concentric X-braced frames with HSS bracing. *International Journal of Steel Structures 12(3): 443 – 459.*

Peres R., Bento R., Castro J.M. 2018. Nonlinear Static Seismic Performance Assessment of Plan-Irregular Steel Structures. *Journal of Earthquake Engineering 24(2): 226 – 253.*

Zareian F., Krawinkler H., Ibarra L., Lignos D. 2010. Basic Concepts and Performance Measures in Prediction of Collapse of Buildings under Earthquake Ground Motions. *The Structural design of Tall and Special Buildings 19: 167 – 181.*

Chapter V

NON-LINEAR DYNAMIC ANALYSIS

V.1 Introduction

The structural response assessment via non-linear dynamic analyses is discussed in this Chapter. The multi-stripe analysis methodology was adopted (Jalayer, 2003, Jalayer and Cornell., 2009), with the aim to obtain collapse fragility curves (discussed in Chapter 6). Numerical simulations were carried out accounting for record-to-record variability through the selection of an adequate number of ground motions (Section V.2).

For a single time-history response analysis with a given ground motion, integration of the equations of motion was carried out using the *OpenSees* software with the application of the implicit integration method proposed by Newmark (1959), in which the two integration parameters were set equal to γ = ½ and β = ¼, thus obtaining stability of the numerical simulation and avoiding introduction of a spurious damping in solving the non-linear equations (Newmark, 1959). Analyses were performed to identify triggering of the collapse limit state, as defined in Chapter III and calculated numerically in Chapter IV.

The first section of the chapter briefly describes the seismic hazard at the selected building site and the hazard-consistent ground motion record selection. Subsequently, the numerical results and a detailed response comparison among the different case studies is presented and discussed. Eventually, sample component responses and specific results concerning selected bins of ground motions are discussed in more detail, also comparing the results with those obtained by the non-linear static analysis (Chapter IV).

V.2 Seismic hazard and record selection

Seismic hazard evaluation and ground motion selection at the building site were carried out within activities of the RINTC research project (Spillatura, 2017). The corresponding seismic hazard curves at the assumed building site are illustrated in Figure IV.1(a) elaborating on information provided by Iervolino *et al.* (2018). For the non-linear dynamic analyses at increasing earthquake intensity levels, the spectral (pseudo-) acceleration at the system fundamental period of vibration ($S_a(T_1)$ or S_a for brevity) was used as the intensity measure (IM). This approach is consistent with the PEER PBEE and FEMA P-58 methodologies and it has already been extended for use in the analysis of 3D structures. The adequacy of such assumption in the case of 3D structures was already discussed in past research (Luco *et al.*, 2005, Faggella *et al*., 2013) in terms of *efficiency* and *sufficiency* of the considered IM (Luco *et al.*, 2001). Results of such research have shown that the use of a scalar IM in assessing seismic response of 3D structures can led to violation of the *sufficiency* property. In these cases, biased results can be obtained. Luco *et al.* demonstrated the promising use of a vector of ground motion parameters (i.e, the IMs) in assessing the response of 3D structures. On the contrary, Faggella *et al.* pointed out that a single IM can be strictly appropriate for cases in which the considered structural response parameter is predominantly correlated to specific spectral ordinate at a single period of the structure.

According to Morelli *et al.* (2018), using the uniform hazard spectrum method (FEMA, 2012), increasing the number of records, conditioning on different IM values, and eventually enveloping the results should lead to improved reliability of the analysis results for building showing significant differences in the vibration periods for the two building directions. Additionally, Morelli *et al.* (2018) show that the most effective scaling technique to reduce the dispersion of EDPs in a desired direction is obtained by using $S_a(T_1)$ as IM. A consequence of such assumption is the amplification of the dispersion of EDPs in the other direction. In this study, the MSA results, which are described in the following sections of this chapter, suggest the large predominance of collapse cases in the transverse building direction, which is the direction showing the first mode of vibration used for the record selection. This result was also a confirmation of the expected high correlation between the identification of the collapse limit state of the building and the selected IM, thus justifying the method adopted in this study.

In the conducted analyses, ten different IM values were considered, corresponding to earthquake return periods (T_R) varying from 10 years to 100000 years. The corresponding values of the mean annual frequency of exceedance of the considered IM are shown in the figure as vertical axes (λ_{Sa}). Two different hazard curves were considered, accounting for variation of the building fundamental period of vibration for the model with and without envelope panels explicitly considered in terms of structural response. At each IM value, 20 pairs of ground motions (GMs) were selected as specified in Iervolino *et al.* (2018) and Spillatura A. (2017). Specifically, the GM selection was carried out using the exact conditional spectrum method (CSM) (Baker, 2011, Lin *et al.*, 2013), but accounting for ground-motion record characteristics other than the spectral shape as specified by Spillatura (2017). The approach used in this dissertation is consistent with the work of the other research units within the RINTC project,

thus allowing comparisons of results which are ultimately addressed to obtain the annual failure rates.

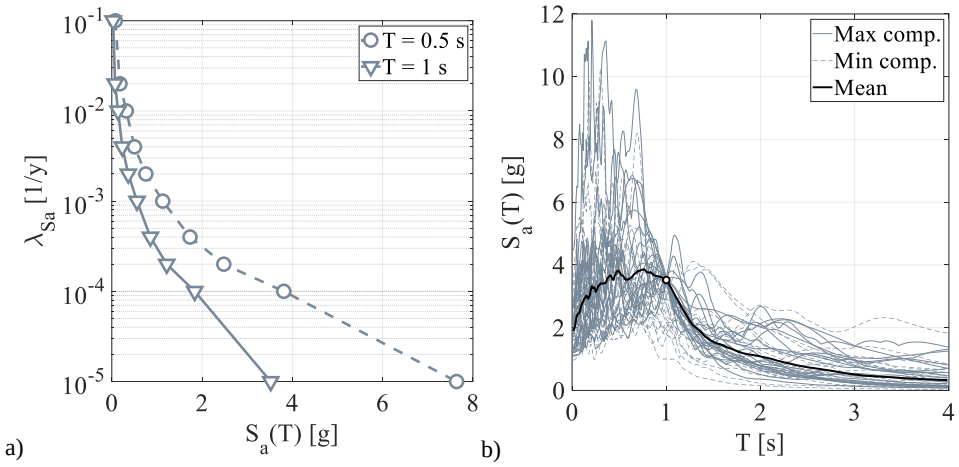

Figure V.1 (a) Hazard curves; (b) Example of ground motion selection.

Figure IV.1(b) shows an example of the GM selection and the corresponding conditional mean spectrum for the maximum intensity level at $T = 1\ s$ (i.e., the conditioning vibration period, T^*). The value of the $S_a(T = 1s)$ of the conditional mean spectrum is highlighted with an empty circle in the figure. Such value is equal to that characterizing the relevant hazard curve in Figure IV.1(a). Per each couple of GMs, one can compute two different spectra. Per each couple of spectra, the one showing the larger value of the relevant S_a at the considered conditioning period shows also the same $S_a(T = 1s)$ value per each of the 20 pairs of GMs considered at such intensity level (continuous line in the plot). This is the mathematical restraint introduced by the CSM. On the contrary, spectra showing the smaller value of the relevant S_a between the generic couple of GMs did not have any limitation or restraint (dashed lines in the plot). Additionally, Figure V.2 shows mean (pseudo-) acceleration response spectra for the considered ground

motions by varying the IM. These spectra were computed starting from GMs selecting with the CSM for a period of vibration equal to $T^* = 1\ s$. Each plot shows ten spectra associated to ten different values of the intensity measure. Such spectra are related to the bi-directional ground motion inputs for the considered 3D numerical models, respectively for the transverse (portal frame) (X) and longitudinal (braced) (Y) building direction. As one can see, mean spectral shapes and values were very similar by varying the considered building direction. A similar plot was built by varying the seismic hazard (and, consequently, the record database) with a conditioning period $T^* = 0.5\ s$.

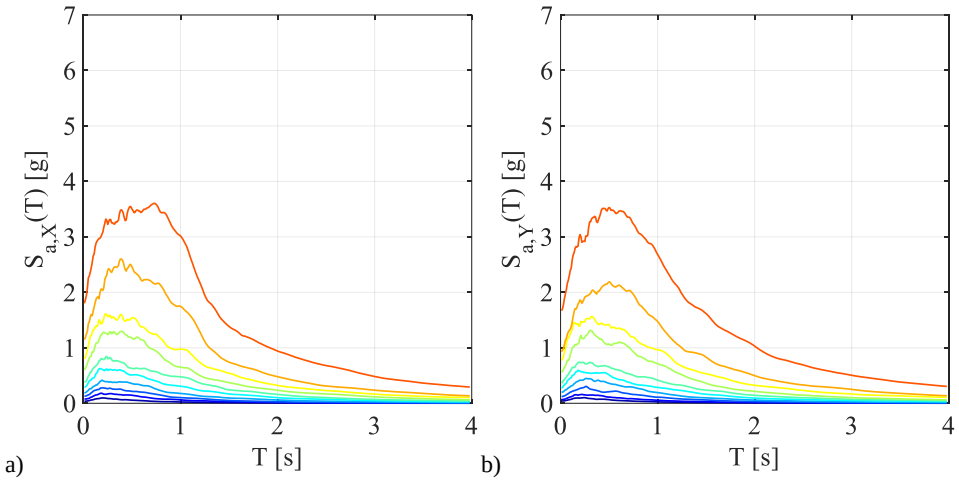

Figure V.2 Mean pseudo-acceleration response spectra for increasing earthquake return periods at T^*=1 s: (a) X-components of GMs; (b) Y-components of GMs.

Figure V.3(a) and (b) show the mean pseudo-acceleration response spectra, for the X and Y building directions, respectively. Such spectra were used to model the seismic actions in the transverse (X) and longitudinal (Y) building directions for the models including the building envelope (for both sandwich panels and trapezoidal sheeting because of the small difference of periods of vibration in the two cases (Chapter IV). As for the cases in Figure I.2, the mean spectral shapes

and values are similar for the two building directions. On the contrary, comparing the plots in Figure V.3 with those in Figure V.2, one can clearly observe variations in both spectral shapes and values. Clearly, the smaller is the conditioning period, the larger is spectral pseudo accelerations.

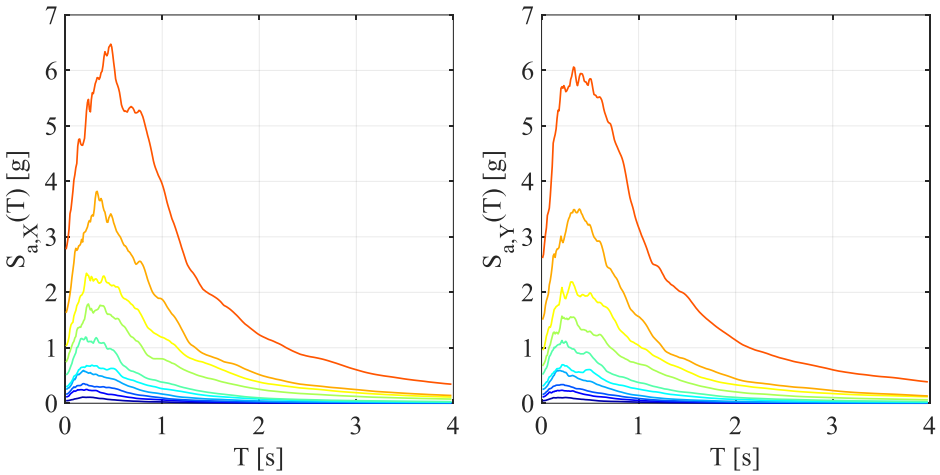

Figure V.3 Mean pseudo-acceleration response spectra for increasing earthquake return periods at T^*=0.5s: (a) X-components of GMs; (b) Y-components of GMs.

In 3D numerical models, the structural response distribution which is estimated by conducting non-linear time history analyses depends on either the orientation (Rigato *et al.*, 2007, Magliulo *et al.* 2014) or the number of records used (Baltzopoulos *et al.*, 2018). However, recent research (Giannopoulos and Vamvatsikos, 2018) proved that the record-to-record variability practically hides the influence of the incident angle. Therefore, the time-history analyses were carried out by choosing randomly the orientation of the X and Y ground motion components. As explained by Giannopoulos and Vamvatsikos (2018), the actual angle of incidence depends on the fault-structure relative orientation, which is generally unknown. The random choice is supposed to avoid a conservative evaluation of the mean annual frequency of exceeding specified limit states (i.e.,

the collapse limit state in this research study). Anyway, additional numerical analyses specifically addressed to investigate the effect of the incidence angle could be foreseen as useful further developments helping in clarifying completely the issue.

V.3 Multi-stripe analysis results

Multi-stripe or multiple-stripe analysis (MSA) (Jalayer and Cornell, 2009) is a method used to perform probabilistic seismic assessment over a wide range of ground motion intensities and multiple performance objectives, such as global collapse. The method uses structural analysis results obtained by non-linear time history analyses (NLTH). As suggested by the name, it refers to a group of stripe analyses performed at multiple spectral acceleration levels (or return period, T_R, of the seismic action), where a stripe analysis consists of structural analyses for several ground motion records that are scaled properly to obtain a common spectral acceleration (this is the case of the CSM). Indeed, the suite of ground motion records used for performing each stripe analysis ideally represents the seismic risk at the corresponding spectral acceleration. Similar to the incremental dynamic analysis procedure (IDA) (Vamvatsikos and Cornell, 2002), the MSA output is a relationship between a chosen engineering demand parameter (EDP) and the value of the intensity measure which represents the seismic intensity at the generic stripe. Because the set of GMs usually changes passing from an intensity measure value to another, the obtained relationship is not a continuous function, rather, a set of points for each different (discrete) intensity level for which the analyses are performed. In the cases described hereafter, each intensity level has 20 couple of values of (IM, EDP), corresponding to the structural response arising from each NLTH performed by using the generic pair of GMs. Differences among GMs can occur due to the record-to-record variability (Shome *et al.*, 1998), thus generating a distribution of the structural response for a given intensity level of the seismic action.

The following sections summarize results obtained computing a set of 20 pair of GMs per 10 different intensity measure values (IMs) of the seismic risk, according to what discussed in section V.2. Therefore, for each considered case study, 200

non-linear time history analyses were performed, considering by-directional ground motion input on the relevant 3D numerical models. A total of 2400 time history analyses were conducted to assess seismic response of the considered archetype non-residential single-story older steel buildings, by varying design assumptions and connections details. In all the examined cases, analyses were artificially interrupted when drifts were predicted to be larger than the maximum (previously defined) threshold value between the two building directions. This artificial cut was done to reduce the computational time, since inelastic response after reaching the considered drift threshold was not realistically represented.

The section is subdivided in 3 sub-sections. In the first sub-section, results of numerical analyses are summarized and discussed. In the second subsection, a wide range of model-to-model comparisons are carried out, emphasizing differences in structural response for intensity measures in which collapse did occur and did not occur. The third subsection highlights the structural response of the relevant components per each considered numerical model. Behavior of the buildings during significant (specific) time history analyses was discussed. The effect of the cladding panel type focusing on the collapse limit state is also extensively discussed.

V.3.1 PCB case studies

V.3.1.1 Bare frame model with SHS braces

Figure V.4(a) shows MSA results for the bare frame model with pinned column base connection in the transverse direction and SHS vertical brace cross sections with welded connections (PCB-SHS-BF). Results are shown as a relationship of the IM value with the corresponding peak values (observed during the generic NLTH) of the transverse drift among the five portal frames ($d_{X,peak}/H$). Also, the plot shows the value of the drift corresponding to 50% of loss in transverse base

shear force resistance with respect to the maximum value ($d_{X,C}/H$) with a vertical dashed line. For each analysis stripe, a box shows the numbers of GMs for which collapse was observed (i.e., exceeding the considered threshold value).

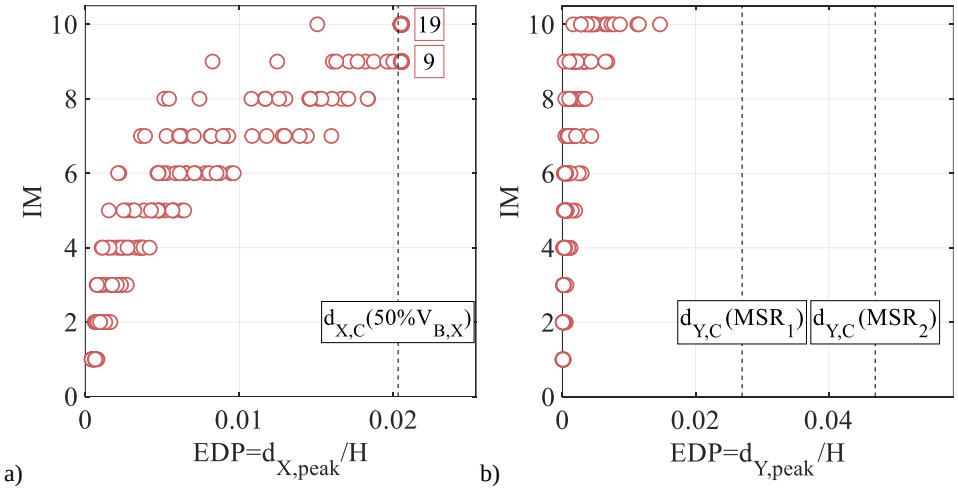

Figure V.4 MSA results for the PCB-SHS-BF model: (a) transverse direction response; (b) longitudinal direction response.

Collapses were computed independently between the two building directions. Distinction in triggering global collapse as a function of the building direction is carried out subsequently. In this case study, only the two larger IM values were interested to failures (i.e., IM = {9, 10}). The record-to-record variability increases with the IM value, since the model experienced large inelastic displacements. The same plot is build considering longitudinal drifts (Figure V.4(b)). In such plot, the two drift values corresponding to the two fracture capacities MSR_i are shown as dashed lines. Longitudinal drifts were predicted to be smaller than the transverse drifts, because of the larger stiffness of the building provided by the vertical braces. No failures occurred in the considered direction.

V.3.1.2 Models with envelope and SHS braces

Similarly, Figure V.5(a) shows the transverse direction MSA results for the PCB-SHS-SP model (i.e., the model with sandwich panels as cladding panels) by using transverse peak drift as EDP, while Figure V.5(b) shows results for the longitudinal direction by changing the relevant EDP (i.e., the longitudinal peak drift). Threshold values corresponding to triggering of the global collapse limit state are plotted as dashed lines. Such limit drift values were that identified by using pushover analysis (Chapter IV). Also, the number of collapse cases are highlighted within a box. Larger orange circles indicate analysis cases for which brace fracture occurred during time history, i.e. the model predicted explicitly brace fracture by reaching the MSR_2 capacity value (the one calculated according to the analytical model proposed by Hsiao *et al.*, 2013). Collapse in the transverse direction was predicted to be always dominant with respect to the longitudinal direction. Collapses started to occur at IM = 7, in the transverse direction. However, only at the larger IM values (i.e., IM = {9,10}), collapses were predicted to occur also in the longitudinal direction. Observed brace fracture cases are in good agreement within the pushover results. However, few cases of brace fractures were observed. Longitudinal drifts for cases exhibiting brace fractures were predicted to be larger than that corresponding to triggering of global collapse for the MSR_1 capacity value within the pushover analysis. Figure V.5(c) and (d) show similar results for the PCB-SHS-TS model (i.e., the model with trapezoidal sheeting as cladding panels). As expected, the worst structural response was predicted with the TSs because of the poorer performance of such cladding panels with respect to the SPs. Particularly, analysis shows an increase in the number of failure cases, which were predicted to start at IM = 6, prior to that observed with the SPs. The model predicted a small number of brace fracture cases with respect to the SP case study. The two end stripes (i.e., IM = {9,10}) were interested by brace fractures. Such cases are highlighted within larger orange circles in the plots.

At IM = 9, brace fractures were predicted to occur for values of the longitudinal drift smaller than that corresponding to triggering of global collapse for the MSR_1 capacity value.

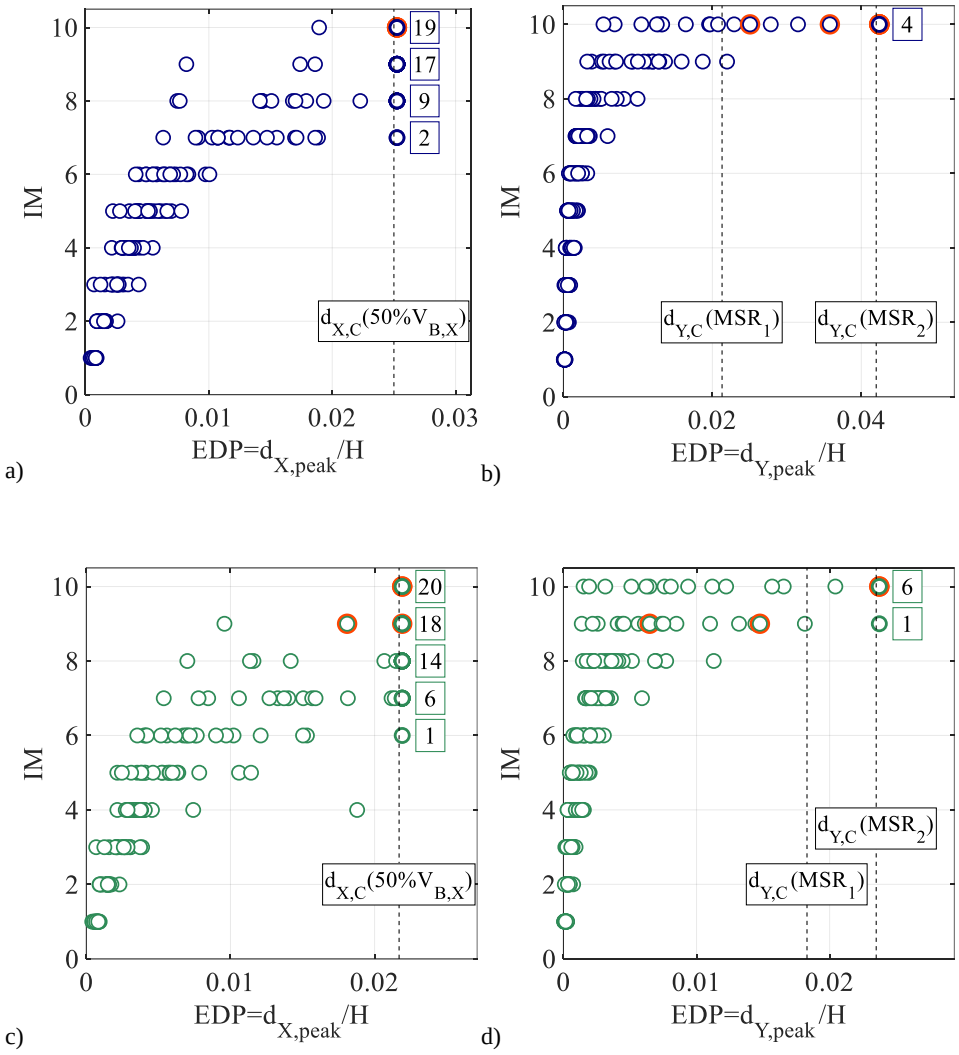

Figure V.5 MSA results for the PCB-SHS model:
SP model response in (a) transverse and (b) longitudinal directions; TS model response in (c) transverse and (d) longitudinal directions.

V.3.1.3 Bare frame model with 2L braces

Figure V.6 shows MSA results for the building with pinned column base in the transverse direction and 2L vertical braces with bolted connections (PCB-2L-BF), for both the transverse (Figure V.6(a)) and the longitudinal (Figure V.6(b)) directions. The same EDPs are used to assess structural response, considering, both transverse and longitudinal, peak drifts among the five portal frames. Because brace connection failure did not depend on the loading history, only one threshold value ($d_{Y,C}/H$) is shown in the plot of the longitudinal direction results. Results were very similar to the previous (i.e., PCB-SHS-BF) with respect to the drifts distribution and collapse cases in the transverse direction.

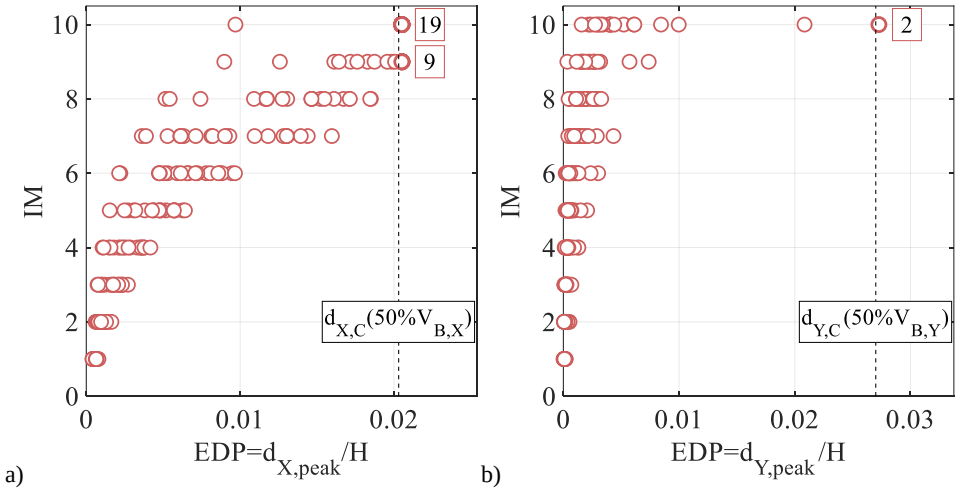

Figure V.6 MSA results for the PCB-2L-BF model:
(a) transverse direction response and (b) longitudinal direction response.

Differences can be observed looking at the longitudinal direction results. Such differences were consequences of the variation of brace cross section and

connections, passing from SHS with welded connections and 2L with bolted connections. Within the 2L solution, 2 new collapse cases were predicted by the numerical model in the longitudinal direction at the highest IM value.

V.3.1.4 Models with envelope and 2L braces

Similarly, MSA results for the numerical models which explicitly include the building envelope are summarized in Figure V.7(a) and (b) (cladding made by SPs) and in Figure V.7(c) and (d) (cladding made by TSs). Both the models predicted increase in global collapse cases with respect to the longitudinal direction. These results were a consequence of the vertical brace connection failures. Such difference in behavior with respect to the SHS brace model was expected and confirmed by pushover analysis results (Chapter III), for which rather brittle structural response were observed looking at cases with 2L vertical braces.

Notwithstanding, only the two end stripes were interested by brace connection failures and, consequently, to global collapse. Also in these cases, the worst structural response was predicted to occur when trapezoidal sheeting were used as cladding panels, in agreement with the results obtained using the non-linear static analysis. Also, effect of the record-to-record variability increased passing from the SP model to the TS model. This was a consequence of the larger inelasticity exhibited by the TSs with respect to the SPs.

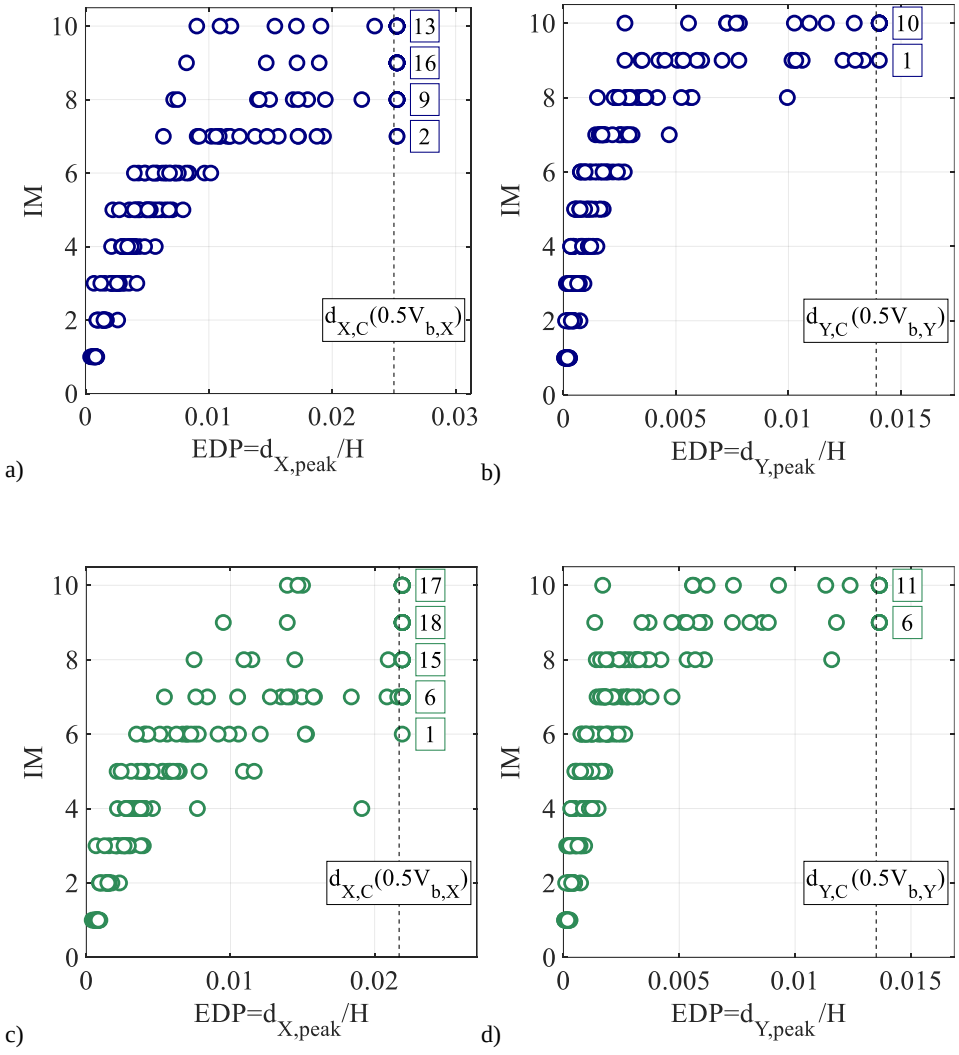

Figure V.7 MSA results for the PCB-2L model:
SP model response in (a) transverse and (b) longitudinal directions; TS model response in (c) transverse and (d) longitudinal directions.

V.3.1.5 Anchor fracture

Fracture of anchors in column base connections of the PCB models can occur prior to exceeding the defined drift thresholds associated with pushover strength degradation for both transverse and longitudinal directions.

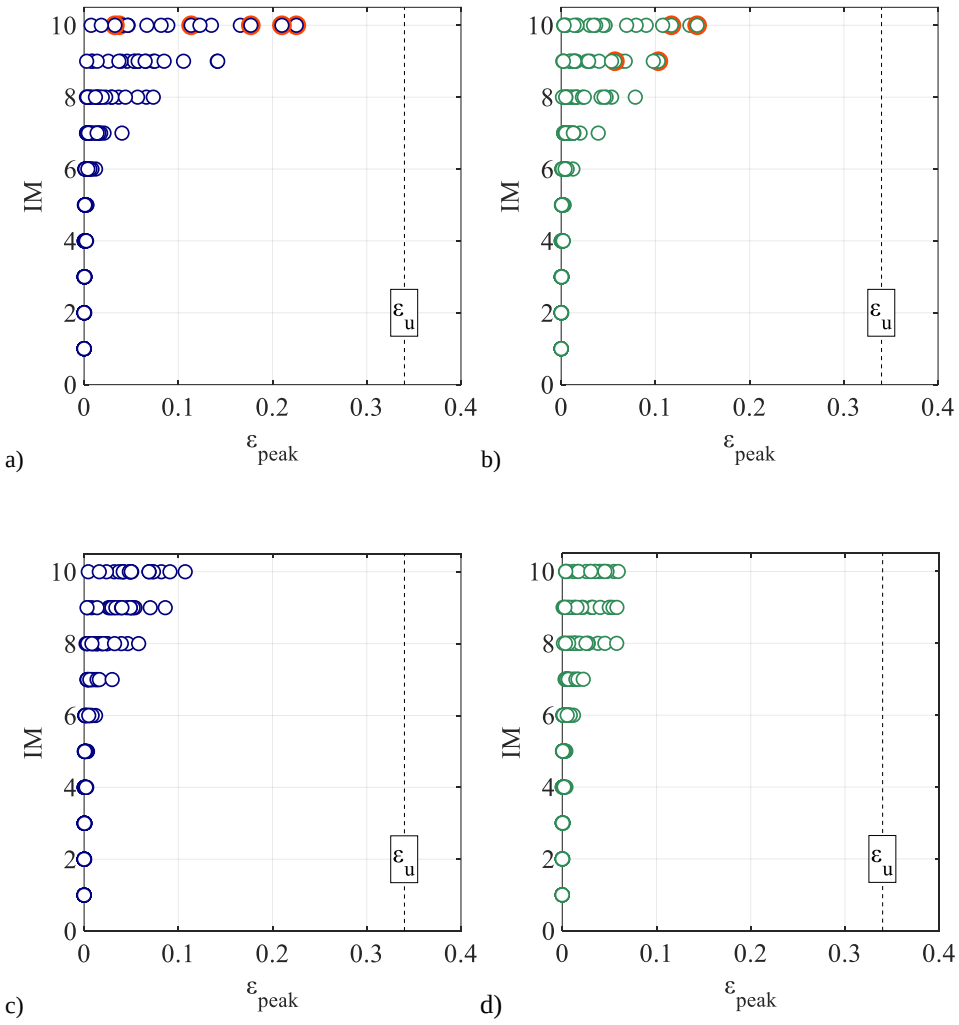

Figure V.8 Peak strain demands in anchors:
(a) PCB-SHS-SP model; (b) PCB-SHS-TS model; (c) PCB-2L-SP model; (d) PCB-2L-TS model.

To assess such failure mechanism during MSAs, anchors peak strains for each NLTH analysis were evaluated and compared to the relevant strain limit value (ε_u). Results are summarized in Figure V.8(a) and (b), respectively for the PCB-SHS-SP and TS model, and in Figure V.8(c) and (d), respectively for the PCB-2L-SP and TS model. Results are shown as relationship between the IM value and the strain peak (ε_{peak}) among all the equivalent anchors at the column base connections. In the plot, the strain anchor capacity (ε_u) is shown with a dashed line. Results show the absence of anchors fracture for all the considered case studies. Models considering SHS brace cross section predicted larger strain peak in anchors, for both the cladding types. However, strain peak results were predicted to be not larger than 22%. Additionally, results show that the peak strains were not necessarily related to triggering of brace fracture. Within the 2L case studies, strain peak values were predicted to be not larger than 10% (SP) or than 8% (TS). In these last cases, results were in line with what observed performing pushovers. Indeed, no failures of anchors were predicted within 2L case studies when structural response was assessed with static methods (Chapter IV).

V.3.1.6 Force-based column checks

Because of the bi-directional ground motion input, columns were subjected to axial forces and bi-directional bending moments, differently from the pushover analyses. For this reason, and also investigating any potential differences in the dynamic response compared with the predictions from the static non-linear analysis, both column buckling and resistance were checked step-by-step during post processing of the numerical results. Since columns were modelled as elastic elements, three checks were necessary: (i) resistance check (labelled as *R*); (ii) in-plane buckling check (labelled as *IPB*); out-of-plane buckling check (labelled as *OPB*). The member capacities for the *R*, *IP* and *OPB* failure modes were evaluated

according to Eurocode 3 (CEN, 2005), by applying Equations (5.1), (5.2) and (5.3) respectively. In the equations: (i) *y* identifies the cross section strong-axis; (ii) *z* identifies the cross section weak-axis; (iii) M_R is the cross section bending moment resistance, while $M_{N,R}$ identify the flexural resistance considering interaction with a concomitant axial force (*n* is the normalized axial force with respect to the cross section plastic resistance); (iv) k_{ij} are the interaction factors, which are a function of the applied axial force and the bending moment distribution; (v) χ_i are the buckling factors for the in-plane buckling (χ_y), out-of-plane buckling (χ_z) and lateral-torsional buckling (χ_{LT}).

$$\left(\frac{D}{C}\right)_R = \left(\frac{M_y}{M_{N,y,R}}\right)^2 + \left(\frac{M_z}{M_{N,z,R}}\right)^{\max(1,\ 5n)} \tag{5.1}$$

$$\left(\frac{D}{C}\right)_{IPB} = \frac{N}{\chi_y N_R} + k_{yy}\frac{M_y}{\chi_{LT} M_{R,y}} + k_{yz}\frac{M_z}{M_{R,z}} \tag{5.2}$$

$$\left(\frac{D}{C}\right)_{OPB} = \frac{N}{\chi_z N_R} + k_{zy}\frac{M_y}{\chi_{LT} M_{R,y}} + k_{zz}\frac{M_z}{M_{R,z}} \tag{5.3}$$

The postprocess of the numerical result was carried out for each analysis step prior to reaching the global collapse condition, thus varying both M_y, M_z, *N* actions and resistances. Figure V.9 shows the peak demand over capacity ratios $(D/C)_R$ in main columns, by varying the considered GM and the seismic intensity (IM). Figure V.9(a) and (b) are related to the PCB-SHS-SP and TS models, respectively, whilst Figure V.9(c) and (d) highlights results concerning the PCB-2L-SP and TS models.

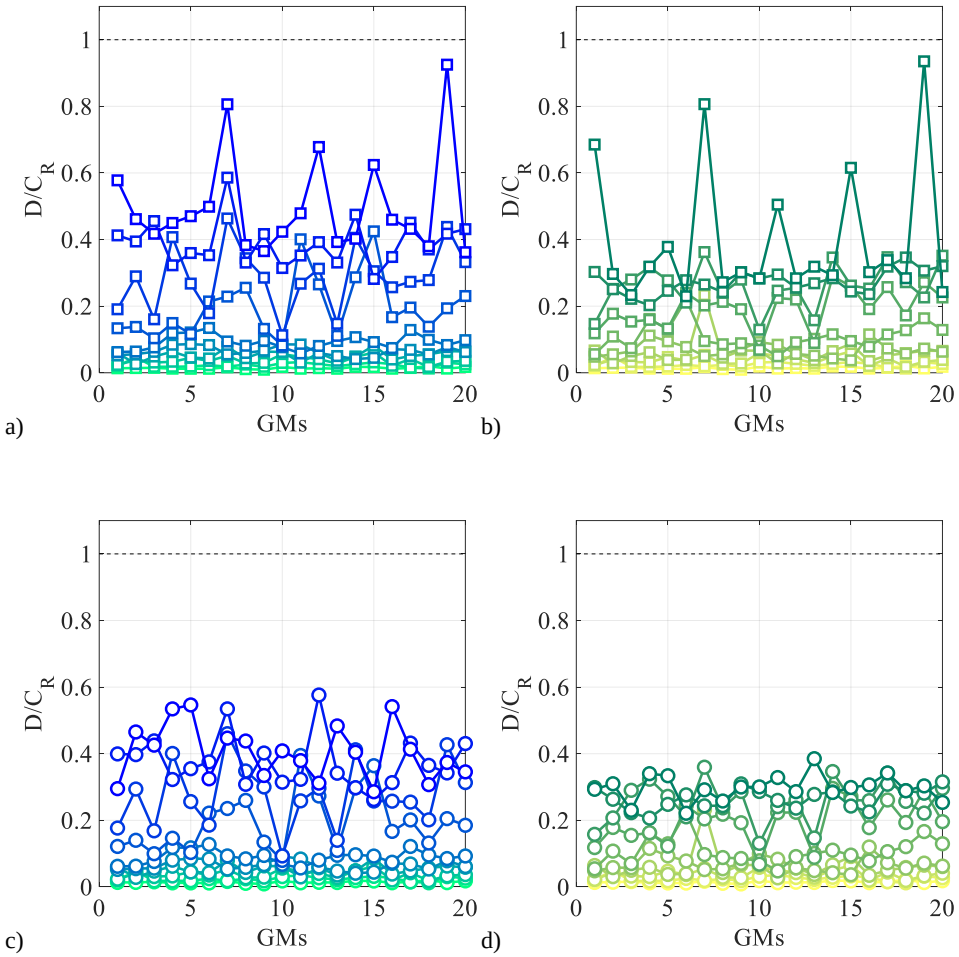

Figure V.9 Cross section plastic resistance checks for columns:
(a) PCB-SHS-SP model; (b) PCB-SHS-TS model; (c) PCB-2L-SP model; (d) PCB-2L-TS model.

MSA confirmed results arising from non-linear static analyses in terms of column cross section resistance. Larger demand over capacity values were observed when SHS brace cross section were used if compared with the 2L solutions. In fact, the brace connection failures in 2L models led to a decrease of the longitudinal drift

demands. SHS brace yielding and strain hardening increased internal actions in column up to 90% of the column cross section resistance, considering both cladding made by SPs and TSs. Values of *D/C* highly reduced moving on 2L brace cross section with bolted connections. Peak values between the 200 analysis results were approximatively equal to 0.60 (PCB-2L-SP) and 0.40 (PCB-2L-TS).

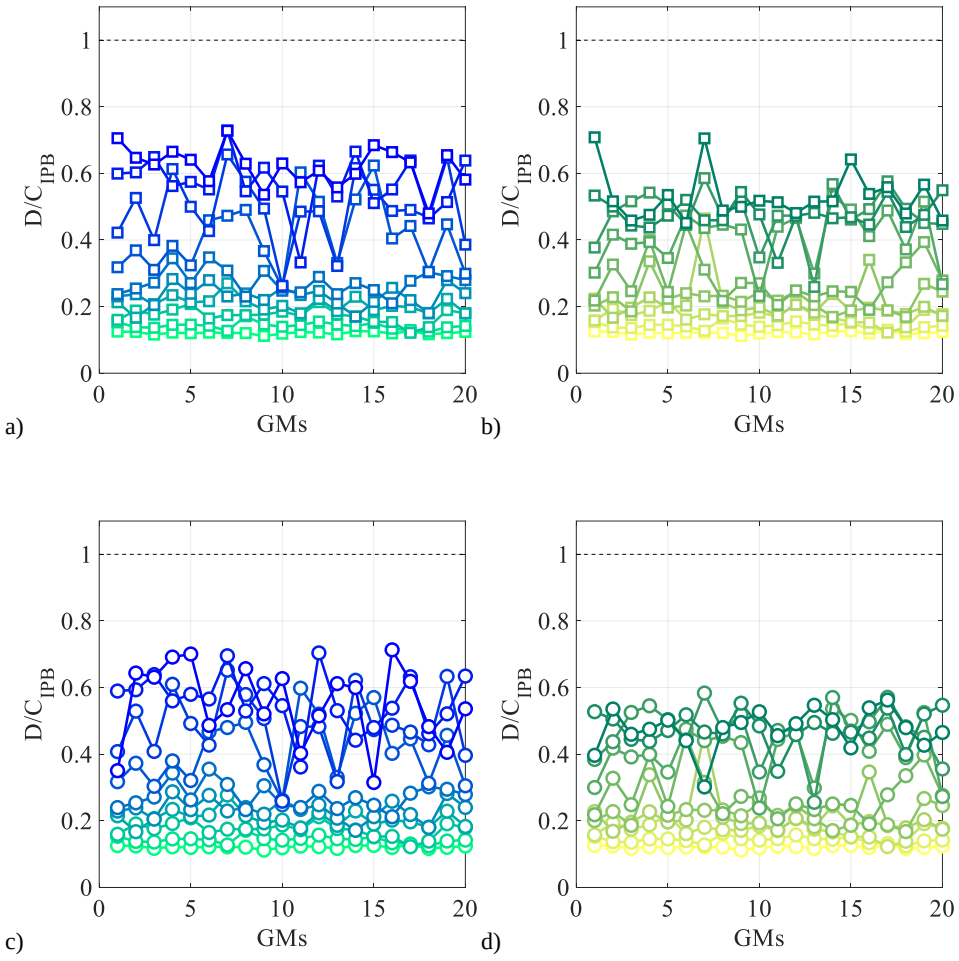

Figure V.10 In-plane buckling checks for columns:
(a)PCB-SHS-SP model; (b)PCB-SHS-TS model; (c)PCB-2L-SP model; (d)PCB-2L-TS model.

Figure V.10(a) and (b) are related to the IPB checks for the PCB-SHS-SP and TS numerical models, respectively, whilst Figure V.10(c) and (d) are related to the PCB-2L-SP and TS numerical models. Both the brace types led to similar results in terms of *D/C* values for IPB checks. Generally, SP cladding type led to larger *D/C* values with respect to the TS cladding type. The brace strain hardening, the secondary frame effect and the larger resistance offered by the SP cladding elements increased internal force in column members. A similar condition was related to the model with TS cladding elements. Maximum *D/C* values are smaller than 0.8 for all the considered numerical models. Larger *D/C* values among all the NLTH analyses passed from 0.75 (PCB-SHS-SP) and 0.70 (PCB-SHS-TS) to 0.70 (PCB-2L-SP) and 0.60 (PCB-2L-TS).

In Figure V.11(a) and (b), results are shown for the OPB checks for PCB-SHS-SP and TS models, whilst Figure V.11(c) and (d) are related to PCB-2L-SP and TS models. As expected, OPB led to the larger *D/C* values in the case of PCB-SHS-SP model. In fact, this is the worst condition due to buckling for the columns. However, results confirmed the columns overstrength caused by design of columns fulfilling serviceability limit state (Chapter II). Maximum *D/C* values are slightly below the unity when SHS braces are considered. It is important to note that, for such cases, global collapse was predicted to occur due to exceedance of the drift threshold in the transverse direction. On the contrary a significant decrease of the *D/C* values is observed in the plot when 2L braces are considered. Maximum *D/C* values passed from 0.98 (PCB-SHS-SP) and 0.97 (PCB-SHS-TS) to 0.82 (PCB-2L-SP) and 0.63 (PCB-2L-TS).

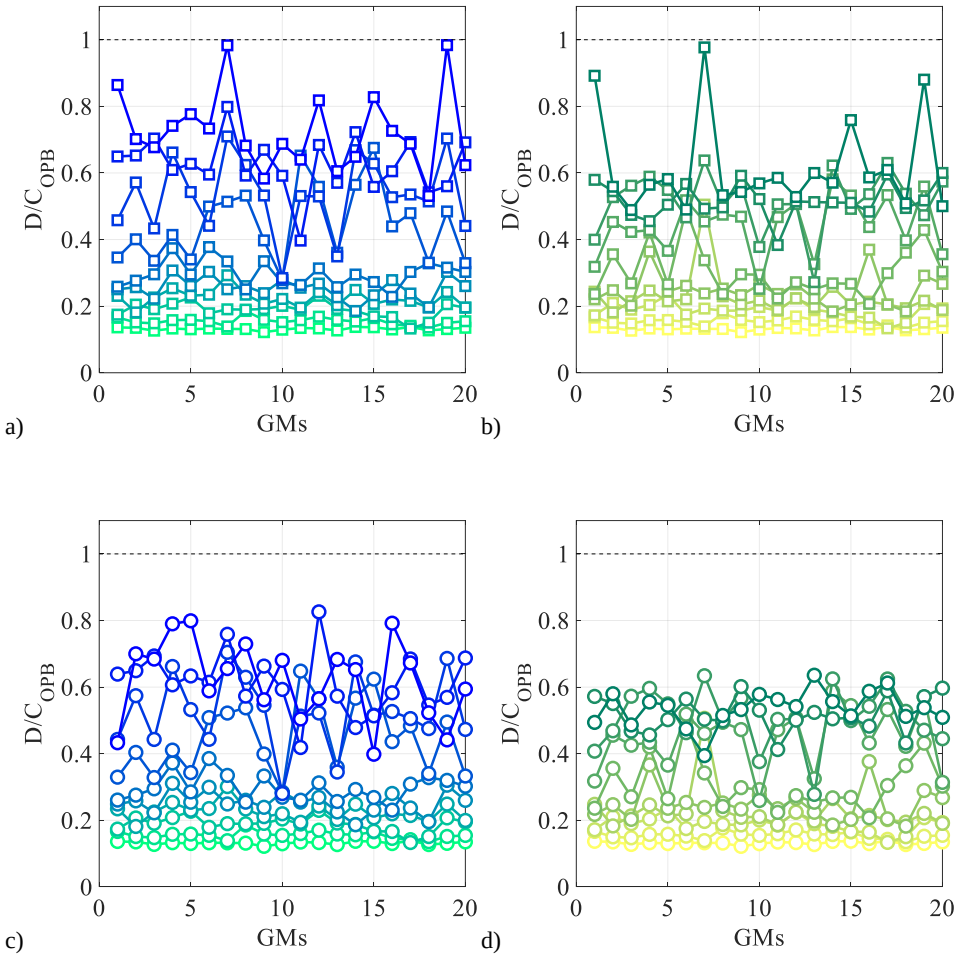

Figure V.11 Out-of-plane buckling checks for columns:
(a)PCB-SHS-SP model; (b)PCB-SHS-TS model; (c)PCB-2L-SP model; (d)PCB-2L-TS model.

V.3.2 SCB case studies

V.3.2.1 Bare frame model with SHS braces

Multi stripe analysis results related to the models with semi-continuous column base connections (SCB) and SHS vertical braces with welded connections are summarized in this section. First, results concerning the dynamic response of the bare frame model (BF) are shown. To easily represent comparison with the numerical models with pinned column base connection (i.e., PCB), the same post-process of the numerical results in shown here.

Figure V.12 shows MSA results for the SCB-SHS-BF case study. Results are shown as a relationship of the IM value with the corresponding peak values (observed during the generic NLTH) of the relevant drift among the five portal frames ($d_{X,peak}/H$ for the transverse direction, $d_{Y,peak}/H$ for the longitudinal direction). Also, the plot in Figure V.12(a) shows the value of the drift corresponding to 50% of loss in the transverse base shear force resistance ($d_{X,C}/H$) with a vertical dashed line. Instead, two vertical dashed lines represent drifts corresponding to 50% of loss in the longitudinal base shear force resistance in the plot of Figure V.12(b). The two corresponding drift values ($d_{Y,C}/H$) were related to the two different MSR_i values used to assess brace fracture and propagation with the non-linear static analysis. Such values, which represents triggering of the collapse limit state, are theoretically defined in Chapter III and numerically evaluated in Chapter IV. For each analysis stripe, a box shows numbers of GMs for which collapse was observed (i.e., counting GMs exceeding the considered threshold value). Only the last three analysis stripes were interested to exceedance of the threshold values. Therefore, collapse limit state was triggered in the transverse building direction.

Brace fractures were predicted at the larger IM value for only two GMs (an orange empty circle highlights such cases). For both the considered GMs, peak longitudinal drifts were similar each other and in between the two drifts corresponding to the loss in longitudinal base shear force resistance as predicted by pushover analysis. For one of the two GMs, collapse in the transverse direction also occurred. Therefore, the building was considered collapsed. On the contrary, peak drift in the transverse direction for the other GM was predicted to be very far from that reaching the threshold value (less than 2%). However, (i) since the analysis was completed (i.e., no numerical instabilities occurred and the whole GM signal was integrated numerically) and (ii) the longitudinal peak drift did not exceed that evaluated using the MSR_2 fracture capacity value, such analysis case was not considered as collapse case. Longitudinal drift demands predicted by the numerical analyses were less than 4%. However, since analysis was interrupted artificially if the transverse drift limit was exceeded, such peak drift demands can be influenced by the behavior of the building in the transverse direction.

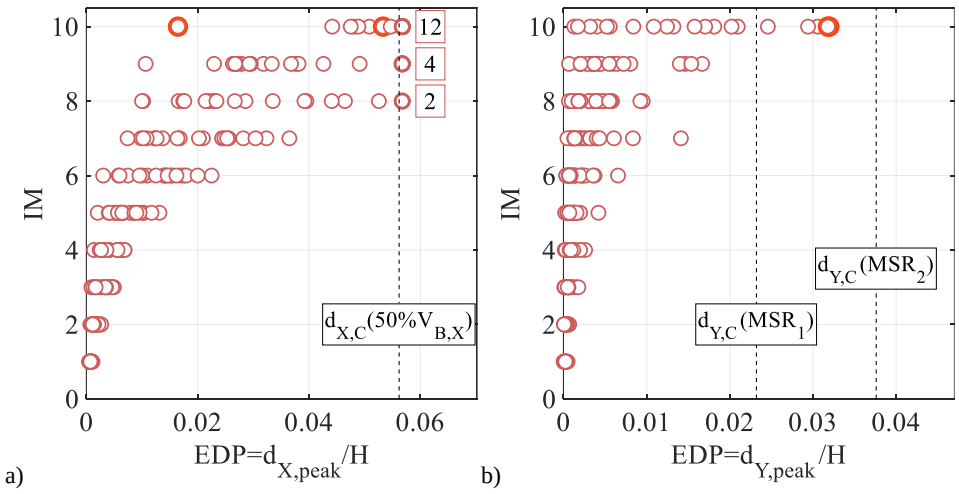

Figure V.12 MSA results for the SCB-SHS-BF model:
(a) transverse and (b) longitudinal direction response.

V.3.2.2 Models with envelope and SHS braces

Figure V.13(a) and (b) summarize MSA results for the SCB-SHS model with explicit numerical consideration of the envelope panels and the secondary steelworks. First, results are described for the cladding made by sandwich panels (SP). The transverse drift peak ($d_{X,peak}/H$) and the longitudinal drift peak ($d_{Y,peak}/H$) among the five portal frames were considered as EDP, respectively for analysis of the transverse and the longitudinal building response. Pushover threshold values corresponding to 50% loss in base shear force resistance, in transverse and longitudinal direction, are shown as dashed lines. In the transverse direction, only one threshold is plot, whilst in the longitudinal direction, the two longitudinal drift values corresponding to the two *MSR* brace fracture capacities are shown. Same results are shown in Figure V.13(c) and (d), considering TSs as cladding elements. Drift limits modelling triggering of global collapse were selected according to the relevant non-linear static analysis results. They are shown as dashed lines in the plots. For the SCB-SHS-SP model, collapse started from IM = 7, predominantly in the transverse direction. Several GMs producing brace fractures were observed at the largest IM value (orange empty circles indicate such cases in the plot). Therefore, collapse was triggered also for exceedance of lateral drifts in the longitudinal direction. The observations hold true for the SCB-SHS-TS model. In this case, structural collapses started at IM = 6, one IM value prior to that observed within the model with SP cladding elements. Collapses in the longitudinal direction were predicted for both IM = 9 and IM = 10. For both the cladding types, brace fractures during the NLTHs were predicted only at the largest IM value (IM = 10). In the braced direction of the SCB-SHS-TS model, the collapse criteria evaluated using the pushover analysis did fail for one GM at IM = 9. In fact, analysis did not predict brace fracture. However, longitudinal drift demand for such GM was larger than that corresponding to the EDP value associated with the

occurrence of brace fracture within pushover analysis. This was a consequence of the interaction between the two building directions.

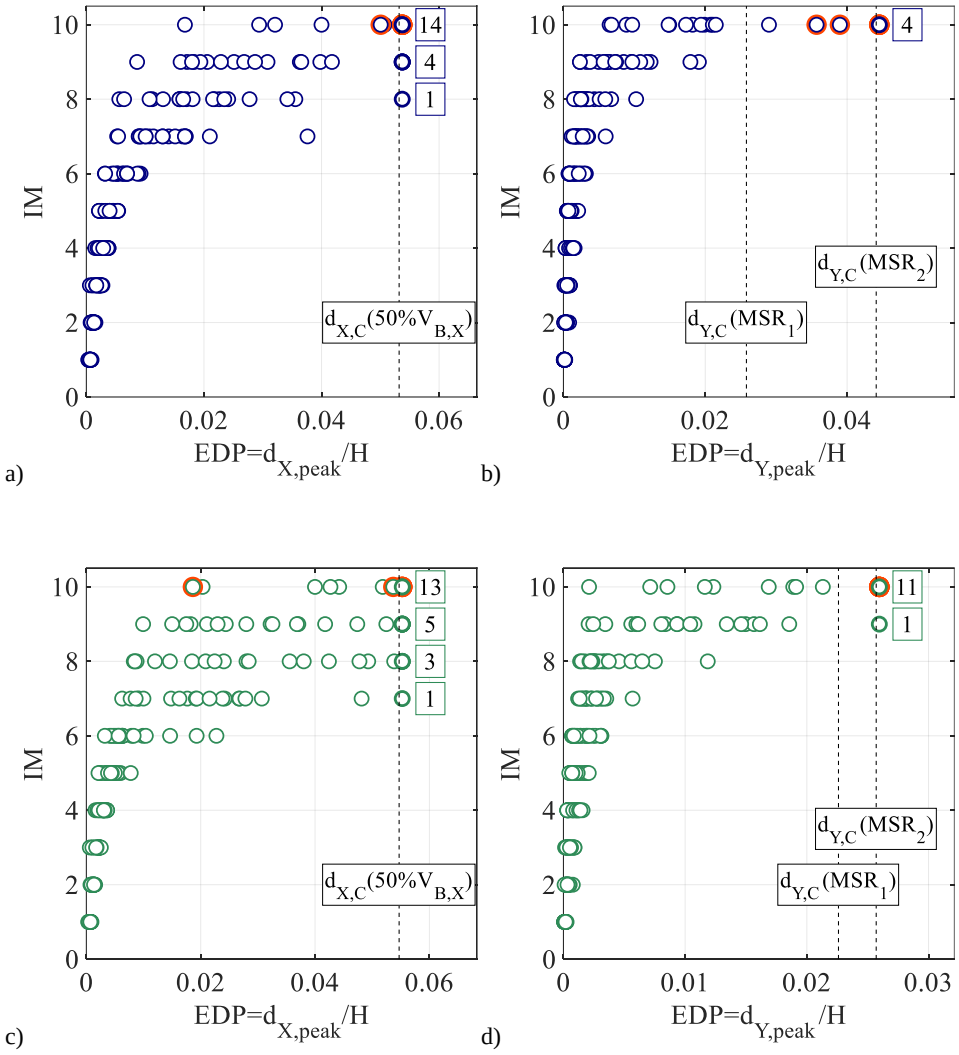

Figure V.13 MSA results for the SCB-SHS model:
SP model response in (a) transverse and (b) longitudinal directions; TS model response in (c) transverse and (d) longitudinal directions.

Particularly, yielding of column base connections in the transverse direction was always predicted to occur when transverse drift demands exceeded 1% (i.e., for IM > 5). Yielding of column base connections implied reduction of the transverse lateral stiffness and a consequent reduction of the longitudinal lateral stiffness. This reduction of the lateral stiffness modified longitudinal structural response with respect to that computed using pushover analysis. Therefore, larger longitudinal drifts associated with the triggering of brace fracture can occur during the dynamic simulation.

V.3.2.3 Bare frame model with 2L braces

Figure V.14(a) and (b) summarize MSA analysis results for the SCB-2L-BF model, considering the transverse building direction and the longitudinal building direction response, respectively.

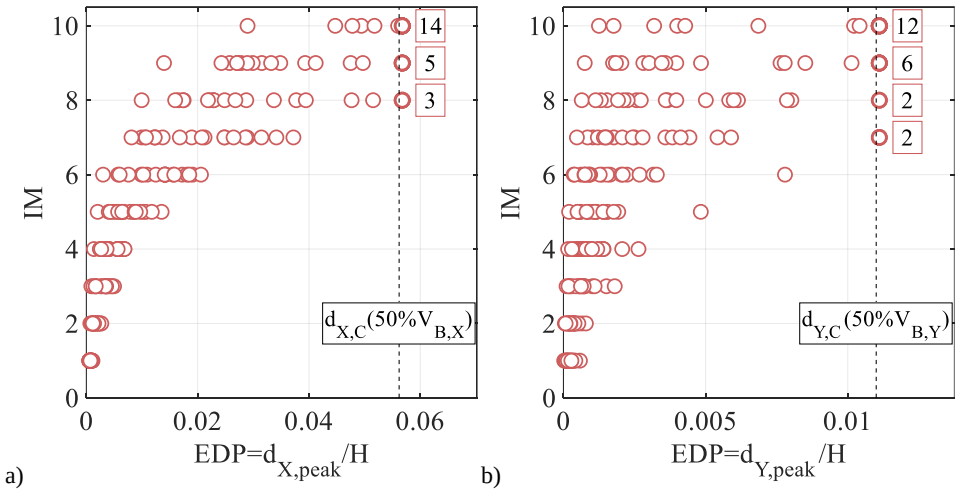

Figure V.14 MSA results for the SCB-2L-BF model:
(a) transverse and (b) longitudinal direction responses.

Results are shown as relationship between the IM values and the relevant EDPs in the considered building direction. Lateral peak drifts during the generic NLTH analysis were considered as relevant EDPs, (labelled as $d_{X,peak}/H$ and $d_{Y,peak}/H$, respectively). In such cases, structural collapse was assessed by only considering one drift threshold per building direction, indicating them in the two plots as $d_{X,C}/H$ and $d_{Y,C}/H$. According to the pushover results, such limits corresponded to collapse due to fracture of column base connection anchors (transverse direction) and due to failure of bolted connections in vertical braces (longitudinal direction). Because of the low ductility exhibited by brace connections, number of collapses in longitudinal direction became similar to that observed in the transverse direction. Indeed, failures were observed starting from IM = 7 (T_R = 2500 *y*) in the longitudinal direction. However, collapse cases in the transverse direction were similar to that observed in the longitudinal direction.

V.3.2.4 Models with envelope and 2L braces

Figure V.15(a) and (b) summarize results concerning SCB-2L-SP model. The same EDP values were considered to assess structural response for both the transverse and the longitudinal direction. Drift limits corresponding to global collapse are shown with dashed lines. In such case, the SP cladding contribution increased the collapse capacity of the building. Consequently, collapse cases in the longitudinal direction drastically decreased from that observed within the bare frame structural response. Collapses started at IM = 8 (T_R = 5000 *y*) in the transverse direction (i.e., due to failures of column base connections in such direction), whilst longitudinal collapses were predicted only at the largest IM value (T_R = 100000 *y*). Similarly, Figure V.15(c) and (d) summarize results concerning the SCB-2L-TS model, by using the same EDP values. Also, drift limits due to triggering of global collapse of the building according to pushover results are shown in the plots as dashed lines. Failure started in the transverse

direction at IM = 7 (T_R = 2500 *y*), while they became predominant in the longitudinal direction as increasing intensity measure value.

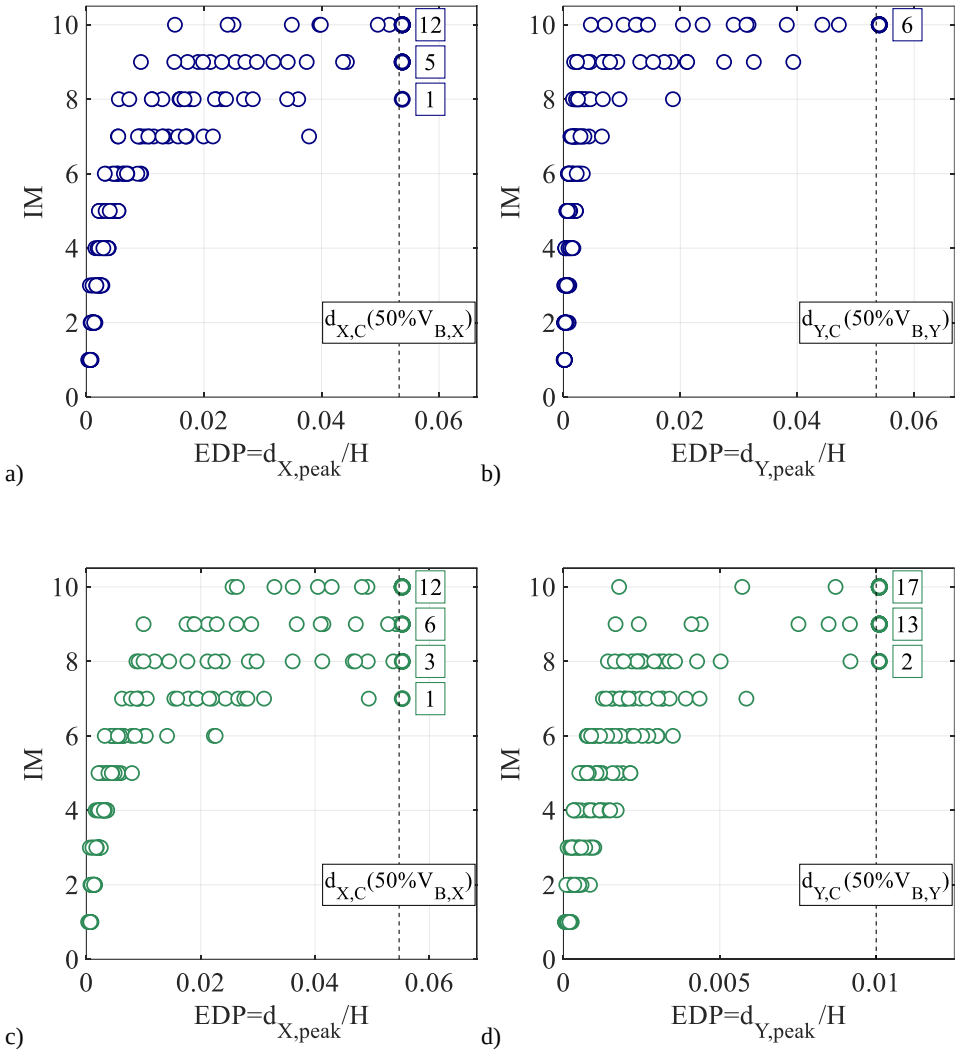

Figure V.15 MSA results for the SCB-2L: SP model response in (a) transverse and (b) longitudinal directions; TS model response in (c) transverse and (d) longitudinal directions.

This was a consequence of the lower $d_{Y,C}/H$ value due to brace bolted connection failures. Since the contribution of the trapezoidal sheeting did not introduce significant improvement with respect to the bare frame response, structural response was very similar to that observed with the bare frame structure, as already observed with the pushover analysis results (Chapter III).

V.3.2.5 Force-based column checks

Main columns of the building were modelled as elastic elements also in the SCB case studies. A confirmation of the accuracy of such modelling strategy can be made by proving such assumption during non-linear time history analyses. Both column resistance and buckling checks were here post-processed for the examined SCB case studies. It can be useful to remember that column cross section slightly reduced passing from the PCB to the SCB structures, from the hot-rolled HE 500 M profile to the HE 450 M profile. This was a consequence of variation in design lateral stiffness passing from the PCB case studies to the SCB case studies (Chapter II). In the SCB case, a perfect fixed column was considered during the design phase, as discussed in the previous chapter. As suggested by pushover analysis results, due to limitation provided by yielding of column base connections in the transverse direction, one can expect local forces in column member smaller than that observed in the PCB case studies (one can simply compare PCB-BF and SCB-BF transverse pushover curve in Chapter IV, looking at the maximum base force resistance developed in both cases). Notwithstanding, variation in column cross section properties did not allow to rule on column stability and/or resistance a-priori: analysis results must be post-processed to obtain an answer. Therefore, the already discussed demand over capacity ratios (*D/C*) for both resistance checks (labelled as R), in-plane buckling checks (labelled as IPB) and out-of-plane buckling checks (labelled as OPB) were calculated. Checks were carried out in order to evaluate differences from pushover

results due to bi-directional ground motion input and to compare column effort by varying design assumptions. It is important to stress the main role offered by columns for the seismic stability of the whole building. Also, such phenomena highly increase the possibility to trigger global collapse. In fact, column buckling due to seismic actions can rapidly trigger structural collapse as a combination of yielding and increase in P-Delta effects during strong events (Lignos and Hartloper, 2020, Suzuki and Lignos, 2021, Elkady and Lignos, 2014).

Comparing cases with SHS and 2L brace cross sections, as well as SP and TS cladding panels, results of such checks are summarized in Figure V.16 (grouping D/C ratios for resistance checks, labelled as R), Figure V.17 (grouping D/C ratios for in-plane buckling checks, labelled as IPB) and Figure V.18 (grouping D/C ratios for out-of-plane buckling checks, labelled as OPB). In all the cases, D/C ratios are largely smaller than the unity. Also in this case, these results confirmed the use of elastic beam-column elements as a modelling choice for assessing structural response of the considered case studies.

Similar *D/C* ratios were observed passing from the SP to the TS case studies, considering both the brace cross section and connections types (i.e., SHS and 2L). Slightly larger *D/C* ratios were predicted for the model with SHS brace cross section. This was in line with the observations already discussed with the PCB case studies. In fact, also for the SCB case studies, failure of brace bolted connections produced a reduction of the longitudinal drifts up to reaching the collapse limit state. Consequently, internal forces in columns reduced.

The maximum *D/C* ratio predicted by the analyses did not exceed 0.30, which is a value much smaller than that predicted within the PCB case studies. Therefore, MSA analysis confirmed the relatively smaller effort of column elements in SCB case studies with respect to that observed in PCB case studies.

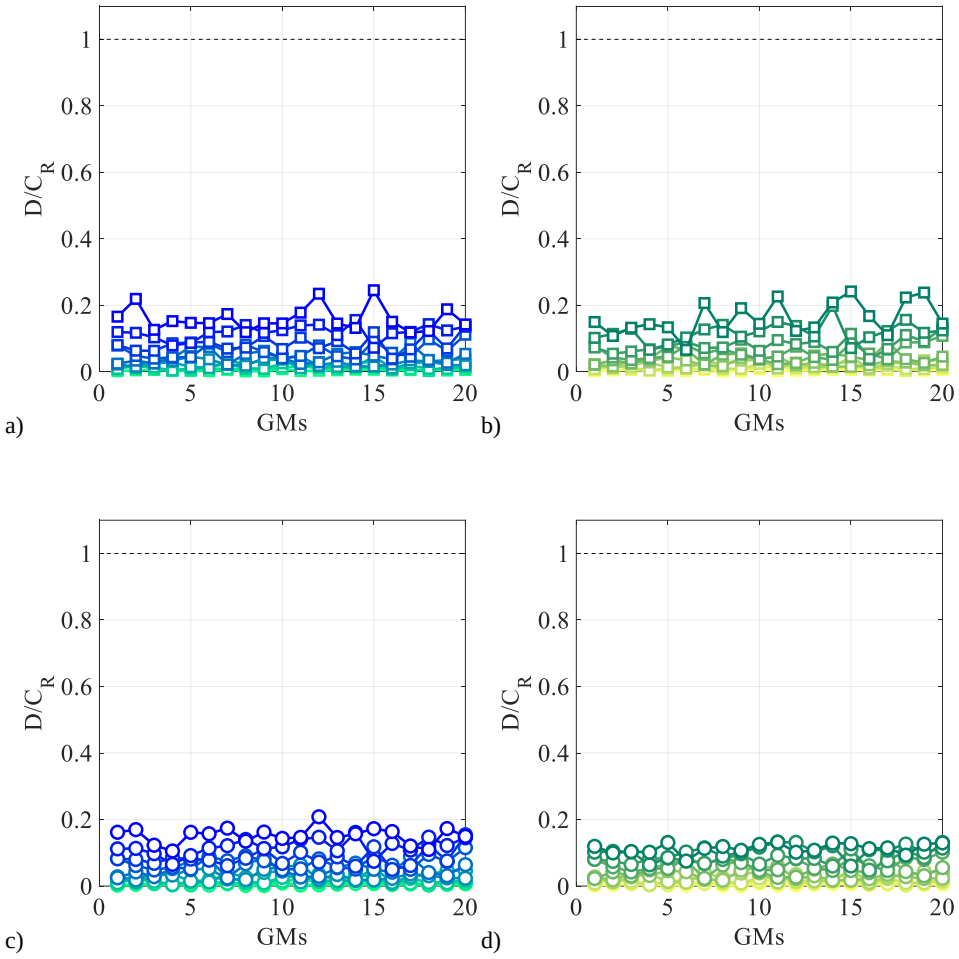

Figure V.16 Cross section plastic resistance checks for columns:
(a) SCB-SHS-SP model; (b) SCB-SHS-TS model; (c) SCB-2L-SP model; (d) SCB-2L-TS model.

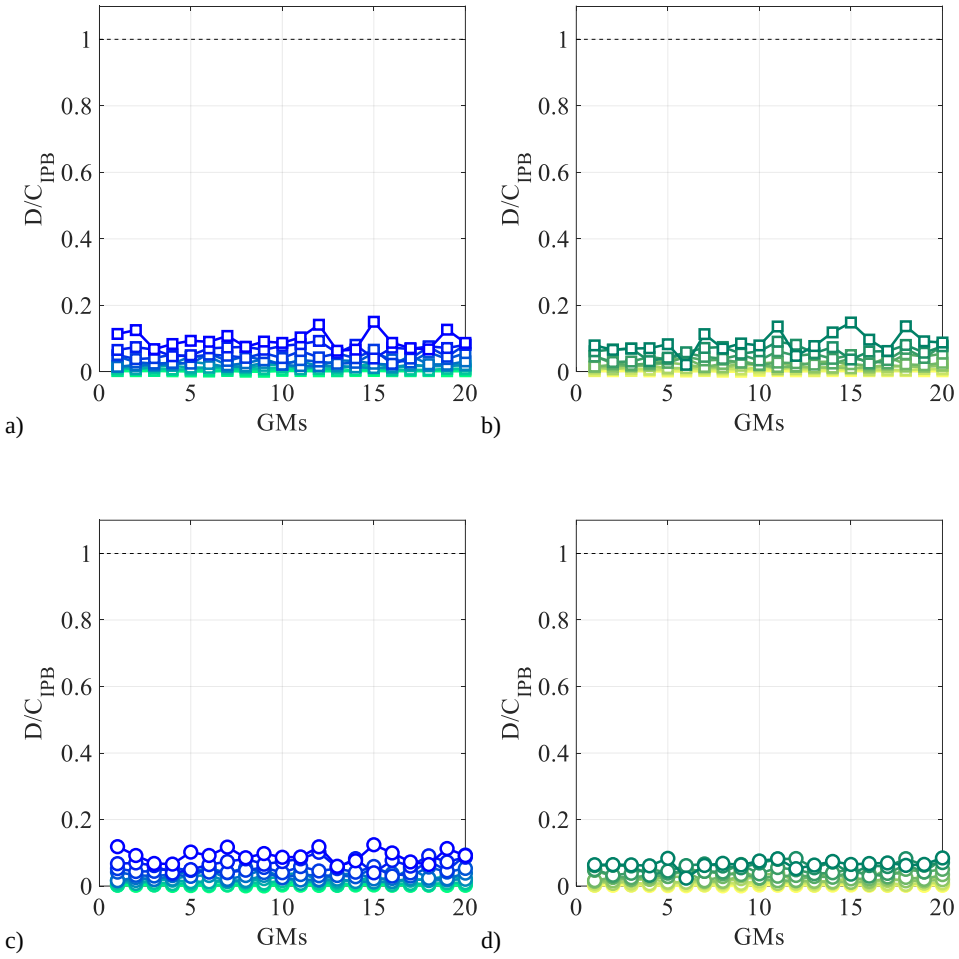

Figure V.17 In-plane buckling checks for columns:
(a) SCB-SHS-SP model; (b) SCB-SHS-TS model; (c) SCB-2L-SP model; (d) SCB-2L-TS model.

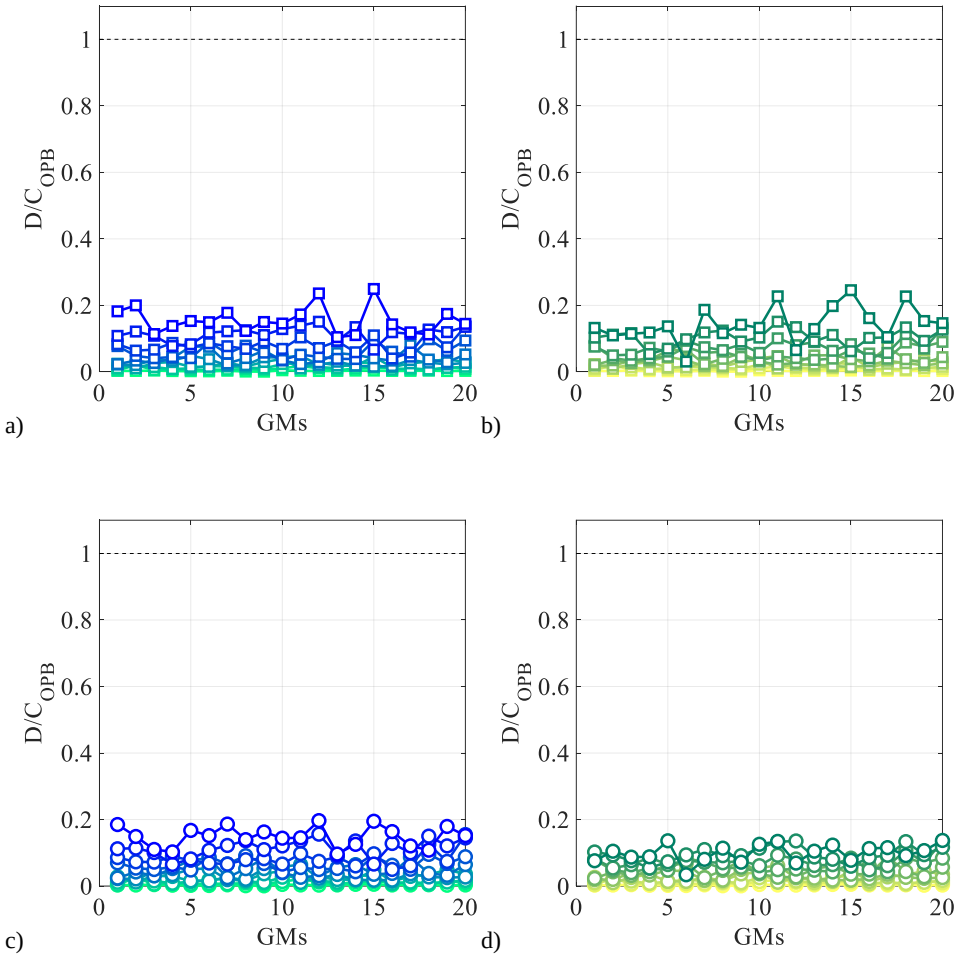

Figure V.18 Out-of-plane buckling checks for columns:
(a) SCB-SHS-SP model; (b) SCB-SHS-TS model; (c) SCB-2L-SP model; (d) SCB-2L-TS model.

V.4 Model-to-model comparison

Interesting observations can be drawn statistically evaluating MSA results obtained for each analysis stripe (i.e., from IM = 1 to IM = 10). Comparisons are made using results previously discussed. Model-to-model comparisons are carried out within three main objectives: (i) to compare structural response in terms of drift demands for analysis stripes in which global collapse did not occur; (ii) to compare number of collapse cases observed by varying design assumptions and structural schemes; (iii) to compare the influence of the building direction on the number of collapse cases. The calculated number of collapse cases will be used as the basic information to build collapse fragility curves described in the next chapter.

V.4.1 Statistical evaluation for non-collapse cases

V.4.1.1 Median values of the X-direction drifts demand

Figure V.19 summarizes model-to-model comparison in terms of median peak drifts in the transverse direction ($(d_{X,peak}/H)_m$), calculating them per each analysis stripe but neglecting GMs in which global collapse drift threshold was reached. In the plots, relationship between the median drift values and the relevant spectral (pseudo) accelerations at the fundamental vibration period ($S_a(T_1)$ or S_a for sake of simplicity) are shown and compared by varying the cladding type, passing from the bare frame model (BF) to the models which considered explicitly claddings (both SPs and TSs). To avoid bias in comparing results for which several collapse cases were predicted, the plot is shown up to a S_a value for which the observed collapse cases are smaller than 5. It is important to highlight that the intensity measure value changed passing from the bare frame model (T^* = 1 *s*) to the numerical models which explicitly considered envelope panels (T^* = 0.5 *s*). Indeed, the calculated values per each stripe are not aligned passing from the BF

to the ENV models. The comparison makes sense if the vertical axis be perceived as a measure of the transverse lateral force acting on the building. In this terms, one can observe that for the same value of the seismic action shaking the structure, envelope panels increased lateral stiffness of the structure itself, thus reducing median values of the displacements per each considered analysis stripe. This observation holds true for all the case studies, either changing brace connection details and brace cross sections (Figure V.19(a) vs. Figure V.19(b), or Figure V.19(c) vs Figure V.19(d)) and varying design assumption concerning the main truss system (Figure V.19(a) vs Figure V.19(c), or Figure V.19(b) vs. Figure V.19(d)). Additionally, the 16^{th} and the 84^{th} percentile of the drifts sample for a given IM are also shown as dashed lines in the plots. As expected, the larger is the S_a value, the larger is the expected dispersion at a given stripe. Also, larger dispersions can be observed within the BF models, reducing them passing from the TS until the SP model. Indeed, severe inelastic behavior of TSs anticipated that corresponding to SPs, thus introducing larger variation due to record-to-record variability starting from lower value of the IM. Looking at the plots, another interesting observation can be traced by comparing the PCB and the SCB numerical models. Comparing plots of Figure V.19(a) and (c), or equivalently Figure V.19(b) and (d), one can observe that differences in median values of the expected transverse drifts between the BF and the ENV models are larger in the SCB cases compared to the PCB cases. Indeed, PCB cases exhibited inelastic response for values of the lateral drift corresponding to truss-to-column connection (TCC) failures (i.e., near collapse). On the contrary, SCB cases exhibited inelastic response starting from lateral drift values corresponding to yielding of column base connections, smaller than that associated with the TCC failures. On the contrary, models explicitly considering envelope panels response allowed to obtain a very similar prediction of the lateral drifts passing from PCB to SCB models. Therefore, envelope panels smoothed differences in drift demands

among models looking at the part of the structural response in which global collapses did not occur.

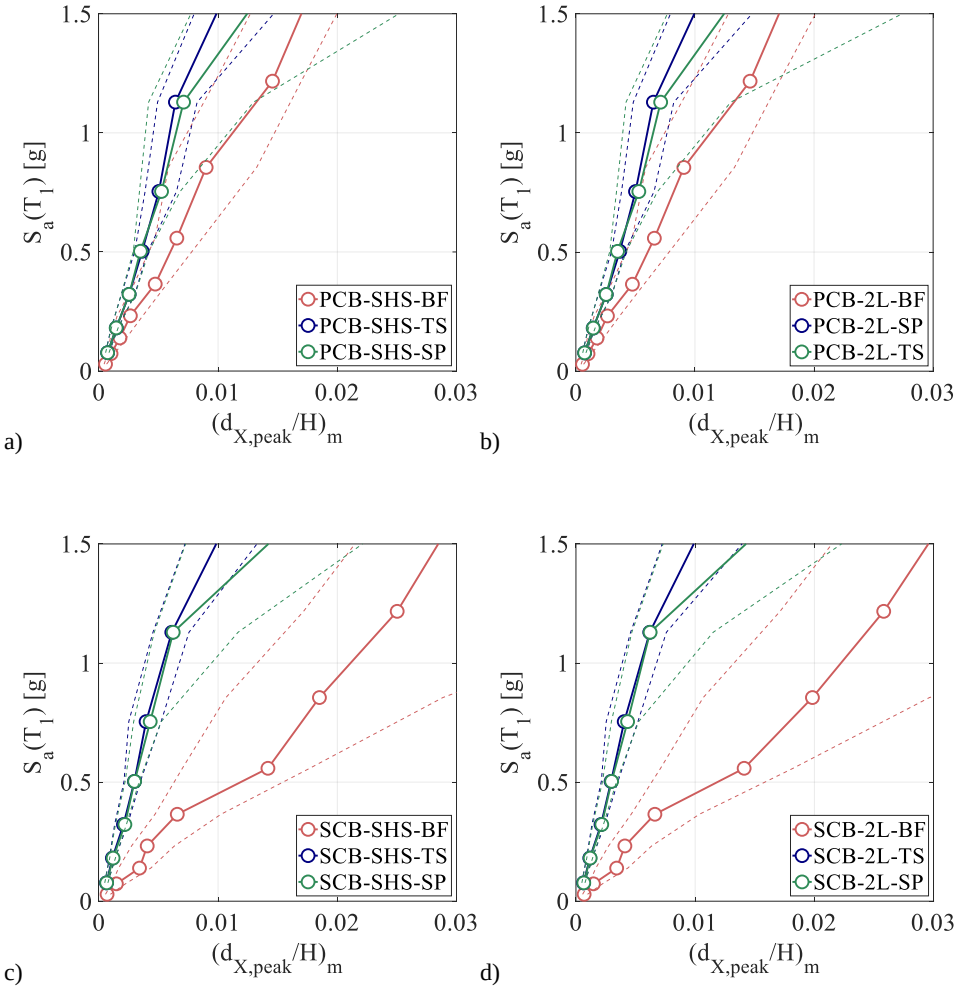

Figure V.19 Model-to-model comparison in terms of median peak drift demand in the transverse direction:
(a) PCB-SHS; (b) PCB-2L; (c) SCB-SHS; (d) SCB-2L.

Finally, comparing response by varying the longitudinal direction brace cross section and connection details, one can observe minor differences in the

distribution of the transverse drifts for both median values and the considered percentiles (i.e., demand dispersion), thus concluding that brace details were irrelevant in assessing transverse direction structural response.

V.4.1.2 COV values of the X-direction drifts demand

Figure V.20 summarizes the calculate COVs of the transverse peak drift values varying the intensity measure level. Also for these plots, calculations were carried out per each analysis stripe but neglecting GMs in which global collapse drift threshold was reached. At the first three stripes, the BF models show larger COV values if compared with both the SP and TS models. Additionally, at the last three stripes, the TS models show the largest COV values among the two envelope types. This was due to premature yielding of screw connections in the case of TSs, which introduced severe inelastic response in cladding panels prior to trigger main structure non-linearity. In all the SP models, COV values are practically the same from IM=1 to IM=6, approximatively equal to 0.20. Comparing results by varying the main truss design assumptions (i.e., switching from PCB to SCB models), one can observe a slight increase of the COVs for the SCB models, passing from 0.18 (PCB models) to 0.22 (SCB models) for IM = 1. This result is a consequence in variation of vibration period between the PCB and the SCB numerical models, either if compared each other (information can be found in the previous chapter) and if compared with the conditioned period used to perform the GM selection. In fact, structural vibration periods of PCB case studies were much closer to the conditioned period if compared to that of the SCB case studies. Also looking at the values of COV, the transverse direction drift assessment is not influenced by the presence of different brace cross section and connection details, as well as buckling deformed shapes (i.e., in-plane buckling in the case of 2L or out-of-plane buckling in the case of SHS).

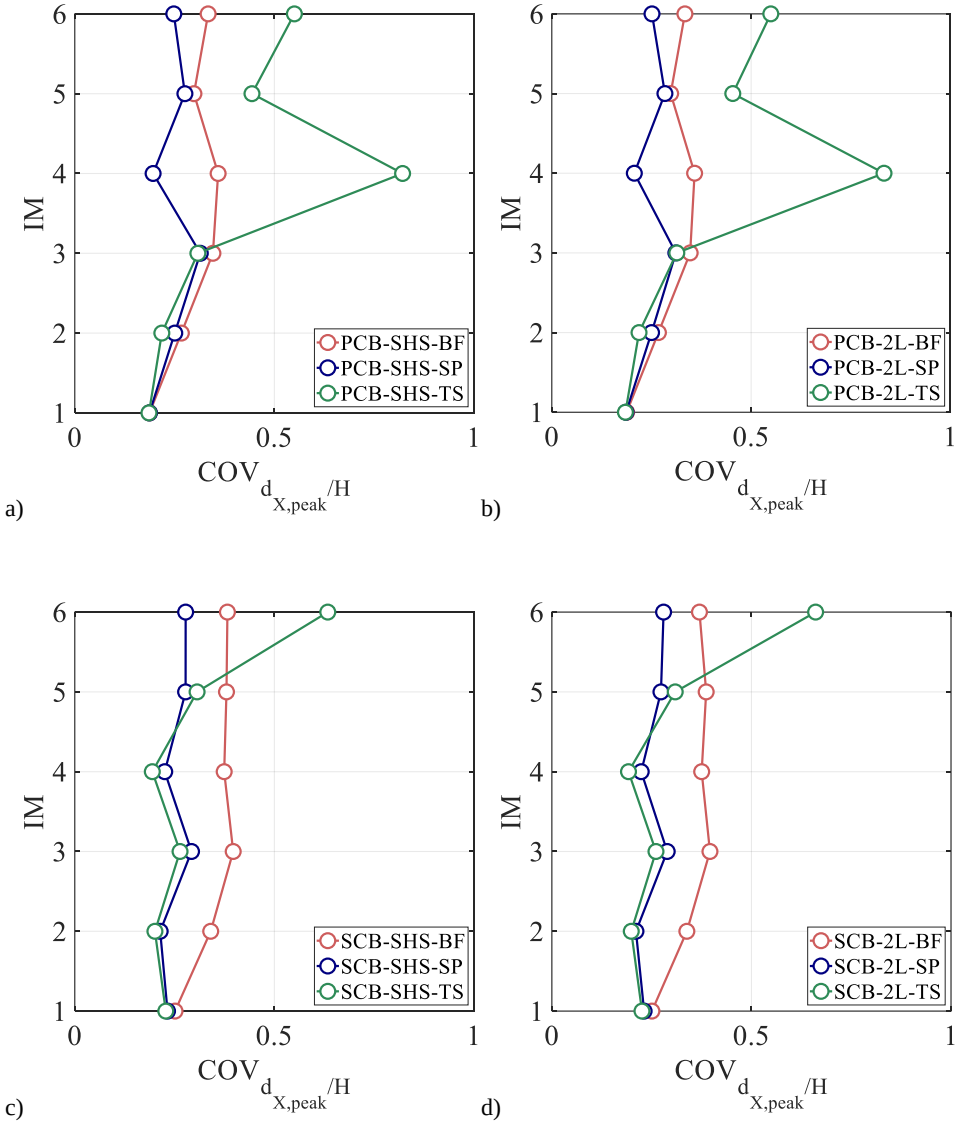

Figure V.20 Model-to-model comparison in terms of COV of peak drift demand in the transverse direction:
(a) PCB-SHS; (b) PCB-2L; (c) SCB-SHS; (d) SCB-2L.

V.4.1.3 Median values of the Y-direction drifts demand

Similarly, statistical results concerning the longitudinal building direction are summarized in Figure V.21 in terms of median peak drifts ($(d_{Y,peak}/H)_m$), calculating them per each analysis stripe but neglecting GMs in which global collapse drift threshold was reached. The plots are built similarly to those concerning the transverse direction, thus allowing comparisons between BF and ENV models, as well as PCB-SHS vs SCB-SHS (Figure V.21(a) and (c)) and PCB-2L vs. SCB-2L (Figure V.21(b) and (d)) comparisons.

First, consider values of median drifts varying the envelope type for the PCB models. One can observe that models predicted practically the same median drift values and dispersions for both the PCB-SHS and PCB-2L models and by varying the cladding type. On the contrary, differences can be observed between the BF model and the SP/TS cladding panels switching to the SCB models. Indeed, the BF model predicted median drift values larger than the SP/TS models, as well as larger values of dispersion per each stripe. Such differences in BF vs. ENV models comparison, observed passing from the PCB to the SCB case studies (either by considering SHS and 2L brace cross sections), are related to the increase of inelastic behavior in the transverse direction in SCB-BF cases with respect to the PCB-BF cases. In fact, in SCB cases, interaction between the two building directions became significant when column base connection started to yield. On the contrary, due to the relatively small amount of ductility exhibited by the truss-to-column connections in the PCB cases, the behavior of such structures can be regarded as elastic-brittle structural response. So that, if connection failure did not occur, interaction between X and Y direction cannot be significant. Therefore, the PCB models allowed to have similar median drift results passing from BF to SP/TS structural response. A relatively small amount inelasticity can be developed up to triggering global collapse of PCB cases.

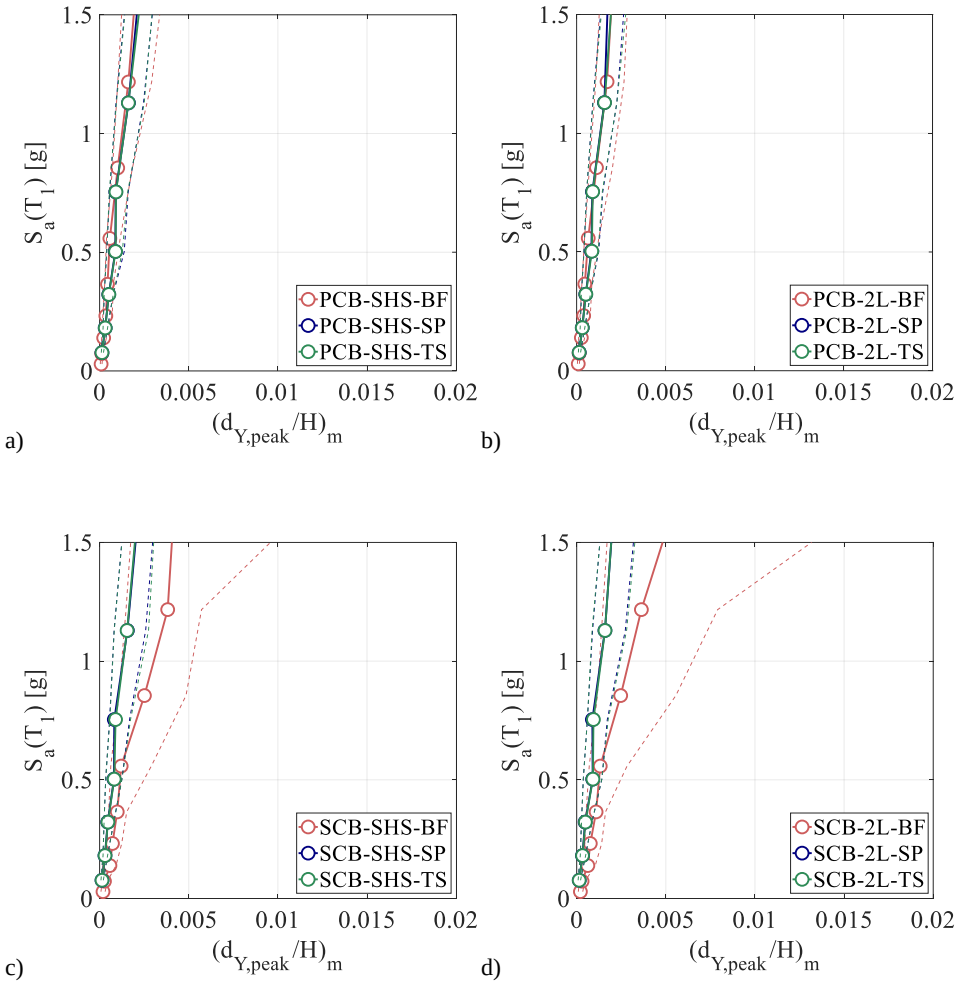

Figure V.21 Model-to-model comparison in terms of median peak drift demand in the longitudinal direction:
(a) PCB-SHS; (b) PCB-2L; (c) SCB-SHS; (d) SCB-2L.

Finally, one interesting observation can be made comparing results in terms of transverse lateral drift demands (Figure V.19) and longitudinal lateral drift demands (Figure V.21). Analyses clearly predicted large differences between drift demands corresponding to the two considered building directions. Particularly, the transverse direction shows median drift demands smaller than 1% (PCB-BF

cases) and 2% (SCB-BF cases) for applied spectral pseudo acceleration smaller than *g*. Such median drifts decrease up to 0.6% when cladding elements were included explicitly in the model (i.e., both the SP and the TS models). On the contrary, either for the PCB and for the SCB cases, with and without considering explicitly envelope panels, the longitudinal direction shows median drift demands smaller than 0.5% for applied spectral pseudo acceleration smaller than 1.5*g*. This is an additional confirmation that longitudinal building direction (i.e., the braced one) is stronger and stiffer than the transverse building direction (i.e., the portal frame direction), as already confirmed by modal analysis results and pushovers.

V.4.1.4 COV values of the Y-direction drifts demand

Results in terms of COVs of the longitudinal peak drift values varying the intensity measure level are summarized in Figure V.22. For all the considered case studies, BF models show COV values larger than 0.5, increasing up to (almost) 1 for IM = 6. On the contrary, models which explicitly include envelope panels (both SPs and TSs) show COV values practically equal to 0.5 from IM = 1 to IM = 6.

Differences between such values from that arising from results of the transverse building direction are explained looking at the considered seismic actions, as discussed previously. First, consider the increase in the COV values with respect to the transverse direction (Figure V.22 vs. Figure V.20). Such increase is a consequence of the procedure used for selecting GMs, which was carried out according to a conditioning period rather different to that associated to the longitudinal building direction. The GM selection was carried out within the activities of the RINTC research project by considering discrete values of the fundamental vibration periods (i.e., T_1 = {0.25 0.5 1 2} *s*). Therefore, one can choose the appropriate set of GMs by matching value of the relevant fundamental

vibration period of the model with that available from the database. Therefore, a slight difference can occur between these two values.

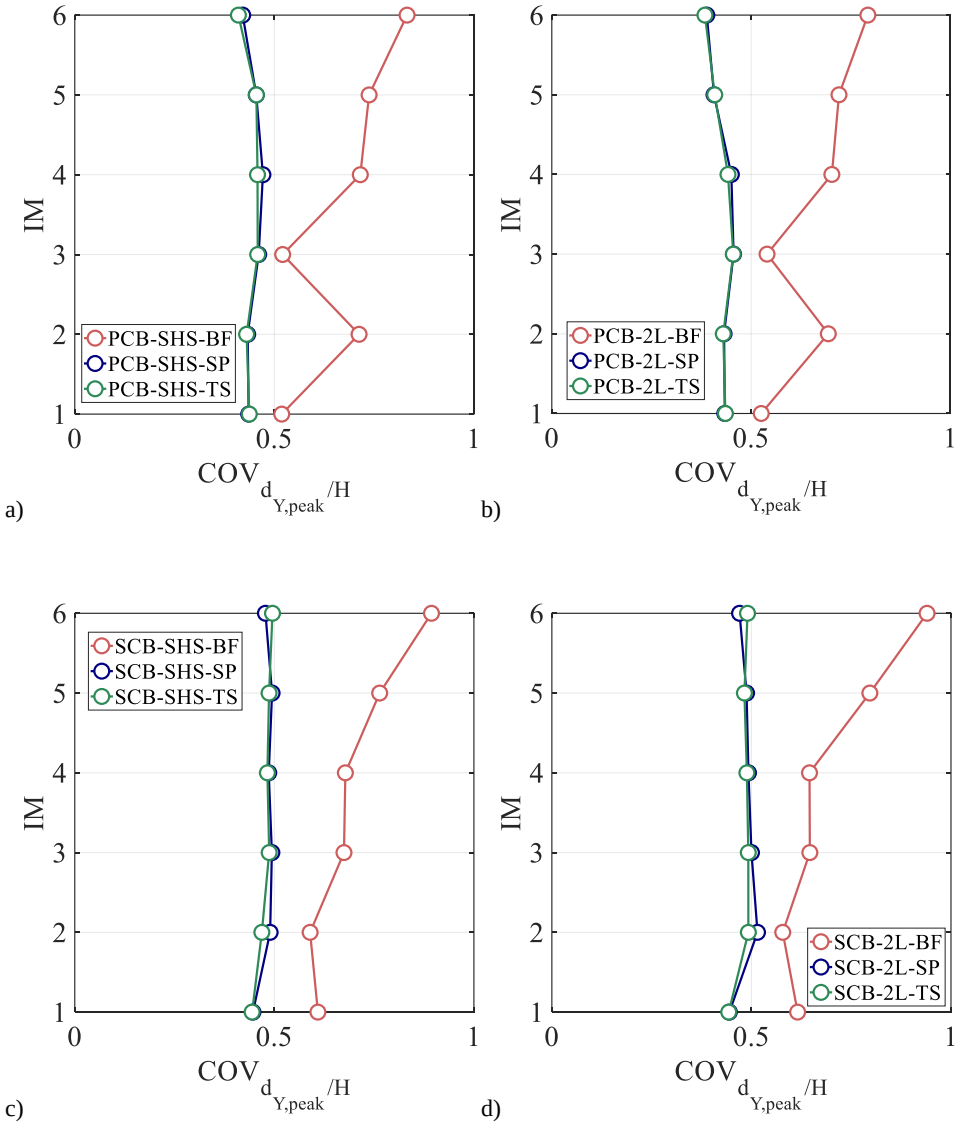

Figure V.22 Model-to-model comparison in terms of COV of peak drift demand in the longitudinal direction:
(a) PCB-SHS; (b) PCB-2L; (c) SCB-SHS; (d) SCB-2L.

As proved by analysis results, the larger was the difference between the T_Y and the corresponding T_1^* chosen from the database, the larger were the COVs predicted by the analyses. Indeed, in BF models the selected conditioned period was fixed as $T_1^* = 1$ *s*, whilst $T_Y = 0.2$ *s*. In the case of ENV models (both SPs and TSs), the selected conditioned period was fixed as $T_1^* = 0.5$ *s*, whilst $T_Y = 0.2$ *s*. Therefore, passing from the BF models to the ENV models, gaps in period reduced and so the predicted COV. Additionally, larger longitudinal COVs with respect to that predicted in the transverse building direction were always observed due to the assumptions made in selecting databases from GM selections.

V.4.2 Number of collapse cases

In this section, comparisons among the number of collapse cases are carried out by switching between the considered numerical models. In all the cases, a figure summarizes results concerning variation of the transverse design assumptions (i.e., PCB vs SCB models) and longitudinal design assumptions (i.e., SHS vs 2L models). The generic plot shows a relationship between the value of the spectral pseudo acceleration at the relevant fundamental vibration period and the number of collapse cases predicted at the generic stripe. Such cases were calculated as the sum of the number of GMs for which the generic NLTH did predict exceedance of the considered threshold limit values or numerical instability. Global collapse cases were calculated once the exceedance of the relevant threshold value was predicted first between the transverse and the longitudinal building direction. Three different curves are depicted in the generic figure: (i) a curve representing relationship between the S_a and the number of transverse (X) collapse cases (empty triangles in the plot); (ii) a curve representing relationship between the S_a and the number of longitudinal (Y) collapse cases (empty squares in the plot); (iii)

a curve representing relationship between the S_a and the number of both transverse (X) and longitudinal (Y) collapse cases (empty circles in the plot). Number of collapse cases reported herein can slightly differ from that shown in the plots of the MSA analysis results. Indeed, analyses were artificially interrupted when the maximum drift limit between the two building directions was reached. Therefore, it can occur that, for a generic couple of GMs, collapse was reached for both the building directions during the time history analysis. Henceforth, results concerning global collapse considers coupling of the building directions in terms of triggering global collapse. Consequently, sum of both X and Y direction collapse cases did produce the total amount of collapse cases registered at a given stripe and for a given numerical model.

V.4.2.1 Bare frame models comparison

Figure V.23 summarizes results concerning the BF models, both for the PCB case studies (Figure V.23(a) and (b), respectively PCB-SHS and PCB-2L) and for the SCB case studies (Figure V.23(c) and (d), respectively SCB-SHS and SCB-2L). First, comparing results concerning the PCB models. In both cases, global collapse started for a value of S_a larger than g. Also, longitudinal global collapses are practically negligible with respect to the transverse ones. Only one case at the largest IM value (S_a = 3.52g, T_R = 100000 y) was observed in the PCB-2L-BF model. In both the models, at the largest IM value practically all the GMs led the building to global collapse. Therefore, variation in vertical brace cross section and connection details did provide negligible effect in assessing global collapse for such archetype bare frame structure made by considering pinned column base connections (i.e., PCB).

Second, comparing results concerning the SCB models. The model which considered SHS brace cross section was not affected by collapse in the

longitudinal direction. Indeed, building collapse was always triggered by transverse column base connection failures. Failure cases started for a value of S_a larger than 1*g* (IM = 8, T_R = 5000 *y*). Maximum number of collapse cases, which occurred at the largest IM value (S_a = 3.52 *g*), was found to be 12.

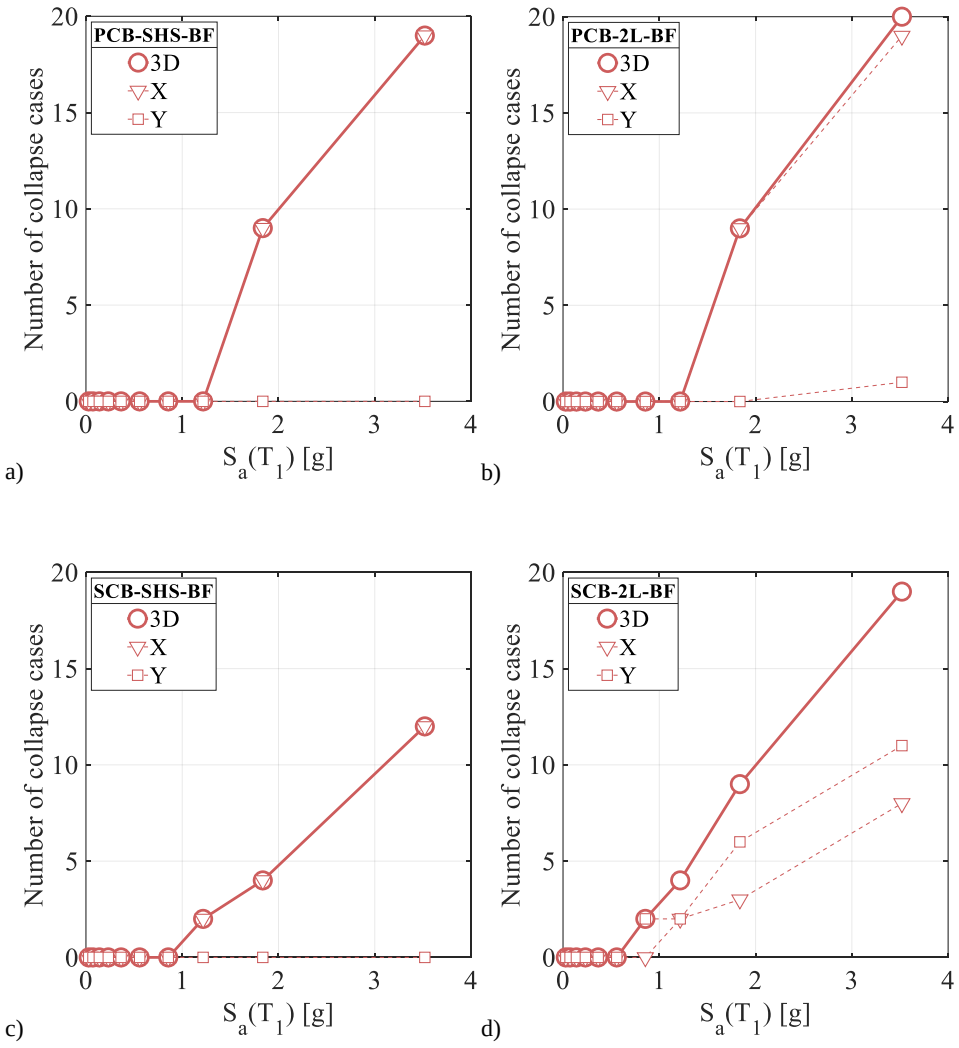

Figure V.23 Number of collapse cases in BF models:
(a) PCB-SHS-BF; (b) PCB-2L-BF; (c) SCB-SHS-BF; (b) SCB-2L-BF.

In the case of 2L brace cross section with bolted connections, both transverse and longitudinal collapse cases contributed significantly to define global collapse of the building. Failure cases started for a value of S_a smaller than 1*g* (IM = 7, T_R = 2500 *y*) due to vertical brace bolted connection failures. At the largest IM value, the model predicted 8 transverse collapses and 11 longitudinal collapses, thus predicting a total of 19 collapses by considering both the building directions. Practically speaking, number of collapse cases almost reached 20, highly increasing from that observed with the SCB-SHS case. Comparing PCB and SCB models, the SCBs provided smaller values of IM for which collapse cases started to occur. This was due to differences in maximum transverse base shear force resistance with respect to the PCB model. However, ductility of SCB column base connections did allow to reduce number of observed collapses if compared with the PCB case studies. In fact, the smaller value of ductility exhibited by truss-to-column connections highly increased collapse cases. Notwithstanding, when 2L braces with bolted connections were used as vertical brace system, number of failures became similar to that observed within the PCB case studies.

V.4.2.2 SP envelope models comparison

Figure V.24 summarizes results concerning the SP models (i.e. case studies which considered sandwich panels with bolted connections as cladding panels), both for the PCB cases (Figure V.24 (a) and (b), respectively PCB-SHS and PCB-2L) and for the SCB case studies (Figure V.24 (c) and (d), respectively SCB-SHS and SCB-2L). First, comparing structural response of the PCB models, thus varying brace cross sections and connection details. Global collapse started for a value of S_a slightly smaller than 2*g* (S_a = 1.73*g*, T_R = 2500 *y*). Either for SHS brace cross section and 2L brace cross section. Transverse failure cases were predominant in defining the building global collapse. Only one case at the largest IM value (S_a = 7.64g, T_R = 100000 y) was observed with the PCB-SHS-SP model. On the

contrary, 8 cases were observed with the PCB-2L-SP model. In both the cases, at the largest IM value practically all the GMs led the building to global collapse (19 cases in the PCB-SHS and 20 cases in the PCB-2L).

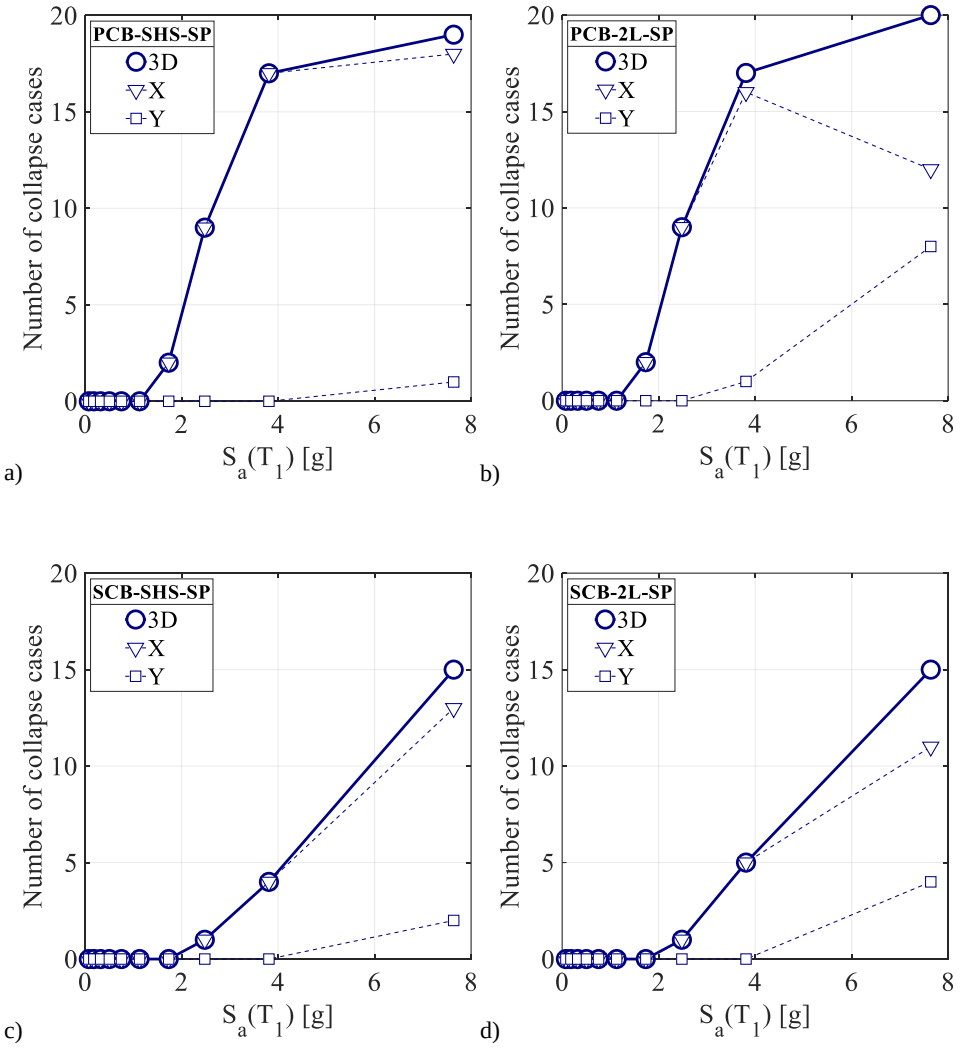

Figure V.24 Number of collapse cases in SP models:
(a) PCB-SHS-SP; (b) PCB-2L-SP; (c) SCB-SHS-SP; (b) SCB-2L-SP.

The SCB models show collapse cases starting from $S_a = 2.5g$ ($T_R = 5000$ *y*). Both the SHS and 2L models were slightly affected by collapse in the longitudinal direction. Therefore, the brace cross section and the connection arrangement did not significantly change the overall building response in terms of collapse assessment. Maximum number of collapse cases, which occurred at the largest IM value, was found to be 15. This was due to both the increase in lateral building strength provided by the SP cladding panels and the larger ductility values exhibited by the column base connections in the transverse building direction. Indeed, comparing PCB and SCB models, the SCBs provide smaller collapse cases for each considered stripe. This observation holds true for any combination of brace cross section investigated, as clearly observed looking at the figure (Figure V.24(a) and (b) vs (c) and (d)).

V.4.2.3 TS envelope models with comparison

Figure V.25 summarizes results related to the TS models (i.e., case studies which considered trapezoidal sheeting with screw connections as cladding panels), respectively for the PCB-SHS and PCB-2L cases (Figure V.25(a) and (b)), as well as SCB-SHS and SCB-2L cases (Figure V.25(c) and (d)). Looking at the PCB cases, results show that transverse collapse is predominant with respect to the longitudinal collapse. Indeed, a significant number of failure cases in longitudinal direction was observed only for the PCB-2L-TS case study, but only looking at the largest IM value ($T_R = 100000$ *y*). For both the PCB models, failures started from $S_a = 1.13g$ ($T_R = 1000$ *y*). For both the brace cross sections and connection arrangements, at the largest IM value, all the GMs led the building to collapse. SCB models predicted beginning of global collapse cases at $S_a = 1.73g$ ($T_R = 2500$ *y*). For SCB-SHS, both transverse and longitudinal collapses did contribute to total collapse cases at the largest IM stripe. For all the other relevant stripes, collapses were predominant in the transverse direction. On the contrary, SCB-2L shows

predominant longitudinal failures (i.e., collapse occurred first in the longitudinal direction due to brace connection failures). 16 cases were predicted at the largest IM value with respect to a total number of cases equal to 19.

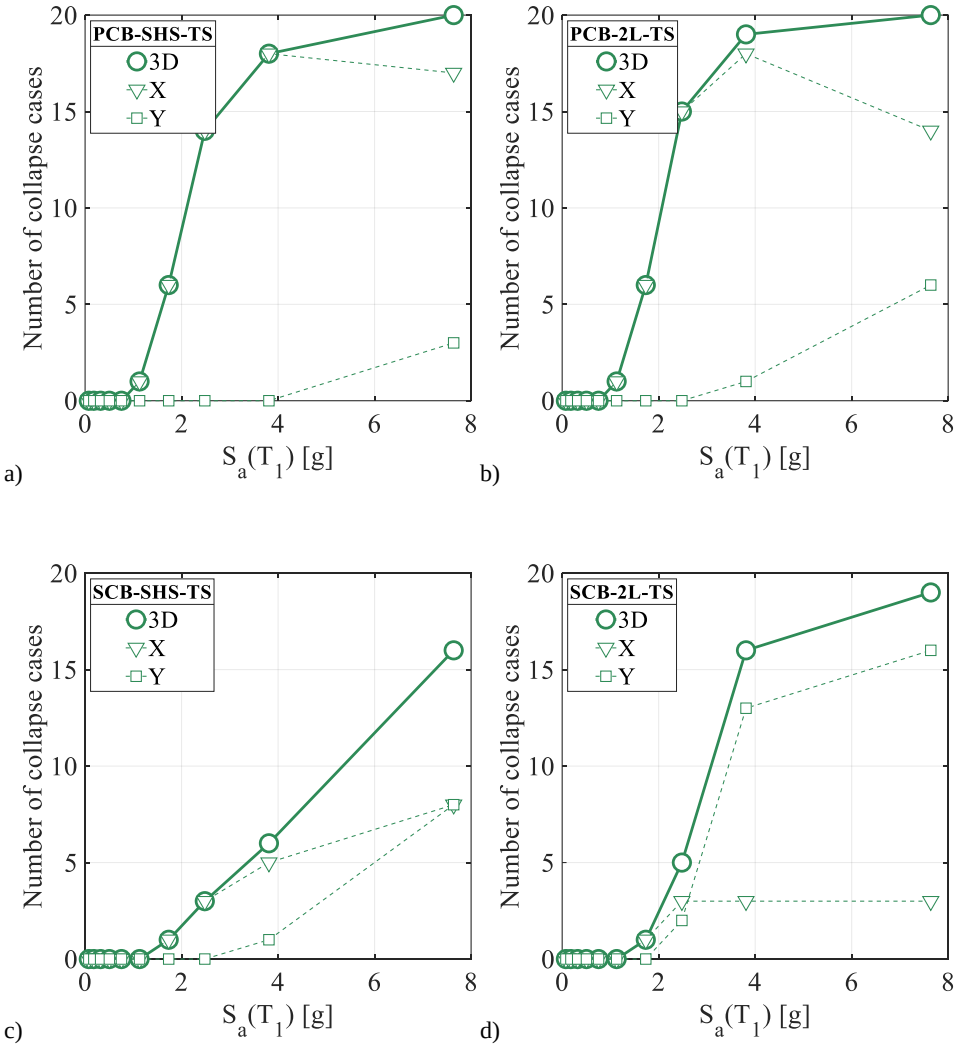

Figure V.25 Number of collapse cases in TS models:
(a) PCB-SHS-TS; (b) PCB-2L-TS; (c) SCB-SHS-TS; (b) SCB-2L-TS.

Comparing PCB and SCB case studies, larger number of collapses were always predicted with the PCB models, especially when 2L brace cross sections and bolted connections were considered as vertical brace arrangement. This was due to the relatively low ductility exhibited by the vertical brace connections and also by the truss-to-column connections in the transverse direction. However, truss-to-column connection failures was always the dominant fragility of the selected buildings (comparing cases arising from PCB-SHS-TS and PCB-2L-TS models).

Also, comparing both the cladding panels type in terms of collapse cases: the TS models always showed collapse cases larger (at least equal) to that observed with the SP models. This prediction is in line with the structural behavior observed within pushover analysis results (Chapter IV), which showed that TSs moderately contributed to the improvement of the building seismic response, if compared with the SPs structural response improvement, both in terms of maximum base shear force resistance and global ductility (i.e., displacement capacity up to collapse).

V.5 Non-linear time history responses

This section highlights some aspects of both local and global responses observed within non-linear dynamic analyses. The section emphasizes inelastic behavior of the relevant building components which can be observed during significant non-linear time history analyses (NLTHs).

Such NLTHs were extracted from the MSAs by varying the considered structural scheme among the several discussed in the previous section of the chapter.

V.5.1 Main Truss connections response

As extensively discussed in the previous sections of this chapter (and in the chapter dedicated to non-linear static analysis results, i.e., Chapter III), main truss connections played a fundamental role in defining condition to trigger global collapse of the buildings made by considering portal frame pinned column base connection (i.e., PCB case studies). The relatively small values of the ductility offered by such components did trigger premature local failures and starting of progressive collapse mechanism, as also preliminary assessed within pushover analyses. Therefore, relevant values of the transverse drifts were considered to define the global threshold value of the relevant EDP triggering global collapse of the buildings, as defined in the Chapter III. A physical proof of the development of such mechanism is illustrated in this section by looking at both local component results and global EDP values. For this purpose, a generic NLTH analysis at the largest IM value (IM = 10, T_R = 100000 *y*) was considered to show local component non-linear response during the time history. As an example, the PCB-SHS-SP model was considered. However, similar structural responses were observed in analysis cases for which the EDP threshold was exceeded, both varying the considered couple of GMs and the structural model. The results confirmed the structural response assessment conducted by using non-linear static analysis.

Figure V.26(a) shows a sketch of the bare frame building with indications concerning labels of portal frames, for both transverse and longitudinal drifts (in plan view) and forces in truss-to-column connections (in transverse view) of the generic portal frame. Additionally, the figure indicates column base connections (in longitudinal view) of the first braced bay (B_1, as already identified in the previous chapter) used to assess structural response of the longitudinal direction.

In Figure V.26Figure V.27, time history analysis results are plotted considering both transverse (Figure V.26Figure V.27(a)) and longitudinal (Figure V.26Figure V.27(b)) drifts of the five portal frames.

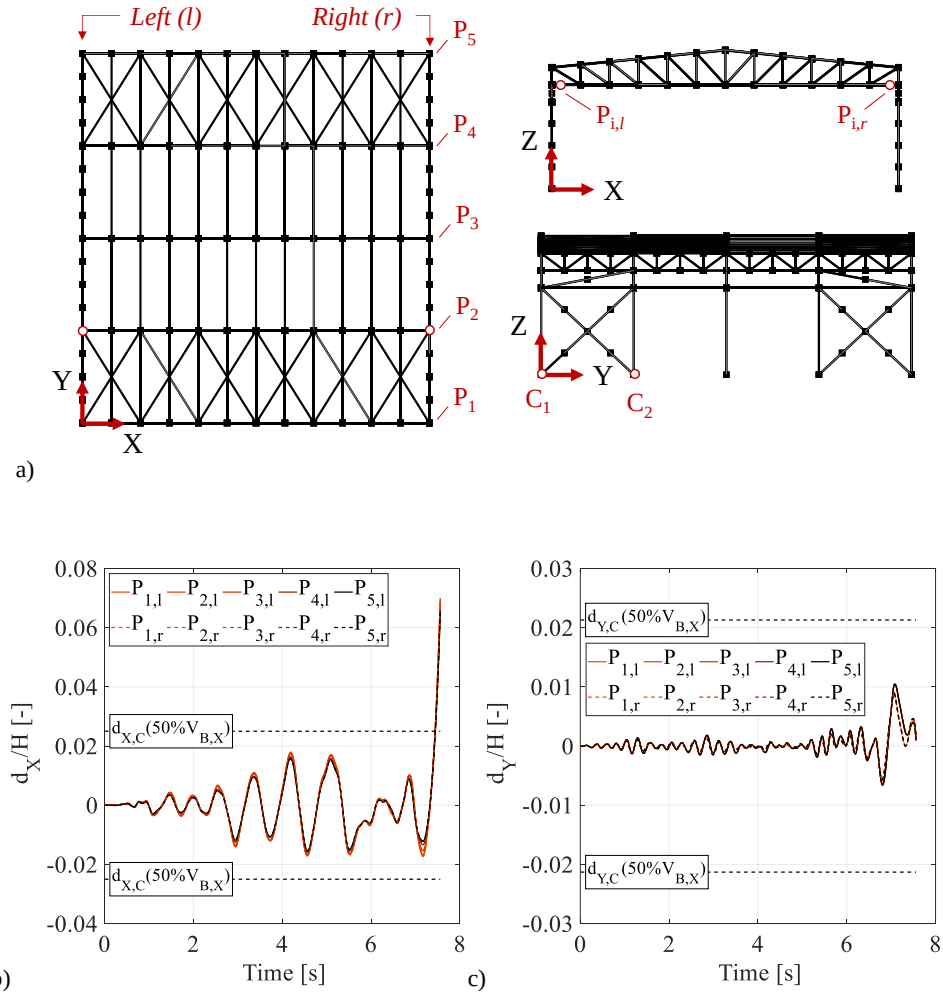

Figure V.26 (a) Schematic view of the building with identification of portal frame labels and connection labels; Sample of time history response at IM = 10 for the PCB-SHS-SP model: (b) transverse direction and (c) longitudinal direction.

Results are shown for both the left (continuous lines) and the right (dashed lines) building side, considering displacements of the nodes at the column tip. Additionally, global drift threshold values evaluated with pushover assessment are shown in the plots as dashed lines. For simplicity, only the longitudinal drift limit corresponding to the MSR_1 brace capacity value is shown. In the transverse direction, results show practically uniform lateral drifts among the portal frames, thus confirming a negligible role of the torsional vibration mode to the building response. All the portal frames did exceed the transverse drift threshold simultaneously. Analysis was performed reaching drifts twice the one associated with collapse. In the longitudinal direction, structural response was found to be bounded in the considered EDP threshold values concerning triggering and propagation of vertical brace fracture (MSR_1). In fact, analysis confirmed the absence of brace fracture during the performed integration time. Additionally, column base connection failure due to anchor fracture was not predicted to occur. However, a relatively small difference between the right side and the left side longitudinal drift values is shown in the plot as a consequence of inelastic deformations exhibited by the anchors of column base connections.

To prove triggering of global collapse accordingly to the pushover analysis results, significant local behavior of components in the transverse direction is postprocessed. Figure V.27 shows local forces in the bottom chord truss-to-column connections for each portal frame, considering both left (continuous lines) and right (dashed lines) side of the building. It is important to clarify that forces in the top chord truss-to-column connections did not exceed their ultimate force capacity. Indeed, pushover analysis did highlight a severe stress in both top and bottom truss-to-column connections. However, failure was always observed for the bottom (both left and right side) truss-to-column connections. MSA results did confirm such sequence of local failure up to exceeding the drift threshold. To better clarify such structural response, Figure V.27(a) shows values of the

connection forces ($F_{N,j}$) as a function of the analysis time. Additionally, the ultimate force connection capacity is plotted as dashed lines to highlight the occurrence of the ultimate failure. Actually, one should consider ultimate connection displacement in doing this check. However, since such displacements were very small values, one can equivalently look at connection forces instead of deformations without changing highlights of the discussion. The plot shows that peak forces in connections are very close to the connection resistance for analysis time smaller than the end time step. However, all connections did reach ultimate strength almost simultaneously within a time step coincident with that related to the exceedance of the global drift threshold.

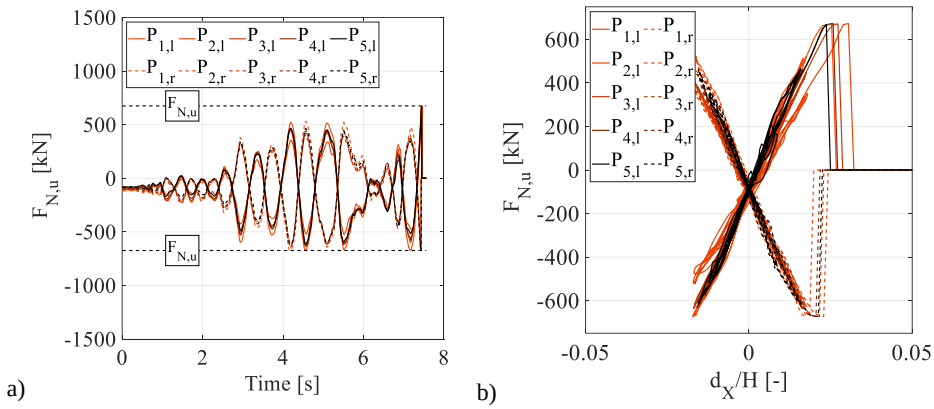

Figure V.27 Sample of time history response at IM = 10 for the PCB-SHS-SP model: Forces on truss-to-column connections as a function of (a) time and (b) transverse drift demand.

In Figure V.27(b), connection forces are plotted as a function of the relevant transverse drift per each portal frame. Two main comments can be stated. First, one can observe the small ductility value which can be developed into such connections prior to trigger bolt failure due to shear forces. Second, the plot confirms results observed with non-linear static analyses. The first failures was observed in right-side connections, whilst collapse was reached with failures in

all truss-to-column connections. Right-side connections were predicted to fail first due to the presence of gravity load compressive axial forces. Indeed, left-side connections had to unload from compression values due to gravity loads prior to develop a significant amount of tension forces.

V.5.2 Column base connections response

For both the considered structural schemes (i.e., PCB and SCB case studies), pushover analyses demonstrated that column base connections played another fundamental role in defining structural response in both the transverse and longitudinal building direction. To better highlight such component contribution, post-processing of the local responses is here reported.

First, consider behavior of column base connections in PCB case studies. As already discussed, PCB structures were modelled considering a pinned column base in the transverse direction, whilst inelastic behavior was explicitly modelled in the longitudinal building direction. This was necessary to consider highly inelastic interaction between shear forces and axial forces acting in the anchors of the column base connections. As a result, inelastic connection behavior influenced structural response of the whole building. Figure V.28(a) shows a sketch of one column where vertical braces are connected in the longitudinal direction, as well as a close-up view of the corresponding column base joint. The sketch of the braced column highlights: (i) the column top displacement ($d_{Y,t}$), (ii) the displacement of the node at the brace-to-column connection (δ_j). Knowing these displacements, it is possible to identify the column relative displacement ($d_{Y,t} - \delta_j$). Finally, the close-up view of the column base highlights the force and displacement parameters used to describe the column base connection response. Figure V.28(b) shows the connection shear force vs. connection displacement relationship for the column base connections in the braced bay labelled as B_1

(information about position of such connections can be found in the longitudinal view of Figure V.26(a)). Results were extracted from the same NLTH analysis used previously.

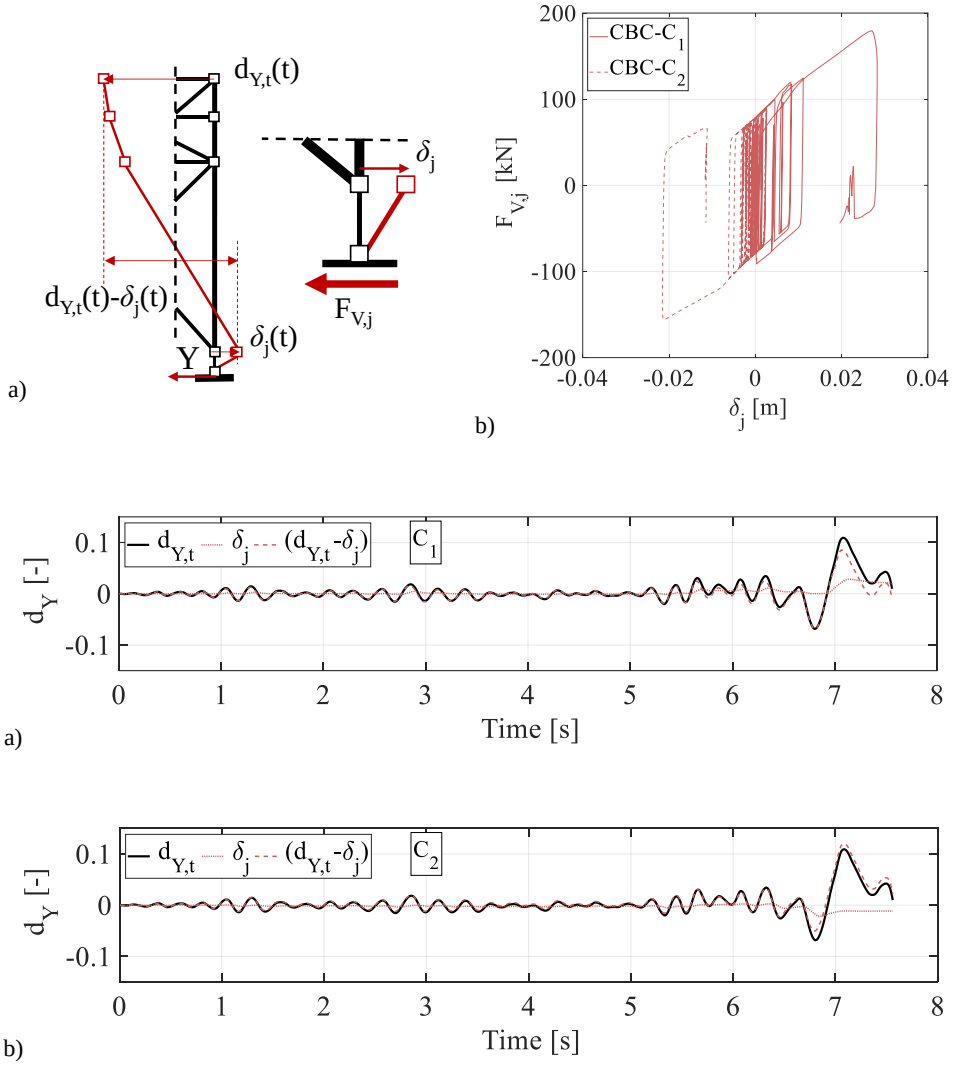

Figure V.28 Column base connection response in the PCB-SHS-SP model:(a) schematic views of the model; (b) force-displacement connection response (c); time history at column C_1; (d) time history at column C_2.

The development of cyclic behavior during time history can be observed in the column base connections. According to pushover analysis results, the non-linear response of the connection was triggered only when tensile forces were developed into the relevant vertical brace. Indeed, brace buckling anticipated column base connection yielding. Figure V.28(a) and (b) show sample response history for the column longitudinal displacements. The connection contribution to the column total displacement was negligible in the first part of the response history, i.e. when the column base connection remained in the elastic range of the response. When yielding of the column base connection started, a difference also started to develop between $d_{Y,t}$ and ($d_{Y,t}$ - δ_j), i.e. a difference between total displacement at the column tip and column displacement relative to the base. The plots show that ($d_{Y,t}$ - δ_j) could either be smaller or larger than $d_{Y,t}$, depending both on the response time and on the considered column. This behavior can be explained because of the connection residual deformation that accumulated during the response history, as shown in Figure V.28(b). Additionally, such type of structural response increased relative drifts for column elements, thus significantly increased their elastic internal actions. However, column yielding, as well as buckling, did not occur (as previously proved).

Consider now one example of NLTH response of column base connections in the SCB-SHS-SP case study. The considered analysis sample was extracted at the largest IM value (T_R = 100000 *y*). Labels follows the same meaning as explained in the previous results (more details in Figure V.26(a)). In Figure V.29(a) and (b), time histories of column drifts are shown for both the main building direction, respectively. Additionally, relevant drift limits concerning triggering of global collapse are shown as dashed lines. In the longitudinal direction (Figure V.29(b)), both the $d_{Y,C}/H$ limit values obtained by varying the *MSR* capacity value are shown. Results predicted collapse in the transverse direction, as the first exceedance of drift limit threshold between the two building directions. However,

numerical analysis was performed increasing analysis time until the occurrence of convergence issues. After predicting global collapse in transverse direction, the numerical model predicted increase of longitudinal drifts (Figure V.29(b)) beyond the $d_{Y,C}/H(MSR_2)$, i.e. considering drift for which in the longitudinal pushover did correspond the occurrence of brace fractures and the consequent 50% loss in base shear force resistance. However, analysis did not indicate any brace fracture for the whole analysis time. This result appeared being in contrast with pushover analysis. However, one should consider that triggering of global collapse drift in transverse direction significantly reduced transverse building stiffness and, consequently, longitudinal building stiffness. So that, interaction between the X and Y direction did not allow to predict brace fracture according to what observed with pushover analysis. In fact, longitudinal pushover analysis was not able to trace structural response after losing significant lateral strength and stiffness in transverse building direction. Therefore, results predicted after reaching failure in one of the two building direction cannot be used in tracing conclusions concerning the accuracy of the pushover in predicting structural response.

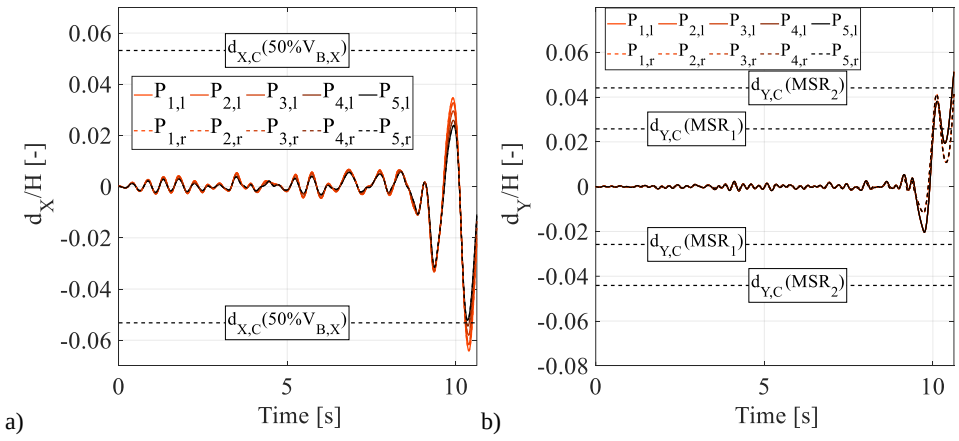

Figure V.29 Sample of time history response at IM = 10 for the SCB-SHS-SP model in (a) transverse and (b) longitudinal directions.

To better clarify the observed structural response arising from time histories of the column drifts, the base shear ($V_{b,X}$) vs. transverse drift (d_X/H, for the first portal frame $P_{1,l}$) and the column base connection response (M_{CBC} vs. θ_j relationship) are plotted in Figure V.30. Looking at the Figure V.30(a), the plot clearly shows the global pinched response developed due to the column base connection cyclic behavior and the SPs inelastic response. Indeed, bearing of bolted connections in sandwich panels developed plastic deformations in holes and, consequently, a typical pinched response of components which experienced bearing. Similarly, at the column base connections, anchor deformation beyond yielding formed a gap between the base plate and the grout, thus generating an elastic unloading which consequently produced a pinched response in the force – displacement global relationship.

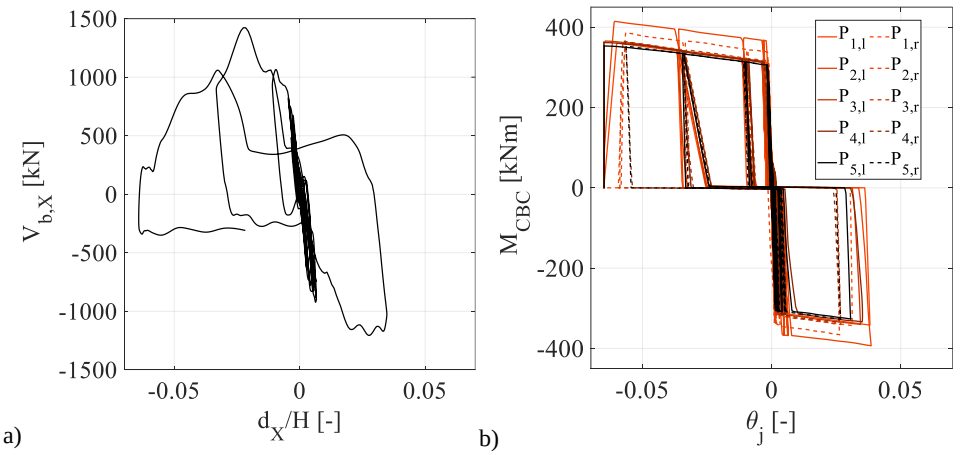

Figure V.30 Sample of time history response at IM = 10 for the SCB-SHS-SP model: (a) transverse base shear force vs. roof drift; (b) column base connection response.

Additionally, the plot clearly shows loss in shear resistance after reaching the peak value, thus confirming results concerning that observed with pushover analysis. Global response of the building was confirmed also by the local response observed

in column base connections (CBCs). Indeed, Figure V.30(b) shows developing of inelastic response in column base connections, according to the analytical model discussed in Chapter III. Several CBCs failed exceeding ultimate connection rotation, which corresponded to anchor fracture due to tensile forces. CBCs for which failure was not mathematically reached did develop large inelastic connection rotation, very close to that corresponding to anchor fracture. Therefore, non-linear time history analysis confirmed results obtained with pushover analysis in assessing response of the SCB case studies, as also suggested by structural responses predicted by other GMs, which were not reported here for the sake of brevity.

V.5.3 Brace connection response with 2L cases

Focusing on structural response in the longitudinal direction, an example of NLTH analysis results is reported here considering structural response of a SCB-2L-TS model. The considered couple of GMs were extracted from analyses performed at the largest stripe (IM = 10, T_R = 100000 *y*). Figure V.31(a) shows time history of longitudinal drifts for each portal frame (labels are shown in Figure V.26(a)), both for the left (continuous lines) and right (dashed lines) side. Additionally, black dashed lines show longitudinal drift limits corresponding to loss in lateral building strength up to 50% with respect to the maximum peak strength of the relevant building direction. Exceedance of such drift limit was predicted by the model around t = 11 *s*, for both the braced sides of the building. However, since drift limit in the transverse direction was much larger than that in the longitudinal direction, analysis was not automatically interrupted after this event. Consequently, numerical integration did allow to obtain solution for the whole input signal. Since brace connections failures were predicted, analysis

shows not negligible residual longitudinal drift at the end of the integration process. Also, one can observe not-uniform drifts between the right-side and the left-side of the building after exceeding the drift threshold. Indeed, as already discussed when processing pushover results, a torsional behavior of the building was expected after reaching failure of brace connections. Figure V.31(b) represents plot of the longitudinal base shear force ($V_{b,Y}$) vs longitudinal drift (d_Y/H, for the first portal frame $P_{1,l}$). As shown in the plot, starting of loss in longitudinal base shear force resistance was predicted corresponding to drift values close to the drift threshold defined with the pushover analysis. After losing lateral strength, the building experienced permanent lateral drifts around 2% with very small value of the longitudinal base shear force resistance. Notwithstanding, according to the seismic collapse criteria used in this dissertation, failure of the building was considered anyway.

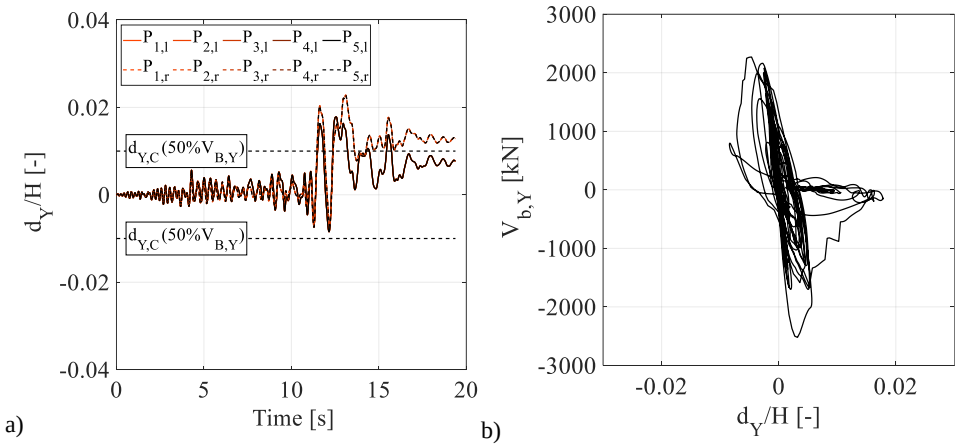

Figure V.31 Sample of time history response at IM = 10 for the SCB-2l-TS model: (a) longitudinal drift demand to portal frames; (b) global force-displacement relationship in the longitudinal direction.

To confirm structural analysis in terms of damaged components with respect to the results highlighting global response of the building, Figure V.31 shows force

($F_{j,BR}$) vs. displacement (δ_j) relationship for bolted connections in vertical braces. The plot was made by distinguish connections in the four braced bays of the building (labelled as B_i in the plots).

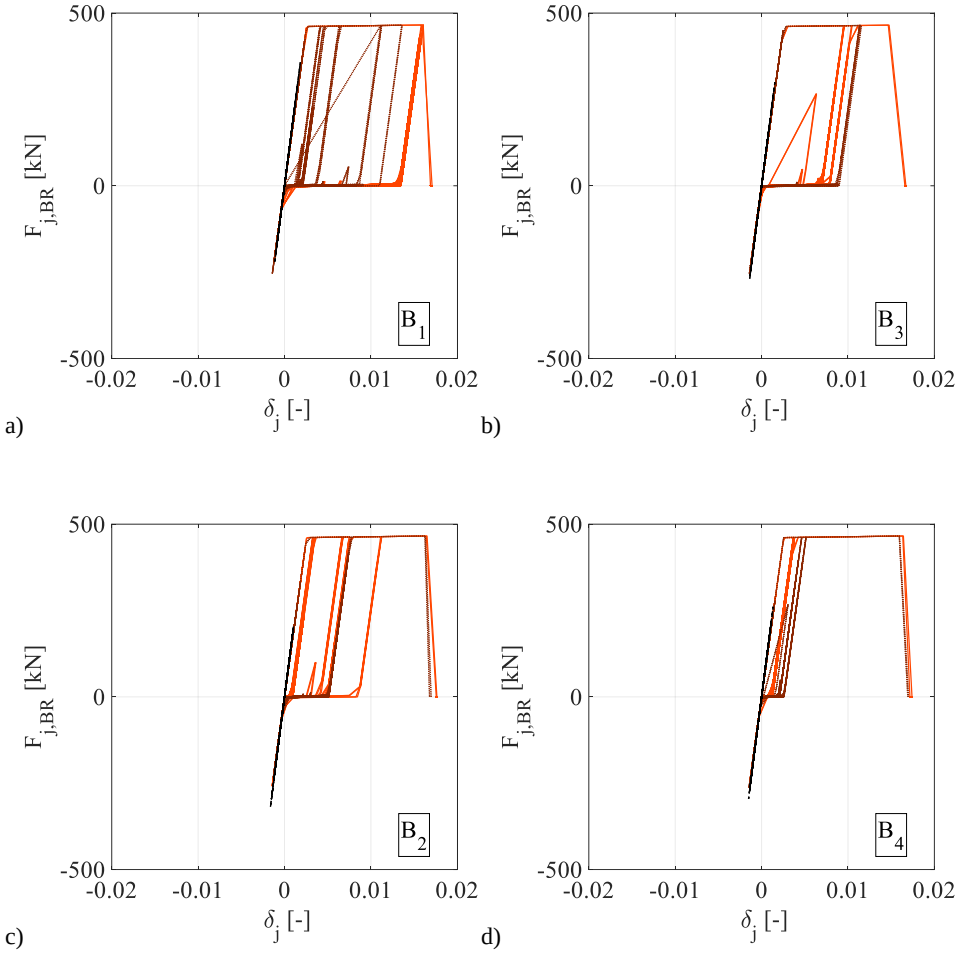

Figure V.32 Brace connection response in the SCB-2L-TS case for a generic GM scaled at IM = 10:
(a) Bay 1; (b) Bay 3; (c) Bay 2; (b) Bay 4.

For each plot, 8 force-displacement relationship are shown, corresponding to the 8 brace connections on the relevant braced bay (6 connections for the X-braces at

the first braced level and 2 connections for the single brace at the second level). Connections on continuous braces are plotted with continuous lines, whilst connections on spliced braces are plotted with dotted lines. Eventually, connections on single braces at the second level are plotted with dashed lines. Clearly, results shows that connection failure was predicted only by considering tensile forces acting on them (which means brace in tension), whilst behaviour in compression was predicted to be elastic. Indeed, buckling of braces did occur prior to reaching connection yielding, as also predicted with pushover analysis. Additionally, pinched response characterized hysteretic cycles of such components, since bearing of bolts dominated the ultimate connection behaviour. According to what observed in the longitudinal drifts plot, all the braced bays did experience connection failures. Analysis confirms that the relatively amount of small ductility which can be developed in bolted connections due to bearing failure mechanism cannot be sufficient to dissipate input seismic energy when strong ground motions shake the structure.

V.5.4 Envelope behavior

In this section, some comparisons between the considered numerical models were made by looking at the envelope response. Since the same GMs were used to perform MSAs for both the envelope types (i.e., both the SPs and the TSs), comparison of the structural response by varying the envelope type can be possible looking at the same couple of GMs input. To this end, two different couple of GMs were selected at IM =7 (T_R = 2500 *y*). For the first comparison, only the transverse response of the buildings is shown here, since global collapse in the longitudinal direction did not take place for the considered earthquake shaking. Figure V.33(a) shows transverse drift response history analysis results by

comparing the PCB-2L-SP and PCB-2L-TS numerical models. All the five portal frame transverse drift responses are shown in the plot. However, since transverse drifts were very similar each other (i.e., this corresponds to pure translations in the transverse direction), the plot shows practically the same drift history responses by varying the considered portal frame. With an empty circle, occurrence of transverse collapse is highlighted in the plot for the TS model, whilst the SP model did not experience global collapse. However, in both cases analyses were performed until the end of the GM input, thus highlighting that divergence of the numerical solution did not occur in the considered TS case. To clarify such aspect, Figure V.33(b) shows relationship between the transverse base shear force resistance ($V_{b,X}$) and the transverse lateral drift of the first portal frame (d_X/H).

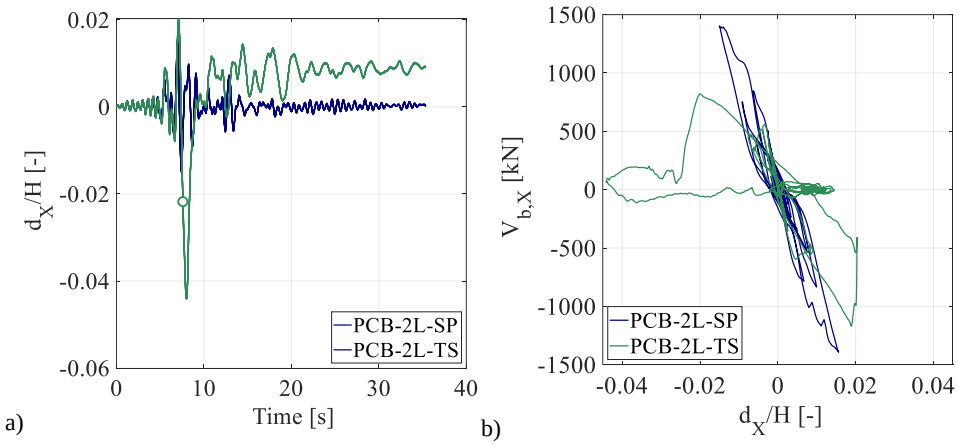

Figure V.33 Sample of time history for a generic GM scaled at IM = 7 for the PCB-2L case studies:
(a) transverse drift time history response; (b) transverse base shear force resistance.

First, one can observe that both the structures experienced practically the same structural behavior for small shaking intensities (small value of the transverse drifts demand). This is consistent with that observed looking at the pushover

response, as well as the modal analysis results. Indeed, the two buildings had the same elastic response. Once the TS cladding resistance was reached, the global force vs. displacement relationship significantly changed passing from the SP to the TS numerical model. Larger resistance offered by SPs if compared with the TSs did allow to overcome the ground shaking with relatively small amount of damage in non-structural elements (i.e., some bearing of bolted connections in cladding elements and failure of secondary siderail-to-column connections). On the contrary, the TS model did experience extensive damage in cladding elements, as well as failures of truss-to-column connections, which were responsible to the observed loss in base shear resistance for lateral drifts larger than 2% (in absolute value). Thus, global collapse in TS model was predicted to occur according to pushover analysis results. However, small but not null values of the lateral strength and stiffness did allow to complete numerical integration of the whole selected signal without showing numerical instabilities and/or divergency of the solution. Notwithstanding, not negligible residual drifts and extensive damages into secondary non-structural elements characterized response of the structure made by trapezoidal sheeting cladding elements.

Similarly, two different couple of GMs were selected at IM =7 (T_R = 2500 *y*) also for comparing structural response for the SCB case studies. Both transverse and longitudinal response of the buildings are shown in Figure V.34(a) and (b), respectively. The plot shows the relationship between the base shear force resistance ($V_{b,X}$ and $V_{b,Y}$) and the relevant column drift (d_X/H and d_Y/H). This comparison was done highlighting the rather different structural behavior by varying the building direction. However, global collapse in the transverse direction, which was the predominant collapse mode in such case studies, did take place for the considered earthquake shaking. As shown in the previous comparison, no differences are shown in the elastic response by varying the cladding type, both for the transverse and for the longitudinal direction. In the

transverse direction (Figure V.34(a)), differences between the two considered numerical model started after reaching the peak strength of trapezoidal sheeting. From that point, the TS model experienced loss in lateral strength, thus showing a (pseudo) vertical plateau corresponding to development of inelastic deformations in column base connections. For the TS model, failure occurred in positive drift direction with transverse drift around 5%. The examination of the local response confirmed triggering of global collapse due to column base connections failure. It is also useful to mention that damage of TSs occurred also for seismic intensity smaller than 7 (as shown previously in processing results by statistically comparing the case studies). On the contrary, the SP model experienced yielding of column base connections, as well as severe cladding-to-frame connections damage. However, collapse due to failure of column base connections did not take place.

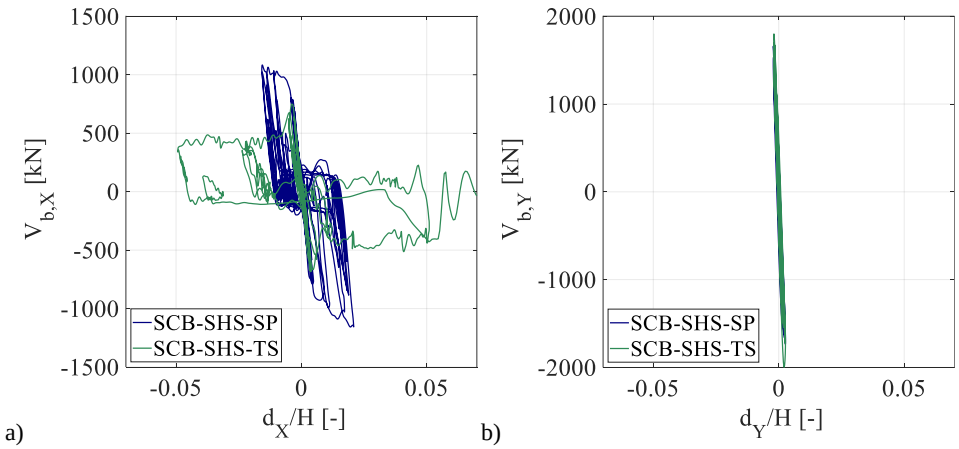

Figure V.34 Global force – displacement response for the SCB-SHS case studies: (a) transverse direction; (b) longitudinal direction.

Response in the longitudinal direction (Figure V.34(b)) is quite simple to describe. The analysis results plotted in the figure shows practically an elastic behavior for

both the considered models. A minor hysteresis response is shown because of the brace buckling, which occurred for very small value of the longitudinal drifts. Therefore, the vertical brace connections overstrength did allow to obtain a relatively stronger longitudinal building direction, both for the SP and TS cladding panel types. However, because of the smaller increase of the lateral building strength, the TS model collapsed as a consequence of the critical response observed in the main structure components, such as column base connections failure.

References

Baker J.W. 2011. Conditional mean spectrum: tool for ground-motion selection. *Journal of Structural Engineering 137: 322 – 331.*

Baltzopoulos G., Baraschino R., Iervolino I. 2018. On the number of records for structural risk estimation in PBEE. *Earthquake Engineering and Structural Dynamics 2018: 1 – 18.*

CEN. 2005. EN 1993-1-1: Design of steel structure – part 1-1: General rules and rules for buildings. *European Committee for Standardization, Brussels, Belgium*.

Elkady A., Lignos D.G. 2015. Analytical investigation of the cyclic behavior and plastic hinge formation in deep wide-flange steel beam-columns. *Bulletin of Earthquake Engineering 13: 1097 - 1118*

Faggella M., Barbosa A.R., Conte J.P., Spacone E., Restrepo J.I. 2013. Probabilistic seismic response analysis of a 3-D reinforced concrete building. *Structural Safety 44: 11 – 27.*

FEMA. 2012. Next-generation methodology for seismic performance assessment of buildings, prepared by the applied technology council for the federal emergency management agency, Report No. FEMA P-58.

Giannopoulos D., Vamvatsikos D. 2018. Ground Motion Records: To rotate or not? *Earthquake Engineering and Structural Dynamics 47(12): 2410 – 2425.*

Hsiao P.C., Lehman D.E., Roeder C.W. 2013. A model to simulate special concentrically braced frames beyond brace fracture. Earthquake Engineering and Structural Dynamics 42: 183 – 200.

Iervolino I., Spillatura A., Bazzurro P. 2018. Seismic Reliability of Code-Conforming Italian Buildings. *Journal of Earthquake Engineering 22:sup2, 5 – 27.*

Jalayer F. 2003. Direct probabilistic seismic analysis: implementing non-linear dynamic assessments. *Ph. D. Thesis, Stanford University*.

Jalayer F., Cornell C.A. 2009. Alternative non-linear demand estimation methods for probability-based seismic assessments. *Earthquake Engineering & Structural Dynamics, 38(8), 951 – 972.*

Lignos D.G., Hartloper A.R. 2019. Steel column stability and implications in the seismic assessment of steel structures according to Eurocode 8 Part 3. *Stahlbau 89(1): 16 – 27.*

Luco N., Manuel L., Baldava S., Bazzurro P. 2005. Correlation of damage of steel moment-resisting frames to a vector-valued set of ground motion parameter. *Proceedings of the 9th International Conference on Structural Safety and Reliability ICOSSAR'05, Rome, Italy.*

Magliulo G., Maddaloni G., Petrone C. 2014. Influence of earthquake direction on the seismic response of irregular plan RC frame buildings. *Earthquake Engineering and Engineering Vibration 13: 243 – 256.*

Morelli F., Laguardia R., Faggella M. Piscini A., Gigliotti R., Salvatore W. 2018. Ground motions and scaling techniques for 3D performance based seismic assessment of an industrial steel structure. *Bulletin of Earthquake Engineering 16: 1179 – 1208.*

Newmark N. M. 1959. A Method of Computation for Structural Dynamics. *Journal of the Engineering Mechanics Division ASCE 85: 67 – 94.*

Rigato A.B., Medina R.A. 2007. Influence of angle of incidence on seismic demands for inelastic single-storey structures subjected to bi-directional ground motions. *Engineering Structures 29: 2593 - 2601.*

Shome N., Cornell C.A., Bazzuro P., Carballo J.E. 1998. Earthquakes, records and nonlinear responses. *Earthquake Spectra 14(3): 469 – 500.*

Spillatura A. 2017. From Record Selection to Risk Targeted Spectra for Risk based Assessment and Design. *PhD Dissertation*, IUSS Pavia, Italy.

Suzuki Y., Lignos D.G. 2021. Experimental Evaluation of Steel Columns under Seismic Hazard-Consistent Collapse Loading Protocols. *Journal of Structural Engineering 147(4): 1 – 18.*

Vamvatsikos D., Cornell C.A. 2002. Incremental Dynamic Analysis. *Earthquake Engineering and Structural Dynamics 31, 491 – 514.*

Chapter VI

COLLAPSE FRAGILITY CURVES

VI.1 Introduction

Fragility is a term which is mostly employed in earthquake engineering to describe the predisposition of a structure, or a part of it, to experience a certain defined seismic damage. Quantification of the structure fragility for a given, already defined, limit state means to convert information observed from the structural behavior (evaluated both numerically or experimentally) in a value of probability that such limit state could be exceeded. The structural fragility can be defined as shown by Equation (6.1), defining it as the conditional probability of exceeding a limit state (LS) given the value of the earthquake intensity measure (IM) (e.g., Bakalis and Vamvatsikos, 2018, Petruzzelli, 2013):

$$F_{LS}(IM) = P\left[LS_{violated} \middle| IM\right] = P\left[D > C \middle| IM\right] \tag{6.1}$$

As shown by Equation (6.1), evaluating the fragility requires comparing the demand (D) with the capacity (C). In practice, this is usually done by introducing an engineering demand parameter (EDP) that is appropriate to describe the limit

state of interest. Using the EDP, Equation (6.1) can be rewritten as shown by Equation (6.2):

$$F_{LS}(IM) = P\left[EDP \geq EDP_C \,\middle|\, IM\right] \tag{6.2}$$

By varying the IM value in a range that is considered adequate to the specific fragility computation, one can obtain a function relating the probability to exceed the limit state vs. the IM (Equation (6.3)).

$$F_{LS}(IM) = P\left[IM \geq IM_C\right] \tag{6.3}$$

The concept of fragility functions in earthquake engineering dates to Kennedy *et al.* (1980), who defined the fragility function as the relationship between the frequency of failure of a component of a nuclear power plant and the peak ground acceleration. Recently, the fragility function was stated as the cumulative distribution function of the capacity of an asset to resist an undesirable limit state, in which the capacity is expressed as the degree of the seismic intensity at which the asset exceeds the undesirable limit state (Porter, 2020). In this definition, the cumulative distribution function is the probability that an uncertain quantity will be less than or equal to a given value, as a function of that value (such definition reflects the mathematical function expressed with Equation 6.3). Depending on the method used to compute the fragility functions, Porter (2020) distinguishes three classes: (i) empirical fragility functions, which are created by fitting a function to approximate observed data from experimental tests or real world; (ii) analytical fragility functions, which are derived from simulation results obtained by using an ad-hoc structural model; (iii) expert opinion or judgment-based

fragility functions, which are built starting from the opinion of people who have experience with the relevant issue. In the latter case, results could be affected by differences in personal judgment of each expert. A combination of these methods can also be used.

In this study, fragility curves were evaluated from data obtained with numerical simulations of the non-linear dynamic response of the archetype buildings discussed in the previous chapter of this dissertation. Hence, the obtained fragility functions can be considered to belong to the second type mentioned by Porter (2020), i.e. they are "analytical" fragilities. In most cases, the analytical fragility curves are fitted by means of a probabilistic model. The typical choice is the lognormal probability model (Porter *et al.*, 2007). The mathematical expression of a lognormal fragility function is given by Equation (6.4).

$$F_{LS}(IM) = \Phi\left(\frac{ln(im) - \eta_{LS}}{\beta_{LS}}\right) \tag{6.4}$$

In Equation (6.4), the operator $\Phi(.)$ represents the standard Gaussian function, while η_{LS} and β_{LS} represent the mean and the standard deviation of the logarithms of the ground motion intensity measure (IM) for which the exceedance of the considered limit state occurs. The unknown parameters of the probability distribution (η_{LS} and β_{LS}) are evaluated starting from the numerical results, according to methods which are better described in the following. The choice of the logarithmic distribution allows to satisfy the basic properties that a fragility curve should possess (Bakalis and Vamvatsikos, 2018): (i) at zero intensity, the probability of exceedance should be null; (ii) as the IM approaches infinity, the probability of failure should approach unity; (iii) the curve should be monotonically increasing.

To build analytical fragility curves starting from structural the response of numerical models, one could follow two standard approaches (Iervolino, 2017): (i) the IM-based approach and (ii) the EDP-based approach. The two methods are summarized in Figure VI.1, with the left and right sub-plots, respectively. With the IM-based approach, one can work with random IM levels, thus identifying a distribution of IMs causing exceedance of the limit state. In the figure, the limit state was considered exceeded when the EDP values cross the corresponding capacity value (EDP_C). In this case, indicating by IM_f the IM causing failure in the generic event, a distribution could be fitted starting from the numerical data (the blue curve in the plot). Subsequently, for a given reference value of the IM (labelled as IM_R in the figure), one can readily calculate the probability of having failure (i.e., limit state exceedance) by means of Equation (6.5). Therefore, the cumulative distribution function of such random variable is the fragility curve for the considered limit state.

$$F_{LS}\left(IM_R\right) = P\left[IM_f \leq IM_R\right] \tag{6.5}$$

The EDP-based approach works considering fixed IM levels. Therefore, it is more suitable to use when the MSA method is adopted. With this approach, one can more directly calculate the probability (or frequency) of exceeding a pre-defined EDP threshold, which is conditioned to a value of the intensity measure (IM) as shown by Equation (6.6):

$$F_{LS}\left(IM_R\right) = P\left[EDP \geq EDP_C \,\middle|\, IM_R\right] \tag{6.6}$$

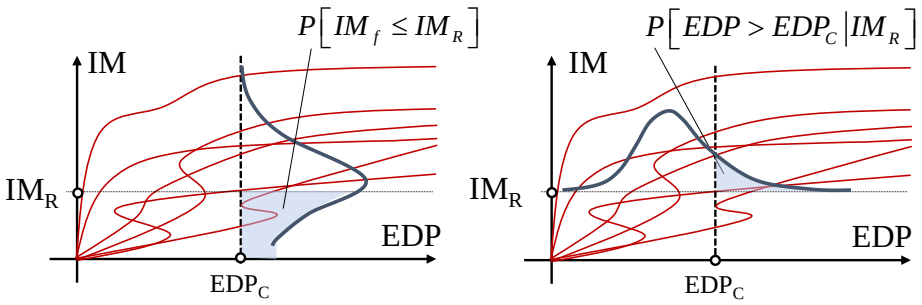

Figure VI.1 IM-based and EDP-based approaches to obtain fragility curves.

If the EDP_C used to build the fragility curves is the value triggering the global collapse of the building, as defined in the previous chapters, then the built fragility curves can be called *collapse* fragility curves.

In this chapter, collapse fragility curves were calculated starting from technical procedures and tools widely used in the literature and extensively described in the next section. The collapse fragility curves will provide a synthetic description of the structural response, allowing also to easily compare the behavior of different structures.

VI.2 Adopted methodology

Collapse fragility curves were built starting from the MSA results and using the software R2R-EU (Baraschino *et al.*, 2020). The software provides several alternatives to calculate the fragilities curves. Since the MSA methodology was adopted to carry out the time-history structural response evaluation, the EDP-based approach was inevitably the choice for the calculation of the fragility functions.

Concerning the numerical strategies aimed to fit a parametric model, one can use several alternatives. Baker (2015) proposed the maximum likelihood method (ML). With the ML method, one evaluates per each stripe the number of GMs exceeding the threshold associated with the limit state. Cases of divergence of the structural response, corresponding to non-convergence of the numerical solution, are automatically treated as cases where the limit state threshold is exceeded. However, with the ML method problems are encountered when the number of collapse cases is small over all the stripes. For this reason, alternative methods are frequently proposed, accounting for collapse cases with the three-parameter-per-intensity model (Shome and Cornell, 2000). In the Shome and Cornell approach (2000), assumptions are made on the distribution of the structural analysis results per each considered stripe. Usually, a lognormal distribution is adopted for the EDP demand at the generic seismic intensity. In this way, a non-null probability of collapse is always obtained even if the structural response obtained from all the analyses does not show any exceedance of the collapse threshold set for the EDP. The failure probabilities per stripe, calculated by using the three-parameter-per-intensity model, are used to estimate parameters of the collapse fragility curve by applying alternative procedures to the ML method. For example, estimates of the fragility parameters can be obtained by means of least square fit (LSF), which consists of fitting a fragility function by minimizing the sum of squared errors by performing a non-linear least squares regression.

For the cases examined in this dissertation, the application of the maximum likelihood method always allowed to obtain fragility curve parameters. Considering that the ML method reduces the number of assumptions needed to obtain fragility parameters, it was selected as the preferred method. However, comparisons with the LSF method were also carried out to evaluate differences due to different assumptions in calculating the failure probability per each stripe, as better described in the following.

Equation (6.7) shows the expression of the considered parametric curve used as collapse fragility function. The spectral pseudo-acceleration at the fundamental vibration period ($S_a(T_1)$, or S_a for brevity) of the relevant structure was used as intensity measure, according to the discussion presented in the previous chapter. The two curve parameters, η_C and β_C, represent the mean and standard deviation of the logarithm of S_a, respectively.

$$P\left[C\middle|S_a\left(T_1\right)\right]=\Phi\left(\frac{ln\left(S_a\right)-\eta_C}{\beta_C}\right) \tag{6.7}$$

As stated previously, the curve parameters were estimated using the maximum likelihood (ML) method, by means of Equation (6.8), which is here rewritten by substituting the number of (bins of) GMs used per each stripe (i.e., 20) and the number of stripes considered in the analysis (i.e., 10). In the equation, $n_{C,j}$ defines the number of collapse cases, which are the total number of cases considering both building directions. Such values were already calculated and discussed in the previous chapter. These are the only numerical results needed for the fragility assessment when the ML method is used.

$$\{\eta_C \quad \beta_C\}=arg\,\underset{\eta,\beta}{max}\left[\sum_{j=1}^{10}\left(ln\binom{20}{n_{C,j}}+n_{C,j}\cdot ln\left\{\Phi\left(\frac{ln\left(S_{a,j}\right)-\eta}{\beta}\right)\right\}+\left(20-n_{C,j}\right)\cdot ln\left\{1-\Phi\left(\frac{ln\left(S_{a,j}\right)-\eta}{\beta}\right)\right\}\right)\right] \tag{6.8}$$

In the case of the least square fit method, parameters of the fragility function are estimated by minimizing the sum of squared errors according to Equation (6.9). In that equation, additional terms with respect to the Equation (6.8) accounted for the application of the three-parameter-per-intensity model in estimating values of the probability of failures for each intensity stripe. In particular, EDP_C represents

the EDP threshold defined triggering of global collapse (as defined in Chapter III), while $\eta_{\ln(EDP,j)}$ and $\beta_{\ln(EDP,j)}$ represent the two parameters of the lognormal distribution of EDP values for the *j* stripe, associated to the non-linear dynamic analysis results which did not experience collapse.

$$\{\eta_C \quad \beta_C\} = arg\min_{\eta,\beta}\left[\sum_{j=1}^{10}\left(\left(1-\frac{n_{c,j}}{20}\right)\cdot\left[1-\Phi\left(\frac{ln(EDP_C)-\eta_{ln(EDP_j)}}{\beta_{ln(EDP_j)}}\right)\right]+\frac{n_{c,j}}{20}-\Phi\left(\frac{ln(S_{a,j})-\eta}{\beta}\right)\right)^2\right] \qquad (6.9)$$

Since the structural fragility function is assumed to be a lognormal distribution, the estimators of the two parameters obtained according to Equation (6.8) or Equation (6.9) have known distributions (Baraschino *et al.* 2020). The R2R software allows to evaluate the mean and variance of such estimators. A parametric bootstrap analysis was selected among the software options (Baraschino *et al.* 2020). In this way, several additional $n_{C,j}$ cases were generated per each stripe (j = 1 to 10), thus obtaining a number of fragility curves depending on the number of performed bootstraps . With these generated data, a measure of the variability of the fragility curve parameters can be obtained, thus quantifying the probability distributions of the estimated η_C and β_C.

VI.3 Analysis results

This section describes the fragility functions obtained using the ML method presented in the previous section. Comparisons between the investigated archetype buildings are also discussed. Eventually, a comparison of fragility functions obtained using the LSF method is also discussed.

VI.3.1 PCB case studies

This section summarizes results concerning the numerical models with pinned column base connections in the transverse direction (i.e., PCB). Figure VI.2(a) and Figure VI.2(b) show the results concerning the PCB-SHS and PCB-2L case studies, respectively, without the building envelope (BF model), and with the SP or TS claddings. As stated previously, the generic collapse fragility curve provides a relationship between the conditional probability of collapse given the first-mode spectral acceleration, S_a. In the plot of Figure VI.2(a), empty triangles are used to plot the numerical results from Chapter V, i.e. the number of collapse cases divided by the number of GMs considered per each stripe (20). The bold continuous curves are the logarithmic cumulative distribution functions whose parameters were obtained per each structural model by means of the ML method. An empty circle is also plotted superimposed to the bold continuous curves to highlight the median value of the relevant S_a. The shaded areas highlight the regions of the plotting plane containing all the individual realizations from the bootstrap analysis (which contained 500 realizations per each individual structural model). Therefore, the larger is the shaded area the larger is the dispersion on the estimated curve parameters (numerical results are summarized at the end of the chapter). It is noted that the boundaries of the shaded area do not generally represent any individual realizations from the bootstrap analysis, but they are envelopes for all the curves.

Figure VI.2(a) (i.e., SHS braces and welded connections) experienced collapse with a median value equal to 2.03g for the BF model, 2.78g for the SP model, and 2.13g for the TS model. All the curves reach a value of approximately 1 for S_a values larger than 7g. The buildings with the 2L braces and bolted connections (Figure VI.2(b)) show similar results, with a median S_a value to collapse equal to 1.85g for the BF model, 2.04g for the TS model, up to 2.64g for the SP model.

Numerical problems were encountered in performing the bootstrap simulations for the BF case study (i.e., the software was not able to perform the resampling of the collapse cases). However, the fragility curve corresponding to the PCB-2L-BF model has practically a value of the dispersion parameter equal to 0. Consequently, intersections with both the TS and the SP curves occurred for values of S_a smaller than $2g$, despite the median value increased from the BF model to the SP/TS models.

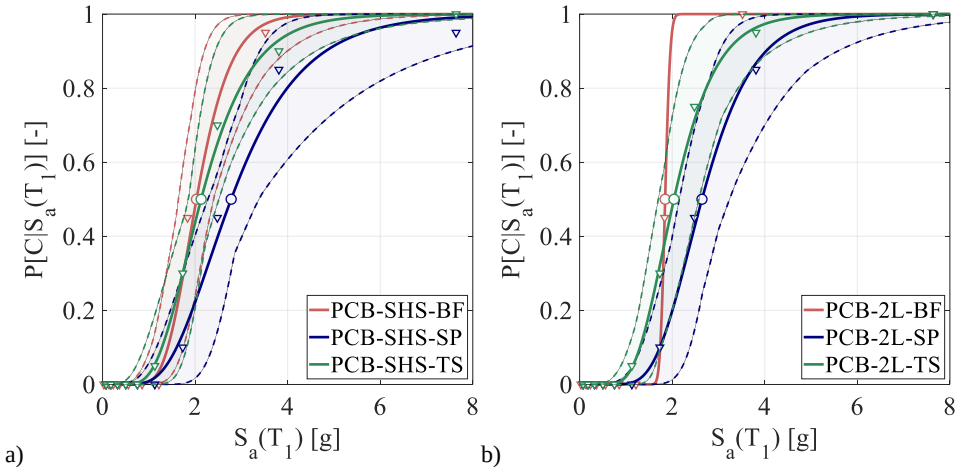

Figure VI.2 Collapse fragility curves for the PCB case studies: (a) SHS braces; (b) 2L braces.

VI.3.2 SCB case studies

This section summarizes results concerning the numerical models with semi-continuous column base connections in the transverse direction (i.e., SCB). Figure VI.3(a) and Figure VI.3(b) show the results for the SCB-SHS case studies. The plots follow the same conventions described in the previous section. In the SCB-SHS cases, the median values of the S_a producing structural collapse resulted equal

to 2.98*g* for the BF model, 4.81*g* for the TS model, up to 5.58*g* for the SP model. Therefore, the differences in the median values of the IM to collapse are appreciable in this case. Additionally, none of the curves predict a probability of collapse equal to 1 in the investigated range of S_a, i.e., from 0 to 8*g*. Also, the shaded areas obtained by the bootstrap procedure appear larger if compared with the corresponding PCB cases. A more detailed description of such comparisons is made in the following. In the SCB-2L cases, larger differences between the models with or without the envelope panels can be observed if compared with the results for the SCB-SHS case studies. The median value of the S_a to collapse varied from 1.80*g* for the BF model, to 3.15*g* for the TS model, up to 5.44*g* for the SP model. Also, the dispersion of the results increases passing from the BF or TS model (similar shaded area can be observed comparing these two models) to the SP model, i.e., the SP model did always show the larger dispersion in terms of bootstrap curves.

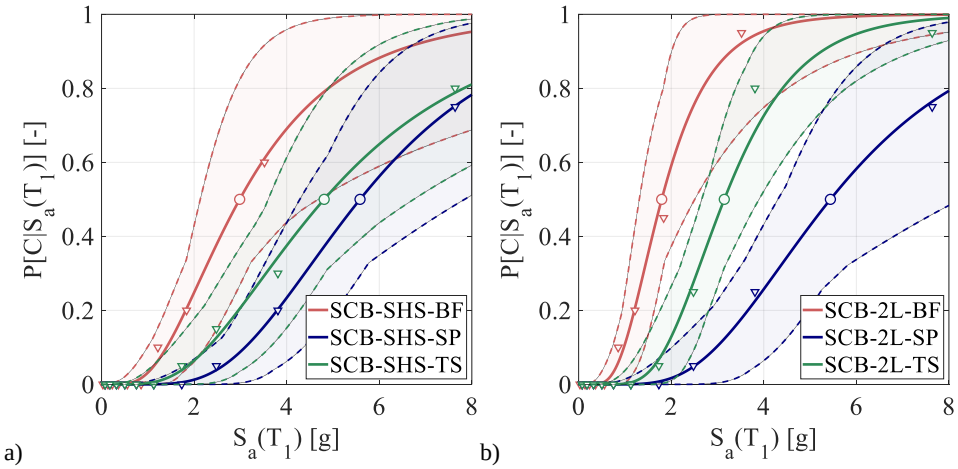

Figure VI.3 Collapse fragility curves for the SCB case studies: (a) SHS braces; (b) 2L braces.

VI.3.1 Model-to-model comparisons

VI.3.1.1 PCB vs. SCB results

First, a comparison among the fragilities of the buildings with portal frames having pinned column base (PCB) or semi-continuous column base (SCB) connections is discussed. It is worth remembering here that the PCB structures exhibited brittle truss-to-column connection failures, while ductile column base connection yielding characterized the response of the SCB cases. This difference in the structural response can be seen clearly reflected in the fragility curves obtained for the structures having SHS braces in the longitudinal direction (Figure VI.4(a)). In fact, the SCB case shows an appreciably larger S_a median value to collapse compared to the PCB case. However, the dispersion of the fragility curves was much larger for the SCB case, thus leading to some overlapping of the shaded regions. On the contrary, using 2L brace cross sections (Figure VI.4(b)) led to approximately the same value of the median S_a to collapse for the PCB and SCB cases. This different result was a consequence of the relatively small ductility exhibited by the 2L bracing, which failed due to end connection failures. Such failures of the bracing system in the longitudinal direction masked the differences in the transverse direction response when comparing the PCB and SCB cases.

Looking at the response with the SP cladding (Figure VI.5), the SCB cases always show larger values of the median and dispersion of the S_a to collapse. In this case, the presence of sandwich panels clearly improved the collapse performance, compensating for the relatively poor response of the 2L brace solution.

Figure VI.6 shows the comparison for the TS models. The results confirm the observations made for the SP model in the case of SHS braces. On the contrary, the gap between the two curves in terms of median values of S_a reduced with respect to the SP models when the 2L brace solution was adopted.

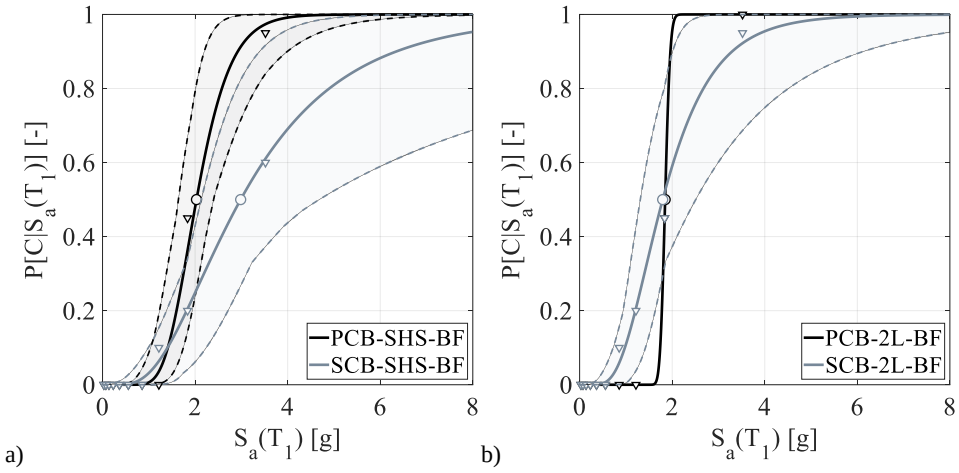

Figure VI.4 PCB-BF vs. SCB-BF model comparisons: (a) SHS braces; (b)2L braces.

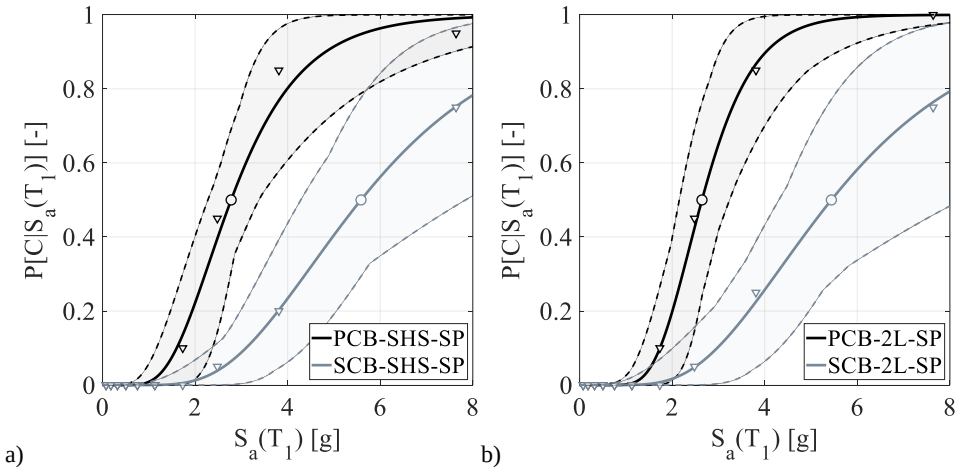

Figure VI.5 PCB-SP vs. SCB-SP model comparisons: (a) SHS braces; (b)2L braces.

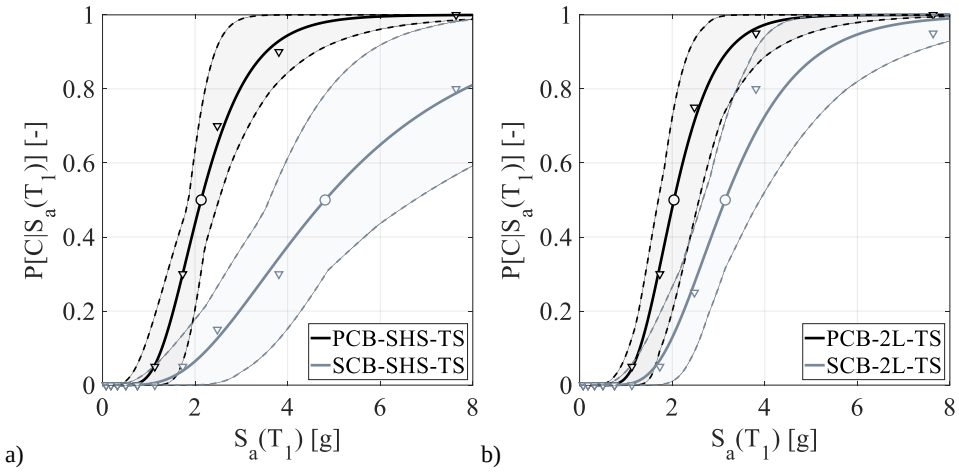

Figure VI.6 PCB-TS vs. SCB-TS model comparisons: (a) SHS braces; (b) 2L braces.

VI.3.1.2 SHS vs. 2L results

A comparison of fragilities by varying the type of the longitudinal brace cross section and connection is provided hereafter. In Figure VI.7(a), fragility curves of the PCB-SHS-BF model are compared to those obtained for the PCB-2L-BF model. As already discussed, the PCB-2L-BF model suffered numerical convergence issues. However, differences between the input data of the two models were practically negligible. In the PCB-SHS-BF model 19 collapse cases were observed at the larger IM value, with respect to 20 collapse cases observed with the PCB-2L-BF. In fact, median S_a values to collapse were predicted to be very similar each other.

In Figure VI.7(b) fragility curves of the SCB-SHS-BF model are compared to those obtained for the SCB-2L-BF model. In this case, both the median S_a values and the dispersions significantly change passing from SHS brace solution to 2L

brace solution. In fact, as suggested by structural analysis results, 2L solutions introduced fragility in the building due to premature failure of bolted connections between braces and gusset plates. This reflected in results of fragility curves.

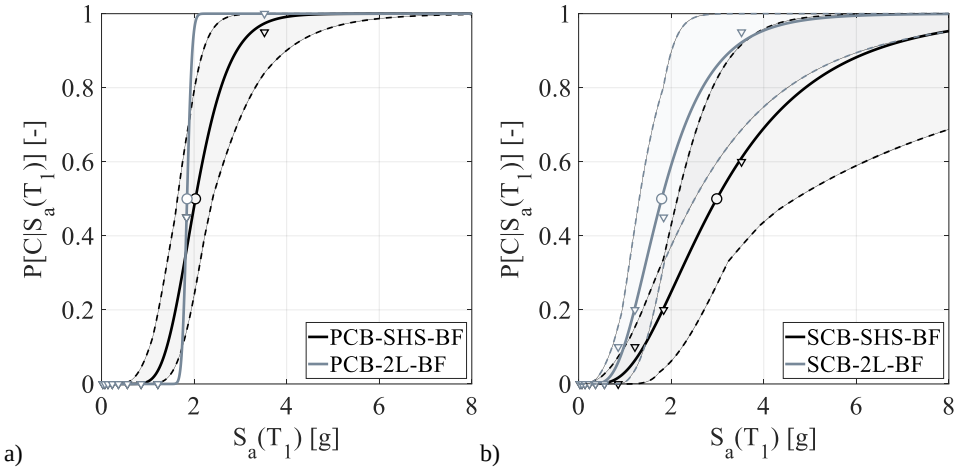

Figure VI.7 SHS vs. 2L model comparisons: (a) PCB-BF cases; (b) SCB-BF cases.

Similar results can be obtained by looking at the SP model (Figure VI.8). Comparing results obtained by varying vertical brace details, on can conclude that brace behaviour represented a minor impact in fragility, both for the PCB and for the SCB cases. Indeed, main source of fragility in the PCB cases was related to failures of truss-to-column connections, which did not change by changing vertical brace behaviour. In the case of SCB models, SP cladding system allowed mitigation of structural fragility introduced within 2L braces, thus obtaining a fragility curves practically equivalent for both the brace typologies.

Figure VI.9 summarize comparison concerning variation in brace details within the TS model. The PCB cases confirmed fragility trend observed for the previous models (Figure VI.9(a)), whilst the SCB cases show a rather large difference, both in terms of median values and dispersions, as well as in terms of bootstrap results.

This was a confirmation of the role of the cladding system in mitigation of structural fragility. Indeed, lateral resistance offered by TSs was not sufficient to mitigate fragility introduced by varying brace connection details, passing from relatively ductile SHS brace solution to practically brittle 2L brace solution.

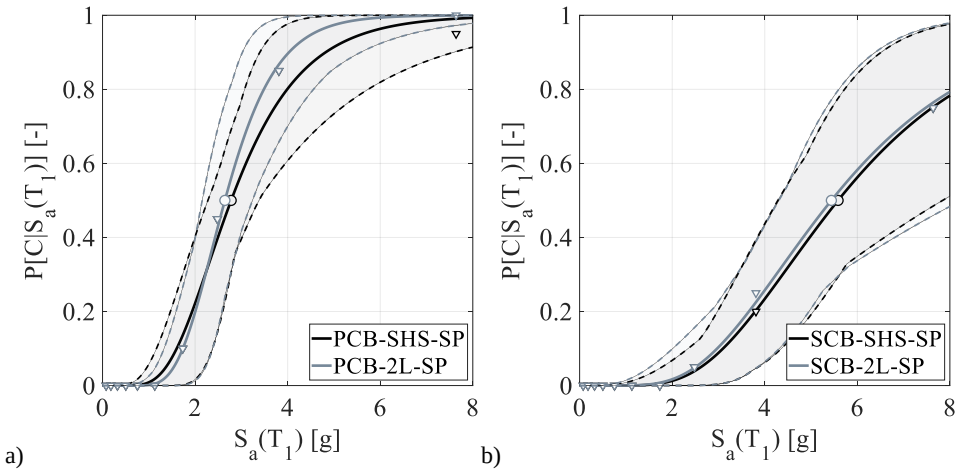

Figure VI.8 SHS vs. 2L comparisons: (a) PCB-SP cases; (b) SCB-SP cases.

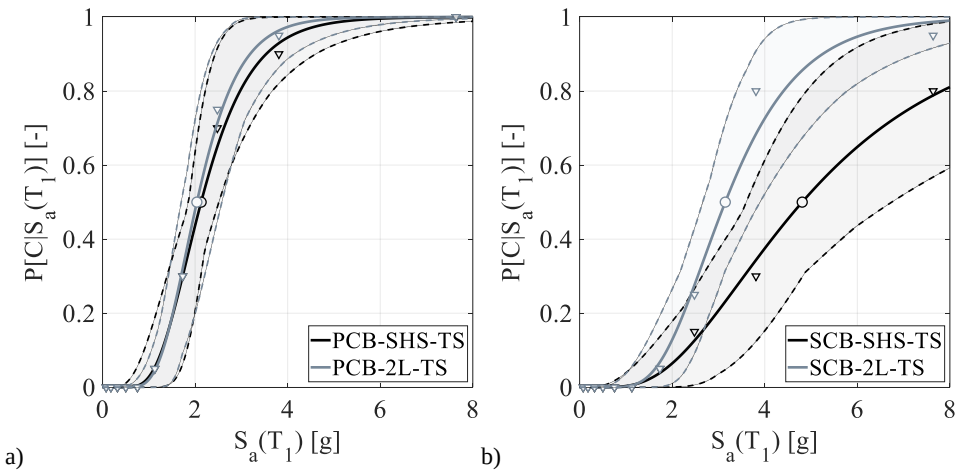

Figure VI.9 SHS vs. 2L comparisons: (a) PCB-TS cases; (b) SCB-TS cases.

VI.3.2 Numerical results and comparisons

Table VI-1 summarizes the numerical results obtained using the parametric bootstrap with the ML method (Baraschino *et al.*, 2020). For completeness, the estimated values of the fragility curve parameters are reported as well. It is noted that no bootstrap analysis results are reported for the PCB-2L-BF model due to the numerical non-convergence previously discussed. As one can see, nearly identical results were obtained either by the ML or the parametric bootstrap. It is also noted that up to 500 simulations were used to generate consistent distributions for the number of collapse cases per each stripe.

Table VI-1 Fragility analysis results using the ML method.

MODEL	η_C	β_C	**E[η_C]**	**E[β_C]**	**VAR [η_C]**	**VAR [β_C]**
PCB-SHS-BF	0.708	0.284	0.709	0.291	0.006	0.002
PCB-SHS-SP	1.022	0.43	1.019	0.411	0.005	0.006
PCB-SHS-TS	0.756	0.395	0.759	0.385	0.004	0.005
PCB-2L-BF	0.614	0.047	-	-	-	-
PCB-2L-SP	0.972	0.329	0.977	0.316	0.004	0.004
PCB-2L-TS	0.712	0.349	0.717	0.334	0.004	0.004
SCB-SHS-BF	1.093	0.589	1.106	0.579	0.016	0.016
SCB-SHS-SP	1.720	0.46	1.729	0.45	0.01	0.009
SCB-SHS-TS	1.571	0.578	1.575	0.566	0.012	0.011
SCB-2L-BF	0.585	0.474	0.588	0.465	0.007	0.007
SCB-2L-SP	1.694	0.472	1.700	0.457	0.011	0.010
SCB-2L-TS	1.147	0.400	1.149	0.386	0.005	0.005

Similarly, Table VI-2 summarizes the numerical results obtained by the LSF method, also implemented in the R2R software. Using the LSF method, bootstrap results were obtained for all the case studies. As one can observe, numerical results in terms of η_C were practically coincident with those obtained by means of the ML method. In terms of β_C, one can observe that the LSF method generally

increased (or slightly decreased) dispersion of the fragility curves. Nearly identical results were obtained using the parametric bootstrap, thus confirming a good estimation of the curve parameter.

Table VI-2 Fragility analysis results using the LSF method.

MODEL	η_C	β_C	**E[η_C]**	**E[β_C]**	**VAR [η_C]**	**VAR [β_C]**
PCB-SHS-BF	0.568	0.306	0.594	0.304	0.005	0.005
PCB-SHS-SP	0.94	0.338	0.941	0.327	0.004	0.007
PCB-SHS-TS	0.684	0.384	0.692	0.369	0.005	0.01
PCB-2L-BF	0.579	0.302	0.585	0.283	0.003	0.002
PCB-2L-SP	0.936	0.339	0.947	0.342	0.005	0.007
PCB-2L-TS	0.659	0.334	0.669	0.32	0.004	0.007
SCB-SHS-BF	1.087	0.652	1.106	0.646	0.028	0.038
SCB-SHS-SP	1.703	0.465	1.707	0.459	0.012	0.014
SCB-SHS-TS	1.542	0.65	1.551	0.64	0.014	0.021
SCB-2L-BF	0.604	0.5	0.601	0.481	0.009	0.012
SCB-2L-SP	1.651	0.488	1.665	0.48	0.01	0.012
SCB-2L-TS	1.051	0.297	1.058	0.302	0.004	0.006

References

Bakalis K., Vamvatsikos D. 2018. Seismic Fragility Functions via Nonlinear Response History Analysis. *Journal of Structural Engineering 144(10): 1 – 15.*

Baker J.W. 2015. Efficient analytical fragility function fitting using dynamic structural analysis. Earthquake Spectra 31: 579 – 99.

Baraschino R., Baltzopoulos G., Iervolino I. 2020. R2R-EU: Software for fragility fitting and evaluation of estimation uncertainty in seismic risk analysis. *Soil Dynamics and Earthquake Engineering 132: 106093*

Iervolino I. 2017. Assessing uncertainty in estimation of seismic response for PBEE. *Earthquake Engineering and Structural Dynamics 46: 1711 – 1723.*

Kennedy R.P., Cornell C.A., Campbell R.D. Kaplan S., and Perla H.F. 1980. Probabilistic seismic safety study of an existing nuclear power plant. *Nuclear Engineering and Design 59: 315 – 338.*

Petruzzelli F. 2013. Scale-dependent procedures for seismic risk assessment and management of industrial building portfolios. *PhD Thesis, Department of Structures for Engineering and Architecture,* Naples, Italy.

Porter K., Kennedy R. and Bachman R. 2007. Creating Fragility Functions for Performance-based Earthquake Engineering. *Earthquake Spectra. 23(2): 471-489.*

Porter K. 2020. A Beginner's Guide to Fragility, Vulnerability, and Risk. *University of Colorado Boulder, 127 pp.* Freely available at: https://www.sparisk.com/pubs/Porter-beginners-guide.pdf.

Zareian F., Krawinkler H., Ibarra L., Lignos D. 2010. Basic Concepts and Performance Measures in Prediction of Collapse of Buildings under Earthquake Ground Motions. *The Structural design of Tall and Special Buildings 19: 167 – 181.*

Chapter VII

CONCLUSIONS AND FUTURE DEVELOPMENTS

Structural collapse due to earthquakes is the main source of injuries and loss of lives and it might contribute significantly to economic losses. Consequently, the evaluation of the collapse risk of buildings is still today a major task in the context of earthquake engineering. However, there are significant difficulties in addressing the task, such as a proper modelling of the inelasticity of structural components accounting for strength and stiffness degradations, and an adequate representation of the seismic actions. The difficulties significantly increase when existing buildings are considered, due to additional lack of adequate knowledge in terms of the cyclic inelastic response of components which would be not designed for such inelastic response in case of a new building. In this context, this dissertation has dealt with the collapse fragility assessment of older non-residential single story steel buildings.

The design of four archetype buildings was simulated according to codes and standards of practice used in Italy in the 1980s-1990s. All the considered archetype buildings comprise portal frames in the transverse (X-) direction and concentric braces in the longitudinal (Y-) direction. The four generated structures

differ each to other because of different design assumptions made in both transverse and longitudinal building directions. In the transverse direction, two alternative schemes were selected: (i) a continuous column for the whole height of the building with a pinned column base (PCB) and a truss beam providing moment action; (ii) a semi-continuous column base (SCB) and a nominally pinned truss-to-column connection. In the longitudinal direction, two brace cross section shapes and two corresponding types of brace connections were selected: (i) square hollow section (SHS) braces with welded gusset plate connections; (ii) two (closely spaced built-up) angle (2L) section braces with bolted gusset plate connections. In addition, per each structural solution, two types of panels for the building envelope were considered: (i) sandwich panels (SP) with bolted cladding-to-frame connections and (ii) trapezoidal sheeting (TS) with screwed cladding-to-frame connections.

The simulated design results have been illustrated in Chapter II, focusing on the main output and issues arising from the older design procedures and standards of the engineering practice. Particularly, design of the main truss system was always governed by gravity loads, resulting in having weaker connections at the truss ends, as well as overstrength of the connected truss members. Columns were designed fulfilling deformability checks due to horizontal actions generated by wind loads. In fact, wind loads were found to be always predominant actions if compared to seismic loads. Design of column base connections was also affected by horizontal loads. Since columns were designed limiting displacements and the relevant connections were designed satisfying resistance checks, semi-rigid and partial-strength column base connections resulting from design. Slenderness limitation for compressed members was critical for selecting cross section of vertical braces. On the contrary, brace connections were designed by using horizontal actions, thus generating partial-strength connections in the case of 2L braces.

In Chapter III, existing models for the identified critical components were first reviewed and discussed. However, either numerical or experimental study on the hysteretic behaviour of structural components which are nowadays designed using capacity design rules (e.g., connections) are totally missed. Starting from information obtained by the available consolidated knowledge, non-linear 3D finite element models were built in the open-source software *OpenSees*. The numerical models were essentially built by mainly exploiting the state-of-art theoretical backgrounds (e.g., the component method) and using engineering judgments. Particularly, a proposal for an improvement over existing models for the building envelope panels, including consideration of the secondary steelwork and relevant connections, has been presented. Eventually, the adopted seismic collapse criterion was described in this chapter. The selected criterion assumes that collapse means a 50% loss of the base shear force resistance with respect to the maximum resistance obtained from a pushover curve.

In Chapter IV, the results of non-linear static (pushover) analysis are described per each structural model. The pushover analysis highlighted that failure in the transverse (portal frame) direction is due to failure of the (partial-strength) truss-to-column connections in the PCB case, while the collapse response is dominated by the column base connections in the SCB case. Regarding the response in the longitudinal (braced frame) direction, the analysis indicates a relative ductile behavior of the SHS braces because of connection strength sufficient to resist brace yielding and buckling. On the contrary, the 2L braces exhibited a quasi-brittle failure due to early failure of the bolted brace to gusset plate connections. Concerning the type of cladding, the buildings with SPs exhibited better structural performance, compared to the buildings with TSs. This was a consequence of the better cladding-to-frame connection details of sandwich panels if compared with the screw connection details of the trapezoidal sheeting.

In Chapter V, the results from the non-linear dynamic analysis are presented per each archetype building. The multi-stripe analysis (MSA) method was adopted with bi-directional ground motion (GM) input. A total of 200 non-linear dynamic analyses were carried out per each numerical model by varying the earthquake return period from 10 *years* to 100000 *years*). The MSA results confirmed the results obtained with the pushover. The collapse cases started to appear for earthquake return period equal to 1000 *years*. At the largest considered earthquake return period, almost all the considered GMs led to collapse of the PCB models. On the contrary, a few collapse cases were observed for the SCB building. The MSA results highlighted that most of the collapses occurred due to the fragility of the transverse portal frames (both for the PCB structures and SCB structures). A small number of collapse cases were triggered by SHS brace fractures and 2L brace connection failure. The SHS brace fracture was triggered for seismic actions with very large return periods $T_R \geq 10000$ *years*. The 2L brace connection failure started to occur for $T_R \geq 5000$ *years*.

Chapter VI describes the collapse fragility curves obtained starting from the MSA results. Lognormal probability distributions were fitted to the numerical data. Each fragility curve parameters were estimated using state-of-the-art methods, which are described in the chapter. The obtained fragility curves very clearly reflected the observations from the structural responses computed via the non-linear dynamic analyses. The results could be used to improve a database of fragility curves for existing buildings.

In conclusion, the results obtained from this study have clearly highlighted the paramount role of connections and the building envelope in assessing the collapse response of existing single-storey steel buildings. Several low-ductility failure modes largely affected both the resistance and drift capacity of such structures. However, results clearly show that larger values of collapse fragility (for example

considering probability larger than 0.80) are associated with very large values of spectral acceleration (larger than 3*g* for the PCB case studies and 4*g* for the SCB case studies). Consequently, mean annual frequencies of collapse are expected to be small enough to be *acceptable* if compared with the available value of the tolerable mean annual frequency of collapse (Chapter III). Also, values of the expected annual losses (EAL) can be predicted to be smaller than those associated with other building types, in line with numerical results of past research (Chapter I). However, though small EAL values are expected to be significantly contributed by the collapse limit state. In fact, as proved by the presented numerical results, the seismic collapse limit state can be triggered with a relatively small number of damaged building components. Since relatively low building damage are expected for drifts smaller than those corresponding to the collapse of the buildings, relatively small economic losses should also be expected if the collapse limit state is not triggered by an earthquake event.

From the overview of the available research results, it was clear that the modelling of connections in this type of buildings poses significant challenges. The connection strain hardening response, the post-peak descending branch, any cyclic strength and stiffness degradation, as well as the possible force interactions are all aspects for which robust analytical models should be developed. From this perspective, additional finite element models and experimental tests, looking more in the detail of the individual structural component response, could improve the current knowledge, either confirming the use of simplified approaches or proving the presence of additional reserve of ductility which could decrease structural fragility.